Dissertation

submitted to the
Combined Faculties for the Natural Sciences and Mathematics
of the Ruperto-Carola University of Heidelberg, Germany
for the degree of
Doctor of Natural Sciences

Put forward by

James Barry

born in: Johannesburg

Oral examination: 29 May 2013

New physics models with sterile neutrinos at different energy scales

Referees:

Dr. Werner Rodejohann

Prof. Dr. Joerg Jaeckel

Abstract

Neutrino mass requires new physics beyond the Standard Model: sterile neutrinos are one such example. In general the mass scale of such particles is unknown, so that different model building scenarios arise. The aim of this thesis is to accommodate light sterile neutrinos in working models and study the phenomenological consequences. Indeed, sterile neutrinos at the eV scale could explain observed short-baseline anomalies, whereas keV-scale warm dark matter particles could resolve tensions in the standard cosmological model. Different A_4 flavour symmetry models are modified to include sterile neutrinos, with the Froggatt-Nielsen mechanism controlling their mass spectrum and higher-order effects explicitly taken into account. The resulting signatures in neutrinoless double beta decay are focussed on. In addition, the connection between that process and neutrino mass is studied in the left-right symmetric model: the multitude of contributions are categorised and various special cases are studied numerically. The role of mixed helicity diagrams is emphasised, and the inverse neutrinoless double beta decay process at a linear collider is analysed in detail. These and other experimental signatures will be crucial in deciphering the nature and origin of neutrino mass.

Zusammenfassung

Neutrinomassen benötigen neue Physik jenseits des Standardmodells, z.B. sterile Neutrinos. Verschiedene Modell-Szenarien sind möglich, da die Masse solcher sterilen Zustände unbekannt ist. Das Ziel dieser Arbeit ist es, leichte sterile Neutrinos in erfolgreiche Modelle einzubauen und die phänomenologischen Konsequenzen zu analysieren. In der Tat könnten sterile Neutrinos an der eV-Skala einige beobachtete Anomalien in Experimenten zu Neutrinooszillationen erklären, während keV sterile Neutrinos als warme dunkle Materie manche Probleme des kosmologischen Standardmodells lösen könnten. Verschiedene auf A_4 basierende flavoursymmetrische Modelle werden mit sterilen Neutrinos erweitert, wobei das Massenspektrum durch den Froggatt-Nielsen-Mechanismus kontrolliert wird; der Einfluss höherer Ordnungen wird explizit berücksichtigt. Die Auswirkungen der Modelle auf neutrinolosen doppelten Betazerfall stehen im Mittelpunkt. Außerdem wird die Verbindung zwischen diesem Prozess und Neutrinomasse in einem links-rechts-symmetrischen Modell untersucht: die Vielzahl von Beiträgen wird kategorisiert und verschiedene Sonderfälle numerisch untersucht. Die Wichtigkeit von Diagrammen mit gemischter Helizität wird betont und der in einem Linearbeschleuniger beobachtbare invertierte neutrinolose doppelte Betazerfall im Detail analysiert. Diese und andere experimentelle Signaturen könnten Licht auf den Ursprung und die Natur der Neutrinomassen werfen.

Acknowledgements

This project would not have been possible without the guidance and support of my supervisor, Werner Rodejohann. I thank you for answering my annoying questions, for giving me the chance to attend summer schools and conferences, for the annual advent calendars and for replying to an e-mail from a stranger from Africa back in 2009! I would also like to thank Manfred Lindner for the vibrant atmosphere in the research group at MPIK, and Anja Berneiser for her tireless help with so many administrative issues.

I am grateful to He Zhang for the fruitful collaboration on two sterile neutrino projects, as well as great Chinese food. Many thanks go out to my office mates, past and present: Hans Hettmansperger, Tibor Frossard and Julian Heeck. I thank you for the lively discussions, coffee breaks, games of billiard and entertaining hat-building sessions. Julian, thanks for insightful whiteboard deliberations, for reading my German abstract and for always keeping me up to date with the latest sterile neutrino trends. Martin Holthausen, thanks for proofreading, for good times over coffee and for interesting newspaper clips. I would also like to thank Alexander Merle for encouraging me to pursue a PhD in theoretical physics, and for good times at conferences. Thank you to Evgeny Akhmedov, Michael Duerr and Thomas Schwetz for useful discussions relating to my research. I thank the other members and ex-members of the theory group for great lunchtime conversations: Adisorn Adulpravitchai, Alexander Dueck, Andreas Hohenegger, Felix Kahlhoeffer, Alexander Kartavtsev, Joachim Kopp, Kher Sham Lim, Lisa Michaels, Viviana Niro, Pavel Fileviez Perez, Daniel Schmidt and Juri Smirnov. Thank you to my experimental colleagues Julia Haser, Sebastian Lindemann, Werner Maneschg, Stefan Wagner and Marc Weber, for allowing me to practice German on many bus rides to the institute.

The friendship and support of Marlin and Carla Watling, Kornelius Israel, Johannes and Esther Welter, Ricardo and Elìs Dettweiler, David and Tina Reeh, Christian Heigoldt, Murat Yulafci, Tilman Gerber, Christian Hoffmann, Ed Einsiedler, Stefanie Linner and Christina Sonntag is gratefully acknowledged. Without you I would have done little else but physics in my time in Heidelberg!

Finally, I would like to thank my parents for their continual support over the years, and my wife Joanne, for her love, encouragement and friendship. I am indebted to you for your patience in the last few months, and for keeping me fed and clothed in the last stages of this work! Above all, I thank the Lord for his presence in my life; He is the source of my strength.

Anybody who has been seriously engaged in scientific work of any kind realises that over the entrance to the gates of the temple of science are written the words: Ye must have faith. It is a quality which the scientist cannot dispense with.

Max Planck

Contents

Abstract i

Acknowledgements iii

1 Introduction 1

2 Beyond the Standard Model with sterile neutrinos 5
2.1 Fermion masses in the Standard Model . . . 5
2.2 Neutrino mass in extensions of the Standard Model . . . 6
2.2.1 Type I seesaw model . . . 7
2.2.2 Type II seesaw model . . . 13
2.2.3 Other neutrino mass models . . . 14
2.3 The left-right symmetric model . . . 15
2.3.1 Background and motivation . . . 15
2.3.2 Theoretical details . . . 16
2.4 Summary . . . 19

3 Phenomenology of sterile neutrinos 21
3.1 Oscillations of active neutrinos . . . 21
3.2 Sterile neutrinos in oscillation experiments . . . 24
3.2.1 Sterile neutrino mixing and mass spectra . . . 24
3.2.2 Sterile neutrino oscillations at short baselines . . . 26
3.2.3 Experimental evidence and global fits . . . 27
3.3 Sterile neutrinos in beta decay . . . 29
3.4 Neutrinoless double beta decay with sterile neutrinos . . . 30
3.4.1 The standard scenario . . . 30
3.4.2 Phenomenological analysis of $0\nu\beta\beta$ with eV-scale sterile neutrinos . . . 32
3.4.3 $0\nu\beta\beta$ with pseudo-Dirac and bimodal neutrinos . . . 36
3.4.4 $0\nu\beta\beta$ in type I seesaw models . . . 39
3.4.5 Experimental situation . . . 41
3.5 Sterile neutrinos from astrophysical sources . . . 42
3.5.1 Astrophysical sources of neutrinos . . . 42
3.5.2 Flavour ratios of pseudo-Dirac and bimodal neutrinos . . . 43
3.6 Sterile neutrinos in cosmology . . . 49
3.6.1 Light (sterile) neutrinos in the early universe . . . 49
3.6.2 Sterile neutrino warm dark matter . . . 54
3.6.3 Leptogenesis and the νMSM . . . 55
3.7 Colliders, lepton flavour violation and EWPO . . . 56
3.7.1 LHC signatures . . . 56
3.7.2 Linear collider signatures . . . 57
3.7.3 Lepton flavour violation and dipole moments . . . 58

3.7.4 Electroweak precision observables . . . 59
3.8 Summary . . . 59

4 Sterile neutrinos in flavour symmetry models **61**
4.1 Introduction to flavour symmetries . . . 61
4.2 A_4 models with light sterile neutrinos . . . 62
4.2.1 Introduction to A_4 symmetry . . . 62
4.2.2 An effective A_4 model with sterile neutrinos . . . 63
4.2.3 A_4 seesaw model with one keV sterile neutrino . . . 71
4.3 Bimodal neutrinos in an S_3 model . . . 84
4.3.1 Pseudo-Dirac vs. bimodal neutrinos . . . 84
4.3.2 Effective S_3 model with one Dirac mass eigenstate . . . 84
4.4 Summary and conclusion . . . 87

5 LNV and LFV in the left-right symmetric model **89**
5.1 Introduction . . . 89
5.2 Neutrinoless double beta decay . . . 90
5.2.1 Particle physics amplitudes . . . 90
5.2.2 Nuclear matrix elements and lifetime . . . 97
5.3 Lepton flavour violation . . . 98
5.4 Signatures at the LHC . . . 100
5.5 $0\nu\beta\beta$ amplitudes in the seesaw limits . . . 101
5.5.1 Type II seesaw dominance . . . 101
5.5.2 Type I seesaw dominance . . . 105
5.6 Inverse neutrinoless double beta decay . . . 109
5.6.1 Relation to $0\nu\beta\beta$ . . . 109
5.6.2 Cross section of $e^-e^- \to W_L^- W_R^-$ . . . 111
5.6.3 Polarised beams . . . 114
5.7 Summary and conclusions . . . 115

6 Conclusion **117**

Appendices **123**

A Flavour conversion probabilities **123**

B Group theory details **125**
B.1 Group theory of A_4 . . . 125
B.2 Residual μ-τ symmetries in extended A_4 models . . . 126

C NLO corrections in the A_4 seesaw model **129**
C.1 Charged lepton sector . . . 129
C.2 Neutrino sector . . . 130

D Form factors and loop functions for LFV processes **135**
D.1 Relevant Lagrangian terms . . . 135
D.2 Decay widths and branching ratios . . . 136
D.3 Loop functions . . . 140

E Helicity amplitudes for $e^-e^- \to W_L^- W_R^-$ **141**

List of Tables **145**

List of Figures **147**

List of Acronyms **149**

References **153**

Chapter 1

Introduction

The Standard Model (SM) of particle physics has been largely successful in explaining the elementary particles that make up our world, and the discovery of a Higgs-like particle at the LHC has provided important confirmation of one of the key ingredients of that model [1, 2]. Be that as it may, many fundamental questions remain unanswered, and experiments at the high-energy frontier have so far been unsuccessful in their quest to uncover physics beyond the SM. There are several theories that predict new particles at the TeV scale, the signatures of which have yet to be discovered.

Indeed, the only real (direct) evidence for new physics comes from neutrinos:[1] oscillation experiments have shown that neutrinos are massive and that they mix, which immediately requires an extension of the SM. The Higgs mechanism gives mass to all known fermions except for neutrinos, due to the fact that there are no right-handed neutral fermions in the theory, so that Dirac mass terms are not allowed. This maximal violation of parity is confirmed from studies of beta decay, in which only neutrinos with left-handed helicity have been observed. A popular way to allow neutrino mass terms in the SM is to introduce right-handed (sterile) neutrinos and/or Higgs triplets, which mediate the type I [3–7] and type II [8–13] seesaw mechanisms, respectively. The right-handed fermions are sterile in the sense that they do not directly interact with SM fields; they can only reveal themselves through mixing with the active sector. However, gauge extensions to the SM elevate sterile neutrinos to be non-singlets, so that they feel gauge interactions from the new physics sector: the left-right symmetric model (LRSM) is one such example.

The term "seesaw" traditionally refers to two widely varying mass scales, thus linking the extremely light (sub-eV) masses of neutrinos to the very heavy Majorana masses of right-handed neutrinos, which are close to the Grand Unified Theory (GUT) [14] scale of order 10^{15} GeV. However, placing right-handed neutrinos at the GUT scale renders them completely unobservable, barring the indirect evidence of leptogenesis, which cannot be empirically proven. For that reason there has been renewed interest in seesaw models at observable energy scales, specifically around the TeV scale, accessible at collider experiments. Although the LHC is unable to detect neutrinos directly it could still observe processes involving heavy neutrinos as mediators. Moreover, there are experimental hints that point towards sterile neutrinos at even lower mass scales, which lead one to consider models with "light" sterile neutrinos. In that sense phenomenology becomes the driving motivation for model building with neutrinos. Chapter 3 provides a summary of the relevant experimental signatures as well as the status of experimental searches.

One example is the idea that sterile neutrinos at the keV scale are a dominant component of the dark matter (DM) [15] in the universe: the so-called "warm dark matter" (WDM) models [16]. A link between neutrino mass and DM has long been postulated [15], since the latter provides an indirect proof of the existence of physics beyond the SM, complementing

[1] Indirect evidence comes from dark matter.

the direct proof of the former. The light neutrinos observed in oscillation experiments are one form of DM, albeit hot dark matter (HDM), which is incompatible with cosmological models. The typical assumption is that the DM particle is much heavier, in other words it is cold dark matter (CDM), usually in the form of a weakly interacting massive particle (WIMP). Several theories such as supersymmetry predict the existence of such particles, and the experimental search for their extremely weak interaction with normal matter is ongoing. Although the standard ΛCDM paradigm is reasonably successful, it still suffers from several inconsistencies at smaller scales. Warm dark matter models have been shown to solve some of those problems, in particular by reducing the number of Dwarf satellite galaxies or smoothing the cusps in DM halos. An ideal candidate for WDM is a sterile neutrino with keV-scale mass and tiny mixing to the active neutrinos, and it is interesting to study how to incorporate such a particle in the usual type I seesaw model.

If one lowers the right-handed neutrino mass scale from the GUT scale to the keV scale then it is not inconceivable that it could be a few orders of magnitude lower, at the eV scale. There are longstanding anomalies in neutrino oscillation physics, specifically the LSND [17] and MiniBooNE [18] results, which could be explained by sterile neutrinos with eV masses. The case for eV-scale sterile neutrinos has recently been strengthened by the so-called "reactor anomaly" [19]: a number of short-baseline (SBL) reactor experiments (past and present) may have observed a flux deficit of electron anti-neutrinos, which went unobserved due to an inaccurate knowledge of the flux of those particles from nuclear reactors. Interestingly, there are also hints for additional relativistic degrees of freedom from cosmology, specifically from studies of the cosmic microwave background (CMB) as well as from Big Bang Nucleosynthesis (BBN), both of which constrain the effective number of neutrino species [20]. Piecing together these different clues leads to a rather incomplete picture, and future experiments must confirm or refute the existence of light sterile neutrinos [21]. The signatures of eV-scale sterile neutrinos in neutrinoless double beta decay ($0\nu\beta\beta$), beta decay and cosmology will be discussed in Chapter 3. From the theoretical point of view it is a challenge to build models that can accommodate such particles; that is one of the goals of this thesis.

Sterile neutrinos are introduced to explain neutrino mass, the evidence for which comes from neutrino mixing. Models to explain the latter are typically based on flavour symmetries, which extend the SM gauge group by further (usually discrete) symmetry groups [22]. It is therefore natural to ask what the effect of light sterile neutrinos is on active neutrino mixing, and whether such particles can be accommodated in flavour symmetry models. One of the most popular symmetry groups is A_4, upon which countless models have been based. The leading order prediction of A_4 (as well as many other) models for active neutrino mixing is tri-bimaximal mixing (TBM), which is now ruled out by data [23], so that higher-order effects must necessarily be taken into account. Those could have various sources, such as renormalisation group running or higher-dimensional operators. Of particular interest in seesaw models are corrections from next-to-leading order (NLO) seesaw terms, in which case there is a definite correlation between active-active mixing and active-sterile mixing. Chapter 4 presents two A_4 models that include sterile neutrinos of varying mass scales: (*i*) an existing effective mass model extended with sterile neutrinos and (*ii*) a seesaw model built to accommodate three sterile neutrino states, one of which is a keV WDM particle. In both cases the sterile neutrino mass spectrum is controlled by the Froggatt-Nielsen (FN) mechanism, NLO terms are studied in detail and phenomenological consequences are discussed. The A_4 seesaw model is the first fully working model of its kind in the literature, combining the known aspects of flavour symmetry models with the FN mechanism and light sterile neutrinos.

Another possibility for neutrino masses is the so-called pseudo-Dirac scenario [24, 25], in

which each active neutrino has a partner of almost the same mass. This could be seen as the opposite extreme to the usual seesaw model, since the Dirac mass terms are now much greater than their Majorana counterparts. The tiny mass-splitting makes these states "pseudo-Dirac", in the sense that a small Majorana mass term is added to a Dirac neutrino term; the mass-squared difference should be smaller than 10^{-11} eV^2 in order to evade bounds from solar neutrino experiments [26]. An intermediate case is the "bimodal" model [27], in which flavour eigenstates receive similar admixtures of Majorana and Dirac type masses. Interesting experimental signatures arise, both in the flavour flux ratios of high energy astrophysical neutrinos measured at neutrino telescopes as well as in $0\nu\beta\beta$, discussed in Chapter 3. A model combining the bimodal scenario with a flavour symmetry will be presented in Chapter 4.

The lepton number violating neutrinoless double beta decay is an important process in particle physics, since it is connected to the generation of neutrino masses and is able to distinguish the Dirac or Majorana nature of the neutrino. All of the above-mentioned neutrino mass models are in some way connected to $0\nu\beta\beta$, and sterile neutrinos at different mass scales give distinctive contributions to this process. In the ideal scenario, one should be able to pin down the absolute scale of neutrino mass with a combination of $0\nu\beta\beta$ and beta decay experiments, as well as with cosmology. However, since several new physics operators could contribute to $0\nu\beta\beta$ it is difficult to draw any conclusions without a comprehensive study of this and other related phenomenology. For instance, lepton flavour violating decays of charged leptons could help restrict the parameter space of models, since such processes depend on similar quantities to $0\nu\beta\beta$ and are experimentally very well constrained. It is this interplay between experimental signatures that forms a large part of this thesis, an approach necessitated by the large number of parameters in the seesaw model.

In what regards neutrino masses, a certain ambiguity still exists due to the presence of both type I and type II seesaw terms, allowed in the most general case. If one approaches the problem from a "top-down" perspective, it is notable that both mechanisms of neutrino mass generation can be embedded into the left-right symmetric model, a theory in which parity symmetry is restored at high energies, following on naturally from the introduction of right-handed neutrinos. Again, if one chooses the scale of new physics to be TeV, there are a variety of experimental signatures. In particular, the TeV-scale LRSM can be tested at both hadron and linear colliders, as well as in lepton flavour violation (LFV) and $0\nu\beta\beta$ experiments. There are many different diagrams leading to $0\nu\beta\beta$ in the LRSM, all of which are connected to neutrino mass in some way. The theoretically distinct cases of type II and type I seesaw dominance will be studied in Chapter 5. In the former case there is a simple relationship between the left- and right-handed sectors, making comparison rather straightforward. The constraints from LFV, $0\nu\beta\beta$ and colliders can be combined to restrict the allowed parameter space. In the context of type I dominance the previously overlooked so-called "mixed" $\lambda-$ and η-diagrams for $0\nu\beta\beta$, proportional to the active-sterile mixing, will be shown to be non-negligible. This will be backed up with a numerical study of a specific matrix texture, where the various bounds from lepton flavour violating processes are explicitly taken into account. The possible observation of the inverse of the λ-diagram at a linear collider running in electron-electron mode will also be discussed.

In summary, this thesis presents a phenomenological analysis of new physics models with sterile neutrinos at different mass scales. Chapter 2 provides the necessary theoretical background; Chapter 3 summarises the various experimental signatures and hints for sterile neutrinos; $0\nu\beta\beta$ and flavour flux ratios are discussed there in detail. Three different flavour symmetry models accommodating sterile neutrinos are presented in Chapter 4, with further details in Appendices B and C. Chapter 5 is a phenomenological study of lepton number and lepton flavour

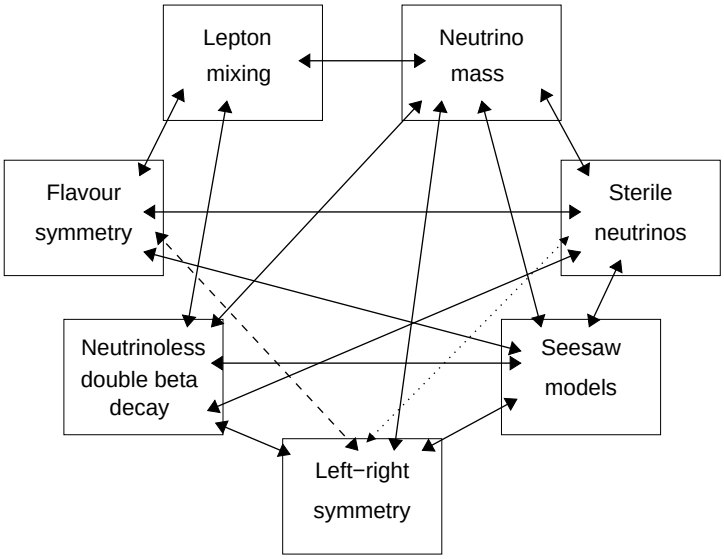

Figure 1.1: Graphic summarising the connections between the main topics of the thesis. The dotted line refers to the fact that the sterile neutrinos in the left-right symmetric model are not fully sterile; the dashed line connects two separate parts – this connection will not be discussed.

violation in the left-right symmetric model, with a focus on $0\nu\beta\beta$ and inverse $0\nu\beta\beta$, and Chapter 6 presents the conclusions. A schematic representation of the most important aspects and their relation to each other can be found in Fig. 1.1.

Parts of this thesis have been published before. Sections 3.2.2, 3.4.2, 4.2, Appendix C and parts of Appendix B are based on Refs. [28, 29], in collaboration with Werner Rodejohann and He Zhang. A summary of those works was presented at the FLASY conference in July 2012, and can be found in the proceedings [30]. Sections 3.4.3, 3.5.2 and 4.3 are based on collaboration with Rabindra Mohapatra and Werner Rodejohann, published in Ref. [31]. Parts of Section 5.6 (and Appendix E) have been published as Ref. [32], with Luis Dorame and Werner Rodejohann.

Chapter 2

Beyond the Standard Model with sterile neutrinos

Active neutrinos participate in weak interactions mediated by gauge bosons, whereas sterile neutrinos have no interactions with SM particles besides through mixing.[1] In order to provide a theoretical background for sterile neutrinos it is appropriate to briefly review the lepton sector of the SM. Extensions to the SM that give neutrinos mass through the introduction of sterile neutrinos will be focussed on here; variants of those models will be used later in the thesis.

2.1 Fermion masses in the Standard Model

Standard Model fermions receive masses via the so-called Higgs mechanism. The Yukawa interaction between the Higgs doublet $\Phi = (\phi^+, \phi^0)^T$ and the SM flavour eigenstate fermion fields is

$$\mathcal{L}_{\rm Y} = -\overline{Q}'_L Y_u \tilde{\Phi} u'_R - \overline{Q}'_L Y_d \Phi d'_R - \overline{L}'_L Y_\ell \Phi \ell'_R + \text{h.c.}\,, \tag{2.1}$$

where $Y_{u,d,\ell}$ are Yukawa coupling matrices, $\tilde{\Phi} = i\sigma_2 \Phi^*$, and the fermions are grouped into left-handed $SU(2)$ doublets and right-handed $SU(2)$ singlets, *viz.*

$$\begin{gathered} L'_{Li} = \begin{pmatrix} \nu'_L \\ \ell'_L \end{pmatrix}_i \sim (\mathbf{2}, -\mathbf{1})\,, \quad Q'_{Li} = \begin{pmatrix} u'_L \\ d'_L \end{pmatrix}_i \sim (\mathbf{2}, \tfrac{\mathbf{1}}{\mathbf{3}})\,, \\ \ell'_{Ri} \sim (\mathbf{1}, -\mathbf{2})\,, \quad u'_{Ri} \sim (\mathbf{1}, \tfrac{\mathbf{4}}{\mathbf{3}})\,, \quad d'_{Ri} \sim (\mathbf{1}, -\tfrac{\mathbf{2}}{\mathbf{3}})\,, \end{gathered} \tag{2.2}$$

where $i = 1, 2, 3$. The subscripts L and R are associated with the projection operators $P_{L,R} = \frac{1}{2}(1 \mp \gamma_5)$ and the numbers in brackets indicate the charges under $SU(2)_L \otimes U(1)_Y$, with electric charge given by $Q = T_L^3 + Y/2$. Note that the SM Lagrangian conserves both total lepton number, i.e., the number of leptons $n_{\ell'}$ minus the number of anti-leptons $n_{\bar{\ell}'}$,

$$L_{\rm tot} \equiv n_{\ell'} - n_{\bar{\ell}'}\,, \tag{2.3}$$

as well as individual family lepton numbers L_e, L_μ and L_τ, where each charged lepton ℓ' (anti-lepton $\bar{\ell}'$) and its associated neutrino ν'_ℓ (anti-neutrino $\bar{\nu}'_\ell$) are assigned $L_\ell = +1$ ($L_{\bar{\ell}} = -1$).

Once the Higgs field develops a non-zero vacuum expectation value (VEV) $\langle\Phi\rangle = (0, v/\sqrt{2})^T$, ($v = 246$ GeV) the electroweak symmetry is broken down to $U(1)_Q$ and the quarks and charged leptons receive mass. The relevant mass matrices are

$$M_u = \frac{v}{\sqrt{2}} Y_u, \quad M_d = \frac{v}{\sqrt{2}} Y_d \quad \text{and} \quad M_\ell = \frac{v}{\sqrt{2}} Y_\ell\,; \tag{2.4}$$

[1] In principle they could interact through Yukawa couplings to the Higgs boson and/or via gravity.

the physical masses are obtained by rotating the fields by unitary matrices, i.e.,

$$u'_{L,R} = V^u_{L,R} u_{L,R}\,, \quad d'_{L,R} = V^d_{L,R} d_{L,R}\,, \quad \text{and} \quad \ell'_{L,R} = V^\ell_{L,R} \ell_{L,R}\,, \tag{2.5}$$

leading to

$$V_L^{u\dagger} Y_u V_R^u = \text{diag}(m_u, m_c, m_t)\,, \quad \text{and} \quad V_L^{d\dagger} Y_d V_R^d = \text{diag}(m_d, m_s, m_b)\,, \tag{2.6}$$

for the quarks and

$$V_L^{\ell\dagger} Y_\ell V_R^\ell = \text{diag}(m_e, m_\mu, m_\tau) \tag{2.7}$$

for the charged leptons.

Since both up and down type quarks have mass, the quarks can mix flavours in the hadronic charged current interaction via the unitary Cabibbo-Kobayashi-Maskawa (CKM) matrix, defined as $V_{\text{CKM}} \equiv V_L^{d\dagger} V_L^u$. The existence of three generations of quarks with different masses is required for CP violation, and the complex phase δ_{CP} of V_{CKM} is the only known source of CP violation in the SM. The elements of the CKM matrix have been measured to relatively high precision [33]: the matrix is close to unity, with small off-diagonal entries. Note that models with four chiral generations are excluded (at $\sim 5\sigma$) by a combination of electroweak precision observables and the latest Higgs results [34].

Despite the remarkable success of the SM it cannot accommodate massive neutrinos. Indeed, from the description given above it is evident that there are no right-handed neutrinos in the model, so that dimension-four neutrino mass terms analogous to those for the quarks and charged leptons in Eq. (2.1) are not allowed. This means that the leptonic charged current is flavour diagonal. However, the established phenomenon of neutrino oscillations (see Section 3.1) requires massive neutrinos and therefore an extension of the SM. Several different models have been proposed and will be reviewed in the following section.

2.2 Neutrino mass in extensions of the Standard Model

Dirac couplings to the Higgs boson [cf. Eq. (2.1)] are responsible for the masses of the quarks and charged leptons in the SM. Augmenting the SM with right-handed neutrinos would allow similar Dirac mass terms for neutrinos, however, this would not explain their smallness. Indeed, light active neutrino masses are commonly believed to be the low-energy manifestation of some new high-energy theory. In that sense, if the SM is treated as an effective low-energy theory one can write down a non-renormalisable dimension-five operator that gives neutrinos a Majorana mass: remarkably there is only one such operator in the SM,

$$\mathcal{L}_{d=5} = \frac{1}{2\Lambda} (\overline{L}'_L \tilde{\Phi}) Y_\nu (\tilde{\Phi}^T L'^{\,c}_L) + \text{h.c.} \xrightarrow{\langle\Phi\rangle = v} \overline{\nu}'_L m_\nu \nu'^{\,c}_L + \text{h.c.}, \tag{2.8}$$

first written down by Weinberg [35]. Here Y_ν is a dimensionless matrix of couplings and Λ is the scale of new physics, which once integrated out leads to a neutrino mass matrix m_ν given by

$$m_\nu = Y_\nu \frac{v^2}{2\Lambda}\,. \tag{2.9}$$

The Weinberg operator violates lepton number L_{tot} by two units, and the smallness of neutrino mass is explained by the large scale Λ. That neutrino mass allows for neutrino mixing can be

seen from the leptonic charged current interaction, which in the diagonal mass basis is given by

$$\mathcal{L}_{CC}^{\text{lep}} = \frac{g}{\sqrt{2}} \overline{\ell_L} \gamma^\mu V_L^{\ell\dagger} V_\nu \nu_L W_{L\mu}^- + \text{h.c.}, \tag{2.10}$$

with V_ν the matrix diagonalising m_ν via $V_\nu^\dagger m_\nu V_\nu^* = \text{diag}(m_1, m_2, m_3)$, V_L^ℓ defined in Eq. (2.7) and m_i $(i = 1, 2, 3)$ the light neutrino masses. The product

$$\tilde{U} = V_L^{\ell\dagger} V_\nu$$

is responsible for neutrino oscillations and is commonly referred to as the Pontecorvo-Maki-Nakagawa-Sakata (PMNS) matrix [36–38], which turns out to be quantitatively very different from the nearly-diagonal CKM matrix. Experimental constraints on the PMNS mixing matrix will be discussed in Sect 3.1. The various UV completions of the operator in Eq. (2.8) are referred to as the seesaw mechanism(s) (see the review in Ref. [39]). The type I and type II seesaw models will be employed later in Chapters 4 and 5 and are reviewed in detail here; other variants are also briefly mentioned.

2.2.1 Type I seesaw model

Lagrangian and mass scales

Extending the particle content in Eq. (2.2) by n_s sterile right-handed neutrinos[2] $\nu'_{Ri} \sim (\mathbf{1}, \mathbf{0})$, of mass M_i $(i = 1, 2, \ldots, n_s)$ results in the Lagrangian

$$\begin{aligned} \mathcal{L}_{\text{type I}} &= \mathcal{L}_{\text{kin}} - \overline{L}'_L Y_\ell \Phi \ell'_R - \overline{L}'_L Y_D \tilde{\Phi} \nu'_R - \frac{1}{2} \overline{\nu'^c_R} M_R \nu'_R + \text{h.c.}, \\ &\xrightarrow{\langle\Phi\rangle = v} \mathcal{L}_{\text{kin}} - \overline{L}'_L M_\ell \ell'_R - \overline{L}'_L M_D \nu'_R - \frac{1}{2} \overline{\nu'^c_R} M_R \nu'_R + \text{h.c.}, \end{aligned} \tag{2.11}$$

which after symmetry breaking leads to an arbitrary $3 \times n_s$ Dirac mass matrix $M_D = v/\sqrt{2} Y_D$ for neutrinos (see Fig. 2.1), i.e., M_D is expected to be at the electroweak scale of $\mathcal{O}(100)$ GeV. The scale of the symmetric $n_s \times n_s$ Majorana mass matrix M_R is as yet unknown and is not protected by any symmetry, since right-handed neutrinos are gauge singlets. One might "naturally" expect M_R to lie at the Planck scale or GUT scale, but this naturalness argument could also be turned around since setting M_R to zero in fact increases the symmetry of the Lagrangian in Eq. (2.11) [40]. Note that the decay width of the Z boson observed at LEP [41] implies that any additional active neutrinos must be at least half as heavy as m_Z, but sterile neutrinos can in principle have any mass scale. The undetermined mass scale M_R is the main subject of this thesis: models which allow for small M_R (light sterile neutrinos) will be focussed on.

In the basis (ν'_L, ν'^c_R) of active and sterile states, the symmetric $(3 + n_s) \times (3 + n_s)$ neutrino mass matrix is

$$M_\nu = \begin{pmatrix} 0 & M_D \\ M_D^T & M_R \end{pmatrix}, \tag{2.12}$$

and the resulting mass spectrum depends on the relative magnitudes of M_D and M_R. There are several distinct possibilities:

[2] Since those fields are gauge singlets, it is possible to add an arbitrary number to the SM without creating anomalies.

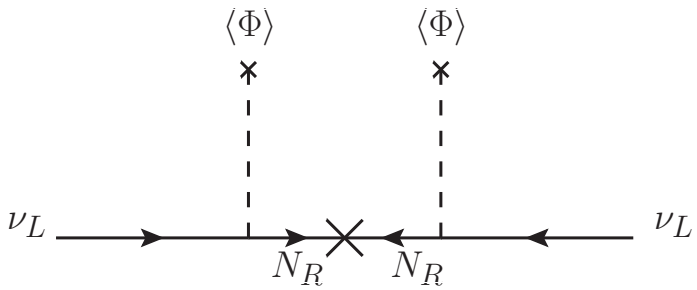

Figure 2.1: Feynman diagram for the type I seesaw model.

- **The seesaw case: $M_D \ll M_R$**
  This is the usual type I seesaw model [3–7], with M_R near the GUT scale [14] of roughly 10^{14} GeV, so that the entries of M_D are much less than the eigenvalues of M_R and the matrix M_ν in Eq. (2.12) can be block-diagonalised [42–44] via

$$W \equiv \begin{pmatrix} V_L^\nu \\ V_R^\nu \end{pmatrix} = \begin{pmatrix} U & S \\ T & V \end{pmatrix} \simeq \begin{pmatrix} \mathbb{1} - \frac{1}{2}BB^\dagger & B \\ -B^\dagger & \mathbb{1} - \frac{1}{2}B^\dagger B \end{pmatrix} \begin{pmatrix} V_\nu & 0 \\ 0 & V_R \end{pmatrix}, \tag{2.13}$$

  to $W^\dagger M_\nu W^* = \text{diag}(m_1, m_2, m_3, M_1, M_2, \ldots, M_{n_s})$, with

$$B = M_D M_R^{-1} + \mathcal{O}\left(M_D^3 (M_R^{-1})^3\right), \tag{2.14}$$

  and $WW^\dagger = \mathbb{1}$. Note that $V_L^\nu = (U \quad S)$ and $V_R^\nu = (T \quad V)$ are unitary 3×6 matrices. This yields the famous seesaw formula,

$$m_\nu = -M_D M_R^{-1} M_D^T + \mathcal{O}\left(\frac{M_D^4}{M_R^3}\right), \tag{2.15}$$

  which means that light neutrinos acquire mass after the heavy neutrinos have been integrated out. Note that at least two sterile neutrinos are required to account for the mass-squared differences of active neutrinos (cf. Section 3.1), and that the higher order term in Eq. (2.15) is negligible in the usual seesaw case. The unitary mixing matrices V_ν and V_R are defined by

$$\begin{aligned} m_\nu &= V_\nu \, \text{diag}(m_1, m_2, m_3) \, V_\nu^T, \\ M_R &= V_R \, \text{diag}(M_1, M_2, \ldots, M_{n_s}) V_R^T, \end{aligned} \tag{2.16}$$

  describing the mixing amongst light active neutrinos and heavy right-handed neutrinos, respectively. The matrix V_R is unphysical, however, so that one can always go to a basis where M_R is diagonal.[3] The mixing between active and sterile neutrinos is negligible, i.e., $M_D/M_R \simeq 10^{-12}$, and can indeed be disregarded in models with $M_R > \mathcal{O}(\text{keV})$, barring cancellations. As one example, in $SO(10)$ models heavy sterile neutrinos are placed into a 16-dimensional representation along with all SM particles, leading to mass relations between the quark and lepton sectors [14, 45].

[3] That is not the case in the LRSM (Section 2.3.2), due to the presence of right-handed currents, or in certain flavour symmetry models where right-handed neutrino transform non-trivially under the flavour group (Section 4.2).

- **The pure Dirac case: $M_R = 0$**
  Although perhaps theoretically unappealing, it is possible to have only the term proportional to Y_D in Eq. (2.11), so that neutrinos are Dirac particles. The smallness of neutrino mass must then be explained by tiny Yukawa couplings of order 10^{-12}, which could be explained by higher-dimensional operators [46] or in theories with large extra dimensions [47]. However in theories without a conserved lepton number the tree level Dirac states will get tiny Majorana corrections at the one-loop level, making neutrinos effectively pseudo-Dirac (see Section 4.3.2).

- **The pseudo-Dirac case: $M_D \gg M_R$**
  Here one cannot use the expansion in Eq. (2.13). As an instructive example, in the case of one generation the approximate (real) mass matrix is

$$m_\nu = m_D \begin{pmatrix} 0 & 1 \\ 1 & \epsilon \end{pmatrix}, \tag{2.17}$$

  which gives the eigenstates $m^\pm = m_D\,(\pm 1 + \epsilon/2)$ and nearly maximal mixing ($\theta \simeq \pi/4$). The resulting neutrino eigenstate is termed pseudo-Dirac [24, 25, 48, 49], with the small term ϵ splitting a Dirac neutrino into two Majorana neutrinos. A variation of the pseudo-Dirac case is the so-called "schizophrenic" or bimodal (BM) scenario, proposed in Ref. [27], where all flavour eigenstates receive comparable contributions from both Dirac and Majorana terms. Interesting signatures result, and will be discussed in the context of $0\nu\beta\beta$ and astrophysical neutrinos in the next chapter; a concrete model will be presented in Section 4.3.

- **The pure Majorana case: $M_D = 0$**
  Here there is no mixing between the active and sterile sectors, so that the sterile neutrino is stable and is an example of fermionic dark matter. This case will not be discussed further here.

- **The intermediate or mixed case: $M_D \simeq M_R$**
  In this phenomenologically interesting case one can expect large mixing between active and sterile states. The block-diagonalisation in Eq. (2.13) is still technically valid as long as $M_D < M_R$, since the remaining off-diagonal terms $BM_D^2/M_R \simeq M_D^3/M_R^2$ are still much smaller than the mass difference between the active and sterile neutrinos. However, the higher order terms in Eqs. (2.13), (2.14) and (2.15) are sizeable and must be taken into account when calculating both active-active and active-sterile neutrino mixing.[4] Those effects are described below, and different ways of achieving this scenario in models will be summarised. In order to keep neutrinos light there are two main alternatives: (*i*) M_R and M_D are both situated at eV or sub-eV scales, so that $m_\nu \simeq M_D^2/M_R \simeq 0.05$ eV, as required;[5] or (*ii*) M_D is at the usual electroweak scale and M_R is only slightly heavier (around the TeV scale), so that cancellations are needed in order to suppress active neutrino masses. Both options will be considered in this thesis: in Chapter 4 a concrete flavour symmetry model with light sterile neutrinos and large mixing is presented and in Chapter 5 the case of cancellations is studied in the LRSM context.

[4] Note that in actual numerical calculations it is often more convenient to simply numerically diagonalise the full neutrino mass matrix M_ν in Eq. (2.12).

[5] There are also various subcases in which the sterile neutrinos are at different mass scales, see Section 2.2.1 and the model in Section 4.2.3.

Neutrino mixing in the type I seesaw model

From Eq. (2.13), the Majorana neutrino mass eigenstates $\nu = \nu_L + \nu_L^c$ and $N = N_R + N_R^c$ are defined by

$$\nu_L' = U\nu_L + SN_R^c\,, \quad \text{and} \quad \nu_R' = T^*\nu_L^c + V^*N_R\,, \tag{2.18}$$

with the $3\times n_s$ ($n_s\times 3$) matrix S (T) describing the mixing between active and sterile neutrino states, see Eq. (2.13). This mixing is the only way to probe the existence of the sterile neutrinos, and will be discussed in more detail in Chapter 3. Note that $UU^\dagger + SS^\dagger = \mathbb{1}$ and $TT^\dagger + VV^\dagger = \mathbb{1}$ [cf. Eq. (2.55)]. The leptonic charged current in Eq. (2.10) now becomes

$$\mathcal{L}_{CC}^{\text{lep}} = \frac{g}{\sqrt{2}}\overline{\ell_L}\gamma^\mu V_L^{\ell\dagger}(U\nu_L + SN_R^c)W_{L\mu}^- + \text{h.c.}\,, \tag{2.19}$$

so that the (non-unitary) PMNS mixing matrix describing the mixing of active neutrino flavours is

$$\tilde{U} \equiv V_L^{\ell\dagger}U \simeq V_L^{\ell\dagger}\left(\mathbb{1} - \tfrac{1}{2}BB^\dagger\right)V_\nu\,, \tag{2.20}$$

whereas the mixing between sterile neutrinos is

$$V = \left(\mathbb{1} - \tfrac{1}{2}B^\dagger B\right)V_R\,. \tag{2.21}$$

In the basis where the charged leptons are diagonal the mixing between the active neutrino ν_α ($\alpha = e,\mu,\tau$) and the sterile neutrino N_{Ri}^c ($i = 1,2,\ldots,n_s$) is given by

$$S_{\alpha i} \equiv [BV_R]_{\alpha i} \simeq \left[M_D(V_R^*\tilde{M}_R^{-1}V_R^\dagger)V_R\right]_{\alpha i} = \frac{[M_DV_R^*]_{\alpha i}}{M_i}\,, \tag{2.22}$$

where $\tilde{M}_R^{-1} = \text{diag}(M_1^{-1}, M_2^{-1}, M_3^{-1})$, illustrating that active-sterile mixing is typically described by a ratio of two scales, M_D and M_R. The mixing between each sterile neutrino N_{Ri}^c and the entire active sector is

$$S_i^2 \equiv \sum_{\alpha=e,\mu,\tau}|S_{\alpha i}|^2\,. \tag{2.23}$$

The seesaw formula in Eq. (2.15) can be re-expressed as

$$[m_\nu]_{\alpha\beta} = -\left[M_DM_R^{-1}M_D^T\right]_{\alpha\beta} = -\sum_{i=1,2,3}S_{\alpha i}S_{\beta i}M_i\,, \tag{2.24}$$

indicating that each sterile neutrino N_{Ri}^c makes a contribution to the active neutrino masses of order $S_i^2M_i$.

A useful parameterisation of the type I seesaw formula in Eq. (2.15) is the orthogonal parameterisation, first written down in Ref. [50], which allows one to express the Dirac mass matrix in terms of a complex orthogonal matrix O, i.e.,

$$M_D = i\,V_\nu\tilde{m}_\nu^{1/2}O\tilde{M}_R^{1/2}V_R^T\,, \quad OO^T = O^TO = \mathbb{1}\,, \tag{2.25}$$

with $\tilde{m}_\nu = \text{diag}(m_1, m_2, m_3)$ and $\tilde{M}_R = \text{diag}(M_1, M_2, M_3)$. In the usual seesaw model this expression can be simplified by setting $V_R = \mathbb{1}$, in the LRSM the full formula should be used. Put into words, Eq. (2.25) is a way of parameterising the unknown right-handed sector via six real (three complex) parameters in O and three real masses in $\tilde{M}_R$, and proves to be convenient for finding Dirac mass matrix textures that reproduce the light neutrino mass and mixing observables for a specific choice of sterile neutrino mass scale(s).

Light sterile neutrinos in type I seesaw models

The seesaw formula in Eq. (2.15) results in light active neutrino masses that are roughly $m_\nu \simeq M_D^2/M_R$, sterile neutrinos of mass M_R and active-sterile mixing of order M_D/M_R [cf. Eq. (2.22)]. Obtaining light sterile neutrinos (M_R) while keeping their mixing with the active sector (M_D/M_R) large essentially requires a mechanism of suppressing both the Dirac and Majorana mass scales, leading to small M_R as well as $M_D \simeq M_R$. If all of the sterile neutrinos are light this is essentially a "mini-seesaw" mechanism [51, 52], where both M_D and M_R are much smaller than usually expected. At the renormalisable level M_D comes from the Yukawa coupling to the electroweak VEV, $v \simeq 246$ GeV; the required suppression could therefore be achieved by introducing higher-dimensional operators. On the other hand, it is also conceivable to have sterile neutrinos at different mass scales, preserving some features of the high-energy seesaw but at the same time having one (or more) sterile neutrino(s) to explain various experimental anomalies (see Chapter 3). The seesaw then proceeds in stages: the heavier particles are integrated out first, followed by the lighter ones, but if $S_i^2 M_i$ is small enough the sterile neutrino N_{Ri}^c is decoupled since it has negligible effect on neutrino masses.

As an explicit example, with three right-handed neutrino mass eigenstates N_{Ri} ($i = 1, 2, 3$) and $M_1 \ll M_{2,3}$, the full 6×6 neutrino mass matrix in the basis where M_R is diagonal is

$$M_\nu^{6\times 6} = \begin{pmatrix} 0 & 0 & 0 & [m_D]_{11} & [M_D]_{11} & [M_D]_{12} \\ 0 & 0 & 0 & [m_D]_{21} & [M_D]_{21} & [M_D]_{22} \\ 0 & 0 & 0 & [m_D]_{31} & [M_D]_{31} & [M_D]_{32} \\ [m_D]_{11} & [m_D]_{21} & [m_D]_{31} & M_1 & 0 & 0 \\ [M_D]_{11} & [M_D]_{21} & [M_D]_{31} & 0 & M_2 & 0 \\ [M_D]_{12} & [M_D]_{22} & [M_D]_{32} & 0 & 0 & M_3 \end{pmatrix}, \tag{2.26}$$

and integrating out N_{R2} and N_{R3} leads to the 4×4 matrix

$$M_\nu^{4\times 4} = \begin{pmatrix} -M_D \tilde{M}_R^{-1} M_D^T & m_D \\ m_D^T & M_1 \end{pmatrix}, \tag{2.27}$$

where $\tilde{M}_R = \mathrm{diag}(M_2, M_3)$. If $M_1 \gg m_D$ one can apply the seesaw formula again to arrive at the light neutrino mass matrix

$$m_\nu \simeq -M_D \tilde{M}_R^{-1} M_D^T - \frac{m_D m_D^T}{M_1}. \tag{2.28}$$

The mixing between N_{R1}^c and the active neutrinos is m_D/M_1, and if it is small enough the second term in Eq. (2.28) is much smaller than the first so that the sterile neutrino N_{R1}^c decouples from the seesaw. There have been several proposals in the literature as to how this can be achieved in a concrete model, some of which are summarised below:

- **Extra dimensional theories**
  By localising one of the right-handed neutrinos on a brane separated from the SM brane it is possible to suppress the mass of N_R due to small wave function overlap. The "split seesaw" model was first proposed in Ref. [53], in the context of keV-scale warm dark matter, and later extended to include an A_4 symmetry in Ref. [54]. The right-handed neutrino mass is suppressed by roughly $e^{-2\tilde{m}k}$, where $\tilde{m}$ is the bulk mass of N_R and k is the distance between the branes.

- **Flavour symmetries**
  Flavour symmetries such as $L_e - L_\mu - L_\tau$ [25, 55] predict one of the sterile neutrino masses to be exactly zero; small breaking of the symmetry (either explicitly or via loop effects) will then generate a small but non-zero mass. This idea has been pursued in the context of keV dark matter [56–58] and could in principle be used for light sterile neutrinos at other mass scales.

- **The Froggatt-Nielsen mechanism**
  The Higgs mechanism described in Section 2.1 above does not predict the masses of fermions: those are governed by the magnitude of the Yukawa couplings $Y_{u,d,\ell}$ in Eq. (2.4). For that reason the FN mechanism [59] attempts to predict fermion mass hierarchies by introducing a new high-energy sector of heavy scalars and fermions charged under a new $U(1)_{\rm FN}$ symmetry. Integrating out the heavy fermions leads to a strong mass suppression, $\lambda \simeq \langle\Theta\rangle/\Lambda$, where Θ is the FN scalar field and Λ the cut-off scale of the theory. This approach is often used to explain the pattern of quark and/or charged lepton masses in flavour symmetry models, in most cases without detailed description of a UV completion.

  An interesting point about the FN mechanism applied to the seesaw model is that the $U(1)_{\rm FN}$ charges of right-handed neutrinos drop out of the seesaw formula [60], so that light neutrino masses are unaffected. This idea will be studied in a concrete A_4 flavour symmetry model in Chapter 4, and it will be shown that several different mass spectra may be achieved. Note that since only right-handed fields may be charged under the $U(1)_{\rm FN}$ symmetry this scenario is incompatible with left-right symmetry, see Ref. [60].

- **Extended seesaw mechanisms**
  In this case one simply extends the type I seesaw model with additional singlet states. In Refs. [61, 62] a concrete model in that regard is described, with three right-handed neutrinos N_{Ri} and another singlet χ_R. The 7×7 neutrino mass matrix in the basis (ν_L, N_R^c, χ_R^c) is

$$M_\nu^{7\times 7} = \begin{pmatrix} 0 & M_D & 0 \\ M_D^T & M_R & M_S^T \\ 0 & M_S & 0 \end{pmatrix}, \tag{2.29}$$

  where certain mass matrix entries are forbidden by flavour symmetries. In the case where $M_R \gg M_S > M_D$, block-diagonalisation leads to the effective neutrino mass matrix

$$M_\nu^{4\times 4} = -\begin{pmatrix} M_D M_R^{-1} M_D^T & M_D M_R^{-1} M_S^T \\ M_S \left(M_R^{-1}\right)^T M_D^T & M_S M_R^{-1} M_S^T \end{pmatrix}, \tag{2.30}$$

  in the basis (ν_L, χ_R^c). With M_S larger than M_D one can apply the seesaw formula again to obtain

$$m_\nu \simeq M_D M_R^{-1} M_S^T \left(M_S M_R^{-1} M_S^T\right)^{-1} M_S \left(M_R^{-1}\right)^T M_D^T - M_D M_R^{-1} M_D^T, \tag{2.31}$$

  for the active neutrinos and

$$m_s \simeq -M_S M_R^{-1} M_S^T, \tag{2.32}$$

  for the sterile ones. The active-sterile neutrino mixing is controlled by

$$B = M_D M_R^{-1} M_S^T \left(M_S M_R^{-1} M_S^T\right)^{-1}. \tag{2.33}$$

Note that the right-hand-side of Eq. (2.31) does not vanish since M_S is a vector rather than a square matrix; if M_S were a square matrix this would lead to an exact cancellation between the two terms of Eq. (2.31).

This model is a "minimal extension" of the type I seesaw in the sense that one needs at least three heavy neutrinos to suppress the masses of both active and sterile neutrinos. Since $M_\nu^{4\times4}$ has rank three, one of the light neutrinos is massless, which means that two of the heavy right-handed neutrinos give rise to two light active neutrinos, while the third one is responsible for the mass of ν_s. The implication is that in order to accommodate more than one light sterile neutrino, more than three heavy neutrinos are required. In addition, this scenario will not be gauge anomaly free if embedded into a GUT, since there is only one generation of χ_R.

2.2.2 Type II seesaw model

It is also possible to generate the dimension-five operator in Eq. (2.8) by the exchange of heavy Higgs triplets of $SU(2)_L$, without introducing right-handed neutrino states: this is known as the type II seesaw [8–13] mechanism, depicted in Fig. 2.2. The triplets can be written in the matrix representation as

$$\Delta \equiv \begin{pmatrix} \delta^+/\sqrt{2} & \delta^{++} \\ \delta^0 & -\delta^+/\sqrt{2} \end{pmatrix} \sim (\mathbf{3},\mathbf{1}), \tag{2.34}$$

and the neutrino mass term comes from the Lagrangian

$$\mathcal{L}_{\text{type II}} = \mathcal{L}_{\text{kin}} + Y_\Delta \overline{L'^c_L} i\sigma_2 \Delta L'_L - V(\Phi,\Delta), \tag{2.35}$$

where Y_Δ is a symmetric matrix of Yukawa couplings and

$$V(\Phi,\Delta) = -m_\Phi^2 \Phi^\dagger\Phi + m_\Delta^2 \text{Tr}\Delta^\dagger\Delta + (\mu_\Delta \Phi^T i\sigma_2 \Delta^* \Phi + \text{h.c.}) + \text{quartic terms}. \tag{2.36}$$

The doublet Φ and the triplet Δ obtain non-zero VEVs $\langle\Phi\rangle = v_\Phi \gg \langle\delta^0\rangle = v_\Delta = \mu_\Delta v_\Phi^2/\sqrt{2}m_\Delta^2$, leading to a seesaw type relation for neutrino mass, *viz.*

$$m_\nu = M_L = \sqrt{2} Y_\Delta v_\Delta = Y_\Delta \frac{\mu_\Delta v_\Phi^2}{m_\Delta^2}\,. \tag{2.37}$$

The electroweak vacuum now becomes

$$v^2 \equiv v_\Phi^2 + 2v_\Delta^2 \simeq (246\text{ GeV})^2\,, \tag{2.38}$$

which leads to a modification of the tree-level ρ parameter,

$$\rho_{\text{tree}} \equiv \frac{m_{W_L}^2}{m_Z^2 \cos^2\theta_W} \simeq 1 - \frac{2v_\Delta^2}{v_\phi^2}\,; \tag{2.39}$$

the experimental constraint $\rho_{\text{exp}} = 1.0008^{+0.0017}_{-0.0007}$ [33] corresponds to the bound $v_\Delta \lesssim 8$ GeV on the triplet VEV. This model has various other experimental signatures [39], some of which will be discussed in the following chapter. Examples include tree-level mediation of LFV processes or collider signatures.

Note that in principle one could have both type I and type II seesaw terms present,

$$m_\nu = M_L - M_D M_R^{-1} M_D^T\,, \tag{2.40}$$

leading to an interplay of the different contributions to neutrino mass: the type I+II seesaw mechanism. Since that scenario is naturally included in the LRSM it will be discussed in more detail in Section 2.3.2 below.

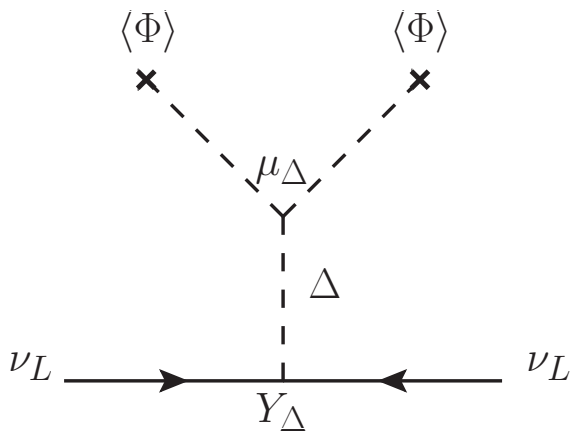

Figure 2.2: Feynman diagram for the type II seesaw model.

2.2.3 Other neutrino mass models

Extended seesaw models

As already discussed above in the context of sterile neutrinos, the usual type I seesaw can be extended in a variety of different ways. In the general case with n right-handed neutrinos N_{Ri} and m additional singlets χ_{Rj} one has a $(3+n+m)\times(3+n+m)$ mass matrix,

$$M_\nu = \begin{pmatrix} M_L & M_D & M_{DS} \\ M_D^T & M_R & M_{RS} \\ M_{DS}^T & M_{RS}^T & M_S \end{pmatrix}, \tag{2.41}$$

in the basis (ν_L, N_R^c, χ_R^c), where the diagonal blocks are symmetric Majorana mass matrices and the off-diagonal ones arbitrary Dirac mass matrices. Setting some of the blocks to zero leads to the double [63, 64], inverse and linear [65, 66] seesaw schemes, depending on the relevant magnitude of the various blocks. As one example, in the inverse seesaw mechanism one sets $M_{DS} = M_R = M_L = 0$ in Eq. (2.41), and with the hierarchy $M_S \ll M_D \ll M_{RS}$ the neutrino mass matrix becomes

$$m_\nu = -M_D (M_{RS}^T)^{-1} M_S M_{RS}^{-1} M_D^T . \tag{2.42}$$

The smallness of neutrino mass now comes directly from M_S, and lepton number is indeed conserved in the limit of $M_S \to 0$.

Type III seesaw

Another alternative is the type III seesaw mechanism [67], in which a set of Majorana $SU(2)_L$ fermion triplets Σ couple with the SM lepton doublets via $f_\Sigma \overline{L}_L \Phi \Sigma$, generating light seesaw neutrino masses. The model is formally analogous to type I seesaw: the neutral components of the fermion triplets play the role of heavy neutrinos. However, since those particles are not gauge singlets they will have interactions with gauge bosons and thus provide various experimental signatures (see Ref. [39] for a review). The type III seesaw model will not be discussed further in this thesis.

Radiative neutrino mass models

It is also conceivable that small neutrino masses are generated at a lower scale, with the required suppression originating from loops. The most famous model in that regard is the two-loop Zee-Babu model [68–70], in which additional singly and doubly charged $SU(2)_L$ singlet scalars h^+ and k^{++} are introduced. Here one expects rich phenomenology, both in $0\nu\beta\beta$ and LFV experiments as well as at colliders [71, 72], illustrating the connection between neutrino mass models and other observables. Note that the Zee-Babu model is just another way of generating the dimension-five operator in Eq. (2.8), at the two-loop level. In fact several authors have performed systematic studies of the Weinberg operator at the one-loop level [73] as well as of loop-induced operators with even higher dimensions [74, 75].

There are also models connecting loop suppressed neutrino mass with dark matter, such as the "scotogenic" model in Ref. [76, 77]. In that case there is usually a discrete Z_2 symmetry introduced to separate the visible and hidden sectors. This idea has also been extended to include an A_4 flavour symmetry in order to predict neutrino mixing patterns [78]. A related model [79, 80] with only one right-handed neutrino and two Higgs doublets exists; in that case the atmospheric and solar mass scales are generated at the tree level and loop level, respectively, providing a natural mass hierarchy that fits the data (see Section 3.1). As in any two Higgs doublet model, the misalignment of charged lepton Yukawa couplings leads to various flavour violating effects.

2.3 The left-right symmetric model

2.3.1 Background and motivation

It is well known that the weak interactions of the SM violate parity maximally, so that left-handed particles participate in gauge interactions with W bosons, while right-handed particles do not. The particle assignments and interactions presented in Eqs. (2.2) and (2.19) show that explicitly. Historically, the $V-A$ structure of the model was inspired by the measurement of the neutrino helicity [81], which implied its masslessness. The LRSM is an attempt to connect those issues: the restoration of parity (the introduction of $V+A$ interactions) is linked to neutrino mass. Put simply, the central idea is that at some high energy scale parity symmetry is restored, so that right-handed fermions are placed on an equal footing with their left-handed counterparts. Right-handed neutrinos are necessary ingredients, and neutrino mass results.

The original model was first constructed by several authors [82–85]. In those papers the parity symmetry is broken by Higgs doublets, which would lead to Dirac neutrino masses. The connection between light (Majorana) neutrino mass and the right-handed scale was made with the introduction of Higgs triplets in Ref. [7], leading to the relation $m_\nu \propto 1/m_{W_R}$, where m_{W_R} is the mass of the right-handed W boson. Massless neutrinos are thus recovered in the limit $m_{W_R} \to \infty$, and the presence of Majorana neutrinos leads to phenomena such as $0\nu\beta\beta$, LFV and collider production of W_R, first discussed in Refs. [11, 86, 87].

As is often the case in new physics models, the requirement of experimental accessibility at the LHC ($m_{W_R} \simeq$ TeV) leads to several undesirable features in the model. This is largely due to the existence of tree level flavour changing neutral currents [88] mediated by the neutral component of the Higgs bi-doublet H_1^0, which place severe constraints on the right-handed scale [89].[6] Explicitly, $m_{H_1^0} > 25$ TeV, so that one has to accept a certain amount of fine-

[6] The physical Higgs state H_1^0 is a linear combination of the ϕ_1^0 and ϕ_2^0 fields, see Eq. (2.46).

tuning in order to keep the right-handed scale low enough for observability.[7] In addition, a detailed analysis [91] of the Higgs sector reveals a "VEV seesaw" relation between parameters at widely differing scales, which will be discussed in Section 2.3.2.

Following Ref. [92], right-handed neutrinos in the LRSM can be termed "weakly sterile", to be distinguished from those introduced in the pure type I seesaw model in Section 2.2.1, which are "fully sterile". The former are charged under a new gauge group but do not feel SM interactions, whereas the latter feel no gauge interactions at all. For that reason the phenomenology of the LRSM is necessarily richer than the type I seesaw model. The features of the type I (heavy neutrinos) and type II (Higgs triplets) seesaw models are all contained within the LRSM. Furthermore, the seesaw terms can be related by the assumption of a discrete symmetry, which allows one to partially solve the type I+II seesaw relation in Eq. (2.40) [93, 94].

The theoretical background for the LRSM is introduced here, and will be applied in the phenomenological analysis of Chapter 5.

2.3.2 Theoretical details

The LRSM is constructed by extending the SM to include the gauge group $SU(2)_R$ (with gauge coupling $g_R \neq g_L$), and right-handed fermions are grouped into doublets under this group. The fermion particle content under $SU(2)_L \otimes SU(2)_R \otimes U(1)_{B-L}$ becomes[8]

$$L'_{Li} = \begin{pmatrix} \nu'_L \\ \ell'_L \end{pmatrix}_i \sim (\mathbf{2}, \mathbf{1}, -\mathbf{1}), \quad L'_{Ri} = \begin{pmatrix} \nu'_L \\ \ell'_L \end{pmatrix}_i \sim (\mathbf{1}, \mathbf{2}, -\mathbf{1}), \tag{2.43}$$

$$Q'_{Li} = \begin{pmatrix} u'_L \\ d'_L \end{pmatrix}_i \sim (\mathbf{2}, \mathbf{1}, \tfrac{\mathbf{1}}{\mathbf{3}}), \quad Q'_{Ri} = \begin{pmatrix} u'_R \\ d'_R \end{pmatrix}_i \sim (\mathbf{1}, \mathbf{2}, \tfrac{\mathbf{1}}{\mathbf{3}}), \tag{2.44}$$

with the electric charge given by $Q = T_L^3 + T_R^3 + \frac{B-L}{2}$ and $i = 1, 2, 3$. The model is similar to the type I seesaw case discussed above, except that the right-handed neutrinos are no longer gauge singlets, so that interactions with new right-handed gauge bosons are possible, and $n_s = 3$ due to the symmetry. An extended Higgs sector is also needed to break the symmetry such that the correct low energy observables are reproduced.

In order to allow Majorana mass terms for neutrinos one introduces the $B-L$ breaking Higgs triplets [7]

$$\Delta_{L,R} \equiv \begin{pmatrix} \delta^+_{L,R}/\sqrt{2} & \delta^{++}_{L,R} \\ \delta^0_{L,R} & -\delta^+_{L,R}/\sqrt{2} \end{pmatrix}, \tag{2.45}$$

with $\Delta_L \sim (\mathbf{3}, \mathbf{1}, \mathbf{2})$ and $\Delta_R \sim (\mathbf{1}, \mathbf{3}, \mathbf{2})$; the electroweak symmetry is broken by the bi-doublet scalar

$$\phi \equiv \begin{pmatrix} \phi^0_1 & \phi^+_2 \\ \phi^-_1 & \phi^0_2 \end{pmatrix} \sim (\mathbf{2}, \mathbf{2}, \mathbf{0}). \tag{2.46}$$

The relevant Lagrangian in the lepton sector is

$$\mathcal{L}_Y^{\text{lep}} = -\overline{L}'_L(f\phi + \tilde{f}\tilde{\phi})L'_R - \overline{L}'^c_L i\sigma_2 \Delta_L h_L L'_L - \overline{L}'^c_R i\sigma_2 \Delta_R h_R L'_R + \text{h.c.}, \tag{2.47}$$

where $\tilde{\phi} \equiv \sigma_2 \phi^* \sigma_2$ and f, g and $h_{L,R}$ are matrices of Yukawa couplings. The additional assumption of a discrete LR symmetry makes the gauge couplings equal ($g_L = g_R \equiv g$), leading to

[7] One way out is to introduced an additional discrete symmetry and another bi-doublet, as presented in Ref. [90].
[8] Notations and conventions are taken from Ref. [95].

relations between the Yukawa coupling matrices in the model. With a discrete parity symmetry it follows that

$$\mathcal{P}:\ L_L \leftrightarrow L_R\,,\quad \phi \leftrightarrow \phi^\dagger\,,\quad \Delta_L \leftrightarrow \Delta_R^*\quad\Rightarrow\quad h_L = h_R^*\,,\quad f = f^\dagger\,,\quad \tilde{f} = \tilde{f}^\dagger\,,$$

with a charge conjugation symmetry one has

$$\mathcal{C}:\ L_L \leftrightarrow (L_R)^c\,,\quad \phi \leftrightarrow \phi^T\,,\quad \Delta_L \leftrightarrow \Delta_R\quad\Rightarrow\quad h_L = h_R\,,\quad f = f^T\,,\quad \tilde{f} = \tilde{f}^T\,.$$

Applying these symmetries simplifies various expressions in the model, as will be discussed later.

Making use of the gauge symmetry to eliminate complex phases, the most general vacuum is

$$\langle\phi\rangle = \begin{pmatrix} \kappa_1/\sqrt{2} & 0 \\ 0 & \kappa_2 e^{i\alpha}/\sqrt{2} \end{pmatrix},\quad \langle\Delta_L\rangle = \begin{pmatrix} 0 & 0 \\ v_L e^{i\theta_L}/\sqrt{2} & 0 \end{pmatrix},\quad \langle\Delta_R\rangle = \begin{pmatrix} 0 & 0 \\ v_R/\sqrt{2} & 0 \end{pmatrix}. \tag{2.48}$$

After spontaneous symmetry breaking, the charged lepton mass matrix is

$$M_\ell = \frac{1}{\sqrt{2}}(\kappa_2 e^{i\alpha} f + \kappa_1 \tilde{f}), \tag{2.49}$$

which can be diagonalised as in Eq. (2.7). With a discrete $\mathcal{P}$ ($\mathcal{C}$) symmetry, M_ℓ becomes Hermitian (symmetric), so that the condition $V_L^\ell = V_R^\ell$ ($V_L^\ell = V_R^{\ell *}$) holds. The neutrino mass Lagrangian contains both type I and type II seesaw terms, *viz.*

$$\mathcal{L}^\nu_{\text{mass}} = -\tfrac{1}{2}\overline{n'_L} M_\nu n'^c_L + \text{h.c.} = -\tfrac{1}{2}\begin{pmatrix} \overline{\nu'_L} & \overline{\nu'^c_R} \end{pmatrix}\begin{pmatrix} M_L & M_D \\ M_D^T & M_R \end{pmatrix}\begin{pmatrix} \nu'^c_L \\ \nu'_R \end{pmatrix} + \text{h.c.}\,, \tag{2.50}$$

with

$$M_D = \frac{1}{\sqrt{2}}(\kappa_1 f + \kappa_2 e^{-i\alpha}\tilde{f})\,,\quad M_L = \sqrt{2} v_L e^{i\theta_L} h_L\,,\quad M_R = \sqrt{2} v_R h_R\,. \tag{2.51}$$

Once again, with a parity (charge conjugation) symmetry the condition $M_D = M_D^\dagger$ ($M_D = M_D^T$) holds. Note that in the most general case the phase θ_L cannot be set to zero. Due to the presence of the so-called "VEV seesaw" relation relating the various VEVs, one expects $x \equiv v_L v_R/\kappa_+^2 = \mathcal{O}(1)$, since x is a function of (order one) couplings in the scalar potential [91]. However, from a purely phenomenological point of view, x can take any value between 0 and 10^{14} [93]. Assuming that $M_L \ll M_D \ll M_R$, the light neutrino mass matrix can be written in terms of the model parameters as

$$m_\nu = M_L - M_D M_R^{-1} M_D^T = \sqrt{2} v_L e^{i\theta_L} h_L - \frac{\kappa_+^2}{\sqrt{2} v_R} h_D h_R^{-1} h_D^T\,, \tag{2.52}$$

where

$$h_D \equiv \frac{1}{\sqrt{2}}\frac{\kappa_1 f + \kappa_2 e^{-i\alpha}\tilde{f}}{\kappa_+}\,,\quad \kappa_+^2 \equiv |\kappa_1|^2 + |\kappa_2|^2\,. \tag{2.53}$$

The 6×6 neutrino mass matrix M_ν in Eq. (2.50) can be diagonalised as in Eqs. (2.13) and (2.16), where in this case the (physical) unitary matrix V_R is the right-handed equivalent of the PMNS matrix. The neutrino mass eigenstates $n = n_L + n_L^c = n^c$ are defined by

$$\begin{aligned} n'_L &= \begin{pmatrix} \nu'_L \\ \nu'^c_R \end{pmatrix} = W n_L = \begin{pmatrix} U & S \\ T & V \end{pmatrix}\begin{pmatrix} \nu_L \\ N_R^c \end{pmatrix}, \\ n'^c_L &= \begin{pmatrix} \nu'^c_L \\ \nu'_R \end{pmatrix} = W^* n_L^c = \begin{pmatrix} U^* & S^* \\ T^* & V^* \end{pmatrix}\begin{pmatrix} \nu_L^c \\ N_R \end{pmatrix}, \end{aligned} \tag{2.54}$$

as before, and the unitarity of W leads to the useful relations

$$\begin{aligned} V_L^\nu V_L^{\nu\dagger} = UU^\dagger + SS^\dagger = \mathbb{1} = V_R^\nu V_R^{\nu\dagger} = TT^\dagger + VV^\dagger\,, \\ V_L^\nu V_R^{\nu\dagger} = UT^\dagger + SV^\dagger = 0\,. \end{aligned} \tag{2.55}$$

In the LRSM there is also a right-handed charged current interaction, so that Eq. (2.19) is extended to

$$\mathcal{L}_{CC}^{\text{lep}} = \frac{g}{\sqrt{2}}\left[\overline{\ell'}\gamma^\mu P_L \nu' W_{L\mu}^- + \overline{\ell'}\gamma^\mu P_R \nu' W_{R\mu}^-\right] + \text{h.c.}, \tag{2.56}$$

in the flavour basis, where

$$\begin{pmatrix} W_L^\pm \\ W_R^\pm \end{pmatrix} = \begin{pmatrix} \cos\xi & \sin\xi\, e^{i\alpha} \\ -\sin\xi\, e^{-i\alpha} & \cos\xi \end{pmatrix} \begin{pmatrix} W_1^\pm \\ W_2^\pm \end{pmatrix} \tag{2.57}$$

characterises the mixing between left- and right-handed gauge bosons, with

$$\tan 2\xi = -\frac{2\kappa_1\kappa_2}{v_R^2 - v_L^2}\,. \tag{2.58}$$

With negligible mixing the gauge boson masses become

$$m_{W_L} \simeq m_{W_1} \simeq \frac{g}{2}\kappa_+ \quad \text{and} \quad m_{W_R} \simeq m_{W_2} \simeq \frac{g}{\sqrt{2}}v_R\,, \tag{2.59}$$

and assuming that[9] $\kappa_2 < \kappa_1$, it follows that

$$\xi \simeq -\kappa_1\kappa_2/v_R^2 \simeq -2\frac{\kappa_2}{\kappa_1}\left(\frac{m_{W_L}}{m_{W_R}}\right)^2, \tag{2.60}$$

so that the mixing angle ξ is at most the square of the ratio of left and right scales $(m_{W_L}/m_{W_R})^2$. Although the experimental limit is $\xi < 10^{-2}$ [33], for $m_{W_R} = \mathcal{O}(\text{TeV})$ one has $\xi \lesssim 10^{-3}$ [96], and supernova bounds for right-handed neutrinos lighter than 1 MeV are even more stringent ($\xi < 3\times 10^{-5}$) [96, 97]. For small ξ the charged current in the mass basis becomes

$$\mathcal{L}_{CC}^{\text{lep}} = \frac{g}{\sqrt{2}}\left[\overline{\ell_L}\gamma^\mu K_L n_L (W_{1\mu}^- + \xi e^{i\alpha} W_{2\mu}^-) + \overline{\ell_R}\gamma^\mu K_R n_L^c(-\xi e^{-i\alpha}W_{1\mu}^- + W_{2\mu}^-)\right] + \text{h.c.}, \tag{2.61}$$

an equation that will be used extensively in the phenomenological analysis of Chapter 5. Here K_L and K_R are 3×6 mixing matrices

$$K_L \equiv V_L^{\ell\dagger} V_L^\nu\,, \quad \text{and} \quad K_R \equiv V_R^{\ell\dagger} V_R^{\nu *}\,, \tag{2.62}$$

with [using Eq. (2.55)] $K_L K_L^\dagger = K_R K_R^\dagger = \mathbb{1}$ and $K_L K_R^T = 0$. The standard neutrino mixing matrix is just the left half of K_L, i.e., $\tilde{U} = V_L^{\ell\dagger} U$ [cf. Eq (2.20)].

There is also a new neutral gauge boson, Z', which mixes with the standard model Z boson. The mass eigenstates $Z_{1,2}$ have the masses

$$m_{Z_1} \simeq \frac{g}{2\cos\theta_W}\kappa_+ \simeq \frac{m_{W_1}}{\cos\theta_W} \quad \text{and} \quad m_{Z_2} \simeq \frac{g\cos\theta_W}{\sqrt{\cos 2\theta_W}}v_R \simeq \sqrt{\frac{2\cos^2\theta_W}{\cos 2\theta_W}}\, m_{W_2}\,, \tag{2.63}$$

where $g = e/\sin\theta_W$ and the $U(1)$ coupling constant is $g' \equiv e/\sqrt{\cos 2\theta_W}$. The mixing is also of order $(m_{W_L}/m_{W_R})^2$, i.e.,

$$\phi = -\frac{1}{2}\sin^{-1}\frac{g^2\kappa_+^2\sqrt{\cos\,2\theta_W}}{2c_W^2(m_{Z_2}^2 - m_{Z_1}^2)} \simeq -\frac{m_{Z_1}^2\sqrt{\cos\,2\theta_W}}{m_{Z_2}^2 - m_{Z_1}^2} \simeq -\sqrt{\cos\,2\theta_W}\left(\frac{m_{Z_1}}{m_{Z_2}}\right)^2. \tag{2.64}$$

Eqs. (2.59) and (2.63) imply that $m_{Z_2} \simeq 1.7 m_{W_2}$. The current limits [33, 98] on the neutral gauge boson parameters are $m_{Z'} > 1.162$ TeV and $|\phi| < 1.2\times 10^{-3}$.

[9] That can be justified by assuming no cancellations in generating quark masses [89].

2.4 Summary

The main message of this chapter is that the SM needs to be extended to accommodate massive neutrinos, with a variety of existing models having been built for this purpose. New particles introduced will invariably produce new experimental signatures, unless the scale of new physics is very high and/or some symmetry forbids couplings to the active sector; the nature of those signatures depends on whether the particles are gauge singlets or not. Models with "light" sterile neutrinos have been focussed on, both as a prelude to the discussions of the next two chapters and because they are in a sense the only "testable" form of sterile neutrinos. Indeed, the only real phenomenological implication of extremely heavy sterile neutrinos is the generation of the baryon asymmetry of the universe via leptogenesis (cf. Sect 3.6.3). The LRSM, an extended gauge theory that naturally accommodates right-handed neutrinos, was also introduced. The theoretical details outlined here support the analysis in Chapter 5. The phenomenology of sterile neutrinos will be presented in the following chapter, with a view to providing a solid motivation for the model building efforts of Chapter 4.

Chapter 3

Phenomenology of sterile neutrinos

Sterile neutrinos at different mass scales have various phenomenological consequences, or, put another way, can be used to explain various observed phenomena, depending on one's viewpoint. The observations serve as both motivations and tests for theoretical models. After an introduction to oscillations amongst active neutrinos this chapter provides a systematic summary of the different signatures of sterile neutrinos, with a brief discussion of the experimental situation in each case. The discussion merges a review of the literature with the original research from Refs. [31, 99], found in Sections 3.2, 3.3, 3.4 and 3.5.2. For a comprehensive review of this topic see Ref. [21].

3.1 Oscillations of active neutrinos

Neutrino oscillations provide proof that neutrinos are massive (see the review in Ref. [33]), so that neutrino flavour eigenstates can be written as a linear combination of mass eigenstates, *viz.*[1]

$$\nu'_\ell = \sum_{i=1}^{3} \tilde{U}_{\ell i} \nu_i \,, \tag{3.1}$$

with $\ell = e, \mu, \tau$. In the standard three-neutrino framework $\tilde{U}$ is a 3×3 unitary matrix [see Eq. (2.20)], and the phenomenon of neutrino oscillations also means that lepton flavour is violated in the charged current interaction in Eq. (2.10). When neutrinos propagate in a vacuum, the probability of a neutrino of initial flavour α oscillating into a neutrino of flavour β at the baseline L is given by

$$\begin{aligned} P_{\nu_\alpha \to \nu_\beta} \equiv P_{\alpha\beta} = \delta_{\alpha\beta} - 4 \sum_{i>j} \mathrm{Re}\left(\tilde{U}^*_{\alpha i} \tilde{U}_{\alpha j} \tilde{U}_{\beta i} \tilde{U}^*_{\beta j}\right) \sin^2\left(\frac{\Delta m^2_{ij} L}{4E}\right) \\ + 2 \sum_{i>j} \mathrm{Im}\left(\tilde{U}^*_{\alpha i} \tilde{U}_{\alpha j} \tilde{U}_{\beta i} \tilde{U}^*_{\beta j}\right) \sin\left(\frac{\Delta m^2_{ij} L}{2E}\right) , \end{aligned} \tag{3.2}$$

where $\Delta m^2_{ij} \equiv m^2_i - m^2_j$; the oscillation probability for anti-neutrinos can be simply obtained from Eq. (3.2) by the replacement $\tilde{U} \to \tilde{U}^*$. In the standard parameterisation [33]

$$\tilde{U} = \begin{pmatrix} 1 & 0 & 0 \\ 0 & c_{23} & s_{23} \\ 0 & -s_{23} & c_{23} \end{pmatrix} \begin{pmatrix} c_{13} & 0 & s_{13} e^{-i\delta} \\ 0 & 1 & 0 \\ -s_{13} e^{i\delta} & 0 & c_{13} \end{pmatrix} \begin{pmatrix} c_{12} & s_{12} & 0 \\ -s_{12} & c_{12} & 0 \\ 0 & 0 & 1 \end{pmatrix} \begin{pmatrix} 1 & 0 & 0 \\ 0 & e^{i\alpha/2} & 0 \\ 0 & 0 & e^{i(\beta/2+\delta)} \end{pmatrix} , \tag{3.3}$$

[1] Active neutrinos are left-handed; the subscript L is dropped for convenience.

where $c_{ij} \equiv \cos\theta_{ij}$, $s_{ij} \equiv \sin\theta_{ij}$ and θ_{ij} $(0 \leq \theta_{ij} \leq \pi/2)$ are the three mixing angles measured in oscillation experiments, δ is the CP-violating Dirac phase and α and β are Majorana phases, with $0 \leq \delta, \alpha, \beta \leq 2\pi$. The diagonal phase matrix has been defined so that only α and β show up in $0\nu\beta\beta$, see Eq. (3.25). The experimental status of each of the six parameters in $\tilde{U}$ will be discussed below.

The factorised form of $\tilde{U}$ is useful for interpreting the data and reflects the fact that it is sufficient to consider two-neutrino mixing in most practical situations. The first matrix contains the parameter θ_{23}, which together with the mass-squared difference $\Delta m^2_{\rm A}$ has been measured in experiments with atmospheric neutrinos (such as Super-Kamiokande [100][2]) and in long baseline accelerator experiments (such as K2K [101], T2K [102, 103] and MINOS [104]). The second matrix depends on θ_{13}, which is accessible to short baseline reactor experiments and has recently been shown to be non-zero by the Daya Bay [105] and RENO [106] experiments, following on from the earlier indications in the Double Chooz [107] reactor experiment and the T2K [107] and MINOS [108] accelerator experiments. The third matrix contains the solar mixing angle θ_{12}, which along with $\Delta m^2_{\rm S}$ is measured in solar neutrino experiments such as SNO [109][3] and Borexino [110, 111], as well as the long baseline reactor experiment KamLAND [112].

The mass eigenstates have been labelled by convention such that

$$\Delta m^2_{\rm S} \equiv \Delta m^2_{21} \quad \text{and} \quad \Delta m^2_{\rm A} \equiv |\Delta m^2_{31}|, \tag{3.4}$$

and the three independent mass-squared differences obey the relations

$$\Delta m^2_{21} \ll |\Delta m^2_{31}| \simeq |\Delta m^2_{32}|\,. \tag{3.5}$$

Although the oscillation term in Eq. (3.2) is insensitive to the sign of Δm^2_{ij}, matter effects (the MSW [113, 114] effect) on the $1-2$ mixing in the Sun have determined Δm^2_{21} to be positive-definite, which means that the electron neutrino ν_e is mostly made up of the lightest mass eigenstate ν_1. The sign of Δm^2_{31} is not known: there are two possible arrangements for the neutrino mass ordering, shown in Fig. 3.1. In the "normal" ordering (NO), the smallest mass-squared difference is between the two lightest eigenstates so that a natural neutrino mass hierarchy can be realised, whereas in the "inverted" ordering (IO), the smallest mass-squared difference is between the two heaviest and almost degenerate eigenstates.

There are various proposals for determining the mass ordering in current and future oscillation experiments. Since matter effects make ν_e heavier (and θ_{13} is now known to be non-zero) one can study $1-3$ mixing for neutrinos and anti-neutrinos, which will show opposite behaviour for the different mass orderings. This is the same principle used to determined the sign of Δm^2_{21} in the Sun. Some ideas include studying the atmospheric neutrino flux with magnetised (INO [116]) or large scale (PINGU [117]) detectors,[4] or using Earth matter effects with long-baseline (LBL) accelerator experiments such as NOνA [118], LBNE [119] or Fermilab–PINGU [120]. Another method would be to compare electron neutrino and anti-neutrino spectra from supernovae [121], but here the differences are very small and a recent study has shown that they will be difficult to observe with current detectors [122]. Spectral analysis of reactor data could also be used, and although limited by experimental sensitivity may indeed be possible with detectors at medium baselines ($L \simeq 50$ km) [123, 124]. Note that neutrino oscillations only yield information on

[2] This was the initial discovery of neutrino oscillations in 1998.

[3] Comparison of charged and neutral current data from the SNO experiment provided definitive proof of solar neutrino oscillations.

[4] The influence of neutrino mass ordering on active-sterile oscillations of atmospheric neutrinos will be discussed in Section 3.2.

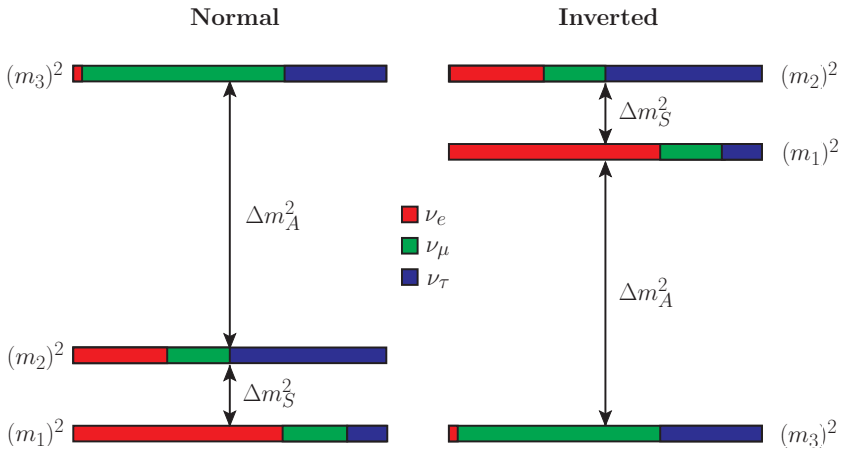

Figure 3.1: The two possible active neutrino mass orderings, adapted from Ref. [115] using current data (Table 3.1) and $\delta = 0$. The colour coding indicates the fraction $|\tilde{U}_{\ell i}|$ of each distinct flavour ν_ℓ, $\ell = e, \mu, \tau$ contained in each mass eigenstate ν_i, $i = 1, 2, 3$.

the mass-squared differences, not the absolute masses themselves. Instead, information on the masses may be obtained from beta decay and neutrinoless double beta decay, as well as from cosmological considerations; all of those probes could also shed light on the neutrino mass ordering, and will be discussed in Sections 3.3, 3.4 and 3.6 below.

There are several global fits [23, 125, 126] to the mass and mixing parameters from neutrino oscillation experiments: the latest best-fit and 3σ ranges are shown in Table 3.1, taken from Ref. [23]. Using the best-fit values for the mixing angles in the normal ordering case, the magnitude of the PMNS matrix is

$$|\tilde{U}|_{\delta=0} \simeq \begin{pmatrix} 0.814 & 0.559 & 0.157 \\ 0.453 & 0.444 & 0.773 \\ 0.362 & 0.701 & 0.614 \end{pmatrix}, \quad |\tilde{U}|_{\delta=0.80\pi} \simeq \begin{pmatrix} 0.814 & 0.559 & 0.157 \\ 0.276 & 0.571 & 0.773 \\ 0.510 & 0.602 & 0.614 \end{pmatrix}, \tag{3.6}$$

for $\delta = 0$ and the best-fit value of $\delta = 0.80\pi$ (the Majorana phases have been set to zero). Explanation of the neutrino mixing pattern, $\tilde{U}$, which is completely different to the small mixing in the quark sector, has prompted research into flavour symmetry models (cf. Section 4.1).

The CP-violating phase δ is only weakly constrained by global fits, but the prospects of its measurement have significantly improved now that $\theta_{13} \neq 0$ (see Ref. [127] for a review). One approach is to compare electron neutrino and anti-neutrino appearance probabilities using LBL experiments such as T2K and NOνA. Due to parameter degeneracies it may also be necessary to examine both the first and the second oscillation maxima, either with two detectors at different baselines, such as at T2KK [128], or with a single detector that measures successive oscillation peaks over a wide energy range [129]. An alternative approach is to use cyclotron stopped-pion decay-at-rest neutrino sources situated at different distances from a single detector, as in the DAEδALUS [130, 131] experiment. However, one of the cleanest ways to measure δ would be at a neutrino factory [132, 133], where the energy spectrum of muon neutrinos is more accurately known.

Note that the Majorana phases α and β do not affect the neutrino oscillation probability; they have physical consequences only if neutrinos are Majorana particles, influencing the amplitude for $0\nu\beta\beta$, discussed in Section 3.4 below.

Table 3.1: Best fit and 3σ ranges of neutrino oscillation parameters, taken from Ref. [23]. For Δm^2_{31}, $\sin^2\theta_{23}$, $\sin^2\theta_{13}$, and δ the upper (lower) row corresponds to normal (inverted) ordering. The number in brackets for $\sin^2\theta_{23}$ is a local minimum in the first octant.

parameter	best fit	3σ range
Δm^2_{21} [10^{-5} eV]	7.62	7.12–8.20
$\lvert\Delta m^2_{31}\rvert$ [10^{-3} eV]	2.55 2.43	2.31–2.74 2.21–2.64
$\sin^2\theta_{12}$	0.320	0.27–0.37
$\sin^2\theta_{23}$	0.613 (0.427) 0.600	0.36–0.68 0.37–0.67
$\sin^2\theta_{13}$	0.0246 0.0250	0.017–0.033
δ	0.80π -0.03π	0–2π

3.2 Sterile neutrinos in oscillation experiments

3.2.1 Sterile neutrino mixing and mass spectra

It is instructive to study sterile neutrino mixing from a purely phenomenological point of view, without introducing a specific theoretical model. In the presence of $n_s = n-3$ sterile neutrinos, the $n \times n$ neutrino mass matrix m_ν can be diagonalised by an $n \times n$ unitary matrix $\tilde{U}$; the linear combination in Eq. (3.1) now becomes

$$\nu'_\ell = \sum_{i=1}^{n} \tilde{U}_{\ell i} \nu_i \,, \tag{3.7}$$

where $\ell = e, \mu, \tau, s_1, s_2, \ldots, s_{n-3}$. In general, for n massive families with $0 \neq n_s = n-3$ massive sterile neutrinos, there are $n-1 = n_s+2$ Majorana phases, $3(n-2) = 3(n_s+1)$ mixing angles and $2n-5 = 2n_s+1$ Dirac phases. The number of angles and Dirac phases is less than the naive $\frac{1}{2}n(n-1)$ angles and $\frac{1}{2}(n-1)(n-2)$ phases, because the $\frac{1}{2}n_s(n_s-1)$ rotations between sterile states are unphysical.[5] As an example, for $n_s = 1$ one can parameterise $\tilde{U}$ as [cf. Eq. (3.3)]

$$\tilde{U} = R_{34}\tilde{R}_{24}\tilde{R}_{14}R_{23}\tilde{R}_{13}R_{12}\tilde{P} \,, \tag{3.8}$$

where the matrices R_{ij} are rotations in ij space, i.e.,

$$R_{34} = \begin{pmatrix} 1 & 0 & 0 & 0 \\ 0 & 1 & 0 & 0 \\ 0 & 0 & c_{34} & s_{34} \\ 0 & 0 & -s_{34} & c_{34} \end{pmatrix} \quad \text{or} \quad \tilde{R}_{14} = \begin{pmatrix} c_{14} & 0 & 0 & s_{14}e^{-i\delta_{14}} \\ 0 & 1 & 0 & 0 \\ 0 & 0 & 1 & 0 \\ -s_{14}e^{i\delta_{14}} & 0 & 0 & c_{14} \end{pmatrix} . \tag{3.9}$$

The diagonal $\tilde{P}$ matrix contains three Majorana phases α, β and γ, *viz.*

$$\tilde{P} = \mathrm{diag}\left(1, e^{i\alpha/2}, e^{i(\beta/2+\delta_{13})}, e^{i(\gamma/2+\delta_{14})}\right) , \tag{3.10}$$

[5] See the discussion below Eq. (2.16), in the seesaw model context.

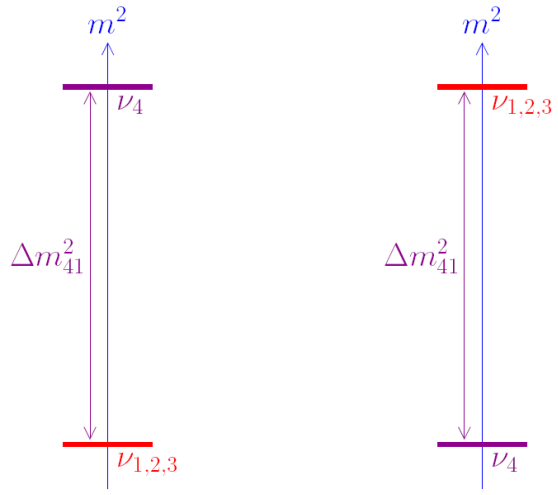

Figure 3.2: (From Ref. [134].) Mass spectra of sterile neutrino schemes with one sterile neutrino: the 3+1 (left) and 1+3 (right) scenarios. In each case the active neutrinos can have normal or inverted mass ordering, and the inequalities $|\Delta m^2_{21}| \ll |\Delta m^2_{31}| \ll |\Delta m^2_{41}|$ hold.

and there are in total three Dirac CP-violating phases δ_{ij}, where again $\tilde{P}$ has been defined so that the effective mass in $0\nu\beta\beta$ can be written in terms of Majorana phases only (see Section 3.4). The probability formula in Eq. (3.2) now contains additional oscillation terms proportional to Δm^2_{4i} $(i = 1, 2, 3)$. In the same vein, one can parameterise the mixing matrix for two sterile neutrinos as

$$\tilde{U} = \tilde{R}_{25} R_{34} R_{25} \tilde{R}_{24} R_{23} \tilde{R}_{15} \tilde{R}_{14} \tilde{R}_{13} R_{12} \tilde{P}\,, \tag{3.11}$$

where $\tilde{P} = \mathrm{diag}(1, e^{i\alpha/2}, e^{i(\beta/2+\delta_{13})}, e^{i(\gamma/2+\delta_{14})}, e^{i(\phi/2+\delta_{15})})$; the additional mass-squared differences are Δm^2_{4i}, Δm^2_{5i} $(i = 1, 2, 3)$ and Δm^2_{54}.

As discussed above, the active neutrinos responsible for solar and atmospheric oscillations can be normally $(m_1 < m_2 < m_3)$ or inversely $(m_3 < m_1 < m_2)$ ordered. The mass-squared differences associated with sterile neutrinos (see Section 3.2.3) are generally much larger[6] than the ones between active mass eigenstates: the sterile states are thus separated in mass from the active ones and can be either much heavier or much lighter than their active counterparts. In the case of one sterile neutrino of mass m_s there are in total four possible mass orderings, divided into the $3 + 1$ case with $m_{1,2,3} \ll m_s$ and the $1 + 3$ case with $m_s \ll m_{1,2,3}$, where the active neutrinos can have normal or inverted ordering in each case. Figure 3.2 shows this distinct difference in the normal ordering case; the phenomenological consequences of different spectra will be presented below.

In the case of two sterile neutrinos with masses m_{s_1} and m_{s_2}, there are three classes of mass spectra: $m_{1,2,3} \ll m_{s_1}, m_{s_2}$ (3+2), $m_{s_1}, m_{s_2} \ll m_{1,2,3}$ (2+3) and $m_{s_1} \ll m_{1,2,3} \ll m_{s_2}$ (1+3+1). In the latter case [135] the active states are sandwiched between the sterile ones, a fact not taken into account in some global fits [136]. Although current oscillation data cannot distinguish 3+1 from 1+3, or 3+2 from 2+3 scenarios, they are sensitive to 1+3+1 vs. 3+2/2+3, as will be discussed below. Note that there are two possible permutations of the mass spectrum in the 1+3+1 case: the sterile neutrino separated from the active ones by a larger mass splitting could

[6] Except in the pseudo-Dirac case.

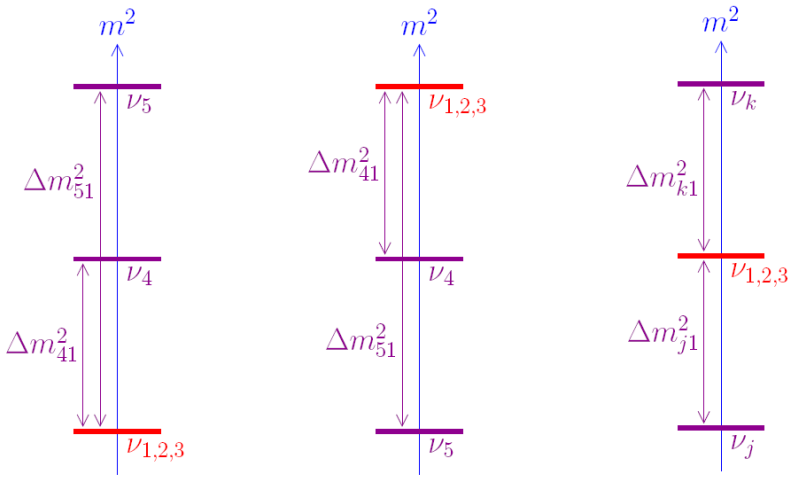

Figure 3.3: (From Ref. [134].) Mass spectra of sterile neutrino schemes with two sterile neutrinos: the 3+2 (left), 2+3 (middle) and 1+3+1 (right) scenarios. In each case the active neutrinos can have normal or inverted mass ordering, and the inequalities $|\Delta m^2_{21}| \ll |\Delta m^2_{31}| \ll |\Delta m^2_{41}| < |\Delta m^2_{51}|$ hold. In the 1+3+1 case the indices k and j are chosen such that $|\Delta m^2_{41}| < |\Delta m^2_{51}|$.

be either the lighter or the heavier of the two sterile states, corresponding to $j = 5$, $k = 4$ or $j = 4$, $k = 5$ in Fig. 3.3, respectively. The individual masses $m_{1,2,3,4,5}$ expressed in terms of the mass-squared differences $\Delta m^2_{\rm S}$, $\Delta m^2_{\rm A}$, Δm^2_{41} and Δm^2_{51} can be found in Ref. [135], where the generalisation to three sterile neutrinos (with sixteen possible mass orderings) is also discussed. It turns out that the 3+2 scenarios are more attractive than the others, due to the cosmological limit on the sum of neutrino masses (see Section 3.6.1).

3.2.2 Sterile neutrino oscillations at short baselines

The presence of sterile neutrinos modifies the oscillation probabilities in appearance and disappearance experiments. As alluded to before, in most experimental situations the full expression in Eq. (3.2) can usually be approximated by a two-neutrino version. In reactor anti-neutrino experiments such as Double Chooz or Daya Bay, the detector is typically located at a baseline of around 1 km, while the average anti-neutrino energy is $\langle E \rangle \simeq 4$ MeV. One can thus estimate that $L/E = \mathcal{O}(10^3)$ eV^{-2}, so that the oscillation term containing Δm^2_{21} can be safely neglected. Since the oscillation frequency related to the mass-squared difference Δ_{4i} (Δm^2_{5i}) is much smaller than the baseline, those terms simply generate a fast oscillation that can be averaged out. In that case the anti-neutrino survival probability approximates to

$$\begin{aligned} P_{\overline{\nu}_e \to \overline{\nu}_e} &\simeq 1 - 2|\tilde{U}_{e4}|^2 - 4|\tilde{U}_{e3}|^2 \sin^2\left(\frac{\Delta m^2_{31} L}{4E}\right) \\ &= 1 - 2\sin^2\theta_{14} - \cos^4\theta_{14} \sin^2(2\theta_{13}) \sin^2\left(\frac{\Delta m^2_{31} L}{4E}\right) , \end{aligned} \tag{3.12}$$

for the case of one sterile neutrino (3+1 and 1+3), and

$$P_{\overline{\nu}_e \to \overline{\nu}_e} \simeq 1 - 2|\tilde{U}_{e4}|^2 - 2|\tilde{U}_{e5}|^2 - 4|\tilde{U}_{e3}|^2 \sin^2\left(\frac{\Delta m^2_{31} L}{4E}\right) , \tag{3.13}$$

for the case of two sterile neutrinos (3+2, 2+3 and 1+3+1): the presence of sterile neutrino(s) thus simply reduces the total neutrino flux seen in reactor neutrino experiments. At even shorter baselines ($L = \mathcal{O}(10)$ m) the Δm^2_{31} contribution can be neglected whereas the oscillation due to Δm^2_{41} is observable, so that the survival probability becomes

$$P_{\overline{\nu}_e \to \overline{\nu}_e} \simeq 1 - 4|\tilde{U}_{e4}|^2 \sin^2\left(\frac{\Delta m^2_{41} L}{4E}\right) = 1 - \sin^2(2\theta_{14}) \sin^2\left(\frac{\Delta m^2_{41} L}{4E}\right) , \tag{3.14}$$

for the 3+1/1+3 case, and

$$P_{\overline{\nu}_e \to \overline{\nu}_e} \simeq 1 - 4|\tilde{U}_{e4}|^2 \sin^2\left(\frac{\Delta m^2_{41} L}{4E}\right) - 4|\tilde{U}_{e5}|^2 \sin^2\left(\frac{\Delta m^2_{51} L}{4E}\right) , \tag{3.15}$$

for the 3+2, 2+3 and 1+3+1 cases. Here the sterile mass splittings mediate very-short-baseline oscillations, which will be discussed in the following section. Note that the oscillation term proportional to $\sin^2\left(\frac{\Delta m^2_{54} L}{4E}\right)$ is suppressed by a factor $|\tilde{U}_{e4}\tilde{U}_{e5}|^2$, and can hence be neglected. Here it is still not possible to distinguish 3+2/2+3 from 1+3+1 scenarios.

Disappearance experiments such as LSND and MiniBooNE (see Section 3.2.3) are characterised by $L/E = \mathcal{O}(1)$ eV^{-2}, and again the oscillation term related to Δm^2_{31} can be ignored. In that case the oscillation probability is given by

$$P_{\overline{\nu}_\mu \to \overline{\nu}_e} \simeq 4|\tilde{U}_{e4}|^2 |\tilde{U}_{\mu 4}|^2 \sin^2\left(\frac{\Delta m^2_{41} L}{4E}\right) , \tag{3.16}$$

for the 3+1/1+3 case, and

$$\begin{aligned} P_{\overline{\nu}_\mu \to \overline{\nu}_e} \simeq\ & 4|\tilde{U}_{e4}|^2 |\tilde{U}_{\mu 4}|^2 \sin^2\left(\frac{\Delta m^2_{41} L}{4E}\right) + 4|\tilde{U}_{e5}|^2 |\tilde{U}_{\mu 5}|^2 \sin^2\left(\frac{\Delta m^2_{51} L}{4E}\right) \\ +\ & 8|\tilde{U}_{e4}\tilde{U}_{\mu 4}\tilde{U}_{e5}\tilde{U}_{\mu 5}| \sin\left(\frac{\Delta m^2_{41} L}{4E}\right) \sin\left(\frac{\Delta m^2_{51} L}{4E}\right) \cos\left(\frac{\Delta m^2_{54} L}{4E} + \tilde{\delta}\right) , \end{aligned} \tag{3.17}$$

for the five neutrino case with $\tilde{\delta} \equiv \arg\left(\tilde{U}^*_{e4}\tilde{U}_{\mu 4}\tilde{U}_{e5}\tilde{U}^*_{\mu 5}\right) \simeq \delta_{14} - \delta_{24} - \delta_{15}$, where the phase is given in the explicit parameterisation of Eq. (3.11). The additional CP-violating phase in Eq. (3.17) leads to a CP asymmetry in the transition probability between the neutrino and anti-neutrino modes. In addition, the last term of Eq. (3.17) shows a distinction between the 3+2/2+3 and 1+3+1 cases due to the presence of Δm^2_{54}: in the 3+2/2+3 cases one has $\Delta m^2_{54} = |\Delta m^2_{51}| - |\Delta m^2_{41}|$ whereas in the 1+3+1 case, $\Delta m^2_{54} \simeq |\Delta m^2_{51}| + |\Delta m^2_{41}|$, which changes the transition probability regardless of the choice of CP-violating phases.

As an example of the effect of sterile neutrino spectra, the oscillation probabilities with respect to the ratio L/E are shown in Fig. 3.4 for the 3+2/2+3 and 1+3+1 cases. It is evident that the appearance probabilities are dependent on the ordering schemes, whereas the disappearance probability is not, since the Δm^2_{54} contributions are suppressed. Furthermore, if non-vanishing CP-violating phases are included there are visible differences between neutrino and anti-neutrino flavour transitions, implying that a detector at very short distances would be an ideal place to search for the CP violation related to sterile neutrinos.

3.2.3 Experimental evidence and global fits

There are several hints for eV-scale sterile neutrinos from oscillation experiments, past and present. The LSND experiment found evidence for $\bar{\nu}_\mu \to \bar{\nu}_e$ oscillations with $\Delta m^2 \simeq 1$ eV^2

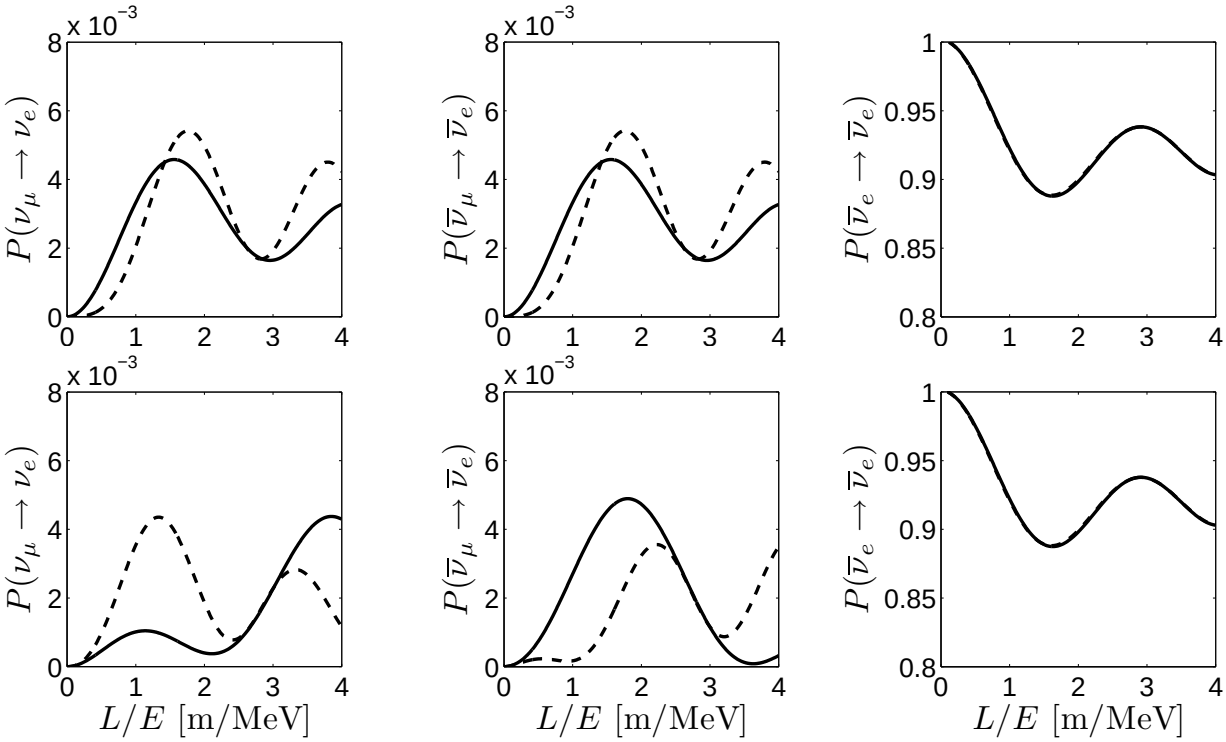

Figure 3.4: The oscillation probabilities with respect to the quantity L/E in the 3+2/2+3 cases (solid lines) and 1+3+1 case (dashed lines). The mixing parameters are the best-fit values from Tables 3.1 and 3.2. In the upper panel all CP-violating phases are set to zero, whereas in the lower panel $\tilde{\delta} = \frac{\pi}{2}$ is assumed.

at 3.8σ [17]. This signal was considered an anomaly for several years, owing to the fact that the KARMEN experiment found no corroborating evidence, although it did not rule out the entire LSND parameter space [137]. The initial results from MiniBooNE (with neutrinos) excluded the oscillation interpretation of LSND at 98% C.L. [138]. However, there is still a poorly understood low-energy excess [139] in both the neutrino and anti-neutrino modes, and the latest combined analysis [18] now shows some consistency with LSND and KARMEN.[7]

Active-sterile oscillations in appearance experiments imply that both $\tilde{U}_{e4}$ and $\tilde{U}_{\mu 4}$ are non-zero [Eq. (3.16)], which means that ν_e and ν_μ disappearance experiments should see a signal as well [Eq. (3.14)]. There are several hints for the former. Firstly, a reanalysis of the GALLEX and SAGE solar neutrino detectors as well as tests carried out with radioactive sources show that the number of measured neutrino events is smaller than expected [142]. This so-called "Gallium anomaly" could be interpreted as ν_e disappearance, i.e., oscillation into eV-scale sterile neutrinos [143]. Secondly, a recent re-evaluation of the anti-neutrino spectra of nuclear reactors leads to increased fluxes [19, 144]. The new calculation combines (*i*) an *ab initio* method that builds up the total anti-neutrino spectrum from a sum of thousands of β-branches with (*ii*) reference electron spectra measured at ILL, which must be converted to anti-neutrino spectra for each isotope. Several effects are taken into account, in particular the Coulomb and weak magnetism corrections to the Fermi theory of β-decay, as well as a new value for the neutron lifetime. The resulting anti-neutrino flux increases by roughly 4%, which means that

[7] Note that the extraction of oscillation parameters depends on the cross section for neutrino detection on carbon [140, 141]; those effects are not fully accounted for in the MiniBooNE analysis.

Table 3.2: Best-fit (from Ref. [153]) and estimated 2σ values of the sterile neutrino parameters.

	parameter	Δm^2_{41} [eV]	$\lvert\tilde{U}_{e4}\rvert^2$	Δm^2_{51} [eV]	$\lvert\tilde{U}_{e5}\rvert^2$
3+1/1+3	best-fit	1.78	0.023		
	2σ	1.61–2.01	0.006–0.040		
3+2/2+3	best-fit	0.47	0.016	0.87	0.019
	2σ	0.42–0.52	0.004–0.029	0.77–0.97	0.005–0.033
1+3+1	best-fit	0.47	0.017	0.87	0.020
	2σ	0.42–0.52	0.004–0.029	0.77–0.97	0.005–0.035

the negative results of previous reactor experiments at short baselines can in fact be interpreted as the observation of a flux deficit. This could be explained by additional sterile neutrinos with masses at the eV scale: the "reactor anomaly". Independent confirmation of this electron (anti-)neutrino disappearance at short baselines poses a new experimental challenge, since the characteristic baseline for eV-scale oscillations at MeV energies is $L \simeq 1 - 10$ m. There are various new experiments planned; one idea is to place a radioactive source inside or next to a large detector such as SNO or KamLAND (see the review in Ref. [145]), another is to use a research reactor with a detector at a baseline of $L \simeq 7$ m, the Nucifer experiment [146].

The results from electron neutrino disappearance are however not confirmed by ν_μ ($\bar{\nu}_\mu$) disappearance results, for example from atmospheric neutrinos, MINOS [147], as well as from a combination of MiniBooNE and SciBooNE data [148]. Future observations of atmospheric neutrinos by IceCube should provide a sensitive probe of $\tilde{U}_{\mu 4}$ [149]. Although disappearance data seem to favour the 3+1 interpretation [150], there is considerable tension when appearance and disappearance experiments are combined [151].[8] Table 3.2 shows the best-fit and 2σ ranges of the relevant parameters used in the present analysis. The best-fit values are taken from the global fit in Table II of Ref. [153].[9] In their analysis of the 3+1/1+3 scenarios, the authors of Ref. [153] find several different allowed regions in the $\Delta m^2_{41} - \sin^2\theta_{14}$ parameter space, at 2σ. In this work the region around the best-fit point is used, and (since the ranges are not available) the parameters in the 3+2, 2+3 and 1+3+1 cases are assigned 2σ uncertainties of the same relative magnitude as those in the 3+1/1+3 scenario. The 1+3+1 scenarios have a slightly better fit than the 3+2/2+3 cases, which is also confirmed from a recent fit [154] that updates the results in Ref. [153].

3.3 Sterile neutrinos in beta decay

Studies of the end-point of the electron energy spectrum in β-decay allow one to probe the so-called "effective electron neutrino mass in β-decay", defined by

$$m_\beta \equiv \sqrt{\sum_{i=1}^{n} |\tilde{U}_{ei}|^2 m_i^2} \ , \tag{3.18}$$

where in the standard case $n = 3$, $\tilde{U}_{ei}$ are the elements of the first row of the PMNS matrix in Eq. (3.3) and m_i are the light neutrino masses. The results of the Mainz [155] and Troitsk [156]

[8] There is also a recent fit that finds slightly less tension between appearance and disappearance data [152], albeit with the inclusion of cosmological data sets.

[9] See also Ref. [134] for another global fit.

Tritium β-decay experiments give the combined upper limit (at 2σ) of [157]

$$m_\beta < 1.8 \text{ eV} . \tag{3.19}$$

The upcoming KATRIN experiment [158] will aim for a sensitivity of $m_\beta \simeq 0.2$ eV. Note that the "direct" search for neutrino mass in β-decay experiments is not sensitive to their Dirac or Majorana nature.

In the presence of n_s sterile neutrinos the sum in Eq. (3.18) runs up to $n = 3+n_s$, so that the sterile states contribute to m_β. It is illustrative to consider the case of $n_s = 1$ and $n_s = 2$, with sterile neutrinos at the eV scale and different spectra (see Figs. 3.2 and 3.3). In the 3+1 and 3+2 cases the active neutrinos are much lighter than the sterile one(s), and m_β is dominated by the sterile contribution, i.e.,

$$\begin{aligned} m_\beta^{3+1} &\gtrsim \sqrt{|\tilde{U}_{e4}|^2 \Delta m^2_{41}} \simeq 0.2 \text{ eV}, \\ m_\beta^{3+2} &\gtrsim \sqrt{|\tilde{U}_{e4}|^2 \, \Delta m^2_{41} + |\tilde{U}_{e5}|^2 \, \Delta m^2_{51}} \simeq 0.16 \text{ eV}. \end{aligned} \tag{3.20}$$

For the cases where the sterile neutrino is lighter than the active ones (1+3 and 2+3) there are three quasi-degenerate neutrinos at the eV scale with mass given by $\sqrt{\Delta m^2_{41}}$ or $\sqrt{\Delta m^2_{51}}$, which effectively governs predictions for m_β, i.e.,

$$\begin{aligned} m_\beta^{1+3} &\gtrsim \sqrt{\sum_{i=1}^{3} |\tilde{U}_{e1}|^2 \Delta m^2_{41}} \simeq \sqrt{\Delta m^2_{41}} \simeq 1.3 \text{ eV}, \\ m_\beta^{2+3} &\gtrsim \sqrt{\sum_{i=1}^{3} |\tilde{U}_{ei}|^2 \, \Delta m^2_{51}} \simeq \sqrt{\Delta m^2_{51}} \simeq 0.93 \text{ eV}. \end{aligned} \tag{3.21}$$

The 1+3+1 cases are similar: the mass gap between the lightest sterile neutrino and the quasi-degenerate active neutrinos (Δm^2_{j1} in Fig. 3.3) again dominates m_β.

Refs. [159, 160] show that sterile neutrinos with masses and mixings in the ranges considered above will be observable in KATRIN, and will be distinguishable from active neutrinos. There are however additional complications for eV-scale neutrinos with mass larger than the energy resolution of KATRIN because the Kurie function cannot be approximated in the usual way (see Ref. [161]). As an aside, the presence of right-handed currents could also affect the electron energy spectrum observed in KATRIN [162].

3.4 Neutrinoless double beta decay with sterile neutrinos

Neutrinoless double beta decay is one of the central themes of this thesis, and will be discussed at length here and in the context of the LRSM in Chapter 5. After a summary of the standard scenario, the particle physics phenomenology of $0\nu\beta\beta$ in the presence of eV-scale sterile neutrinos as well as pseudo-Dirac neutrinos is presented, and several special features of $0\nu\beta\beta$ in the type I seesaw model are described. The final subsection provides an overview of the experimental situation and the calculation of nuclear matrix elements (NMEs).

3.4.1 The standard scenario

Observation of the lepton number violating decay,

$$(A, Z) \to (A, Z+2) + 2e^- , \tag{3.22}$$

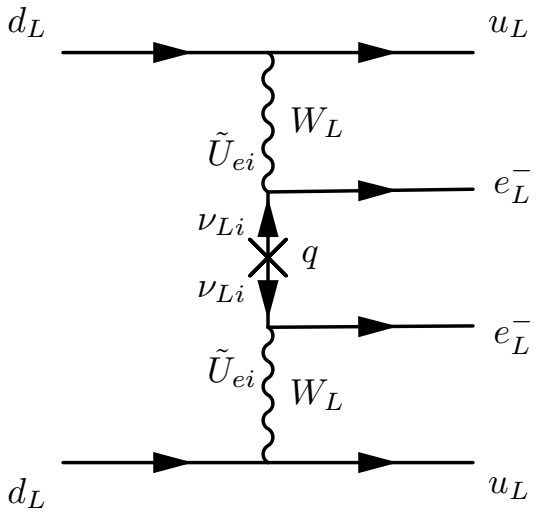

Figure 3.5: Feynman diagram of $0\nu\beta\beta$ in the standard case of light active neutrino exchange ($\mathcal{A}_\nu$), where q is the momentum of the neutrino.

would imply that neutrinos are Majorana particles [163], but extracting more specific information requires an assumption as to the underlying mechanism of the process. New physics beyond the SM is required to make it observable, and the necessary operators arise in several different theoretical frameworks (see the reviews in Refs. [164, 165]). The standard case of light active Majorana neutrino exchange is depicted in Fig. 3.5, with an amplitude proportional to

$$\mathcal{A}_\nu \simeq G_F^2 \frac{\langle m_{ee}\rangle_{3\nu}}{q^2}\,, \tag{3.23}$$

where the effective Majorana mass is

$$|\langle m_{ee}\rangle_{3\nu}| = \left|\sum_{i=1}^{3} \tilde{U}_{ei}^2\, m_i\right| \tag{3.24}$$

$$= \left|c_{12}^2 c_{13}^2 m_1 + s_{12}^2 c_{13}^2 m_2 e^{i\alpha} + s_{13}^2 m_3 e^{i\beta}\right|, \tag{3.25}$$

with α and β the Majorana phases. This equation holds for mass eigenstates lighter than $|q| \simeq 100$ MeV, the characteristic momentum of the process. The current limit is $|\langle m_{ee}\rangle_{3\nu}| \lesssim 0.4$ eV, from the KamLAND-Zen experiment with ^{136}Xe [166].

The currently allowed regions of the effective mass are plotted against the lightest mass in Fig. 3.6, using data from Table 3.1, with CP-conserving and CP-violating areas indicated. The coherent sum $|\langle m_{ee}\rangle_{3\nu}|$ contains 7 out of 9 parameters of the neutrino mass matrix and is the only observable carrying information about the Majorana phases. As can be seen in the left panel of Fig. 3.6, it is possible for $|\langle m_{ee}\rangle_{3\nu}|$ to vanish in the case of normal neutrino mass ordering, equivalent to a zero in the (1,1) element of the low energy Majorana neutrino mass matrix m_ν. In the inverted ordering case $|\langle m_{ee}\rangle_{3\nu}|$ cannot vanish, and the lower limit is given by

$$|\langle m_{ee}\rangle_{3\nu}| \simeq \left|(c_{12}^2 + s_{12}^2 e^{i\alpha})\sqrt{\Delta m_{\rm A}^2}\right| \gtrsim (c_{12}^2 - s_{12}^2)\sqrt{\Delta m_{\rm A}^2} \simeq \frac{\sqrt{\Delta m_{\rm A}^2}}{3} \simeq 17 \text{ meV}, \tag{3.26}$$

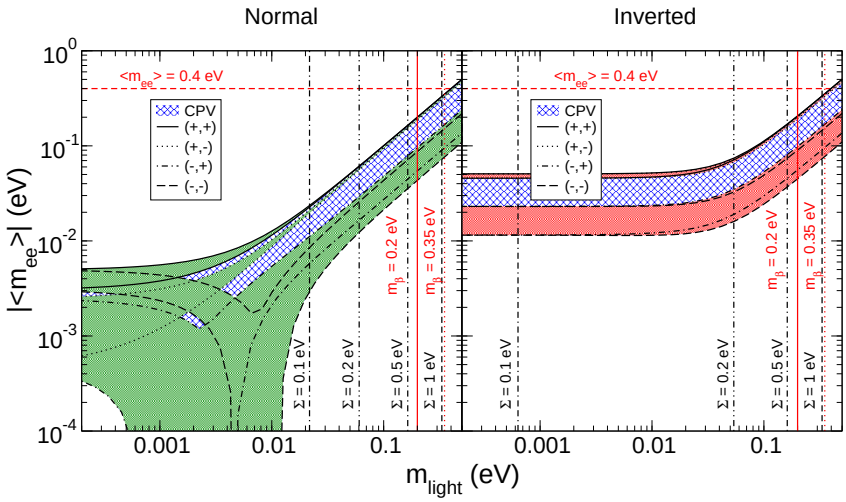

Figure 3.6: The effective mass $|\langle m_{ee}\rangle|$ as a function of the lightest neutrino mass in both the normal and inverted ordering, with the oscillation parameters varied in their 3σ ranges [23]. CP-conserving (violating) areas are indicated by black lines (blue hashes), and prospective values of $\sum m_\nu$ and m_β are shown. The latest limit on $|\langle m_{ee}\rangle|$ is indicated by the red horizontal dashed line.

where $\Delta m^2_{\rm A}$ is the mass-squared difference of atmospheric neutrinos. The final extraction of the decay halflife is affected by uncertainties in the NMEs, to be discussed in Section 3.4.5.

The standard scenario is by no means the only one: there are several particle physics candidates that can lead to $0\nu\beta\beta$ [164, 167]. Other contributions could come from heavy neutrinos, particles in R-parity violating supersymmetric theories, leptoquarks, Majorons, as well as particles arising in extra-dimensional and left-right symmetric theories. Current limits on the lifetime of $0\nu\beta\beta$ can be used to set constraints on different particle physics parameters [164]. The presence of light sterile neutrinos can significantly alter the predictions shown in Fig. 3.6, and the specific model of neutrino masses also plays a decisive role. Several different situations will be discussed below; $0\nu\beta\beta$ in the LRSM will be discussed in Section 5.2.

3.4.2 Phenomenological analysis of $0\nu\beta\beta$ with eV-scale sterile neutrinos

With n_s massive sterile neutrinos in the eV range the sum in Eq. (3.25) will extend to $n = 3{+}n_s$, and there will be $n_s + 2$ Majorana phases. The allowed regions for the modified effective mass $|\langle m_{ee}\rangle_{n\nu}|$ $(n = 4, 5)$ can be found from the parameter ranges in Tables 3.1 and 3.2, updating the results in Refs. [135, 168].

One sterile neutrino

In the presence of one sterile neutrino, the effective neutrino mass in $0\nu\beta\beta$ is given by

$$|\langle m_{ee}\rangle_{4\nu}| = \left| c^2_{12}c^2_{13}c^2_{14}m_1 + s^2_{12}c^2_{13}c^2_{14}m_2 e^{i\alpha} + s^2_{13}c^2_{14}m_3 e^{i\beta} + s^2_{14}m_4 e^{i\gamma} \right| , \tag{3.27}$$

using the parameterisation in Eq. (3.8). If the sterile neutrino is heavier than the active ones, the approximation

$$|\langle m_{ee}\rangle_{(3+1)\nu}| \simeq \left| c^2_{14}\langle m_{ee}\rangle_{3\nu} + s^2_{14}\sqrt{\Delta m^2_{41}}\, e^{i\gamma} \right| \tag{3.28}$$

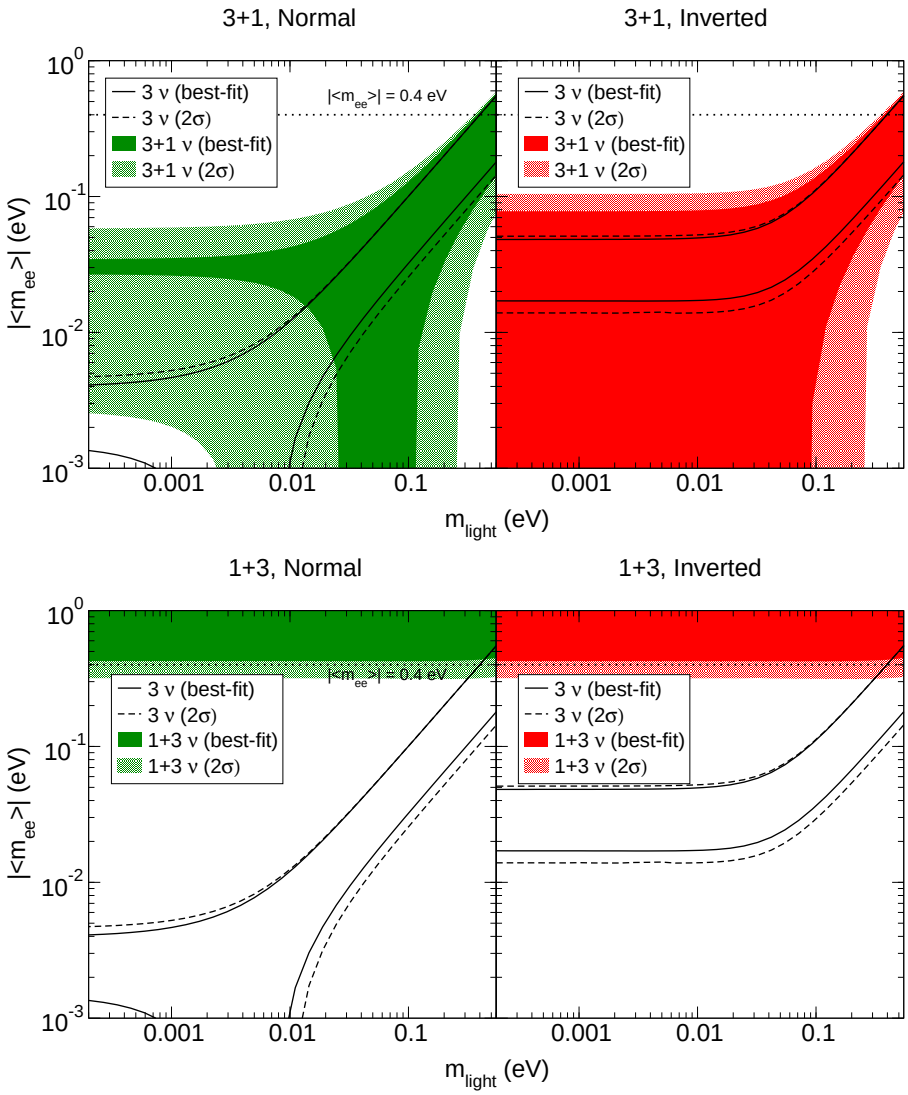

Figure 3.7: The allowed ranges in the $|\langle m_{ee}\rangle| - m_{\text{light}}$ parameter space, both in the standard three-neutrino picture (unshaded regions) and with one sterile neutrino (shaded regions), for the 3+1 (top) and 1+3 (bottom) cases. The latest limit on $|\langle m_{ee}\rangle|$ is indicated by the horizontal dotted line.

holds, where $\langle m_{ee}\rangle_{3\nu}$ is the standard expression in Eq. (3.25). The upper panel of Fig. 3.7 displays the allowed range of $|\langle m_{ee}\rangle_{(3+1)\nu}|$ as a function of the lightest mass $m_{\rm light}$. Also shown in this plot and the following ones is the allowed range of $|\langle m_{ee}\rangle_{3\nu}|$, as in Fig. 3.6, and it is evident that the usual situation is completely altered by the presence of one or more sterile neutrinos. If the lightest neutrino mass is reasonably small, e.g., $m_{\rm light} < 0.01$ eV, the allowed range of $|\langle m_{ee}\rangle_{(3+1)\nu}|$ is dominated by the term $s^2_{14}\sqrt{\Delta m^2_{41}} \simeq 0.031$ eV, which means that $|\langle m_{ee}\rangle_{(3+1)\nu}|$ cannot vanish in the normal ordering case (the contribution of the two light active neutrinos cannot cancel that of the sterile neutrino).

The inverted ordering shows noticeable modifications to the standard case, since $|\langle m_{ee}\rangle_{(3+1)\nu}|$ can vanish for a large range of lightest masses, including the regime where the active neutrinos are quasi-degenerate ($m_{\rm light} > 0.1$ eV). This means that the usual lower bound on the effective mass (cf. Eq. (3.26) and the solid and dashed lines in Fig. 3.7) is no longer valid. If future $0\nu\beta\beta$ experiments measure a tiny effective mass and the neutrino mass ordering is confirmed to be inverted from oscillation experiments (see Section 3.1), the sterile neutrino hypothesis would be an attractive explanation for this inconsistency.

The lower panel of Fig. 3.7 shows the effective mass when the sterile neutrino is lighter than the active ones (the 1+3 scenario). In that case there are three quasi-degenerate neutrinos at the eV scale, with their mass given by $\sqrt{\Delta m^2_{41}} \simeq 1.3$ eV, which also governs predictions for other observables. The effective mass then takes its standard form for quasi-degenerate neutrinos:

$$|\langle m_{ee}\rangle_{(1+3)\nu}| \simeq \sqrt{\Delta m^2_{41}}\,\sqrt{1 - \sin^2 2\theta_{12}\,\sin^2\alpha/2}\,. \tag{3.29}$$

However, this situation is relatively disfavoured by cosmological bounds on the sum of neutrino masses (cf. Section 3.6.1). Note that if the current limit of about 0.4 eV on the effective mass is taken at face value, then $\sqrt{1 - \sin^2 2\theta_{12}\,\sin^2\alpha/2} \lesssim 0.3$, thus already putting strong constraints on the solar neutrino mixing angle and in particular on the Majorana phase.

Two sterile neutrinos

If there are two sterile neutrinos, the effective mass is

$$|\langle m_{ee}\rangle_{5\nu}| = \left|c^2_{12}c^2_{13}c^2_{14}c^2_{15}m_1 + s^2_{12}c^2_{13}c^2_{14}c^2_{15}m_2e^{i\alpha} + s^2_{13}c^2_{14}c^2_{15}m_3e^{i\beta} + s^2_{14}c^2_{15}m_4e^{i\gamma} + s^2_{15}m_5e^{i\phi}\right|, \tag{3.30}$$

with ϕ the additional Majorana phase. In the 3+2 cases where both of the sterile neutrinos are at the eV scale, $|\langle m_{ee}\rangle_{(3+2)\nu}|$ can be approximated by

$$|\langle m_{ee}\rangle_{(3+2)\nu}| \simeq \left|c^2_{14}c^2_{15}\langle m_{ee}\rangle_{3\nu} + s^2_{14}\sqrt{\Delta m^2_{41}}e^{i\gamma} + s^2_{15}\sqrt{\Delta m^2_{51}}e^{i\phi}\right|, \tag{3.31}$$

in analogy to the 3+1 case. The upper panel of Fig. 3.8 shows the allowed regions in this case: the phenomenology is similar to that discussed for 3+1 above, except that the presence of two sterile terms in Eq. (3.31) allows $|\langle m_{ee}\rangle_{(3+2)\nu}|$ to take smaller values in the hierarchical region for the normal ordering. The inverted ordering is essentially the same as in the 3+1 case.

The lower panel of Fig. 3.8 displays the 2+3 cases, where the sterile neutrinos are lighter than the active ones. The three active neutrinos are quasi-degenerate at the eV scale, with their mass given by the largest sterile mass-squared difference $\sqrt{\Delta m^2_{51}} \simeq 0.93$ eV, so that Eq. (3.29) applies for $|\langle m_{ee}\rangle_{(2+3)\nu}|$, with Δm^2_{41} replaced by Δm^2_{51}. The mass ordering of the active states plays no role. Once again these scenarios are disfavoured by cosmology. There is little difference between this case and the 1+3+1 case; plots for the latter can be found in Ref. [99].

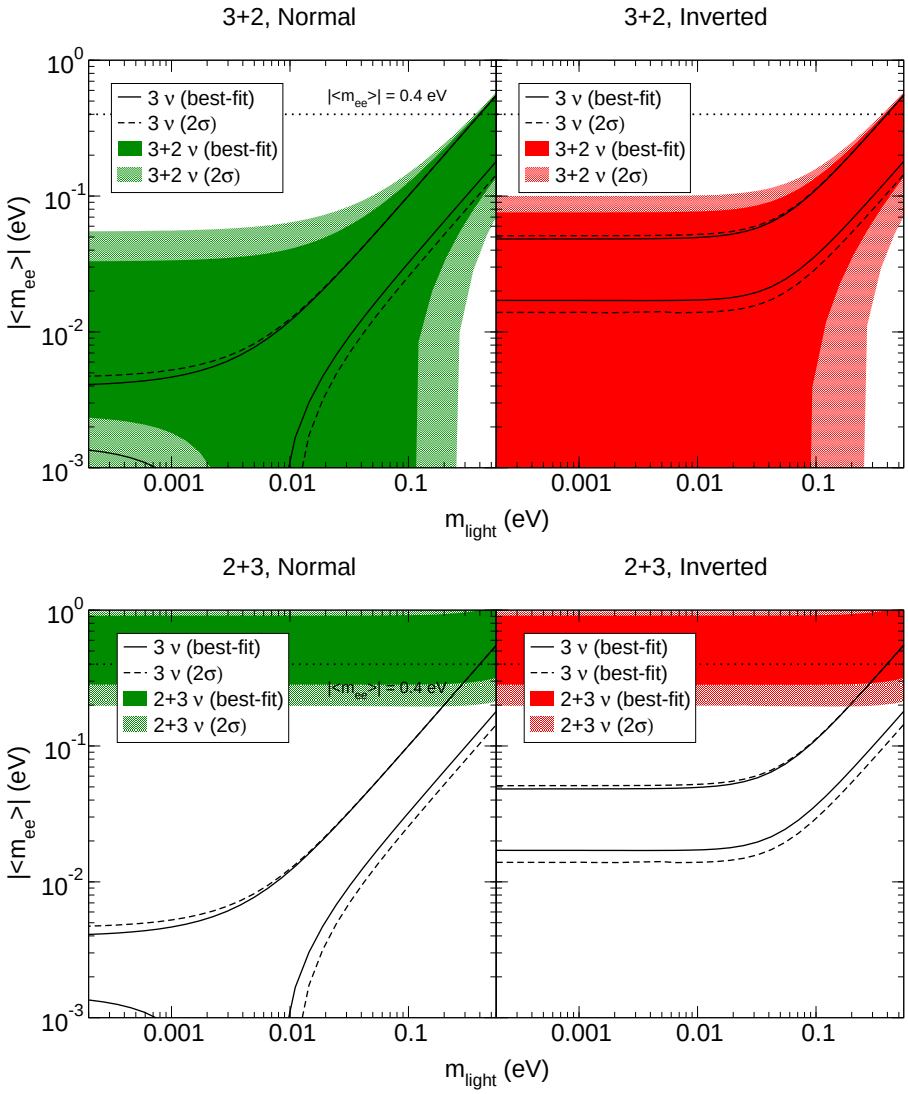

Figure 3.8: Same as Fig. 3.7, for the 3+2 (top) and 2+3 (bottom) cases.

In summary, the presence of eV-scale sterile neutrinos can significantly modify the predictions for $0\nu\beta\beta$, which provides a complementary test of the existence of those particles and could be used to constrain the sterile neutrino explanation of oscillation anomalies.

3.4.3 $0\nu\beta\beta$ with pseudo-Dirac and bimodal neutrinos

The approximately degenerate eigenstates, $m_i^{\pm}$, of the pseudo-Dirac pair have opposite CP parities, see Eq. (2.17). With three pseudo-Dirac neutrinos (six Majorana neutrinos), the expression in Eq. (3.25) becomes

$$|\langle m_{ee}\rangle_{\rm PD}| = \frac{1}{2}\left|\sum_{i=1}^{3}\tilde{U}_{ei}^2(m_i^+ + m_i^- e^{i\pi})\right| \simeq \left|\sum_{i=1}^{3}\tilde{U}_{ei}^2\frac{\delta m_i^2}{2m_i}\right|, \tag{3.32}$$

where $\delta m_i^2 \equiv (m_i^+)^2 - (m_i^-)^2$. Stringent limits on the pseudo-Dirac mass splitting exist from oscillation experiments: $\delta m_i^2 \lesssim 10^{-11}$ eV^2 for m_1 and m_2 from solar neutrino data [26][10] and $\delta m_i^2 \lesssim 10^{-3}$ eV^2 for m_3 from atmospheric data [169]. The contribution in Eq. (3.32) is therefore effectively vanishing ($|\langle m_{ee}\rangle_{\rm PD}| \lesssim 10^{-4}$ eV) and can be neglected. However, if only one or two neutrino mass eigenstates are pseudo-Dirac (the BM scenario), one effectively has a combination of the standard case in Eq. (3.25) and the pure pseudo-Dirac case in Eq. (3.32). Those neutrinos that are pseudo-Dirac do not significantly contribute to $|\langle m_{ee}\rangle_{\rm PD}|$, whereas the normal Majorana mass eigenstates contribute as in Eq. (3.25).

Figures. 3.9 and 3.10 show the allowed ranges in $|\langle m_{ee}\rangle| - \sum m_\nu$ parameter space, for different combinations of pseudo-Dirac neutrinos and both normal and inverted neutrino mass ordering, using data from Ref. [170]. The parameter space in the standard case is included for comparison. In each case, the contribution from the pseudo-Dirac pair is assumed to be vanishing so that

$$|\langle m_{ee}\rangle_{\rm BM}| = \left|\sum_{j=1}^{N}\tilde{U}_{ej}^2 m_j\right|, \tag{3.33}$$

where the index j runs over the neutrinos that are *not* pseudo-Dirac, and $N = 1$ or $N = 2$. For instance, in the case where only ν_2 is pseudo-Dirac, the effective Majorana mass becomes

$$|\langle m_{ee}\rangle_{\rm BM}^{\nu_2}| = \left|c_{12}^2 c_{13}^2 m_1 + s_{13}^2 m_3 e^{i\beta}\right|, \tag{3.34}$$

and there is only one phase, β. One can see from the plots in Figs. 3.9 and 3.10 that in the cases of ν_2 and $\nu_{2,3}$ pseudo-Dirac and inverted mass ordering, the lower limit for $|\langle m_{ee}\rangle|$ is increased by a factor of two [27]. Explicitly, the lower bound for the inverted ordering becomes

$$|\langle m_{ee}\rangle_{\rm BM}^{\nu_2}| \simeq c_{12}^2\sqrt{\Delta m_{\rm A}^2} \gtrsim \frac{2\sqrt{\Delta m_{\rm A}^2}}{3} \simeq 34 \text{ meV}, \tag{3.35}$$

to be compared with the bound for the standard case in Eq. (3.26). Due to the fact that $c_{12}^2 - s_{12}^2 \simeq s_{12}^2$, the case in which ν_1 is pseudo-Dirac results in $|\langle m_{ee}\rangle|$ taking its minimal value in the inverted ordering. Another interesting case is when $\nu_{1,3}$ are pseudo-Dirac with normal ordering, where the lower limit of $|\langle m_{ee}\rangle|$ is given by ($\Delta m_{\rm S}^2$ is the mass-squared difference of solar neutrinos)

$$|\langle m_{ee}\rangle_{\rm BM}^{\nu_{1,3}}| \gtrsim s_{12}^2\sqrt{\Delta m_{\rm S}^2} \simeq 2.9 \text{ meV}, \tag{3.36}$$

[10] Note that ν_1 and ν_2 contain a large amount of ν_e, see Fig. 3.1.

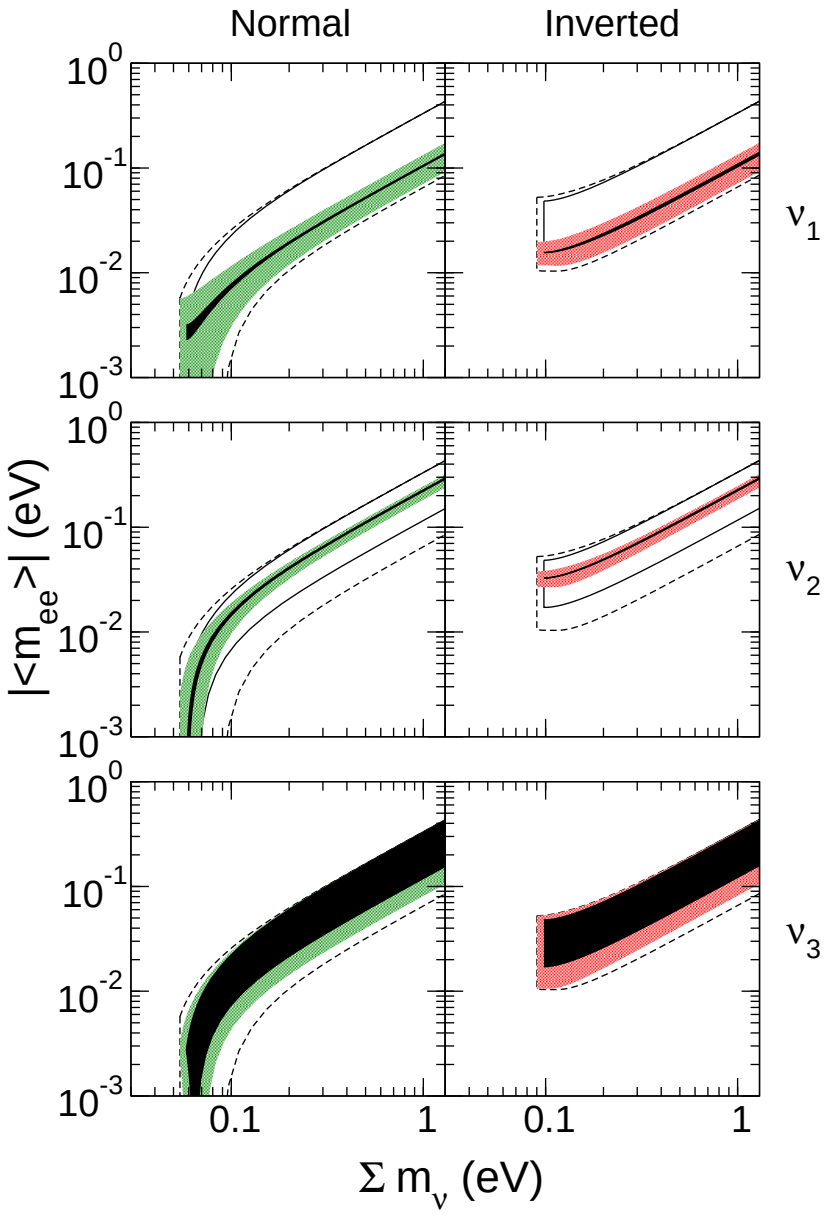

Figure 3.9: Allowed regions in the $|\langle m_{ee}\rangle| - \sum m_\nu$ plane for the three different cases of one pseudo-Dirac neutrino (indicated on the right of each row). The black regions are for exact TBM, and the light green (red) shaded regions correspond to the 3σ ranges of the oscillation parameters for normal (inverted) ordering. The solid (dashed) lines indicate the best-fit (3σ) allowed regions in the standard three-neutrino scenario.

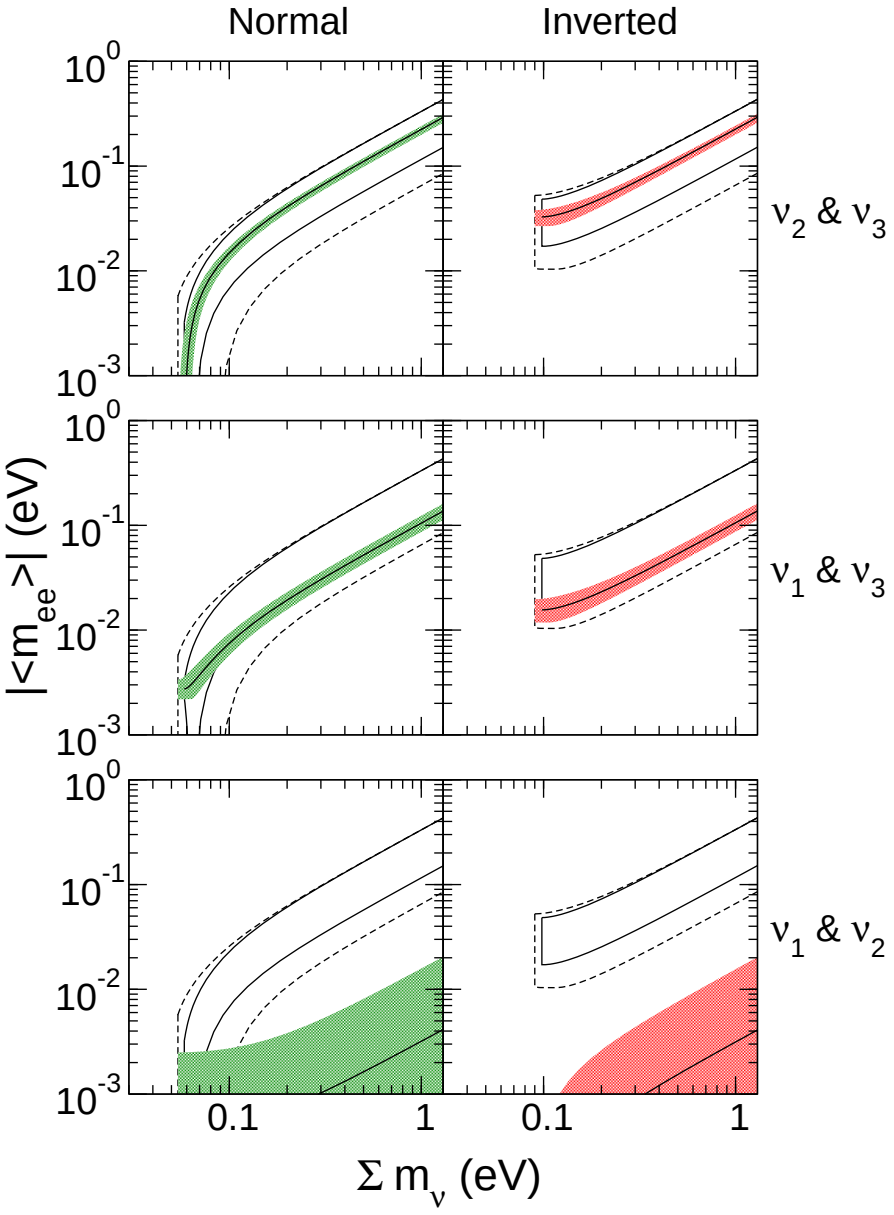

Figure 3.10: Same as Fig. 3.9 for the three different cases of two pseudo-Dirac neutrinos (indicated on the right of each row).

and the amplitude for $0\nu\beta\beta$ can never vanish, in contrast to the usual normal ordering case.

The cases where both ν_1 and ν_2 are pseudo-Dirac obviously lead to small values of $|\langle m_{ee}\rangle|$, since the only term contributing is $s_{13}^2 m_3$. In those cases the effective mass can lie outside the regions in which one expects it in the general case. Another interpretation of this would be that one of the non-standard mechanisms of $0\nu\beta\beta$ destructively interferes with the usual mass mechanism. The strategy to test this would be to perform multi-isotope investigation, as the cancellation is not expected to be on the same level in different nuclei. However, the pseudo-Dirac suppression discussed here is the same for all nuclei.

In summary, there are several cases for which there is a significant difference from the standard case of pure Majorana neutrinos. If long baseline oscillation experiments establish the neutrino mass ordering, and/or the neutrino mass scale is pinned down by cosmology or direct searches, neutrinoless double beta decay can distinguish the different cases, once again illustrating the discriminative power of the process.

3.4.4 $0\nu\beta\beta$ in type I seesaw models

The type I seesaw model contains n_s sterile neutrinos N_{Ri}^c, which can contribute to the amplitude for $0\nu\beta\beta$ through mixing with the active neutrinos. The relevant Lagrangian (in the diagonal charged lepton basis) is [cf. Eq. (2.19)]

$$\mathcal{L}_{CC}^{\text{lep}} = \frac{g}{\sqrt{2}} \overline{e_L} \gamma^\mu \left(\sum_{i=1}^{3} U_{ei} \nu_{Li} + \sum_{i=1}^{n-3} S_{ei} N_{Ri}^c \right) W_{L\mu}^- \,, \tag{3.37}$$

with U and S describing active-active and active-sterile mixing, respectively. The mass scale of the sterile states (M_R) is essentially unknown, and there are various special cases, outlined in Section 2.2.1. Neutrinos with mass below $|q| \simeq 100$ MeV will contribute to the $0\nu\beta\beta$ process via the effective mass defined in Eq. (3.25), where the sum is extended to included the new mass eigenstates. However, examination of the neutrino propagator,[11]

$$\frac{M_i}{q^2 - M_i^2} \simeq \begin{cases} \dfrac{M_i}{q^2} \text{ for } M_i^2 \ll q^2 \\ -\dfrac{1}{M_i} \text{ for } M_i^2 \gg q^2 \end{cases} \,, \tag{3.38}$$

shows that the contribution of right-handed neutrinos with masses much larger than $|q|$ is suppressed by the inverse of their mass. The $0\nu\beta\beta$ amplitude thus depends on the relative magnitudes of M_i and $|q|$: three different cases are outlined below, see also Ref. [171].

- **All sterile states heavier than $|q|$**
  If all of the heavy neutrinos M_i have mass at the GUT scale, their mixing contribution to $0\nu\beta\beta$ is negligible, as it is proportional to $1/M_i$, *viz.*

$$\mathcal{A}_{N_R}^L \simeq G_F^2 \sum_{i=1}^{n-3} \frac{S_{ei}^2}{M_i} \,, \tag{3.39}$$

  shown in Fig. 3.11. This contribution can only become relevant for sterile neutrinos at or below the TeV scale with sizeable mixing ($S \simeq 0.01 - 0.001$) to the active sector, which will be discussed in the context of the LRSM in Section 5.2. Note that in the language of effective operators the exchange of heavy neutrinos is short range, i.e., the interaction is point like, so that the NMEs differ from the standard case.

[11] The momentum-dependent term in the numerator vanishes due to chirality, see Eq. (5.3).

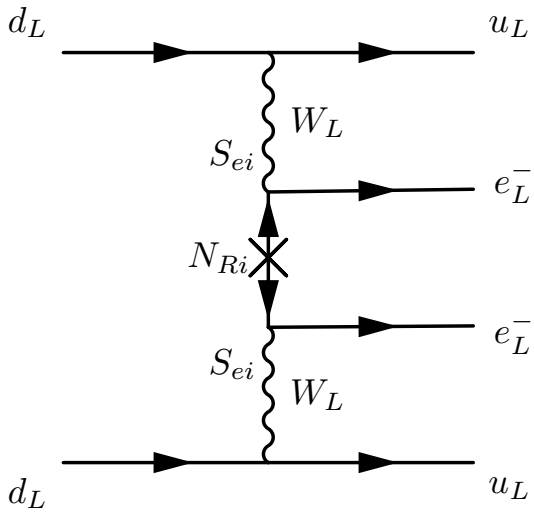

Figure 3.11: Heavy neutrino contribution to $0\nu\beta\beta$ in the type I seesaw model ($\mathcal{A}^L_{N_R}$), with the matrix S characterising the mixing between active and sterile neutrinos.

- **All sterile states lighter than $|q|$**
  If all of the $n_s = n - 3$ right-handed neutrinos are light, $M_i^2 \ll q^2$, the effective mass becomes

$$|\langle m_{ee}\rangle| = \left|\sum_{i=1}^{3} U_{ei}^2 m_i + \sum_{i=1}^{n-3} S_{ei}^2 M_i\right| = \left[M_\nu^{n\times n}\right]_{ee} = 0\,, \tag{3.40}$$

  showing that the effective mass cancels exactly, since the $(1,1)$ entry of the full $n \times n$ neutrino mass matrix in Eq. (2.12) is vanishing. However, the cancellation is not realised as soon as one of the right-handed neutrinos is heavier than $|q|$, which will be discussed below.

  The result in Eq. (3.40) holds in the general framework of type I seesaw models. However, in certain flavour symmetric seesaw models in which neutrino mixing is entirely determined by the Dirac mass term, M_D can be expressed as [172, 173]

$$M_D = V_\nu \,\mathrm{diag}\left(\sqrt{-m_1 M_1}, \sqrt{-m_2 M_2}, \ldots, \sqrt{-m_i M_i}\right) V_R^T\,, \tag{3.41}$$

  which also corresponds to $O = \mathbb{1}$ in the parameterisation of Eq. (2.25). The active-sterile mixing in Eq. (2.22) is now given by $S_{\alpha i} = (V_\nu)_{\alpha i}\sqrt{-m_i/M_i}$, which (for $i = 1,2,3$) is merely a rescaling of each column of V_ν, indicating a direct connection between active and sterile sectors. Interestingly, this implies that the above-mentioned cancellation for light right-handed neutrinos in $|\langle m_{ee}\rangle|$ occurs pairwise, since

$$S_{ei}^2 M_i = \left[-(V_\nu^2)_{ei}\frac{m_i}{M_i}\right] M_i = -U_{ei}^2 m_i\,, \quad (i = 1,2,3)\,, \tag{3.42}$$

  neglecting terms of order B^2 in Eq. (2.13). Here M_ℓ is assumed to be diagonal, but the result still holds with non-trivial V_L^ℓ, which can be factored out from both U_{ei} and S_{ei}. Put into words, this result means that the contribution to $|\langle m_{ee}\rangle|$ from the i-th active neutrino is exactly cancelled by the contribution from the i-th sterile neutrino, for $i = 1,2,3$, where the latter is responsible for the mass of the former via seesaw. The

computation of $|\langle m_{ee}\rangle|$ is now simplified since in Eq. (3.40) one only needs to count the effects of those active neutrinos whose corresponding sterile neutrinos are heavier than $|q|$, which will be applied to the model in Section 4.2.

- **Mixed case, with heavy and light sterile neutrinos**
  In this case some sterile neutrinos are heavier than $|q|$ while others are lighter than $|q|$. This is the most interesting case from a phenomenological point of view, since in addition to the usual light neutrino term there are two types of sterile contributions, i.e.,

$$\mathcal{A}^L_{N_R}\left(M_i < |q|\right) \propto \frac{S^2_{ei} M_i}{q^2} \quad \text{and} \quad \mathcal{A}^L_{N_R}\left(M_i > |q|\right) \propto \frac{S^2_{ei}}{M_i} \tag{3.43}$$

  for light and heavy states, respectively. Heavy neutrinos at the GUT scale should be integrated out first (their "direct" contribution is suppressed by the inverse of their mass), so that their only contribution to $0\nu\beta\beta$ is "indirect", via the masses of the light active neutrinos. However, heavy neutrinos close to the TeV scale could in fact dominate via the contribution on the right side of Eq. (3.43), as long as the active and light sterile contributions cancel each other [cf. Eq. (3.40)]. An example of this case will be given in Section 4.2. Note that the NMEs for light and heavy neutrino exchange are also different, as discussed in Section 3.4.5 below.

The Higgs triplets in the type II seesaw model introduced in Section 2.2.2 can also contribute to $0\nu\beta\beta$, which will be discussed in the context of the LRSM in Chapter 5.

3.4.5 Experimental situation

A conclusive measurement of $0\nu\beta\beta$ requires improved precision in both particle and nuclear physics parameters. The decay rate for $0\nu\beta\beta$ is often written as

$$[T^{0\nu}_{1/2}]^{-1} = \Gamma^{0\nu} \equiv G_k(Q, Z)|\mathcal{M}_k(A, Z)\eta_k|^2\,, \tag{3.44}$$

where $G_k(Q, Z)$ is the phase space factor, $\mathcal{M}_k(A, Z)$ the nuclear matrix element and η_k the lepton number violating particle physics parameter; the subscript k refers to different contributing mechanisms. The phase space factor comes from integrating over the wave functions of the electrons in the final state, and depends on the Q-value for the decay and to an extent on the particle physics process involved. The NME depends on the nucleus as well as whether the mechanism is mediated by long or short range forces, i.e., by light or heavy particles.

The current best limits on the lifetime for the $0\nu\beta\beta$ of ^{136}Xe are

$$\begin{aligned} T^{0\nu}_{1/2} &> 1.9 \times 10^{25}\ \text{yrs}\,, \\ T^{0\nu}_{1/2} &> 1.6 \times 10^{25}\ \text{yrs}\,, \end{aligned} \tag{3.45}$$

which come from the KamLAND-Zen [166] and EXO [174] experiments, respectively. The Heidelberg-Moscow (HM) experiment [175] sets an upper limit of $T^{0\nu}_{1/2} > 1.9 \times 10^{25}$ yrs using ^{76}Ge, and although part of the collaboration [176] claims a positive signal, this is somewhat controversial [177, 178] and requires independent confirmation. Ref. [164] lists the upper limits from various other experiments. Future experiments such as GERDA [179] and SuperNEMO [180] aim to reach a sensitivity for $|\langle m_{ee}\rangle|$ of order 10 meV and should thus be able to rule out the inverted mass ordering [cf. Eq. (3.26)], as long as the relevant parameter uncertainties are reduced.

Table 3.3: Phase-space factors $G_{01}^{0\nu}$ [182] and nuclear matrix elements for light ($\mathcal{M}_\nu^{0\nu}$) [181] and heavy ($\mathcal{M}_N^{0\nu}$) [183, 184] neutrino exchange, for different isotopes, for $g_A = 1.25$ and $r_0 = 1.1$ fm.

Isotope	$G_{01}^{0\nu}$ [10^{-14} yrs^{-1}]	$\mathcal{M}_\nu^{0\nu}$	$\mathcal{M}_N^{0\nu}$
^{76}Ge	0.686	2.58–6.64	233–412
^{82}Se	2.95	2.42–5.92	226–408
^{130}Te	4.13	2.43–5.04	234–384
^{136}Xe	4.24	1.57–3.85	160–172

The extraction of limits on particle physics parameters requires knowledge of the NMEs, which are difficult to calculate and prone to large theoretical uncertainties due to the overlap of nuclear wave functions. Several methods have been used in the literature, ranging from Nuclear Shell Model (NSM) to Quasi-Random Phase Approximation (QRPA) techniques, and although there is some consensus this varies for different nuclei. The reader is referred to Refs. [164, 181] for a comprehensive discussion of those issues. The analysis in Chapter 5 will make use of several different NMEs (cf. Table 5.2); for illustration the results for the standard mechanism ($\mathcal{M}_\nu^{0\nu}$) and heavy neutrino exchange ($\mathcal{M}_N^{0\nu}$) are shown in Table 3.3, for various nuclei. In the standard case the dimensionless particle physics parameter is

$$|\eta_\nu| = \frac{|\langle m_{ee}\rangle_{3\nu}|}{m_e} \lesssim 7.1 \times 10^{-7}\,, \tag{3.46}$$

whereas in the heavy neutrino case it is

$$|\eta_{N_R}^L| = m_p \left|\sum_i \frac{S_{ei}^2}{M_i}\right| \lesssim 7.0 \times 10^{-9}\,. \tag{3.47}$$

using the most conservative value for the NME and the KamLAND-Zen limit. Figure 3.12 shows the variation of the lifetime for the $0\nu\beta\beta$ of ^{76}Ge with light neutrino mass for normal and inverted mass ordering, assuming only light neutrinos contribute via Eq. (3.46) and using the smallest matrix element ($\mathcal{M}_\nu^{0\nu} = 2.58$). Comparison with Fig. 3.6 shows that the lifetime is obviously just the inverse of the effective mass squared, with various numerical prefactors. The variation in $\mathcal{M}_\nu^{0\nu}$ can bring the minimum allowed lifetime down by one order of magnitude.

3.5 Sterile neutrinos from astrophysical sources

3.5.1 Astrophysical sources of neutrinos

The experimental evidence for neutrino oscillations described in Section 3.1 stems partly from the detection of astrophysical neutrinos, either those from the Sun or those produced in the atmosphere by cosmic-ray collisions. There are various other astrophysical neutrino sources, and their detection by neutrino telescopes would provide complementary information to other probes of the universe (see the review in Ref. [185]). For instance, neutrinos radiate from objects such as supernovae, neutron stars and red giants. In addition, scattering of ultra-high-energy cosmic rays off photons produce pions, which decay to (anti-)neutrinos. Sources capable of

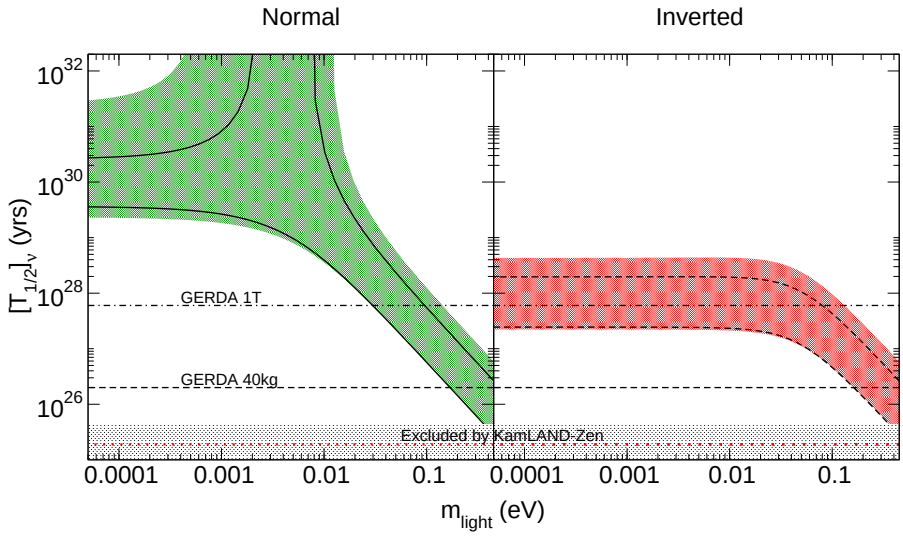

Figure 3.12: The standard light neutrino contribution to the $0\nu\beta\beta$ halflife of ^{76}Ge plotted against the lightest light neutrino mass, using best fit values (lines) and 3σ ranges (shaded regions) of the oscillation data from Ref. [23] as well as the relevant coefficients from Table 3.3. The grey shaded region is excluded by the KamLAND-Zen experiment [166], the horizontal dashed (dashed-dotted) lines show the planned sensitivities of the GERDA [179] experiment, with 40 kg (1 ton) of isotope. The Heidelberg-Moscow limit is indicated by a horizontal (red) dotted line.

accelerating particles to such high energies (greater than 10^{19} eV) include supernovae, active-galactic nuclei (AGN), quasars and gamma-ray bursts (GRBs).

Sterile neutrinos at the eV-scale have various effects on astrophysical processes. In the Sun, one expects an upturn of the energy spectrum of low-energy events; the absence of that feature can be attributed to sterile neutrinos [186, 187] (see Ref. [188] for a general discussion of solar neutrino phenomenology in the presence of sterile states). Another example is the influence of active-sterile oscillations on r-process nucleosynthesis in core collapse supernovae [189]. The heavy element yield seems to be too low in standard calculations, and sterile neutrinos have been proposed as a way to increase it, see e.g., Refs. [190–192].

The latest search for high energy neutrino point sources in IceCube finds no evidence for a neutrino signal [193], which places a strong bound on the neutrino flux of GRBs. Nevertheless, extra-galactic neutrinos are a useful probe of neutrino properties: studying the evolution of the neutrino flux flavour ratios not only provides information about astrophysical sources but also constrains neutrino mass and mixing (see Ref. [194, 195] for reviews). In the following section the case of pseudo-Dirac neutrinos is analysed in detail, and flavour ratios are shown to be useful in constraining the bimodal scenario (cf. Sections 2.2.1 and 4.3). The effect of eV-scale sterile neutrinos on flavour ratios was studied in Ref. [196].

3.5.2 Flavour ratios of pseudo-Dirac and bimodal neutrinos

Extra-galactic neutrinos travel large distances in space and have different energies, depending on their source. In most cases [197] the neutrinos originate from pion (and kaon) decay, followed

by muon decay, *viz.*

$$\pi^- \to \mu^- + \bar{\nu}_\mu \quad \text{and} \quad \mu^- \to e^- + \bar{\nu}_e + \nu_\mu \,, \tag{3.48}$$

leading to the initial flavour flux ratios $\Phi_e^0 : \Phi_\mu^0 : \Phi_\tau^0 = 1 : 2 : 0$. However, in neutron sources the initial ratios are $1 : 0 : 0$, with electron anti-neutrinos originating from β-decays [198, 199]; in muon-damped sources they become $0 : 1 : 0$, since the muons (but not pions) lose energy before they decay [200, 201]. Although the latter two sources are presumably less common and harder to measure (there is less total neutrino flux), they allow for interesting comparative studies with the usual pure pion source.

In general, the initial flux composition may be described as [202]

$$(\Phi_e^0 : \Phi_\mu^0 : \Phi_\tau^0) = (1 : n : 0) \,. \tag{3.49}$$

Here the parameter n distinguishes the different types of neutrino sources: for neutron sources, the initial ratio of $1 : 0 : 0$ is represented by the limit $n \to 0$, whereas in muon-damped sources the initial ratio of $0 : 1 : 0$ is the limit $n \to \infty$. Pure pion sources have $n = 2$. In each case neutrino mixing will affect the final flavour flux ratios at Earth detectors, and those ratios will also depend on whether the neutrinos are pseudo-Dirac or bimodal. It is well known that for the initial ratios of $1 : 2 : 0$, the final ratios turn out to be $1 : 1 : 1$ [197], assuming μ-τ symmetry (actually, it suffices to assume that $\mathrm{Re}(\tilde{U}_{e3}) = 0$ and $\theta_{23} = \pi/4$) and three standard neutrinos. Deviations from this symmetry limit will be discussed below.

If some or all of the neutrinos are pseudo-Dirac, the detected flux ratios are modified, and it is possible to study the effects of deviations in each different case [203]. In the standard three-neutrino scenario (no pseudo-Dirac effects), the flavour conversion probability for extra-galactic neutrinos is

$$P_{\alpha\beta} = \delta_{\alpha\beta} - 2 \sum_{i>j} \mathrm{Re}(\tilde{U}_{\alpha j} \tilde{U}^*_{\alpha i} \tilde{U}^*_{\beta j} \tilde{U}_{\beta i}) = \sum_i |\tilde{U}_{\alpha i}|^2 |\tilde{U}_{\beta i}|^2 \,, \tag{3.50}$$

where the oscillation term in Eq. (3.2) has been averaged out due to the large propagation distance ($L \simeq 100$ Mpc). However, it can be shown that if all neutrinos are pseudo-Dirac [204],

$$P^{\mathrm{PD}}_{\alpha\beta} = \sum_i |\tilde{U}_{\alpha i}|^2 |\tilde{U}_{\beta i}|^2 \cos^2 \left(\frac{\delta m_i^2 L}{4E} \right) , \tag{3.51}$$

where $\delta m_i^2 = (m_i^+)^2 - (m_i^-)^2$ is the small mass-squared difference between the pseudo-Dirac pairs, so that Eq. (3.50) is recovered for $\delta m_i^2 = 0$. Here the oscillations due to the atmospheric and solar mass-squared differences are decoherent, whereas those due to the tiny pseudo-Dirac mass splittings (δm_i^2) remain coherent. The bimodal flavour neutrino case is different in that not all of the three states ν_i are pseudo-Dirac, but only one or two (see Section 4.3). If the corresponding $\delta m_i^2 L/4E \gg 1$, in other words if L/E is large enough, the cosine term averages out to $1/2$. The standard effects from neutrino mixing are therefore modified and neutrinos from very distant sources could probe the tiny pseudo-Dirac mass-squared differences [203–206]. As discussed in Section 3.4.3, mass splittings of less than about 10^{-11} eV^2 have no effect on the solar neutrino flux.

If one assumes that only one neutrino is pseudo-Dirac (say ν_2), then the corresponding term ($i = 2$) of the sum in Eq. (3.51) is modified by a factor of $1/2$, leading to the probability

$$P^{\nu_2}_{\alpha\beta} = |\tilde{U}_{\alpha 1}|^2 |\tilde{U}_{\beta 1}|^2 + \frac{1}{2} |\tilde{U}_{\alpha 2}|^2 |\tilde{U}_{\beta 2}|^2 + |\tilde{U}_{\alpha 3}|^2 |\tilde{U}_{\beta 3}|^2 \,. \tag{3.52}$$

This can be extended to cases in which different combinations of neutrinos are pseudo-Dirac; the reduction factor of $1/2$ is applied to the relevant terms in each case. The measured neutrino

Table 3.4: The observed Φ_μ/Φ_e neutrino flux ratio at the detector for different combinations of pseudo-Dirac neutrinos, assuming the initial flux ratios of $1:2:0$ and exact μ-τ symmetry. Numerical values are calculated from the global fit data in Ref. [170]; the value of $\sin^2\theta_{12}$ is approximately the same as in Table 3.1.

Pseudo-Dirac neutrinos	Φ_μ/Φ_e		
	General case	Best-fit	3σ
None & all	$1:1$	1.00	1.00
ν_1	$1-\frac{1}{4}\sin^2\theta_{12} : \frac{1}{2}(1+\sin^2\theta_{12})$	1.40	1.32−1.46
ν_2 & ν_3	$\frac{1}{4}(2+\sin^2\theta_{12}) : 1-\frac{1}{2}\sin^2\theta_{12}$	0.67	0.66−0.73
ν_2	$\frac{1}{4}(3+\sin^2\theta_{12}) : 1-\frac{1}{2}\sin^2\theta_{12}$	0.99	0.95−1.04
ν_1 & ν_3	$\frac{1}{4}(3-\sin^2\theta_{12}) : \frac{1}{2}(1+\sin^2\theta_{12})$	0.58	0.55−0.60
ν_3	$\frac{3}{4}:1$	0.75	0.75
ν_1 & ν_2	$\frac{3}{2}:1$	1.50	1.50

flux, Φ_α, is the sum of the product of each initial flux Φ^0_α with the relevant flavour conversion probability,

$$\Phi_\alpha = \sum_\beta P_{\beta\alpha}\Phi^0_\beta \,, \tag{3.53}$$

so that the presence of one or more pseudo-Dirac neutrinos will change the final detected flux (and flux ratios) compared to the standard case. Table 3.4 shows the observable Φ_μ/Φ_e ratio as a function of θ_{12} for the different combinations of pseudo-Dirac neutrinos, for μ-τ symmetry and initial fluxes of $1:2:0$. Note that if all three neutrinos are pseudo-Dirac the observed flux ratio is again $1:1$, with an overall reduction in flux of $1/2$. In several cases the ratio is independent of θ_{12}. In addition, if ν_2 or $\nu_{1,3}$ are pseudo-Dirac, then Φ_μ/Φ_e is $1:1$ only if $\sin^2\theta_{12} = \frac{1}{3}$, i.e., for exact TBM (see Section 4.1), which is now ruled out by neutrino data.

Indeed, the data in Table 3.1 indicate deviation from μ-τ symmetry as well as non-zero θ_{13}, so that the simple picture presented in Table 3.4 will be modified. Flux ratios can be expressed in terms of the deviation parameter

$$\epsilon = \frac{\pi}{4} - \theta_{23} \,, \tag{3.54}$$

as well as the correction parameters Δ and Γ, defined in Eqs. (A.2) and (A.4), respectively. Explicit expressions for the relevant flavour conversion probabilities can be found in Appendix A, and can be used to calculate the final flux ratios in each case. The ratio Φ_μ/Φ_e is the most straightforward to measure and will be discussed below; results for the ratio Φ_e/Φ_τ, which is harder to measure, are also displayed.

The plots in Figs. 3.13 and 3.14 show the variation in the flux ratios Φ_μ/Φ_e and Φ_e/Φ_τ with $\sin^2\theta_{12}$ for the different possible combinations of one or two pseudo-Dirac neutrinos, assuming the standard case of an initial flux ratio of $1:2:0$ (a pure pion source) and using data from Ref. [170]. For comparison, the standard case without any pseudo-Dirac nature is also shown, for which the ratios can be approximated by

$$\frac{\Phi_\mu}{\Phi_e} \simeq \frac{1-\Delta}{1+2\Delta} \simeq 1-3\Delta \quad \text{and} \quad \frac{\Phi_e}{\Phi_\tau} \simeq \frac{1+2\Delta}{1-\Delta} \simeq 1+3\Delta \,, \tag{3.55}$$

using Eq. (A.3) and neglecting quadratic terms. One can see from the plots in Figs. 3.13 and 3.14 that the two cases in which ν_3 and $\nu_{1,2}$ are pseudo-Dirac show very little dependence on θ_{12} (compare with Table 3.4), even with deviations applied. The ratio Φ_μ/Φ_e differs considerably from the standard case if either ν_1 or both ν_1 and ν_2 are pseudo-Dirac, and can be approximated by

$$\begin{aligned}\frac{\Phi_\mu^{\nu_1}}{\Phi_e^{\nu_1}} &\simeq \{1-3\Delta\} + \frac{2-s_{12}^2-3s_{12}^4}{2(1+s_{12}^2)^2} - \frac{2\epsilon(s_{12}^2+s_{12}^4)}{(1+s_{12}^2)^2} \\ &\quad - \frac{3\Delta(3-4s_{12}^2-2s_{12}^4)}{2(1+s_{12}^2)^2} + \frac{2\Gamma(1-4s_{12}^2)}{(1+s_{12}^2)^2}\,, \\ \frac{\Phi_\mu^{\nu_{1,2}}}{\Phi_e^{\nu_{1,2}}} &\simeq \{1-3\Delta\} + \frac{1}{2} - 2\epsilon - \Delta\,.\end{aligned} \tag{3.56}$$

In both cases the expressions are given to first order in the deviation parameters and the curly brackets correspond to the standard case [Eq. (3.55)]. For the ratio Φ_e/Φ_τ, Fig. 3.14 shows that there are potentially strong effects if either ν_3 or both ν_2 and ν_3 are pseudo-Dirac, in which case

$$\begin{aligned}\frac{\Phi_e^{\nu_3}}{\Phi_\tau^{\nu_3}} &\simeq \{1+3\Delta\} + \frac{1}{3} + \frac{13}{9}\Delta\,, \\ \frac{\Phi_e^{\nu_{2,3}}}{\Phi_\tau^{\nu_{2,3}}} &\simeq \{1+3\Delta\} + \frac{8+4s_{12}^2-8c_{12}^2s_{12}^2-18s_{12}^4-3s_{12}^6}{(2+s_{12}^2)^3} \\ &\quad + \frac{3\Delta(8+4s_{12}^2-6s_{12}^4-s_{12}^6)}{(2+s_{12}^2)^3} + \frac{32\Gamma(2+s_{12}^2)}{(2+s_{12}^2)^3}\,.\end{aligned} \tag{3.57}$$

As mentioned above, the initial flavour ratios of other interesting neutrino sources, such as neutron or muon-damped sources, can be parameterised as in Eq. (3.49). Figures 3.15 and 3.16 indicate the dependence of the ratios Φ_μ/Φ_e and Φ_e/Φ_τ on n for the different pseudo-Dirac combinations. It is evident that in certain cases the observed ratio can be much larger than in the standard case. Specifically, in the case of ν_2 being pseudo-Dirac, the ratios Φ_μ/Φ_e and Φ_e/Φ_τ can become large for $n\to\infty$ and $n\to 0$, respectively. Expanding to first order in the deviation parameters, the ratios are given in those cases by

$$\begin{aligned}\frac{\Phi_\mu^{\nu_2}}{\Phi_e^{\nu_2}} \xrightarrow{n\to\infty} \frac{P_{\mu\mu}^{\nu_2}}{P_{e\mu}^{\nu_2}} &\simeq \left\{\frac{1-c_{12}^2s_{12}^2}{2c_{12}^2s_{12}^2} - \frac{1+c_{12}^2s_{12}^2}{2c_{12}^4s_{12}^4}\Delta\right\} \\ &\quad - \frac{1+4\epsilon}{6s_{12}^2} + \frac{1+12\Gamma}{6c_{12}^2s_{12}^2} + \frac{3\Delta+4\Gamma}{18c_{12}^2s_{12}^4} - \frac{3\Delta+16\Gamma}{18c_{12}^4s_{12}^4}\,, \\ \frac{\Phi_e^{\nu_2}}{\Phi_\tau^{\nu_2}} \xrightarrow{n\to 0} \frac{P_{ee}^{\nu_2}}{P_{e\tau}^{\nu_2}} &\simeq \left\{\frac{1-2c_{12}^2s_{12}^2}{c_{12}^2s_{12}^2} + \frac{1-2c_{12}^2s_{12}^2}{c_{12}^4s_{12}^4}\Delta\right\} \\ &\quad + \frac{1}{3c_{12}^2s_{12}^2} - \frac{6\Delta+8\Gamma}{9c_{12}^4s_{12}^2} + \frac{3\Delta+16\Gamma}{9c_{12}^4s_{12}^4}\,.\end{aligned} \tag{3.58}$$

The terms in curly brackets again denote the flux ratios corresponding to the general case, without pseudo-Dirac neutrinos, in the same limit ($n\to\infty$ or $n\to 0$). Additionally, if both ν_1 and ν_2 are pseudo-Dirac, the ratio Φ_μ/Φ_e becomes large for $n\to\infty$,

$$\frac{\Phi_\mu^{\nu_{1,2}}}{\Phi_e^{\nu_{1,2}}} \xrightarrow{n\to\infty} \frac{P_{\mu\mu}^{\nu_{1,2}}}{P_{e\mu}^{\nu_{1,2}}} \simeq \left\{\frac{1-c_{12}^2s_{12}^2}{2c_{12}^2s_{12}^2} - \frac{1+c_{12}^2s_{12}^2}{2c_{12}^4s_{12}^4}\Delta\right\} + \frac{1-4\epsilon}{4c_{12}^2s_{12}^2} - \frac{1}{c_{12}^4s_{12}^4}\Delta\,, \tag{3.59}$$

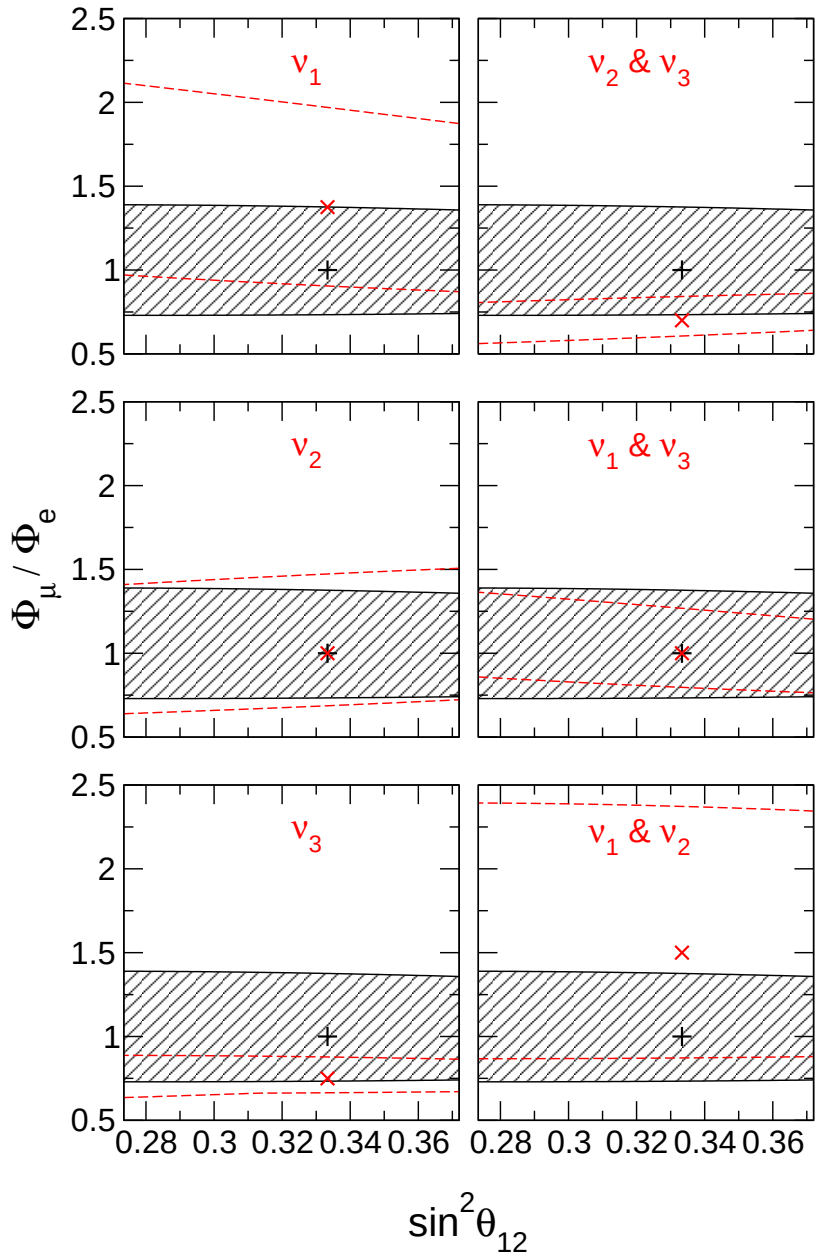

Figure 3.13: The observable flux ratio Φ_μ/Φ_e against $\sin^2\theta_{12}$, assuming the initial neutrino flux ratios of $1:2:0$ and different combinations of pseudo-Dirac neutrinos (denoted by red dashed lines), with the parameters θ_{13}, θ_{23}, and δ varying in their allowed 3σ ranges. The black hatched region shows the general case with no pseudo-Dirac neutrinos; the red cross (black plus sign) shows the value of Φ_μ/Φ_e in each pseudo-Dirac case (the general case), assuming TBM.

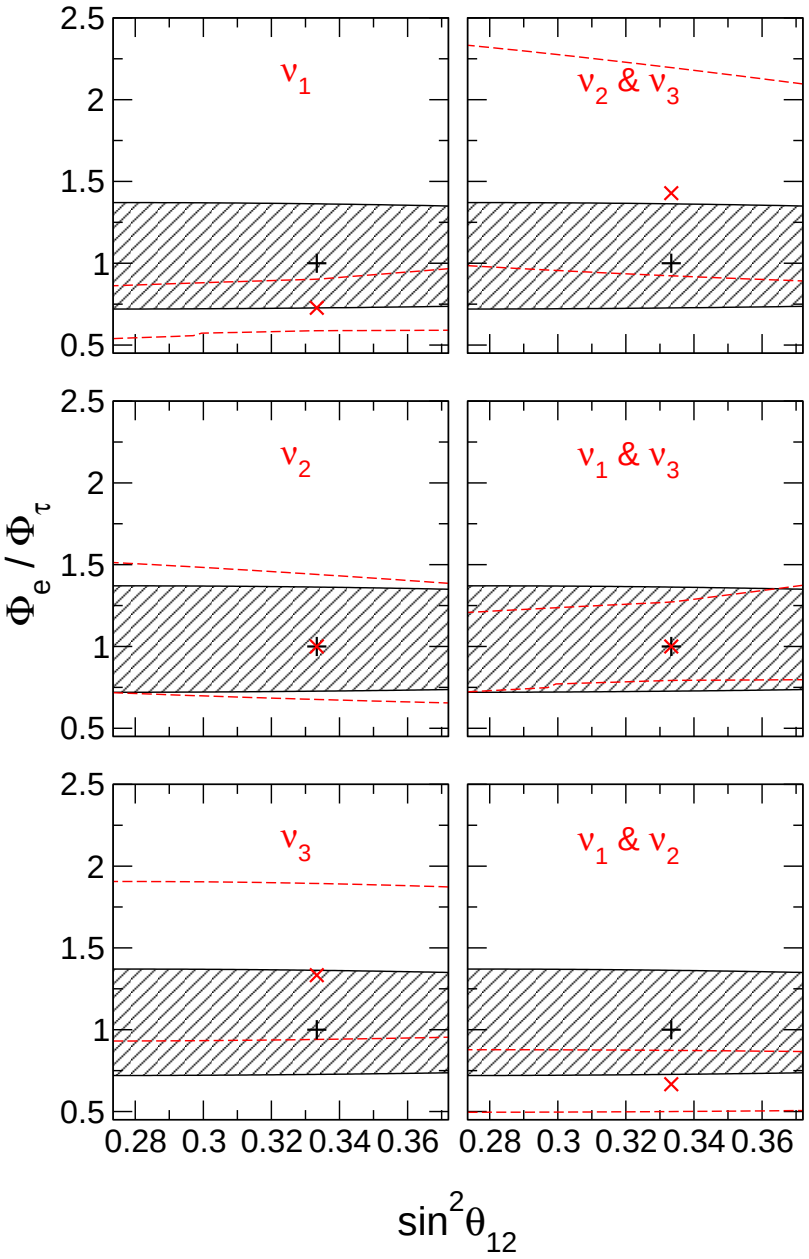

Figure 3.14: Same as Fig. 3.13 for the observable flux ratio Φ_e/Φ_τ.

and if both ν_2 and ν_3 are pseudo-Dirac, the ratio Φ_e/Φ_τ becomes large for $n \to 0$,

$$\frac{\Phi_e^{\nu_2,3}}{\Phi_\tau^{\nu_2,3}} \xrightarrow{n\to 0} \frac{P_{ee}^{\nu_2,3}}{P_{e\tau}^{\nu_2,3}} = \frac{P_{ee}^{\nu_2}}{P_{e\tau}^{\nu_2}} \simeq \left\{ \frac{1-2c_{12}^2 s_{12}^2}{c_{12}^2 s_{12}^2} + \frac{1-2c_{12}^2 s_{12}^2}{c_{12}^4 s_{12}^4}\Delta \right\} + \frac{1}{3c_{12}^2 s_{12}^2} - \frac{6\Delta + 8\Gamma}{9c_{12}^4 s_{12}^2} + \frac{3\Delta + 16\Gamma}{9c_{12}^4 s_{12}^4} \,. \tag{3.60}$$

The plots in Figs. 3.15 and 3.16 could in principle be used to rule out certain cases. If, for instance, measurements of the neutrino flux ratios from a muon-damped source give $\Phi_\mu/\Phi_e \gtrsim 5$, four of the six possibilities would be ruled out so that either ν_2 or both ν_1 and ν_2 would have to be pseudo-Dirac neutrinos. A similar result applies for the case of $\Phi_e/\Phi_\tau \gtrsim 7$ and neutron sources, where only ν_2 or ν_2 and ν_3 could be pseudo-Dirac.

In conclusion, the flux ratios of extra-galactic high energy neutrinos are a good test of the bimodal scenario, complementing the non-standard signatures in $0\nu\beta\beta$ (cf. Section 3.4.3). A combination of measurements of flux ratios and the effective mass in $0\nu\beta\beta$ should be able to rule out or confirm this scenario, using Figs. 3.9, 3.10, 3.13, 3.14, 3.15 and 3.16.

3.6 Sterile neutrinos in cosmology

Neutrinos play a vital role in our understanding of cosmology, and their properties are therefore constrained by cosmological data sets (see the reviews in Refs. [20, 207, 208]). New particles such as sterile neutrinos affect different parts of the evolution of the universe, depending on their mass, and can also be used to explain features such as dark matter [209] or the baryon asymmetry of the universe (BAU) [210]. This section provides a summary of the most relevant constraints on eV-scale light sterile neutrinos, an introduction to sterile neutrino WDM, as well as a brief discussion of leptogenesis, the process of producing the BAU by the decay of right-handed neutrinos.

3.6.1 Light (sterile) neutrinos in the early universe

In the expanding universe, the light neutrinos of the SM decouple at $T \simeq 1$ MeV, which means that they are relativistic. Annihilation of electrons and positrons at $T \simeq m_e/3 \simeq 0.2$ MeV leads to a reheating of the photon plasma, but the decoupled neutrinos are unaffected. The relation $T_\nu = \left(\frac{4}{11}\right)^{1/3} T_\gamma \simeq 1.95\,\mathrm{K} \simeq 10^{-4}$ eV follows from entropy conservation arguments and provides a reasonably good estimate of the temperature of relic neutrinos, still valid today. However, there are corrections from QED effects and a slight reheating of neutrinos, which lead to a small increase in the neutrino energy density, parameterised by

$$\sum_i \rho_{\nu,i} \equiv N_{\text{eff}}\, \rho_{\nu,0} \,. \tag{3.61}$$

Here $\rho_{\nu,0} = \frac{7}{8}\frac{\pi^2}{15} T_\nu^4$ is the energy density in a single neutrino flavour, assuming complete decoupling, and N_{eff} is the effective number of neutrino species. The SM prediction is $N_{\text{eff}} = 3.046$ [211], where the calculation assumes that the additional relativistic energy density is in the form of neutrinos. However, the cosmological parameter N_{eff} is often used to refer to any weakly interacting particle light enough to be relativistic at the time of CMB decoupling. Sterile neutrinos are obvious candidates, but others include axions, dark photons or even gravitons.

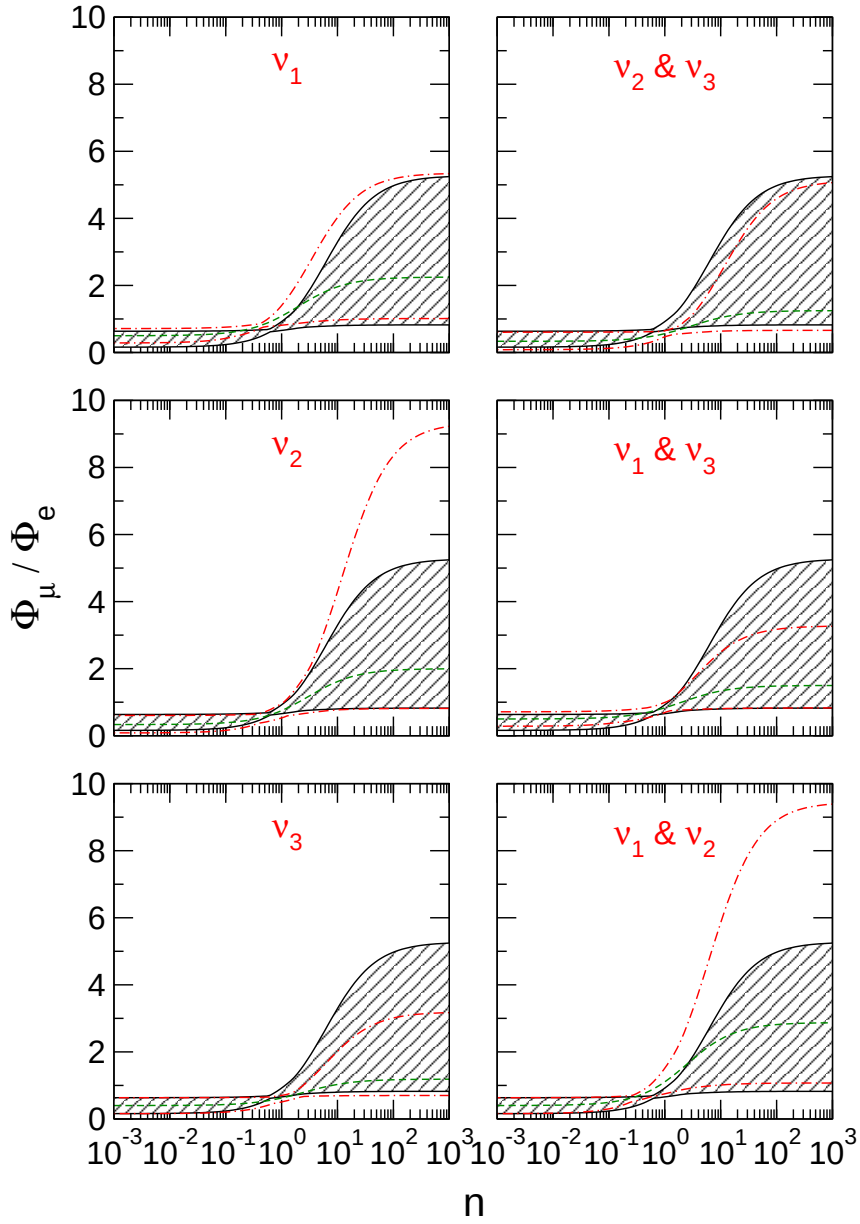

Figure 3.15: The observable flux ratio Φ_μ/Φ_e against n, assuming the initial neutrino flux ratios of $1 : n : 0$ and different combinations of pseudo-Dirac neutrinos (denoted by red dashed-dotted lines), with the parameters θ_{13}, θ_{23}, and δ varying in their allowed 3σ ranges. The black hatched region shows the general case with no pseudo-Dirac neutrinos; the green dashed line shows the value of Φ_μ/Φ_e in each pseudo-Dirac case, assuming TBM.

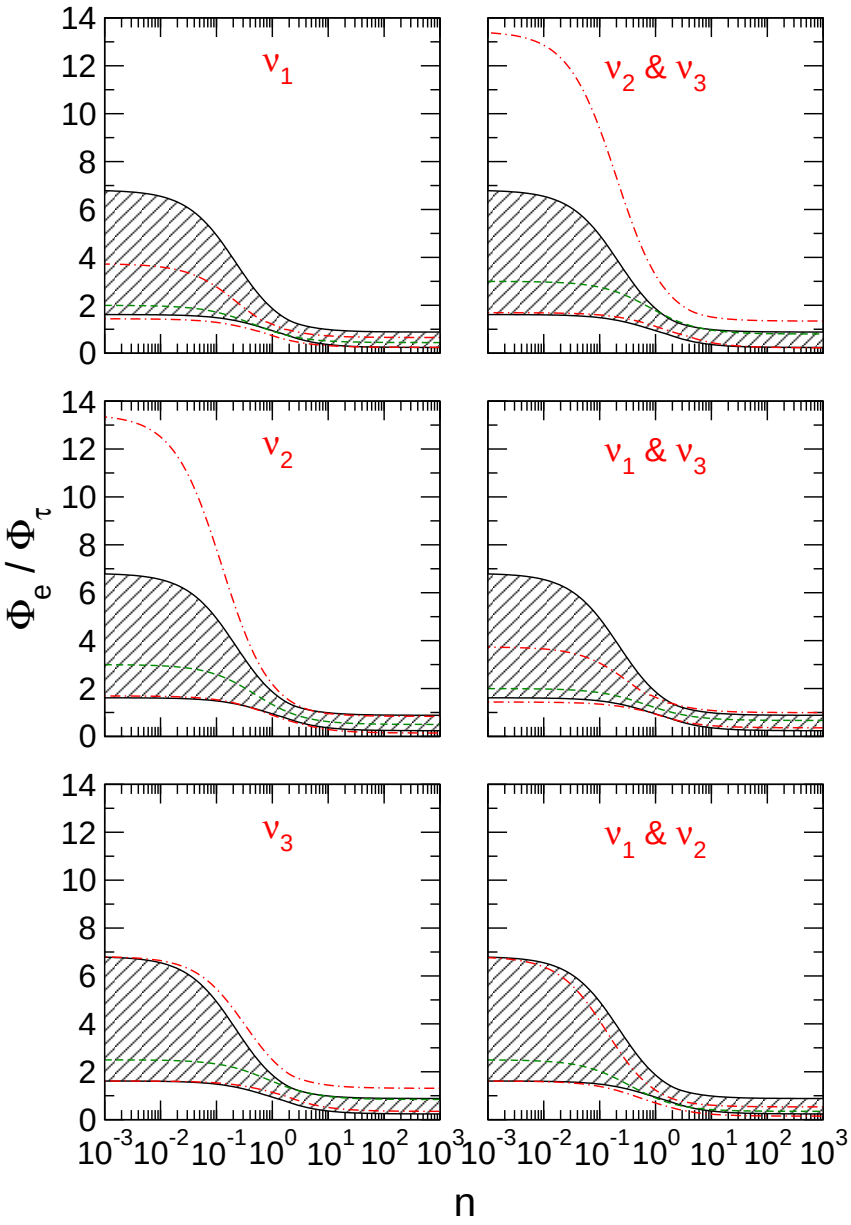

Figure 3.16: Same as Fig. 3.15 for the observable flux ratio Φ_e/Φ_τ.

In order for sterile states to contribute to N_{eff} they must be thermalised, which is usually accomplished via oscillations with active neutrinos [212, 213]. This would indeed be the case for sterile neutrinos with the mass and mixing parameters from Table 3.2.

The expansion of the universe during the epoch of radiation domination is directly proportional to the energy density stored in radiation, which at the time of photon decoupling ($T \simeq 0.26$ eV) is given by

$$\rho_{\text{rad}} = \rho_\gamma + \sum_i \rho_{\nu,i} = \rho_\gamma \left[1 + \frac{7}{8}\left(\frac{4}{11}\right)^{4/3} N_{\text{eff}}\right] \simeq \rho_\gamma (1 + 0.2271\, N_{\text{eff}})\,, \tag{3.62}$$

where $\rho_\gamma = \frac{\pi^2}{15} T_\gamma^4$. The effective number of neutrinos thus controls the expansion rate of the universe, which shows up in measurements of the temperature anisotropy spectrum of the CMB and affects the predictions for the primordial abundances of light elements from BBN. Oscillation experiments (cf. Section 3.1) have shown that at least two neutrinos are heavier than the relic neutrino background temperature $T_\nu \simeq 10^{-4}$ eV, so that those neutrinos are non-relativistic and their contribution to the energy density of the universe is given by

$$\Omega_\nu\, h^2 \simeq \frac{1}{94\ \text{eV}} \sum m_\nu\,, \tag{3.63}$$

where $\sum m_\nu$ is the sum of neutrino masses and $H_0 = 100\, h\ \text{km}\,\text{s}^{-1}\,\text{Mpc}^{-1}$ is the Hubble parameter today. Requiring that $\Omega_\nu < 1$ places a bound [214, 215] on the sum of neutrino masses, which can be strengthened by assuming that all dark matter is in the form of neutrinos: $\sum m_\nu \lesssim 11$ eV. However, bounds from large scale structure formation turn out to be far more stringent, as will be seen below.

Neutrinos and any other relativistic energy density affect the CMB power spectrum in several different ways, summarised in Ref. [216]. Sub-eV mass neutrinos effectively increase the ratio of radiation to matter at the time photons decouple, which is shortly after the epoch of matter-radiation equality ($T \simeq 1$ eV). Thus N_{eff} affects the positions of the peaks in the spectrum, as well as their height (via the early integrated Sachs-Wolfe effect). In addition, the growth of perturbations during the radiation era can be affected by N_{eff}, and the diffusion damping tail can be enhanced. The latest nine-year WMAP data [216], combined with ACT and SPT data (from 2011) leads to

$$N_{\text{eff}}^{\text{CMB}} = 3.89 \pm 0.67\ (68\%\ \text{C.L.})\,; \tag{3.64}$$

the inclusion of measurements of H_0 as well as BAO data changes the result to $N_{\text{eff}} = 3.84 \pm 0.40$ (68% C.L.). The result is consistent with the SM within 2σ, but the existence of one additional relativistic species has not yet been definitively ruled out. A new analysis [217] combining nine-year WMAP data with the latest ACT or SPT data gives $N_{\text{eff}} = 3.23 \pm 0.47$ or $N_{\text{eff}} = 3.76 \pm 0.34$, respectively. The situation is more complex since the new ACT and SPT data contradict each other, with the former favouring the standard value for N_{eff} [152]. Note that heavier particles ($m_\nu \gg 10$ eV) are non-relativistic at matter-radiation equality and thus do not affect N_{eff}.

A complementary probe of N_{eff} is the observed primordial abundance of ^{4}He, Y_P, which depends on the neutron-to-proton (n/p) ratio at the start of BBN, i.e., at $T \simeq 0.07$ MeV. Once the rate of charged current weak interactions equals the rate of expansion, the reactions freeze out and the n/p ratio is fixed. As discussed above, the expansion rate of the universe is increased by additional relativistic particles [cf. Eq. (3.62)], which leads to earlier freeze-out and thus increases Y_P. Current data [218–220] support a higher ^{4}He abundance and lead to [221]

$$N_{\text{eff}}^{\text{BBN}} = 3.77^{+0.47}_{-0.45}\,, \tag{3.65}$$

which is consistent with the existence of one additional sterile neutrino [222, 223]. Once again, this effect could be mimicked by another type of relativistic particle, or even by other effects such as a non-zero lepton asymmetry [224] or the decay of heavy particles [225]. The joint CMB and BBN constraints reported in Ref. [216] are consistent with the SM value as well as with $N_{\rm eff} = 4$; an extensive list of the results of various authors can be found in Ref. [21].

CMB data is also sensitive to the sum of neutrino masses via the effects described above, as long as $\sum m_\nu \gtrsim 1.8$ eV. From WMAP data alone [216],

$$\sum m_\nu^{\rm CMB} < 1.3 \text{ eV } (95\% \text{ C.L.}) \,, \tag{3.66}$$

whereas adding ACT, SPT, HST as well as BAO data leads to $\sum m_\nu < 0.44$ eV (95% C.L.), which is a very tight constraint. It is important to note that changes in the neutrino mass inferred from cosmology can also be compensated for by changing the Hubble parameter H_0, which warrants the combination of different data sets in order to reduce parameter degeneracies.

The theory of large scale structure (LSS) formation in the early universe places a strong bound on the sum of neutrino masses. Free-streaming of neutrinos affects the large-scale matter power spectrum, suppressing the growth of fluctuations on scales below the horizon when they become non-relativistic (the free-streaming length). That suppression is proportional to the neutrino-to-matter fraction Ω_ν/Ω_m, which can also be affected by sterile neutrinos. Thus LSS can be used to "weigh neutrinos" [226]: the Sloan Digital Sky Survey (SDSS) reports a bound of $\sum m_\nu < 0.62$ eV (95% C.L.) [227].[12] In addition the matter power spectrum on small scales can be probed by the Lyman-alpha (Ly-α) forest data, corresponding to the absorption of photons from distant quasars by neutral hydrogen in the intergalactic medium. Density fluctuations of the gas along the line of sight allow reconstruction of the matter density profile, although the processes involved are not entirely well understood. In spite of this, various authors have obtained even more stringent bounds on $\sum m_\nu$ by combining various data sets, see for example Ref. [231]. The bottom line is that there is no single cosmological bound for $\sum m_\nu$, and values in the range 0.2–1.5 eV can be found in the literature.

As mentioned above, the sterile neutrinos required to explain the oscillation anomalies outlined in Section 3.2.3 will be thermalised and thus effect $N_{\rm eff}$. However, eV-scale sterile states are in danger of contradicting cosmological constraints on the sum of neutrino masses. Data from Table 3.2 lead to

$$\sum m_\nu^{3+1} \gtrsim \sqrt{\Delta m^2_{41}} \simeq 1.3 \text{ eV}, \tag{3.67}$$

$$\sum m_\nu^{3+2} \gtrsim \sqrt{\Delta m^2_{41}} + \sqrt{\Delta m^2_{51}} \simeq 1.6 \text{ eV}, \tag{3.68}$$

for the 3+1 and 3+2 cases, respectively. The sum of masses is much higher in the cases where the sterile neutrinos are heavier than the active ones (1+3, 2+3, 1+3+1), e.g.,

$$\sum m_\nu^{1+3} \gtrsim 3\sqrt{\Delta m^2_{41}} \simeq 4 \text{ eV}, \tag{3.69}$$

$$\sum m_\nu^{2+3} \gtrsim 3\sqrt{\Delta m^2_{51}} + \sqrt{\Delta m^2_{51} - \Delta m^2_{41}} \simeq 3.4 \text{ eV}, \tag{3.70}$$

for the 1+3 and 2+3 cases, respectively. The analyses of Refs. [222, 223] find the upper bound $M_s < 0.45$ eV (68% C.L.) on the sterile neutrino mass, assuming the 3+1 mass spectrum

[12] Although LSS measurements are generally only sensitive to the sum of neutrino masses, some authors have argued that future experiments may be able to constrain the neutrino mass ordering [228, 229], but a recent analysis [230] using simulations of Planck and EUCLID data shows that that is rather unlikely.

($N_{\text{eff}} = 4$); the bound for the 3+2 case is similar. However, recent works have shown that in general one needs exotic modifications to cosmology in order to explain all of the data [232–235]. For instance, a large initial lepton asymmetry could lead to partial thermalisation of one or more of the sterile states, which alleviates the constraints to some extent, but tension with the data still remains, especially when adding two sterile neutrinos. A new analysis [152] has shown that there is reasonable agreement between SBL data and cosmology, as long as at least one of the sterile neutrinos are not completely thermalised.

The present hints for extra radiation will soon be constrained by Planck data, with a precision of $\Delta N_{\text{eff}} \sim \pm 0.3$ [222]. This means that Planck could in fact constrain the existence of a sterile neutrino species before beta decay or $0\nu\beta\beta$ experiments see a signal. However, cosmological data are rather model-dependent, so that a definitive exclusion or confirmation is not so straightforward. If Planck restricts the effective number of light neutrinos to be close to the SM value one could still build exotic models to explain the oscillation anomalies, for instance by introducing an MeV dark matter particle with different couplings to electrons than to neutrinos [236, 237] or even by modifying gravity [238]. On the other hand, confirmation of sterile neutrinos by Planck may provoke a re-examination of the standard cosmological model. Whatever the outcome, the hints from short-baseline and reactor experiments described in Section 3.2.3 remain and require independent verification from other terrestrial experiments.

3.6.2 Sterile neutrino warm dark matter

Massive neutrinos affect structure formation and are thus a source of dark matter, but simulations [239] of the evolution of LSS have shown that the light active neutrinos of the SM cannot make up all of the DM in the universe, since their free-streaming length[13] would erase observed small scale structures. In contrast to HDM in the form of neutrinos, the WIMPs of the ΛCDM model are cold thermal relics with negligible free-streaming length, which clump together to allow structures to form. There are several particle physics candidates with the required properties [15], one example would be the neutralino in supersymmetric theories.

Although the ΛCDM model is remarkably successful on larger scales, several hints for DM with a non-negligible free-streaming length have emerged on smaller scales. Firstly, the ΛCDM model predicts the number of dwarf satellite galaxies to be too large, in conflict with observations. Secondly, CDM simulations produce halos with concentrated cores whereas rotation curves of galaxies imply low-density cores. In addition, observations have shown that faint dwarf galaxies do not fill voids in the bright galaxy distribution, so that smaller halos are correlated with large scale structures, which one would not expect with CDM. These problems can be alleviated by WDM, primarily due to its velocity, which damps structures on sub-Mpc scales [240].

Sterile neutrinos at the keV scale are good candidates for WDM [16, 241, 242],[14] since their maximal free-streaming length is given by [209]

$$\lambda_{\text{FS}} \simeq 1 \text{ Mpc} \left(\frac{\text{keV}}{M_i} \right) . \tag{3.71}$$

This value can be slightly smaller depending on the way the WDM is produced. There are various constraints on the WDM mass and its mixing with the active sector, some of which depend on the production mechanism. The universal Tremaine-Gunn bound [245] means that

[13] For eV-scale neutrinos, $\lambda_{\text{FS}} \simeq 100$ Mpc (eV/m_ν).
[14] keV sterile neutrinos could also provide an explanation for pulsar kicks [243, 244].

any fermionic DM should be heavier than about 0.4 keV, from arguments about the phase-space density of a Fermi gas; this bound increases to roughly 1 keV in specific WDM models. Furthermore, the radiative decay of a sterile neutrino (N_1) would lead to a monochromatic X-ray line of energy $E_\gamma = M_1/2$ and decay width

$$\Gamma_{N_1\to\gamma\nu} \simeq 5.5\times 10^{-27}\left(\frac{S_1^2}{10^{-5}}\right)\left(\frac{M_1}{\text{keV}}\right)^5 \text{ s}^{-1}\,, \tag{3.72}$$

where S_1 is the mixing defined in Eq. (2.23); non-observation of that line leads to the bound [246]

$$S_1^2 \lesssim 1.8\times 10^{-5}\left(\frac{\text{keV}}{M_1}\right)^5. \tag{3.73}$$

The constraint of DM stability requires $\tau_1 > \tau_{\text{universe}} \simeq 10^{17}$ s, where the lifetime comes from the tree-level decay into three (anti-)neutrinos, with a decay width roughly given by $\Gamma_{N_1\to 3\nu} \simeq G_F^2 S_1^2 M_1^5$. This is easily fulfilled with a keV-mass particle and mixing satisfying Eq. (3.73), since

$$\tau_{N_1\to 3\nu} \simeq 5\times 10^{23}\text{ s}\left(\frac{\text{keV}}{M_1}\right)^5\left(\frac{10^{-5}}{S_1^2}\right). \tag{3.74}$$

In realistic sterile neutrino WDM models, a specific mechanism for the relic production of sterile neutrinos is required. The Dodelson-Widrow scenario [16] employs non-resonant production via active-sterile mixing. In that case, if one assumes that the sterile neutrino N_1 with mass M_1 and mixing S_1 makes up all the DM in the Universe, its abundance is given by [209]

$$\Omega_{N_1} \simeq 0.2\left(\frac{S_1^2}{3\times 10^{-9}}\right)\left(\frac{M_1}{3\text{ keV}}\right)^{1.8}, \tag{3.75}$$

so that the mass is bounded to be around 1-3 keV. However, Ly-α constraints lead to $M_1 \gtrsim 8$ keV [247], which combined with the X-ray bound in Eq. (3.73) effectively excludes non-resonant production. In the so-called Shi-Fuller mechanism [248], production proceeds via resonant flavour oscillations (the MSW effect), which require a significant primordial lepton asymmetry. The Ly-α bounds are weaker in this case, roughly $M_1 \gtrsim 2$ keV [249]. Other approaches discussed in the literature include production via the decay of scalar singlets [250, 251] as well as thermal production achieved by extending the gauge group to that of the LRSM [252, 253] (cf. Section 2.3). A specific model encompassing both sterile neutrino WDM as well as the BAU is the neutrino Minimal Standard Model (νMSM) [254, 255], discussed in Section 3.6.3 below, in which three sterile neutrinos below the electroweak scale are introduced.

Equation (3.75) is used as a guideline for the model building efforts of Chapter 4, without too much concern for the production mechanism. The main challenge from a particle physics perspective is how to obtain a sterile neutrino with keV mass and mixing of order $S_1^2 \simeq 10^{-8}$ in a realistic model. Several approaches have already been discussed in Section 2.2.1. Note that a sterile neutrino characterised by Eq. (3.75) results in a contribution $S_1^2 M_1 \lesssim 10^{-5}$ eV to the active neutrino masses, which means that one of the active neutrinos is effectively massless.

3.6.3 Leptogenesis and the νMSM

The discussion of sterile neutrinos in cosmology would not be complete without mentioning leptogenesis, which is a mechanism to generate the baryon asymmetry of the universe,

$$\eta_B \equiv \frac{n_B - n_{\bar{B}}}{n_\gamma} \simeq 6\times 10^{-10}\,, \tag{3.76}$$

from the decays of heavy sterile neutrinos, where n_B ($n_{\bar{B}}$) refers to the number of baryons (anti-baryons), and n_γ to the number of photons. Indeed, the only known source of CP violation in the SM comes from the CKM matrix (cf. Section 2.1), which is not enough to explain the number in Eq. (3.76). The type I seesaw mechanism introduced in Section 2.2.1 provides the setting for the standard thermal leptogenesis scenario, in which the out-of-equilibrium decays of GUT-scale heavy neutrinos generate a lepton asymmetry that is subsequently converted into baryon asymmetry via sphaleron processes. The lepton asymmetry is proportional to $Y_D^\dagger Y_D$, where Y_D is the Dirac coupling defined in Eq. (2.11). If the heavy neutrinos are thermally produced they need to be heavier than about 10^9 GeV to give large enough η_B [256].

In the νMSM, N_1 is the keV WDM particle whereas the two heavier sterile neutrinos $N_{2,3}$ are at the GeV scale; the required baryon asymmetry is produced via CP-violating oscillations [257] of $N_{2,3}$. In order to simultaneously explain the BAU and DM production one needs resonant enhancement [258], which implies that the right-handed neutrinos are nearly degenerate, roughly $|M_2 - M_3|/M_2 \simeq 10^{-11}$ [259]. A comprehensive study of the parameter space of the model was performed in Ref. [260], and models that achieve the required mass spectrum have been considered in the literature, see Section 2.2.1 as well as Ref. [261]. The A_4 model in Chapter 4 can indeed accommodate the νMSM scenario presented here.

3.7 Colliders, lepton flavour violation and electroweak precision observables

Sterile neutrinos can also be probed at hadron and lepton colliders, and in charged lepton flavour violating processes. In some cases they can lead to a modification of the electroweak precision observables (EWPO). After a brief discussion of LHC signals the interesting case of inverse double beta decay at a linear collider is introduced, as a prelude to the analysis of the LRSM in Chapter 5. The constraints from searches for charged lepton flavour violation are also relevant for that case; and will be summarised here. For completeness the constraints from electroweak physics are briefly mentioned.

3.7.1 LHC signatures

Although (sterile) neutrinos are not directly detectable at the LHC, their presence could still be felt through couplings to other particles. In particular, heavy neutrinos can be produced in pp collisions via a process that can be obtained by rotating the $0\nu\beta\beta$ diagram in Fig. 3.11, and they subsequently decay to two like-sign dileptons and two jets. However, since the relevant energy scale is $\mathcal{O}$(TeV), the requirement of observation at the LHC places several restrictions on models of neutrino mass. In the type I seesaw mechanism with TeV-scale right-handed neutrinos, tiny Dirac Yukawa couplings Y_D are required in order to suppress light neutrino mass [see Eqs. (2.11) and (2.15)]. A signal at the LHC is therefore unlikely, unless cancellations are at play [262–265],[15] which could be due to a flavour symmetry [263, 265], for example. In that case, if the Yukawas are large enough there could be other signatures such as modified Higgs decays [266–268]. A similar situation occurs in the inverse seesaw model, and bounds on Yukawa couplings have been derived in Ref. [269] using recent LHC data.

The situation is quite different in the type II seesaw model, since the Higgs triplet mass need not be large for neutrino mass to be small [see Eq. (2.37)]. The phenomenology is also richer due to the gauge couplings of Higgs triplets, which allow for both single and pair production

[15] See the analysis in Chapter 5 for an explicit example of this.

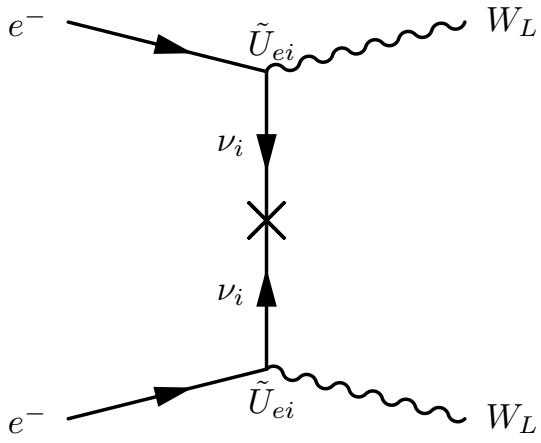

Figure 3.17: Lepton number violating inverse double beta decay, mediated by light Majorana neutrinos.

via charged and neutral gauge bosons [270–272], as long as the triplets are not too heavy. In addition, the striking signature of their decay into like-sign dileptons is related to the neutrino mass matrix [271, 273–275]. The latest results from ATLAS [276] give the exclusion limits $m_{\delta_L^{\pm\pm}} > 409$ GeV for $e^\pm e^\pm$ final states and assuming a branching ratio of 100% to each final state. For a comprehensive analysis of seesaw models at the LHC see Ref. [277].

The LRSM contains all the features of the type I and type II seesaw mechanisms, but the additional gauge symmetries allow production of heavy right-handed neutrinos via the right-handed W boson [11, 86, 87]. Furthermore, the new neutral gauge boson Z' could in principle be seen at the LHC [278], although the relation $m_{Z'} \simeq 1.7 m_{W_R}$ [see Eq. (2.63)] means that the cross sections for processes such as $pp \to Z' \to \ell^+\ell^-$ will be lower than those involving charged gauge bosons (see Ref. [279] for a review and further references). The latest ATLAS limits for the right-handed Higgs triplet are $m_{\delta_R^{\pm\pm}} > 322$ GeV [276]. Several authors have analysed the phenomenology of the LRSM at hadron colliders, see e.g., Refs. [278, 280–283]. The relationship between collider and $0\nu\beta\beta$ phenomenology in the LRSM will be discussed in Chapter 5.

3.7.2 Linear collider signatures

A linear collider provides an extremely clean environment to test lepton number violation, in comparison to $0\nu\beta\beta$, which suffers from nuclear physics uncertainties (cf. Table 3.3). Indeed, the process

$$e^- e^- \to W^- W^- , \tag{3.77}$$

shown in Fig. 3.17, directly tests the central part of the $0\nu\beta\beta$ diagram in Fig. 3.11, and has often been called inverse neutrinoless double beta decay. Observation at a linear collider running in like-sign electron mode would provide a cross-check for the mechanism of $0\nu\beta\beta$, and has been proposed by several authors in the past [284–296].

As discussed in the case of the LHC, the like-sign dilepton signature from the decay of Higgs triplets could also be seen at a linear collider. Here the relevant s-channel process is $e^- e^- \to \alpha\,\beta$, mediated by the doubly charged Higgs δ^{--}, which has been studied in Refs. [297, 298].

The direct connection to neutrino mass and LFV allows one to probe the couplings Y_Δ in Eq. (2.35).

The LRSM can also be studied at a linear collider, and the various diagrams that mediate $0\nu\beta\beta$ could in principle be tested: this topic will be discussed in detail in Chapter 5. At an e^+e^- collider the Z' could mediate new four fermion interactions, i.e., $e^+e^- \to Z' \to f\bar{f}$, and could be detected due to interference with the virtual γ and Z contributions [299]. In addition, the doubly charged components of the left- and right-handed Higgs triplets could be produced in e^+e^- collisions [275, 300].

3.7.3 Lepton flavour violation and dipole moments

The oscillation results presented in Section 3.1 show that lepton flavour is violated in the neutrino sector, implying new physics in the form of neutrino mass. However, the small active neutrino masses "GIM suppress" charged lepton flavour violating processes, making them experimentally inaccessible. For instance, the branching ratio for $\mu \to e\gamma$ mediated by light neutrinos is

$$\mathrm{BR}_{\mu\to e\gamma} = \frac{3\alpha}{32\pi}\left|\sum_i \tilde{U}^*_{\mu i}\tilde{U}_{ei}\frac{m_i^2}{m_{W_L}^2}\right|^2 \simeq \frac{3\alpha}{32\pi}\left(\frac{\Delta m^2_{\mathrm{A}}}{m^2_{W_L}}\right)^2 \simeq 10^{-52}\,, \tag{3.78}$$

where α is the fine-structure constant and Δm^2_{A} the atmospheric mass squared difference, and here $\tilde{U}$ is unitary. In seesaw models $\tilde{U}$ is no longer unitary [cf. Eq. 2.20], and the existence of heavy right-handed neutrinos and/or Higgs triplets allow the LFV decays $\mu \to e\gamma$ and $\mu \to 3e$ as well as $\mu \to e$ conversion in nuclei to occur at rates observable in current experiments.[16] Those decay rates will be proportional to similar combinations of mass and mixing parameters as the $0\nu\beta\beta$ amplitudes, thus providing complementary constraints. Defining

$$\Gamma_\nu \equiv \Gamma(\mu^- \to e^-\nu_\mu\bar{\nu}_e) \quad \text{and} \quad \Gamma_{\mathrm{capt}} \equiv \Gamma(\mu^- + \mathrm{A(Z,N)} \to \nu_\mu + \mathrm{A(Z-1,N+1)}), \tag{3.79}$$

the relevant branching ratios

$$\begin{aligned} \mathrm{BR}_{\mu\to e\gamma} &\equiv \frac{\Gamma(\mu^+ \to e^+\gamma)}{\Gamma_\nu}\,, \\ \mathrm{R}^A_{\mu\to e} &\equiv \frac{\Gamma(\mu^- + A(N,Z) \to e^- + A(N,Z))}{\Gamma_{\mathrm{capt}}}\,, \\ \mathrm{BR}_{\mu\to 3e} &\equiv \frac{\Gamma(\mu^+ \to e^+e^-e^+)}{\Gamma_\nu}\,, \end{aligned} \tag{3.80}$$

are constrained at 90% C.L. to[17]

$$\mathrm{BR}_{\mu\to e\gamma} < 2.4\times10^{-12}\ [302], \quad \mathrm{R}^{\mathrm{Au}}_{\mu\to e} < 7.0\times10^{-13}\ [303] \quad \text{and} \quad \mathrm{BR}_{\mu\to 3e} < 1.0\times10^{-12}\ [304]$$

by experiment. Future experiments aim for even greater precision: the MEG upgrade aims at a sensitivity of 6×10^{-14} for $\mu \to e\gamma$ [305], whereas the Mu3e experiment aims to get down to 10^{-16} for $\mu \to 3e$ [306]. The COMET and PRISM/PRIME experiments will constrain the rate of $\mu \to e$ conversion down to 10^{-16} [307] and 10^{-18} [308], respectively. A complementary test of the lepton flavour violating decay of the muon is via the process $\mu^-e^- \to e^-e^-$ in a muonic atom, proposed in Ref. [309].

[16] Tau decays are also searched for in experiments, but will not be analysed here.

[17] During the preparation of this thesis a stronger limit on the branching ratio for $\mu \to e\gamma$ was published [301], but the limit from Ref. [302] will be used in the analysis of Chapter 5.

A detailed discussion of LFV in the framework of the LRSM will be presented in Chapter 5. In that context another relevant observable is the dipole moment of the electron, which depends on similar parameters to $\mu \to e\gamma$. The current experimental limit is

$$|d_e| < 10^{-27}\, e \text{ cm [310]}.$$

3.7.4 Electroweak precision observables

The introduction of sterile neutrinos has several other consequences, mostly related to the non-unitarity of the lepton mixing matrix [311], shown explicitly in Eq. (2.19). Some examples include a modification of the invisible Z decay width, violation of the universality of lepton couplings, or additional contributions to the electroweak precision parameters. Those effects all constrain the magnitude of the active-sterile mixing (S), and were recently studied in Ref. [312]. However, for the most part it is the stringent bounds from LFV and $0\nu\beta\beta$ that constrain the elements of S the most, as will be seen in the analysis of Chapter 5.

3.8 Summary

The discussions and analyses of this chapter have shown that sterile neutrinos may be tested in a multitude of different physical processes, all of which constrain their mixing to the active sector. Although the standard three-neutrino oscillation framework described in Section 3.1 is well-established, the hints for eV-scale sterile neutrinos in short-baseline experiments remain. The cosmological data on N_{eff} seem to point in the same direction, but this is quite model dependent and more precision is required in order to draw any reliable conclusions. $0\nu\beta\beta$ processes are very sensitive to additional eV-scale sterile states: the effective mass can behave quite differently to the normal case. Heavier keV sterile neutrinos could explain dark matter, whereas even heavier particles could generate the required baryon asymmetry of the universe. The signatures of sterile neutrinos at the TeV scale are varied, ranging from collider signals to $0\nu\beta\beta$ and LFV.

The remainder of this thesis is devoted to (*i*) flavour symmetry models with light sterile neutrinos and (*ii*) a phenomenological analysis of lepton number and lepton flavour violation in the left-right symmetric model.

Chapter 4

Sterile neutrinos in flavour symmetry models

4.1 Introduction to flavour symmetries

The data in Table 3.1 summarise the current status of neutrino physics: the era of precision measurements has begun, with the aim of constraining the mixing parameters even further, determining the mass hierarchy and measuring CP violation. On the theoretical side, the majority of research in the past decade has centred on explaining the peculiar mixing in the neutrino sector [see Eq. (3.6)] by employing flavour symmetries [22, 313]. However, sterile neutrinos somewhat complicate the simple three-neutrino framework, and one needs to expand flavour symmetry models to take them into account. In addition, since many models predict $\theta_{13} = 0$ at the leading order, the recent evidence for non-zero θ_{13} requires that they be extended. This chapter will provide several examples of flavour symmetry models, modified to include sterile neutrinos at different mass scales.

The SM symmetries discussed in Section 2.1 do not constrain the form of the mass matrices: M_ℓ is an arbitrary 3×3 matrix and m_ν must be symmetric if neutrinos are Majorana particles. The idea of flavour symmetries is to extend the SM by a so-called flavour (or family) symmetry, i.e.,

$$G = SU(3)_C \otimes SU(2)_L \otimes U(1)_Y \otimes G_{\text{family}} \,, \tag{4.1}$$

so that invariance under G_{family} leads to further restrictions on the mass matrices. By assigning the lepton doublets and singlets to different representations of the symmetry group one obtains specific matrix structures once the symmetry is broken. Models in the literature look to find an underlying symmetry that can explain the pattern of neutrino mixing, in a sense employing a "bottom-up" approach. A popular starting point is the TBM pattern,

$$U_{\text{TBM}} \equiv \begin{pmatrix} \frac{2}{\sqrt{6}} & \frac{1}{\sqrt{3}} & 0 \\ -\frac{1}{\sqrt{6}} & \frac{1}{\sqrt{3}} & -\frac{1}{\sqrt{2}} \\ -\frac{1}{\sqrt{6}} & \frac{1}{\sqrt{3}} & \frac{1}{\sqrt{2}} \end{pmatrix} \simeq \begin{pmatrix} 0.816 & 0.577 & 0. \\ -0.408 & 0.577 & -0.707 \\ -0.408 & 0.577 & 0.707 \end{pmatrix} , \tag{4.2}$$

proposed in Ref. [314], which implies

$$\sin^2\theta_{12} = \frac{1}{3} \,, \quad \sin^2\theta_{23} = \frac{1}{2} \quad \text{and} \quad \sin^2\theta_{13} = 0 \,, \tag{4.3}$$

for the neutrino mixing angles. However, comparison with Eq. (3.6) shows that the TBM hypothesis is ruled out, primarily because $\theta_{13} \neq 0$. This has led to other alternatives being considered in the literature, see for instance Ref. [315]. Several authors have also performed scans over discrete groups in order to find candidates that fit the data [316–318].

The leading-order TBM prediction could be modified by higher-order effects, such as those from NLO operators or VEV misalignment [319]. Corrections to the leptonic mixing pattern could also arise from the charged lepton sector [cf. Eq. (2.20)] or from renormalisation group

Table 4.1: Classification of A_4 models in the literature, simplified from Ref. [28]. Lepton doublets, charged lepton singlets and right-handed neutrinos are denoted by L_i, ℓ_i^c and ν_i^c, respectively.

Type	L_i	ℓ_i^c	ν_i^c	Examples
A	$\underline{3}$	$\underline{1}$, $\underline{1}'$, $\underline{1}''$	$\cdots$	[328, 329]
B	$\underline{3}$	$\underline{1}$, $\underline{1}'$, $\underline{1}''$	$\underline{3}$	[330, 331]
E	$\underline{3}$	$\underline{3}$	$\underline{1}$, $\underline{1}'$, $\underline{1}''$	[332, 333]
G	$\underline{3}$	$\underline{1}$, $\underline{1}'$, $\underline{1}''$	$\underline{1}$, $\underline{1}'$, $\underline{1}''$	[334]
I	$\underline{3}$	$\underline{1}$, $\underline{1}$, $\underline{1}$	$\underline{1}$, $\underline{1}$, $\underline{1}$	[335]

running [320–322]. On the other hand, since the parameters in Eq. (3.6) are all roughly order one, it is conceivable that neutrino mixing does not originate from a symmetry at all: the anarchy hypothesis [323, 324]. In that case one obtains no concrete predictions, barring a parameterisation-dependent probability distribution for the elements of $\tilde{U}$. This idea has received recent attention due to evidence for non-zero θ_{13} [325], and has also been extended to the sterile neutrino case in Ref. [326]. There have even been attempts at combining anarchy and symmetry in specific models, e.g., Ref. [327]. One could argue as to whether the order one "random" mixing in the lepton sector is more natural than the small mixing in the quark sector. Nevertheless, the idea that some underlying symmetry is behind the observed fermion mixing patterns still seems more appealing, and that approach will be followed here.

A_4 models accommodating light (eV-scale) as well as keV-scale sterile neutrinos will be discussed in Section 4.2. Flavour symmetries are introduced to explain the observed mixing parameters, but in most cases mass scales and hierarchies remain free parameters. One way to explain the charged lepton mass hierarchy is the Froggatt-Nielsen (FN) mechanism [59], already mentioned in Section 2.2.1. In the models in Section 4.2 the FN mechanism will be used for both the charged lepton and sterile neutrino mass hierarchies. In Section 4.2.2 the original model from Ref. [328] is outlined and then modified, following Ref. [99]. As mentioned before, the seesaw model in Section 4.2.3 (based on Ref. [29]) is the first of its kind in the literature. In Section 4.3 an S_3 flavour symmetry model for the bimodal scenario is briefly outlined, following Ref. [31]. The phenomenology of this interesting and exotic case for $0\nu\beta\beta$ and astrophysical flavour ratios has already been described in Sections 3.4.3 and 3.5.2, respectively.

4.2 A_4 models with light sterile neutrinos

4.2.1 Introduction to A_4 symmetry

The non-Abelian discrete symmetry group A_4 is the smallest group that contains a three dimensional irreducible representation, which is one of the main reasons it has been employed as a symmetry group for leptons. A discussion of the relevant group theory aspects can be found in Appendix B. Its connection to TBM can be seen from the fact that the most general mass matrix leading to TBM is invariant under one of the generators of the group, see Eq. (B.7). The economical structure of A_4 models has led to their relative popularity in the literature: around 100 papers have been devoted to this topic. For that reason a classification table for

A_4 models has been drawn up in Ref. [28] (see also Ref. [336]); a simplified version is shown in Table 4.1, with several categories and subcategories omitted. The models presented here belong to category G, since right-handed neutrinos need to be in singlet representations in order to separate their mass scales.

Before discussing A_4 models it should be noted that the symmetry group needs to be broken in a specific way in order to generate TBM. Explicitly, the group should be broken down to Z_3 in the charged lepton sector and Z_2 in the neutrino sector, implying particular symmetry-breaking vacua as well as a separation between the neutral and charged sectors. It turns out that one requires two triplet flavons with different VEV alignments, and in the end those alignments are not a natural minimum of the scalar potential. This is the so-called "vacuum alignment problem", for which several solutions have been proposed. Some of those include extra-dimensional models, where the flavons are localised on different branes [328], or supersymmetric models with an additional R-symmetry [331]. Extensions of the flavour group provide another solution [337, 338]. This general problem will not be tackled here, since the focus is on including sterile neutrinos in existing flavour models.

In the following section a popular A_4 model is modified in order to accommodate one or two eV-scale sterile neutrinos; the resulting deviations from exact TBM as well as the effect of higher-order operators will be discussed. keV sterile neutrinos, which could be a candidate for WDM, will also be added to the same model. Section 4.2.3 details an A_4 seesaw model with one of the three right-handed neutrinos at the keV scale. Various cases for the mass scales of the other two neutrinos are discussed, along with the resulting phenomenological consequences. The role of higher-order corrections is described in detail, both here and in Appendix C.

4.2.2 An effective A_4 model with sterile neutrinos

Original model

In the Altarelli-Feruglio A_4 model [328], neutrinos get mass from effective operators [cf. Eq. (2.8)], and the judicious choice of particle and flavon content along with the correct VEV alignment leads to TBM, at leading order. The relevant particle assignments are shown in Table 4.2, where the additional Z_3 symmetry separates the neutrino and charged lepton sectors, and the $U(1)_{\mathrm{FN}}$ symmetry reproduces the charged lepton mass hierarchy via the FN mechanism, with the FN charges F_ℓ ($\ell = e, \mu, \tau$) assigned to the right-handed charged leptons. The additional sterile neutrino ν_s with FN charge F_ν will be discussed below.

The particle assignments along with the A_4 multiplication rules (see Appendix B) lead to the A_4-invariant Lagrangian

$$\begin{aligned}\mathcal{L}_{\mathrm{Y}} = {} & \frac{y_e}{\Lambda}\lambda^{F_e} e^c (\varphi L) h_d + \frac{y_\mu}{\Lambda}\lambda^{F_\mu} \mu^c (\varphi L)' h_d + \frac{y_\tau}{\Lambda}\lambda^{F_\tau} \tau^c (\varphi L)'' h_d \\ & + \frac{x_a}{\Lambda^2}\xi (L h_u L h_u) + \frac{x_d}{\Lambda^2}(\varphi' L h_u L h_u) + \text{h.c.} + \ldots ,\end{aligned} \tag{4.4}$$

where Λ is the cut-off scale and the dots stand for higher-dimensional operators. The notation $(ab)'$ means that the product of the fields a and b transforms as $\underline{1}'$, which will be used from now on. $\lambda \equiv \langle\Theta\rangle/\Lambda < 1$ is the FN suppression parameter, where Λ is assumed to be the cut-off scale of both the A_4 and $U(1)_{\mathrm{FN}}$ symmetries. If one chooses the real basis for A_4 (see Appendix B), along with the flavon VEV alignments[1] $\langle\xi\rangle = u$, $\langle\varphi\rangle = (v, 0, 0)$ and $\langle\varphi'\rangle = (v', v', v')$, then the

[1] Note that the model contains two Higgs doublets for the up- and down-sector, respectively, and therefore can be accommodated within supersymmetry. The VEV alignment could in that case be arranged by "driving fields" [331]. In the SM $h_u = i\sigma_2 h_d^*$, see Eq. (2.1).

Table 4.2: Particle assignments of the A_4 model, modified from Ref. [328] to include a sterile neutrino ν_s. The additional Z_3 symmetry decouples the charged lepton and neutrino sectors; the $U(1)_{\rm FN}$ charge generates the hierarchy of charged lepton masses and regulates the scale of the sterile state.

Field	L	e^c	μ^c	τ^c	$h_{u,d}$	φ	φ'	ξ	Θ	ν_s
$SU(2)_L$	2	1	1	1	2	1	1	1	1	1
A_4	$\underline{3}$	$\underline{1}$	$\underline{1}''$	$\underline{1}'$	$\underline{1}$	$\underline{3}$	$\underline{3}$	$\underline{1}$	$\underline{1}$	$\underline{1}$
Z_3	ω	ω^2	ω^2	ω^2	1	1	ω	ω	1	1
$U(1)_{FN}$	-	F_e	F_μ	F_τ	-	-	-	-	-1	F_ν

charged lepton mass matrix is diagonal, whereas the neutrino mass matrix,

$$m_\nu = \frac{v_u^2}{\Lambda}\begin{pmatrix} a' + \frac{2d'}{3} & -\frac{d'}{3} & -\frac{d'}{3} \\ \cdot & \frac{2d'}{3} & a' - \frac{d'}{3} \\ \cdot & \cdot & \frac{2d'}{3} \end{pmatrix}, \tag{4.5}$$

is diagonalised by the TBM matrix in Eq. (4.2). Here $a' = 2x_a\frac{u}{\Lambda}$ and $d' = 2x_d\frac{v'}{\Lambda}$, and the light active neutrino masses are

$$m_1 = a' + d', \quad m_2 = a', \quad m_3 = a' - d', \tag{4.6}$$

This means that m_ν is form-diagonalisable: the eigenvectors are independent of the parameters in the neutrino mass matrix, and there is a sum rule between the light masses, $2m_2 = m_1 + m_3$ [339].

The charged lepton mass hierarchy is generated by the FN mechanism: the negative unit of $U(1)_{\rm FN}$ charge carried by the flavon Θ suppresses each mass term by powers of the small parameter $\langle\Theta\rangle/\Lambda = \lambda < 1$. Explicitly,

$$m_\ell = y_\ell v_d \frac{v}{\Lambda}\lambda^{F_\ell}, \tag{4.7}$$

where F_ℓ is the relevant $U(1)_{\rm FN}$ charge. The relevant mass scales are obtained by assuming that (*i*) the Yukawa couplings y_ℓ, x_a and x_d remain in the perturbative regime; (*ii*) the flavon VEVs are smaller than the cut-off scale and (*iii*) all flavon VEVs fall in approximately the same range, which leads to the relation [328]

$$0.004 < \frac{v'}{\Lambda} \simeq \frac{v}{\Lambda} \simeq \frac{u}{\Lambda} < 1, \tag{4.8}$$

with the cut-off scale Λ ranging between 10^{12} and 10^{15} GeV, and $v_u \simeq 174$ GeV. As an explicit example, if one assumes that $v'/\Lambda \approx v/\Lambda \approx u/\Lambda \simeq 10^{-1.5}$, in keeping with the constraints from Eq. (4.8), and that the cut-off scale is $\Lambda \simeq 10^{12.5}$ GeV, the charged lepton masses are

$$m_\ell = y_\ell v_d \frac{v}{\Lambda}\lambda^{F_\ell} \simeq 3\left(\frac{v_d}{10^2\ \text{GeV}}\right)\left(\frac{v}{10^{11}\ \text{GeV}}\right)\left(\frac{10^{12.5}\ \text{GeV}}{\Lambda}\right)\left(\frac{\lambda}{10^{-1.5}}\right)^{F_\ell}\ \text{GeV}, \tag{4.9}$$

where $\lambda \simeq 10^{-1.5}$ means that $\langle\Theta\rangle$ is in the same range as the other flavon VEVs. The $U(1)_{\rm FN}$ charges $F_{e,\mu,\tau} = (3,1,0)$ result in the correct mass spectrum, with $y_\ell = \mathcal{O}(1)$. The light neutrino

mass scale is roughly

$$\frac{v_u^2}{\Lambda}a' \simeq \frac{v_u^2}{\Lambda}d' \simeq 0.1\left(\frac{u}{10^{11}\text{ GeV}}\right)\left(\frac{v_u}{10^2\text{ GeV}}\right)^2\left(\frac{10^{12.5}\text{ GeV}}{\Lambda}\right)^2\text{ eV}\,, \tag{4.10}$$

with $\mathcal{O}(1)$ Yukawa couplings.

The leading order TBM prediction of the model depends on the triplet VEV alignments in the scalar sector. In the general case [28, 340], those alignments could be modified to $\langle\varphi\rangle = (v, v\,\epsilon_1^{\text{ch}}, v\,\epsilon_2^{\text{ch}})$ and $\langle\varphi'\rangle = (v', v'(1+\epsilon_1), v'(1+\epsilon_2))$, where the deviation parameters come from higher-dimensional operators or renormalisation group effects. Mixing angles will then receive corrections of the same order, proportional to $\epsilon_{1,2}^{\text{ch}}$ and $\epsilon_{1,2}$. The effects of next-to-leading order (NLO) operators, suppressed by additional powers of the cut-off scale Λ, will be considered below, following Ref. [331].

In the charged lepton sector, corrections to M_ℓ come from terms like

$$\frac{1}{\Lambda^2}\left[y'_e\lambda^{F_e}\left(\varphi\varphi L h_d\right)e^c + y'_\mu\lambda^{F_\mu}\left(\varphi\varphi L h_d\right)'\mu^c + y'_\tau\lambda^{F_\tau}\left(\varphi\varphi L h_d\right)''\tau^c\right], \tag{4.11}$$

which replicate the leading order patterns and can thus be simply absorbed into the coefficients y_ℓ. The higher-order operators contributing to light neutrino masses are of order $1/\Lambda^3$. There exist only three such terms that cannot be absorbed by a redefinition of the parameters a' and d' [331], *viz.*

$$\frac{x_1}{\Lambda^3}(\varphi\varphi')'(Lh_uLh_u)''\,, \quad \frac{x_2}{\Lambda^3}(\varphi\varphi')''(Lh_uLh_u)'\,, \quad \text{and} \quad \frac{x_3}{\Lambda^3}\xi(\varphi Lh_uLh_u)\,, \tag{4.12}$$

so that the light neutrino mass matrix is modified to

$$m_\nu = m_\nu^{(0)} + m_\nu^{(1)} = \begin{pmatrix} a' + \frac{2d'}{3} & -\frac{d'}{3} & -\frac{d'}{3} \\ \cdot & \frac{2d'}{3} & a' - \frac{d'}{3} \\ \cdot & \cdot & \frac{2d'}{3} \end{pmatrix} + \begin{pmatrix} \frac{2}{3}\eta_3 & \eta_2 & \eta_1 \\ \cdot & \eta_1 & -\frac{1}{3}\eta_3 \\ \cdot & \cdot & \eta_2 \end{pmatrix}, \tag{4.13}$$

where $\eta_1 = 2x_1\frac{vv'v_u^2}{\Lambda^3}$, $\eta_2 = 2x_2\frac{vv'v_u^2}{\Lambda^3}$ and $\eta_3 = 2x_3\frac{uvv_u^2}{\Lambda^3}$. The η_i terms are a factor of $v/\Lambda \simeq 0.03$ smaller than the terms in Eq. (4.10). The neutrino masses become

$$\begin{aligned} m_1 &\simeq a' + d' - \frac{1}{2}(\eta_1+\eta_2) + \frac{1}{3}\eta_3\,, \\ m_2 &\simeq a' + \eta_1 + \eta_2\,, \\ m_3 &\simeq -a' + d' + \frac{1}{2}(\eta_1+\eta_2) + \frac{1}{3}\eta_3\,, \end{aligned} \tag{4.14}$$

to first order in η_i, and the corrected mixing angles are

$$\sin^2\theta_{13} \simeq \frac{(\eta_1-\eta_2)^2}{8a'^2}\,, \quad \sin^2\theta_{12} \simeq \frac{1}{3}\left(1 - \frac{2\eta_3}{3d'}\right), \quad \sin^2\theta_{23} \simeq \frac{1}{2}\left(1 - \frac{\eta_1-\eta_2}{4a'}\right). \tag{4.15}$$

It is possible to find numerical values that generate a large enough value of θ_{13}, although one must carefully choose the relative signs of η_1 and η_2. In the following the focus will be on introducing one or more sterile neutrino(s) into the model.

One eV sterile neutrino

It is possible to add an additional sterile singlet, ν_s,[2] transforming as $\underline{1}$ under A_4 and 1 under Z_3 (see Table 4.2). The A_4 invariant dimension-5 operator $\frac{1}{\Lambda}(\varphi' L h_u)\nu_s$ is not allowed by the Z_3 symmetry; the remaining terms are

$$\mathcal{L}_{\mathrm{Y}_s} = \frac{x_e}{\Lambda^2}\lambda^{F_\nu}\xi(\varphi' L h_u)\nu_s + \frac{x_f}{\Lambda^2}\lambda^{F_\nu}(\varphi'\varphi' L h_u)\nu_s + m_s\lambda^{2F_\nu}\nu_s^c\nu_s + \text{h.c.}, \tag{4.16}$$

where for now m_s is a bare Majorana mass. The modified 4×4 mass matrix is [cf. Eq. (4.5)]

$$M_\nu^{4\times 4} = \begin{pmatrix} a+\frac{2d}{3} & -\frac{d}{3} & -\frac{d}{3} & e \\ \cdot & \frac{2d}{3} & a-\frac{d}{3} & e \\ \cdot & \cdot & \frac{2d}{3} & e \\ \cdot & \cdot & \cdot & m_s \end{pmatrix}, \tag{4.17}$$

where $a = 2x_a\frac{uv_u^2}{\Lambda^2}$, $d = 2x_d\frac{v'v_u^2}{\Lambda^2}$ and $e = \sqrt{2}x_e\frac{uv'v_u}{\Lambda^2}$ have dimensions of mass. Note that the first three elements of the fourth row of $M_\nu^{4\times 4}$ are identical because of the VEV alignment $\langle\varphi'\rangle = (v', v', v')$, which was necessary to generate TBM in the 3 neutrino case; that alignment combined with the A_4 multiplication rules also causes the second term in Eq. (4.16) (proportional to x_f) to vanish.[3]

With the mass scales discussed above one obtains $a \simeq d \simeq 0.1$ eV, as before, as well as

$$e \simeq 0.1\left(\frac{\lambda}{10^{-1.5}}\right)^6\left(\frac{u}{10^{11}\text{ GeV}}\right)\left(\frac{v'}{10^{11}\text{ GeV}}\right)\left(\frac{v_u}{10^2\text{ GeV}}\right)\left(\frac{10^{12.5}\text{ GeV}}{\Lambda}\right)^2\text{ eV}, \tag{4.18}$$

again with the assumption that the Yukawa couplings $x_{a,d,e}$ are of order 1. The $U(1)_{\mathrm{FN}}$ charge of $F_\nu = 6$ has been assigned to ν_s, in analogy to the mechanism used in the charged lepton sector. Indeed, in order to fit the data, the parameters a and d should be between 10^{-3} and 10^{-1} eV, the ratio $e/m_s = \mathcal{O}(10^{-1})$ to generate sufficient mixing, and $m_s \simeq 1$ eV for the sterile neutrino mass. The Majorana mass term $m_s\lambda^{2F_\nu}\nu_s^c\nu_s$ is doubly suppressed by the $U(1)_{\mathrm{FN}}$ charge, and the leading order contribution is

$$\frac{x_s}{\Lambda}(\varphi\varphi)\lambda^{2F_\nu}\nu_s^c\nu_s \Longrightarrow x_s\frac{v^2}{\Lambda}\lambda^{2F_\nu}, \tag{4.19}$$

resulting in a Majorana mass of order eV, i.e.,

$$m_s \simeq 10^{0.5}\left(\frac{\lambda}{10^{-1.5}}\right)^{12}\left(\frac{v}{10^{11}\text{ GeV}}\right)^2\left(\frac{10^{12.5}\text{ GeV}}{\Lambda}\right)\text{ eV}. \tag{4.20}$$

This shows that usual choice of scales and charges easily allows $a \simeq d \simeq e < m_s$ in the mass matrix in Eq. (4.17); higher-order terms will be discussed below.

Assuming that the parameters are all real, Eq. (4.17) is exactly diagonalised by

$$U = \begin{pmatrix} \frac{2}{\sqrt{6}} & \frac{1}{6e}\frac{K_-}{N_-} & 0 & \frac{1}{6e}\frac{K_+}{N_+} \\ -\frac{1}{\sqrt{6}} & \frac{1}{6e}\frac{K_-}{N_-} & -\frac{1}{\sqrt{2}} & \frac{1}{6e}\frac{K_+}{N_+} \\ -\frac{1}{\sqrt{6}} & \frac{1}{6e}\frac{K_-}{N_-} & \frac{1}{\sqrt{2}} & \frac{1}{6e}\frac{K_+}{N_+} \\ 0 & \frac{1}{N_-} & 0 & \frac{1}{N_+} \end{pmatrix}, \tag{4.21}$$

[2] The notation in this chapter conforms to that usually employed in flavour symmetry models, and primes for flavour eigenstates are omitted.

[3] Since no additional flavons are introduced, one can assume that the solution of the VEV alignment problem remains valid.

where $K_\pm = a - m_s \pm \sqrt{12e^2 + (a-m_s)^2}$ and $N_\pm^2 = 1 + \frac{\left(a-m_s\pm\sqrt{12e^2+(a-m_s)^2}\right)^2}{12e^2}$. For $a < m_s$, expansion in e/m_s results in the mixing matrix

$$U \simeq \begin{pmatrix} \frac{2}{\sqrt{6}} & \frac{1}{\sqrt{3}} & 0 & 0 \\ -\frac{1}{\sqrt{6}} & \frac{1}{\sqrt{3}} & -\frac{1}{\sqrt{2}} & 0 \\ -\frac{1}{\sqrt{6}} & \frac{1}{\sqrt{3}} & \frac{1}{\sqrt{2}} & 0 \\ 0 & 0 & 0 & 1 \end{pmatrix} + \begin{pmatrix} 0 & 0 & 0 & \frac{e}{m_s} \\ 0 & 0 & 0 & \frac{e}{m_s} \\ 0 & 0 & 0 & \frac{e}{m_s} \\ 0 & -\frac{\sqrt{3}e}{m_s} & 0 & 0 \end{pmatrix} + \begin{pmatrix} 0 & -\frac{\sqrt{3}e^2}{2m_s^2} & 0 & 0 \\ 0 & -\frac{\sqrt{3}e^2}{2m_s^2} & 0 & 0 \\ 0 & -\frac{\sqrt{3}e^2}{2m_s^2} & 0 & 0 \\ 0 & 0 & 0 & -\frac{3e^2}{2m_s^2} \end{pmatrix}, \tag{4.22}$$

giving the eigenvalues

$$m_1 = a + d\,, \quad m_2 = a - \frac{3e^2}{m_s}\,, \quad m_3 = -a + d\,, \quad m_4 = m_s + \frac{3e^2}{m_s}\,. \tag{4.23}$$

It is evident that $M_\nu^{4\times4}$ is not form-diagonalisable anymore: the second and fourth column of U are sensitive to the entries of $M_\nu^{4\times4}$. The sum rule between light active neutrino masses will be violated, leading to different predictions for $0\nu\beta\beta$ [339]. The mass-squared differences as well as the active-sterile mixing angles $\sin^2\theta_{i4}$ $(i = 1, 2, 3)$ are controlled by the four parameters in Eq. (4.17), with the mixing most sensitive to the ratio e/m_s. Note that both the normal and inverted orderings are allowed, in contrast to the standard three neutrino version of the model, which only allowed the normal ordering. By fitting the parameters a, d, e and m_s to the allowed range of the four parameters $\Delta m^2_{\rm S}$, $\Delta m^2_{\rm A}$, Δm^2_{41} and $\sin^2\theta_{14}$, one can show that the masses are arbitrary, are not constrained to any particular region, and are in general uncorrelated with the mixing parameters. However, the lightest mass increases with $\sin^2\theta_{14}$, which means that the effective mass in $0\nu\beta\beta$, $|\langle m_{ee}\rangle| \equiv \left|a + \frac{2d}{3}\right|$, also increases with $\sin^2\theta_{14}$, as expected from Eq. (3.28). Fig. 4.1 shows the allowed ranges of a, d, e. In general, a and d are approximately inversely proportional to each other.

Comparison of Eqs. (3.8) and (4.22), shows that $\sin\theta_{13} = 0$, i.e., this parameter retains its TBM value, whereas $\sin^2\theta_{12}$ and $\sin^2\theta_{23}$ receive small corrections:[4]

$$\begin{aligned} \sin^2\theta_{12} &= \frac{|U_{e2}|^2}{1-|U_{e4}|^2} \simeq \frac{1}{3}\left[1 - 2\left(\frac{e}{m_s}\right)^2\right], \\ \sin^2\theta_{23} &= \frac{|U_{\mu3}|^2(1-|U_{e4}|^2)}{1-|U_{e4}|^2-|U_{\mu4}|^2} \simeq \frac{1}{2}\left[1 + \left(\frac{e}{m_s}\right)^2\right]. \end{aligned} \tag{4.24}$$

Note the correlation $\sin^2\theta_{23} \simeq \frac{3}{4}(1-\sin^2\theta_{12})$ following from the above expressions. Other results of the model are $U_{s1} = U_{s3} = 0$ and $U_{e4} = U_{\mu4} = U_{\tau4}$. The three active-sterile mixing angles can be expressed in terms of the matrix elements $U_{\ell4}$ as

$$\sin^2\theta_{14} = |U_{e4}|^2\,, \quad \sin^2\theta_{24} = \frac{|U_{\mu4}|^2}{1-|U_{e4}|^2}\,, \quad \sin^2\theta_{34} = \frac{|U_{\tau4}|^2}{1-|U_{e4}|^2-|U_{\mu4}|^2}\,, \tag{4.25}$$

and the model predicts them all to be of similar magnitude:

$$\sin^2\theta_{14} \simeq \sin^2\theta_{24} \simeq \sin^2\theta_{34} \simeq \left(\frac{e}{m_s}\right)^2 \simeq \frac{1}{2}(1 - 3\sin^2\theta_{12}) \simeq 2\sin^2\theta_{23} - 1\,, \tag{4.26}$$

to second order in the ratio e/m_s. The correlation [see Eqs. (4.24) and (4.26)] between the solar and atmospheric mixing parameters ($\sin^2\theta_{12}$ and $\sin^2\theta_{23}$) and the active-sterile mixing parameter ($\sin^2\theta_{14}$) is shown in Fig. 4.2, and is the same for both mass orderings.

[4] Since the charged lepton sector is diagonal, $V_L^\ell = \mathbb{1}$ so that $U = \tilde{U}$.

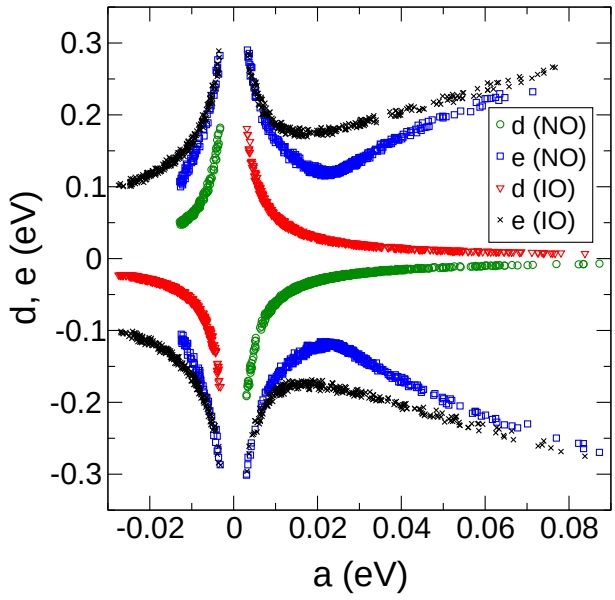

Figure 4.1: The allowed values in $a-d$ and $a-e$ parameter space for normal (NO) and inverted (IO) ordering, obtained by varying each parameter between -0.5 and 0.5 eV, varying m_s between -1.5 and 1.5 eV, and requiring that the oscillation parameters lie in the correct range [153, 341].

In the general sense, small mixing with sterile neutrinos will modify active mixing angles. The active-sterile mixing is of order e/m_s, where e is any of the entries $(M_\nu^{4\times4})_{\ell s}$ with $\ell = e, \mu, \tau$. Deviations from initial mixing angles $\theta_{12,13,23}$ are then of the same order. Although the example discussed here has the particular feature that $U_{e4} = U_{\mu4} = U_{\tau4}$ and that the first and third row of U are identical to TBM (see the discussion in Section B.2), this will be different in other cases.

Higher-order operators modify both active and sterile sectors; the former have been discussed above. The NLO corrections to m_s are given by

$$\left(\frac{x_{s'}}{\Lambda^2}\xi\xi\xi + \frac{x_{s''}}{\Lambda^2}(\varphi'\varphi')\xi\right)\lambda^{2F_\nu}\nu_s^c\nu_s^c \Longrightarrow \left(x_{s'}\frac{u^3}{\Lambda^2} + x_{s''}\frac{3v'^2u}{\Lambda^2}\right)\lambda^{2F_\nu}\,, \tag{4.27}$$

which for the scales chosen above give contributions of $\mathcal{O}(0.1)$ eV, thus not significantly affecting the scale of m_s [cf. Eq. (4.20)]. Note that the term proportional to $(\varphi'\varphi'\varphi')\nu_s^c\nu_s^c$ is in principle also allowed, but vanishes after A_4 symmetry breaking, just like the x_f term in Eq. (4.16). Next-to-leading order corrections to the e parameter come from terms like

$$\frac{x'_e}{\Lambda^3}\lambda^{F_\nu}\xi(\varphi'\varphi L h_u)\nu_s\,, \tag{4.28}$$

which lead to

$$e' \simeq 0.01\left(\frac{\lambda}{10^{-1}}\right)^8\left(\frac{u\,v'}{(10^{10}\text{ GeV})^2}\right)\left(\frac{v}{10^{11}\text{ GeV}}\right)\left(\frac{v_u}{10^2\text{ GeV}}\right)\left(\frac{10^{12}\text{ GeV}}{\Lambda}\right)^3\text{ eV}\,, \tag{4.29}$$

indicating that the active-sterile mixing [Eq. (4.26)] is hardly affected.

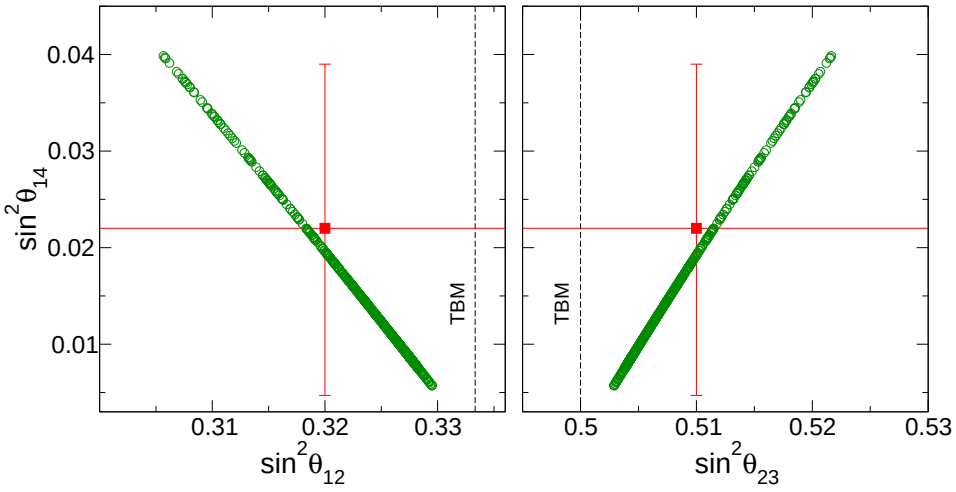

Figure 4.2: $\sin^2\theta_{14}$ against $\sin^2\theta_{12}$ and $\sin^2\theta_{23}$, for both the normal and inverted ordering. The dashed (black) lines corresponds to the TBM values of $\sin^2\theta_{12}$ and $\sin^2\theta_{23}$, the solid (red) lines indicate the 2σ ranges of the parameters and the (red) square is the best-fit point [153, 341].

Two eV sterile neutrinos

In order to have two sterile neutrinos in the A_4 model one can simply add a second sterile singlet ν_{s_2}, which is a singlet $\underline{1}$ under A_4 and 1 under Z_3, and carries the $U(1)_{\rm FN}$ charge $F_\nu = 6$, as before. In the basis where the sterile sector of the mass matrix is diagonal, the symmetric 5×5 mass matrix is

$$M_\nu^{5\times5} = \begin{pmatrix} a+\frac{2d}{3} & -\frac{d}{3} & -\frac{d}{3} & e & f \\ \cdot & \frac{2d}{3} & a-\frac{d}{3} & e & f \\ \cdot & \cdot & \frac{2d}{3} & e & f \\ \cdot & \cdot & \cdot & m_{s_1} & 0 \\ \cdot & \cdot & \cdot & \cdot & m_{s_2} \end{pmatrix}. \tag{4.30}$$

Note that one always has the freedom to work in this basis, since the rotations between sterile states are unphysical in this case, and mixing in the sterile sector can be absorbed by redefining e and f. Since f and m_{s_2} arise in the same way as e and m_s in the case of one sterile neutrino, one expects that e and f, as well as m_{s_1} and m_{s_2}, are each of similar magnitude, respectively. In analogy to the case discussed in the previous subsection, the mass matrix is approximately

diagonalised by

$$U = \begin{pmatrix} \frac{2}{\sqrt{6}} & \frac{1}{\sqrt{3}} & 0 & 0 & 0 \\ -\frac{1}{\sqrt{6}} & \frac{1}{\sqrt{3}} & -\frac{1}{\sqrt{2}} & 0 & 0 \\ -\frac{1}{\sqrt{6}} & \frac{1}{\sqrt{3}} & \frac{1}{\sqrt{2}} & 0 & 0 \\ 0 & 0 & 0 & 1 & 0 \\ 0 & 0 & 0 & 0 & 1 \end{pmatrix} + \begin{pmatrix} 0 & 0 & 0 & \frac{e}{m_{s_1}} & \frac{f}{m_{s_2}} \\ 0 & 0 & 0 & \frac{e}{m_{s_1}} & \frac{f}{m_{s_2}} \\ 0 & 0 & 0 & \frac{e}{m_{s_1}} & \frac{f}{m_{s_2}} \\ 0 & -\frac{\sqrt{3}e}{m_{s_1}} & 0 & 0 & 0 \\ 0 & -\frac{\sqrt{3}f}{m_{s_2}} & 0 & 0 & 0 \end{pmatrix} + \begin{pmatrix} 0 & -\frac{\sqrt{3}}{2}\left(\frac{e^2}{m_{s_1}^2} + \frac{f^2}{m_{s_2}^2}\right) & 0 & 0 & 0 \\ 0 & -\frac{\sqrt{3}}{2}\left(\frac{e^2}{m_{s_1}^2} + \frac{f^2}{m_{s_2}^2}\right) & 0 & 0 & 0 \\ 0 & -\frac{\sqrt{3}}{2}\left(\frac{e^2}{m_{s_1}^2} + \frac{f^2}{m_{s_2}^2}\right) & 0 & 0 & 0 \\ 0 & 0 & 0 & -\frac{3e^2}{2m_{s_1}^2} & -\frac{3ef}{2m_{s_1}m_{s_2}} \\ 0 & 0 & 0 & -\frac{3ef}{2m_{s_1}m_{s_2}} & -\frac{3f^2}{2m_{s_2}^2} \end{pmatrix}, \tag{4.31}$$

assuming that $a < m_{s_{1,2}}$ and that the ratios e/m_{s_1} and f/m_{s_2} are small. The mass eigenvalues are

$$\begin{aligned} m_1 &= a + d\,, \quad m_2 = a - \frac{3e^2}{m_{s_1}} - \frac{3f^2}{m_{s_2}}\,, \quad m_3 = -a + d\,, \\ m_4 &= m_{s_1} + \frac{3e^2}{m_{s_1}}\,, \quad m_5 = m_{s_2} + \frac{3f^2}{m_{s_2}}\,, \end{aligned} \tag{4.32}$$

to second order in the ratios e/m_{s_1} and f/m_{s_2}.

Once again, the reactor mixing angle retains its TBM value, and the predictions for $\sin^2\theta_{12}$ and $\sin^2\theta_{23}$ are

$$\begin{aligned} \sin^2\theta_{12} &\simeq \frac{1}{3}\left[1 - 2\left(\left(\frac{e}{m_{s_1}}\right)^2 + \left(\frac{f}{m_{s_2}}\right)^2\right)\right], \\ \sin^2\theta_{23} &\simeq \frac{1}{2}\left[1 + \left(\frac{e}{m_{s_1}}\right)^2 + \left(\frac{f}{m_{s_2}}\right)^2\right], \end{aligned} \tag{4.33}$$

in analogy to the 4×4 case. Using the explicit parameterisation [Eq. (3.11)] of the 5×5 mixing matrix, the six active-sterile mixing angles can be approximated by

$$\sin^2\theta_{i4} \simeq \left(\frac{e}{m_{s_1}}\right)^2, \quad \sin^2\theta_{i5} \simeq \left(\frac{f}{m_{s_2}}\right)^2 \quad (i = 1, 2, 3)\,, \tag{4.34}$$

with the additional assumption that U is real.

One keV sterile neutrino

It is straightforward to recast the model above in the context of keV sterile neutrino WDM rather than eV-scale sterile neutrinos. With the same particle assignments as in Table 4.2, the $U(1)_{\rm FN}$ charge of $F_\nu = 8$ and the correct choice of scales one can have m_s at the desired keV scale with active-sterile mixing, $e/m_s = \mathcal{O}(10^{-4})$. For instance, with

$$\begin{aligned} u \simeq v' \simeq 10^{10}\ \text{GeV}\,, \quad v \simeq 10^{11}\ \text{GeV}\,, \quad \Lambda \simeq 10^{12}\ \text{GeV}\,, \\ v_{u,d} \simeq 10^{2}\ \text{GeV}\,, \quad \langle\Theta\rangle \simeq 10^{11}\ \text{GeV}\,, \end{aligned} \tag{4.35}$$

which means that $\lambda = \langle\Theta\rangle/\Lambda \simeq 0.1$, one obtains

$$\begin{aligned} a \simeq d &\simeq 0.1 \left(\frac{u}{10^{10}\text{ GeV}}\right)\left(\frac{v_u}{10^2\text{ GeV}}\right)^2\left(\frac{10^{12}\text{ GeV}}{\Lambda}\right)^2 \text{ eV}\,, \\ e &\simeq 0.1 \left(\frac{\lambda}{10^{-1}}\right)^8\left(\frac{u}{10^{10}\text{ GeV}}\right)\left(\frac{v'}{10^{10}\text{ GeV}}\right)\left(\frac{v_u}{10^2\text{ GeV}}\right)\left(\frac{10^{12}\text{ GeV}}{\Lambda}\right)^2 \text{ eV}\,, \end{aligned} \tag{4.36}$$

with order one Yukawas. From Eq. (4.19), the leading order contribution to m_s is

$$\left(\frac{x_s}{\Lambda}\varphi\varphi\right)\lambda^{16}\nu_s^c\nu_s^c \Longrightarrow \left(x_s\frac{v^2}{\Lambda}\right)\lambda^{16}\,; \tag{4.37}$$

the resulting Majorana mass is

$$m_s \simeq \left(\frac{\lambda}{10^{-1}}\right)^{16}\left(\frac{v}{10^{11}\text{ GeV}}\right)^2\left(\frac{10^{12}\text{ GeV}}{\Lambda}\right)\text{ keV}\,. \tag{4.38}$$

The active-sterile mixing is given by

$$\frac{e}{m_s} \simeq 10^{-4}\,, \tag{4.39}$$

in accordance with the astrophysical constraints discussed in Section 3.6.2. Next-to-leading order contributions in Eq. (4.27) are of order 10^{-4} keV, and do not affect the scale of m_s significantly. The contribution to m_2 proportional to e^2/m_s is negligible in this case [cf. Eq. (4.23)], so that the sum rule holds to good approximation.

With the scales in Eq. (4.35), the FN charges $F_{e,\mu,\tau} = (4, 2, 0)$ give the correct charged lepton mass spectrum, using

$$m_\ell = y_\ell v_d \frac{v}{\Lambda}\lambda^{F_\ell} \simeq 10\left(\frac{v_d}{10^2\text{ GeV}}\right)\left(\frac{v}{10^{11}\text{ GeV}}\right)\left(\frac{10^{12}\text{ GeV}}{\Lambda}\right)\left(\frac{\lambda}{10^{-1}}\right)^{F_\ell}\text{ GeV}\,. \tag{4.40}$$

Summary

In summary, an effective flavour symmetry model has been extended to include light sterile neutrino(s) at different scales, with their mass suppressed by the Froggatt-Nielsen mechanism. This is one of the first working models that combines flavour symmetries with light eV-scale sterile neutrinos. Corrections to the leading order mixing pattern amongst active neutrinos are correlated with the active-sterile mixing, which is a general feature of such approaches. Indeed, one could imagine using a different flavour symmetry group as a starting point for such models, since in the A_4 case the leading order prediction of TBM is ruled out by current data, and NLO terms are required. Those extra terms could come from higher-order operators, which give sizeable modifications to active neutrino mixing but have little effect on the active-sterile mixing. The smallness of θ_{13} is a general problem in A_4 models, but the main point here is that sterile neutrinos can be added to flavour symmetry models. The effective model presented here can be extended to a seesaw version, discussed in the following section.

4.2.3 A_4 seesaw model with one keV sterile neutrino

Introduction

The type I seesaw model has been introduced in Chapter 2, and different ways (including the FN mechanism) to achieve light sterile neutrinos within that model have been summarised in

Section 2.2.1. In this section an A_4 seesaw model with three right-handed neutrinos is described, with one sterile state at the keV scale and the other two at either the eV scale, the heavy scale ($\gtrsim$ GeV), or both. The FN mechanism is used to control the mass spectrum of right-handed neutrinos and to set the charged lepton mass hierarchy. There are various possible scenarios, differing by the mass spectra of both active and sterile neutrinos, and each scheme exhibits distinct phenomenology.

Due to the fact that most A_4 seesaw models place right-handed neutrinos in the triplet representation (see the full classification table in Ref. [28]), one has to make non-trivial modifications to those models in order to assign different FN charges to each sterile neutrino.[5] Indeed, in order to get TBM at leading order with diagonal right-handed neutrinos as A_4 singlets, one must choose the VEV alignments of the flavon fields Φ_i along the directions of the columns of the TBM matrix, i.e., $\Phi_1 \simeq (2,-1,-1)^T$, $\Phi_2 \simeq (1,1,1)^T$, $\Phi_3 \simeq (0,-1,1)^T$, similar to the method outlined in Refs. [342–344]. The crucial point is that each light neutrino mass eigenvalue m_i is then suppressed by only one of the heavy right-handed neutrinos M_i, *viz.*

$$m_1 \simeq \frac{\Phi_1 \Phi_1^T}{M_1}\,, \quad m_2 \simeq \frac{\Phi_2 \Phi_2^T}{M_2}\,, \quad m_3 \simeq \frac{\Phi_3 \Phi_3^T}{M_3}\,, \tag{4.41}$$

so that one can decouple any one of the right-handed neutrinos and still achieve TBM with the remaining two columns, at the price of one massless active neutrino. Since $m_2 \neq 0$ (see Fig. 3.1), it is only viable to decouple the neutrinos that correspond to the first or third columns, giving normal ($m_1 = 0$) or inverted ($m_3 = 0$) ordering, respectively. The decoupled right-handed neutrino becomes the keV WDM candidate. It is worth stressing that the phenomenology of $0\nu\beta\beta$ will now be different to the effective model discussed above, since in that case sterile states are simply added to an existing model and the analysis in Section 3.4.2 applies.

Outline of the leading order model

Table 4.3 shows the particle assignments of the A_4 seesaw model, with right-handed neutrinos ν_i^c ($i = 1,2,3$) transforming as singlets under A_4. Three triplet flavons φ, φ' and φ'' are needed to construct the columns of M_D as well as the charged lepton mass matrix, and the singlet flavons ξ, ξ' and ξ'' are introduced in order to give masses to the right-handed neutrinos and keep M_R diagonal at leading order. The NLO terms implied by the presence of the flavons will be discussed later. The Lagrangian invariant under the SM gauge group and the additional $A_4 \otimes Z_3 \otimes U(1)_{\rm FN}$ symmetry is

$$\begin{aligned} -\mathcal{L}_{\rm Y} = {} & \frac{y_e}{\Lambda}\lambda^3 \left(\varphi L h_d\right) e^c + \frac{y_\mu}{\Lambda}\lambda \left(\varphi L h_d\right)' \mu^c + \frac{y_\tau}{\Lambda} \left(\varphi L h_d\right)'' \tau^c \\ & + \frac{y_1}{\Lambda}\lambda^{F_1}(\varphi L h_u)\nu_1^c + \frac{y_2}{\Lambda}\lambda^{F_2}(\varphi' L h_u)''\nu_2^c + \frac{y_3}{\Lambda}\lambda^{F_3}(\varphi'' L h_u)\nu_3^c \\ & + \frac{1}{2}\left[w_1 \lambda^{2F_1}\xi \nu_1^c \nu_1^c + w_2 \lambda^{2F_2}\xi' \nu_2^c \nu_2^c + w_3 \lambda^{2F_3}\xi'' \nu_3^c \nu_3^c\right] + \text{h.c.}, \end{aligned} \tag{4.42}$$

at leading order, with the same notation as before, where Λ is the cut-off scale and y_ℓ, y_i and w_i are coupling constants.

Once again, with the vacuum alignment $\langle\varphi\rangle = (v,0,0)$, the charged lepton mass matrix is

[5] The model in Ref. [335] also has right-handed neutrinos as singlets, but instead of the FN mechanism a hierarchy amongst the flavons is assumed.

Table 4.3: Particle assignments of the A_4 type I seesaw model, with three right-handed sterile neutrinos and additional Z_3 and $U(1)_{\rm FN}$ symmetries, as before.

Field	L	e^c	μ^c	τ^c	$h_{u,d}$	φ	φ'	φ''	ξ	ξ'	ξ''	Θ	ν_1^c	ν_2^c	ν_3^c
$SU(2)_L$	2	1	1	1	2	1	1	1	1	1	1	1	1	1	1
A_4	$\underline{3}$	$\underline{1}$	$\underline{1}''$	$\underline{1}'$	$\underline{1}$	$\underline{3}$	$\underline{3}$	$\underline{3}$	$\underline{1}$	$\underline{1}'$	$\underline{1}$	$\underline{1}$	$\underline{1}$	$\underline{1}'$	$\underline{1}$
Z_3	ω	ω^2	ω^2	ω^2	1	1	ω	ω^2	ω^2	ω	1	1	ω^2	ω	1
$U(1)_{\rm FN}$	-	3	1	0	-	-	-	-	-	-	-	-1	F_1	F_2	F_3

diagonal, *viz.*[6]

$$M_\ell = \frac{v_d\, v}{\Lambda} \begin{pmatrix} y_e\lambda^3 & 0 & 0 \\ 0 & y_\mu\lambda & 0 \\ 0 & 0 & y_\tau \end{pmatrix} , \tag{4.43}$$

where $v_d = \langle h_d \rangle$ and the charged lepton mass hierarchy is generated by the FN mechanism, as already described in Section 4.2.2. The same mechanism will be used in the right-handed neutrino sector; for the moment the FN charges of the right-handed sterile neutrinos are left as free parameters.

As discussed in Section 2.2.1, a sterile neutrino ν_i^c with mass $M_i = \mathcal{O}(\text{keV})$ and mixing of order $S_i^2 \simeq 10^{-8}$ will give a negligible contribution to neutrino mass, i.e., $m_i \simeq S_i^2 M_i \simeq 10^{-5}$ eV, and can thus be decoupled from the seesaw mechanism. It is then expedient to work in a 5×5 basis, with the Dirac mass matrix M_D a 3×2 matrix and M_R a 2×2 symmetric matrix. This is similar to the minimal seesaw model [345, 346] and the νMSM (cf. Section 3.6.3), in which the lightest active neutrino is massless. The mass spectrum of active neutrinos can either have normal ordering, with $m_3 \gg m_2 \gg m_1 \simeq 0$, or inverted ordering, with $m_2 \gtrsim m_1 \gg m_3 \simeq 0$. However, there exist different scenarios depending on the FN charges assigned to the remaining right-handed neutrinos. General analytical formulae are given in this subsection, whereas specific mass spectra will be discussed later on.

The sterile neutrino ν_1^c is assumed to be the WDM candidate, with a mass given by

$$M_1 = w_1 u \lambda^{2F_1}, \tag{4.44}$$

where $u = \langle \xi \rangle$. The full 6×6 neutrino mass matrix takes the form in Eq. (2.12); the vacuum alignment $\langle \varphi \rangle = (v, 0, 0)$ means that at leading order the first column of the Dirac mass matrix is $(y_1 v v_u \lambda^{F_1}/\Lambda, 0, 0)^T$, so that the sterile neutrino ν_1^c only mixes with the electron neutrino.[7] From Eqs. (2.22) and (2.23), the active-sterile mixing is

$$S_{e1} \simeq \frac{[M_D]_{e1}}{M_1} = \frac{y_1 v v_u}{w_1 u \Lambda} \lambda^{-F_1} , \tag{4.45}$$

so that the FN charge F_1 actually enhances the active-sterile mixing, and the contribution of the sterile neutrino ν_1^c to the lightest neutrino mass is

$$m_{1,3} = \frac{y_1^2 v^2 v_u^2}{w_1 u \Lambda^2} , \tag{4.46}$$

[6] Next-to-leading order operators will modify the structure of M_ℓ, introducing non-trivial mixing in the charged lepton sector (see Appendix C).

[7] Next-to-leading order terms will induce mixing between ν_1^c and $\nu_{\mu,\tau}$ (cf. Section 4.2.3).

which turns out to be negligible. Once the scale of the various flavon VEVs are fixed then F_1 is fixed by the WDM constraints [cf. Eq. (3.75)], and the various scenarios to be discussed will differ only by the choice of the FN charges F_2 and F_3, i.e., the scale of the remaining two sterile neutrinos.

With the keV sterile neutrino ν_1^c decoupled, the seesaw proceeds with the remaining two right-handed neutrinos, ν_2^c and ν_3^c. For the NO case, the triplet VEV alignments[8]

$$\langle\varphi'\rangle = (v', v', v'), \quad \langle\varphi''\rangle = (0, v'', -v'') \,, \tag{4.47}$$

result in the following 5×5 neutrino mass matrix in the basis $(\nu_e, \nu_\mu, \nu_\tau, \nu_2^c, \nu_3^c)$:

$$M_\nu^{5\times5} = \begin{pmatrix} 0 & M_D \\ M_D^T & M_R \end{pmatrix} , \tag{4.48}$$

with the Dirac mass matrix

$$M_D^{(\mathrm{NO})} = \frac{v_u}{\Lambda} \begin{pmatrix} y_2 v' \lambda^{F_2} & 0 \\ y_2 v' \lambda^{F_2} & -y_3 v'' \lambda^{F_3} \\ y_2 v' \lambda^{F_2} & y_3 v'' \lambda^{F_3} \end{pmatrix} \tag{4.49}$$

and the right-handed neutrino mass matrix

$$M_R = \begin{pmatrix} w_2 u' \lambda^{2F_2} & 0 \\ 0 & w_3 u'' \lambda^{2F_3} \end{pmatrix} , \tag{4.50}$$

where $u' = \langle\xi'\rangle$ and $u'' = \langle\xi''\rangle$.

The neutrino masses and flavour mixing can be obtained by the full diagonalisation of $M_\nu^{5\times5}$, i.e., $U^\dagger M_\nu^{5\times5} U^* = \mathrm{diag}(m_1, m_2, m_3, m_4, m_5)$, where m_4 and m_5 denote the masses of right-handed neutrinos. Since eV-scale sterile neutrinos may be present, one should include NLO seesaw terms, as discussed in Section 2.2.1. Using Eq. (2.13) and assuming real matrices for simplicity, one arrives (up to order ϵ_i^2) at

$$\begin{aligned} U^{(\mathrm{NO})} \simeq & \begin{pmatrix} \frac{2}{\sqrt{6}} & \frac{1}{\sqrt{3}} & 0 & 0 & 0 \\ -\frac{1}{\sqrt{6}} & \frac{1}{\sqrt{3}} & -\frac{1}{\sqrt{2}} & 0 & 0 \\ -\frac{1}{\sqrt{6}} & \frac{1}{\sqrt{3}} & \frac{1}{\sqrt{2}} & 0 & 0 \\ 0 & 0 & 0 & 1 & 0 \\ 0 & 0 & 0 & 0 & 1 \end{pmatrix} + \begin{pmatrix} 0 & 0 & 0 & \epsilon_1 & 0 \\ 0 & 0 & 0 & \epsilon_1 & -\epsilon_2 \\ 0 & 0 & 0 & \epsilon_1 & \epsilon_2 \\ 0 & -\sqrt{3}\epsilon_1 & 0 & 0 & 0 \\ 0 & 0 & -\sqrt{2}\epsilon_2 & 0 & 0 \end{pmatrix} \\ & + \begin{pmatrix} 0 & -\frac{\sqrt{3}}{2}\epsilon_1^2 & 0 & 0 & 0 \\ 0 & -\frac{\sqrt{3}}{2}\epsilon_1^2 & \frac{1}{\sqrt{2}}\epsilon_2^2 & 0 & 0 \\ 0 & -\frac{\sqrt{3}}{2}\epsilon_1^2 & -\frac{1}{\sqrt{2}}\epsilon_2^2 & 0 & 0 \\ 0 & 0 & 0 & -\frac{3}{2}\epsilon_1^2 & 0 \\ 0 & 0 & 0 & 0 & -\epsilon_2^2 \end{pmatrix} , \end{aligned} \tag{4.51}$$

where the expansion parameters are given by

$$\epsilon_1 = \frac{y_2 v' v_u}{w_2 u' \Lambda} \lambda^{-F_2} \quad \text{and} \quad \epsilon_2 = \frac{y_3 v'' v_u}{w_3 u'' \Lambda} \lambda^{-F_3}, \tag{4.52}$$

[8] Ref. [335] employs a radiative symmetry breaking mechanism in order to achieve this VEV alignment.

in analogy to Eq. (2.22). The ϵ_i parameters control the size of active-sterile mixing and NLO corrections to neutrino masses and mixing, and will be important in the discussions of various scenarios in the following subsections. The neutrino mass eigenvalues are

$$\begin{aligned} m_1^{(\mathrm{NO})} &= 0\,, \\ m_2^{(\mathrm{NO})} &= m_2^{(0)}\left(1-3\epsilon_1^2\right), \\ m_3^{(\mathrm{NO})} &= m_3^{(0)}\left(1-2\epsilon_2^2\right), \\ m_4^{(\mathrm{NO})} &= w_2 u' \lambda^{2F_2} - m_2^{(0)}\left(1-3\epsilon_1^2\right), \\ m_5^{(\mathrm{NO})} &= w_3 u'' \lambda^{2F_3} - m_3^{(0)}\left(1-2\epsilon_2^2\right), \end{aligned} \tag{4.53}$$

plus higher-order terms, where

$$m_2^{(0)} \equiv -\frac{3y_2^2 v'^2 v_u^2}{w_2 u' \Lambda^2}\,, \quad m_3^{(0)} \equiv -\frac{2y_3^2 v''^2 v_u^2}{w_3 u'' \Lambda^2}\,, \tag{4.54}$$

are the leading order seesaw terms in the NO.

For the IO case the following VEV alignments are assumed:

$$\langle\varphi'\rangle = (v', v', v'), \quad \langle\varphi''\rangle = (2v'', -v'', -v'')\,. \tag{4.55}$$

The Dirac mass matrix is modified to

$$M_D^{(\mathrm{IO})} = \frac{v_u}{\Lambda}\begin{pmatrix} y_2 v' \lambda^{F_2} & 2y_3 v'' \lambda^{F_3} \\ y_2 v' \lambda^{F_2} & -y_3 v'' \lambda^{F_3} \\ y_2 v' \lambda^{F_2} & -y_3 v'' \lambda^{F_3} \end{pmatrix}, \tag{4.56}$$

while the right-handed neutrino mass matrix M_R remains unchanged. In this case the diagonalisation matrix approximates (up to order ϵ_i^2) to

$$\begin{aligned} U^{(\mathrm{IO})} \simeq{}& \begin{pmatrix} \frac{2}{\sqrt{6}} & \frac{1}{\sqrt{3}} & 0 & 0 & 0 \\ -\frac{1}{\sqrt{6}} & \frac{1}{\sqrt{3}} & -\frac{1}{\sqrt{2}} & 0 & 0 \\ -\frac{1}{\sqrt{6}} & \frac{1}{\sqrt{3}} & \frac{1}{\sqrt{2}} & 0 & 0 \\ 0 & 0 & 0 & 1 & 0 \\ 0 & 0 & 0 & 0 & 1 \end{pmatrix} + \begin{pmatrix} 0 & 0 & 0 & \epsilon_1 & 2\epsilon_2 \\ 0 & 0 & 0 & \epsilon_1 & -\epsilon_2 \\ 0 & 0 & 0 & \epsilon_1 & -\epsilon_2 \\ 0 & -\sqrt{3}\epsilon_1 & 0 & 0 & 0 \\ -\sqrt{6}\epsilon_2 & 0 & 0 & 0 & 0 \end{pmatrix} \\ &+ \begin{pmatrix} -\sqrt{6}\epsilon_2^2 & -\frac{\sqrt{3}}{2}\epsilon_1^2 & 0 & 0 & 0 \\ \sqrt{\frac{3}{2}}\epsilon_2^2 & -\frac{\sqrt{3}}{2}\epsilon_1^2 & 0 & 0 & 0 \\ \sqrt{\frac{3}{2}}\epsilon_2^2 & -\frac{\sqrt{3}}{2}\epsilon_1^2 & 0 & 0 & 0 \\ 0 & 0 & 0 & -\frac{3}{2}\epsilon_1^2 & 0 \\ 0 & 0 & 0 & 0 & -3\epsilon_2^2 \end{pmatrix}, \end{aligned} \tag{4.57}$$

and the neutrino masses are given by

$$\begin{aligned} m_1^{(\mathrm{IO})} &= m_1^{(0)}\left(1-6\epsilon_2^2\right), \\ m_2^{(\mathrm{IO})} &= m_2^{(0)}\left(1-3\epsilon_1^2\right), \\ m_3^{(\mathrm{IO})} &= 0\,, \\ m_4^{(\mathrm{IO})} &= w_2 u' \lambda^{2F_2} - m_2^{(0)}\left(1-3\epsilon_1^2\right), \\ m_5^{(\mathrm{IO})} &= w_3 u'' \lambda^{2F_3} - m_1^{(0)}\left(1-6\epsilon_2^2\right), \end{aligned} \tag{4.58}$$

where

$$m_1^{(0)} \equiv -\frac{6y_3^2 v''^2 v_u^2}{w_3 u'' \Lambda^2} \tag{4.59}$$

is the leading order expression for the lightest mass in the IO and $m_2^{(0)}$ is defined in Eq. (4.54). Note from Eqs. (4.51) and (4.57) that the mixing pattern $|U_{e3}| = 0$ and $|U_{\mu 3}| = |U_{\tau 3}|$ is stable with respect to higher-order seesaw terms, which is actually true to all orders in ϵ_i [44].

It deserves to be mentioned that the leading order contributions to the active neutrino masses in Eqs. (4.54) and (4.59) do not depend on the FN charges assigned to the right-handed neutrinos, a feature of the seesaw model already discussed in Section 2.2.1. In general, the leading seesaw mass term is M_D^2/M_i, so that the one unit of FN charge λ^{F_i} from M_D cancels with the two units λ^{2F_i} from M_i. On the other hand, the NLO term $M_D^4/M_i^3 \propto \epsilon_i^2$ does depend on the FN charge, which therefore controls the magnitudes of NLO corrections. The larger the charge F_i (equivalent to a smaller sterile neutrino mass), the larger the correction parameters ϵ_i become, and thus the larger the corrections to the leading order seesaw masses.

In addition to NLO seesaw terms, one would expect higher-dimensional operators to modify the leading order predictions of the model, which has so far been constructed from the leading order Lagrangian in Eq. (4.42). The magnitude of those corrections depends largely on the actual numerical values chosen in the model, since they are suppressed by additional powers of the cut-off scale Λ. It therefore makes sense to use leading order predictions as a guide for mass scales. The requirements are that (*i*) the sterile neutrino mass [Eq. (4.44)] and mixing [Eq. (4.45)] satisfy Eq. (3.75), (*ii*) active neutrino masses are at the correct scale and (*iii*) Yukawa couplings are $\leq \mathcal{O}(1)$. A rough numerical estimate shows that with the mass scales

$$v \simeq 10^{11}\ \text{GeV}, \quad u \simeq 10^{12}\ \text{GeV}, \quad \Lambda \simeq 10^{13}\ \text{GeV}\,, \tag{4.60}$$

the Higgs VEV $v_u = \langle h_u \rangle \simeq 174$ GeV and $\lambda \simeq 0.1$, one needs the FN charge

$$F_1 = 9 \tag{4.61}$$

to obtain a sterile neutrino of mass $M_1 \simeq 1$ keV with the desired mixing angle $S_1^2 \simeq 10^{-8}$, with $y_1, w_1 \leq \mathcal{O}(1)$. In order to stabilise the active neutrino masses around the sub-eV scale, one can choose [together with the numbers in Eq. (4.60)] the scales

$$v' \simeq v'' \simeq u' \simeq u'' \simeq 10^{11}\ \text{GeV} \tag{4.62}$$

for the other flavon VEVs, and the mass splitting among active neutrinos can be achieved by properly choosing the corresponding Yukawa couplings, i.e., y_i and w_i ($i = 2, 3$). The scale choices are fixed from now on.

Mixing corrections from higher-order terms

As has already been described in the effective model context, the presence of gauge singlet flavons in the model will inevitably induce NLO corrections, which may modify the leading order picture and affect both active and active-sterile neutrino mixing. Modifications to active mixing are in fact desirable in order to generate non-zero θ_{13}, and will be achieved by adding higher-order operators to the Lagrangian in Eq. (4.42). Other methods of introducing corrections have been mentioned in Section 4.1.

Since the charged lepton and right-handed neutrino mass matrices are diagonal at leading order, TBM comes solely from the structure of the Dirac mass matrix. Without performing

a detailed numerical analysis, one can show that the higher-order corrections affect all three mass matrices: M_ℓ, M_D and M_R. The impact of those corrections is controlled by the ratios of flavon VEVs to the cut-off scale, *viz.*

$$r_1 \equiv \frac{u}{\Lambda} \simeq 0.1 \quad \text{and} \quad r_2 \equiv \frac{u'}{\Lambda} \simeq \frac{u''}{\Lambda} \simeq \frac{v}{\Lambda} \simeq \frac{v''}{\Lambda} \simeq 0.01\,. \tag{4.63}$$

The terms containing the VEV $\langle\xi\rangle = u = r_1\Lambda$ have the largest effect, and will be included in the analysis (see Appendix C); terms containing the VEVs u', u'', v, v' and v'' are all of relative order $r_2 \simeq 0.01$ and can be safely neglected. The correction terms turn out to have a negligible effect on the keV sterile neutrino mass, as well as its mixing with the active sector. Explicitly, from Eqs. (C.12), (C.14) and (C.15), the corrected active-sterile mixing is

$$\theta'_{e1}{}^{(\mathrm{NO})} \simeq \theta_{e1}\left(1 + \frac{y'_1 v'}{y_1 v} r_1\right) \quad \text{and} \quad \theta'_{e1}{}^{(\mathrm{IO})} \simeq \theta_{e1}\left[1 + \left(\frac{y'_1 v'}{y_1 v} + 2\frac{y_3 v''}{y_1 v}\frac{w'_1}{w_1}\right) r_1\right], \tag{4.64}$$

where the dimensionless couplings y'_1 and w'_1 are defined in Eqs. (C.5) and (C.8), respectively, and the leading order expression for θ_{e1} is given in Eq. (4.45). In addition, the mixing angles $\theta_{\mu 1}$ and θ_{τ_1} become non-zero, but of the same magnitude as θ_{e1}, i.e.,

$$\theta'_{\mu,\tau 1}{}^{(\mathrm{NO})} \simeq \theta_{e1}\left(\frac{y'_1 v'}{y_1 v} \mp \frac{y_3 v''}{y_1 v}\frac{w'_1}{w_1}\right) r_1 \quad \text{and} \quad \theta'_{\mu,\tau 1}{}^{(\mathrm{IO})} \simeq \theta_{e1}\left(\frac{y'_1 v'}{y_1 v} - \frac{y_3 v''}{y_1 v}\frac{w'_1}{w_1}\right) r_1\,. \tag{4.65}$$

This shows that the active-sterile mixing is stable, illustrating the point that unlike active neutrino mixing it is related to the ratio of two large scales, so that small changes in M_D and M_R will have little effect on $\theta_{\ell i}$ (assuming that $|w'_1| \lesssim |w_1|$). The WDM particle remains decoupled from the seesaw and one can still work in the 5×5 basis. The relevant mixing matrix elements are given here; details of the diagonalisation procedure and modified neutrino mass eigenvalues can be found in Appendix C.

The final lepton mixing matrix is a 3×5 matrix connecting the three flavours of lepton doublets to the five neutrino mass eigenstates. Corrections from the charged lepton sector [Eq. (C.3)] and the neutrino sector [Eq. (C.16)] can be combined via Eq. (2.20) to give the approximate mixing matrix elements

$$\begin{aligned}
|\tilde{U}_{e3}|^2 &\simeq \frac{r_1^2}{2}\left[\left(\frac{y'_\mu}{y_\mu} - \frac{y'_\tau}{y_\tau}\right)^2\right] + \frac{1}{2}(\chi-\rho_3)^2 - (\chi-\rho_3) r_1 \left(\frac{y'_\mu}{y_\mu} - \frac{y'_\tau}{y_\tau}\right), \\
|\tilde{U}_{e2}|^2 &\simeq \frac{1}{3}\left[1 - 3\epsilon_1^2 - 2\rho_2 - 2r_1\left(\frac{y'_\mu}{y_\mu} + \frac{y'_\tau}{y_\tau}\right)\right], \\
|\tilde{U}_{\mu 3}|^2 &\simeq \frac{1}{2}\left[1 - 2\epsilon_2^2 + 2\frac{y'_\tau}{y_\tau} r_1 + \frac{2}{3}\sigma_+^N \mathcal{R}\right],
\end{aligned} \tag{4.66}$$

for active neutrino mixing and

$$\begin{aligned}
|\tilde{U}_{e,\mu 4}|^2 &\simeq \epsilon_1^2\left[1 \mp 2\rho_2 \mp 2r_1\left(\frac{y'_\mu}{y_\mu} \pm \frac{y'_\tau}{y_\tau}\right)\right], \\
|\tilde{U}_{e5}|^2 &\simeq \epsilon_2^2\left[r_1^2\left(\frac{y'_\mu}{y_\mu} - \frac{y'_\tau}{y_\tau}\right)^2 - 2r_1\left(\frac{y'_\mu}{y_\mu} - \frac{y'_\tau}{y_\tau}\right)(\chi-\rho_3) + (\chi-\rho_3)^2\right], \\
|\tilde{U}_{\mu 5}|^2 &\simeq \epsilon_2^2\left(1 + 2r_1\frac{y'_\tau}{y_\tau}\right),
\end{aligned} \tag{4.67}$$

for active-sterile mixing, in the NO. Here the ϵ_i are generated by NLO seesaw terms, $y'_{\mu,\tau}$ stem from corrections to the charged lepton mass matrix, while the other parameters come from corrections to M_D and M_R. For the inverted ordering,

$$\begin{aligned}
|\tilde{U}_{e3}|^2 &\simeq \frac{r_1^2}{2}\left(\frac{y'_\mu}{y_\mu}-\frac{y'_\tau}{y_\tau}\right)^2 - \rho_2 r_1\left(\frac{y'_\mu}{y_\mu}-\frac{y'_\tau}{y_\tau}\right)+\frac{\rho_2^2}{2}\,,\\
|\tilde{U}_{e2}|^2 &\simeq \frac{1}{3}\left[1-3\epsilon_1^2-2\rho_2-2r_1\left(\frac{y'_\mu}{y_\mu}+\frac{y'_\tau}{y_\tau}\right)-\frac{2}{3}\sigma_+^I\mathcal{G}\right],\\
|\tilde{U}_{\mu 3}|^2 &\simeq \frac{1}{2}\left[1+2\rho_2+2\frac{y'_\tau}{y_\tau}r_1\right],
\end{aligned} \tag{4.68}$$

and

$$\begin{aligned}
|\tilde{U}_{e,\mu 4}|^2 &\simeq \epsilon_1^2\left[1-2\rho_2\mp 2r_1\left(\frac{y'_\mu}{y_\mu}\pm\frac{y'_\tau}{y_\tau}\right)\right],\\
|\tilde{U}_{e5}|^2 &\simeq 4\epsilon_2^2\left[1+r_1\left(\frac{y'_\mu}{y_\mu}+\frac{y'_\tau}{y_\tau}\right)-(\chi-\rho_3)\right],\\
|\tilde{U}_{\mu 5}|^2 &\simeq \epsilon_2^2\left[1-2r_1\left(2\frac{y'_\mu}{y_\mu}+\frac{y'_\tau}{y_\tau}\right)\right],
\end{aligned} \tag{4.69}$$

for active-active and active-sterile mixing, respectively. The parameters

$$\begin{aligned}
\sigma_\pm^N &\equiv \chi\pm\rho_2-\rho_3\,, \quad \sigma_\pm^I \equiv \chi\pm 3\rho_2-\rho_3\,,\\
\chi &\equiv \frac{y_1 v}{y_3 v''}\frac{w'_1}{w_1}r_1\,, \quad \rho_2 \equiv \frac{y'_2 v''}{y_2 v'}r_1\,, \quad \rho_3 \equiv \frac{y'_3 v}{y_3 v''}r_1\,,\\
\mathcal{R} &\equiv \frac{m_2^{(0)}}{m_3^{(0)}} \simeq \sqrt{\frac{\Delta m_\mathrm{S}^2}{\Delta m_\mathrm{A}^2}} = \mathcal{O}(10^{-1})\,,\\
\mathcal{G} &\equiv \frac{m_1^{(0)}}{m_2^{(0)}-m_1^{(0)}} \simeq \frac{2\Delta m_\mathrm{A}^2}{\Delta m_\mathrm{S}^2} \simeq \frac{2}{\mathcal{R}^2} = \mathcal{O}(10^2)\,,
\end{aligned} \tag{4.70}$$

control the size of the mixing terms, where Δm_S^2 and Δm_A^2 are the solar and atmospheric mass squared differences, respectively. The dimensionless couplings $y'_{2,3}$ are defined in Eq. (C.5). $\mathcal{R}$ and $\mathcal{G}$ contain the leading order neutrino masses from Eqs. (4.54) and (4.59): while $\mathcal{R}$ is quite small, $\mathcal{G}$ is large, which is a consequence of the two relatively large but nearly degenerate neutrino masses in the IO, $m_1^{(0)} \simeq m_2^{(0)} \simeq 0.05$ eV. Thus an expansion to first order has been performed in $\mathcal{R}$, whereas $\mathcal{G}$ remains an exact expression in the mixing matrix. This means that keeping the corrections to $|\tilde{U}_{e2}|^2$ under control in the IO requires $\sigma_+^I = \chi + 3\rho_2 - \rho_3$ to be $\mathcal{O}(10^{-3})$, which in turn puts a constraint on the Yukawa couplings $y'_{2,3}$ and w'_1 in Eqs. (C.5) and (C.8). The approximations $r_1 \simeq 0.1$ and $v \simeq v' \simeq v''$ [cf. Eq. (4.63)] imply the relations

$$\rho_{2,3} \simeq 0.1\frac{y'_{2,3}}{y_{2,3}} \quad \text{and} \quad \chi \simeq 0.1\frac{y_1}{y_3}\frac{w'_1}{w_1}\,, \tag{4.71}$$

so that $y'_{2,3} \simeq 0.01 y_{2,3}$ and $y_1 w'_1 \simeq 0.01 y_3 w_1$ are required in the inverted ordering. The full neutrino mass eigenvalues are given in Eqs. (C.18) and (C.20): despite the appearance of $\mathcal{G}^2$ terms in the IO mass eigenvalues they will always be suppressed by $(\sigma_+^I)^2$, which is constrained to be small from the mixing matrix element $\tilde{U}_{e2}$.

As expected, by setting y'_2, y'_3, w'_1, y'_μ and y'_τ to zero in Eqs. (4.66) to (4.69) one recovers the matrix elements in Eqs. (4.51) and (4.57). Note that without the higher-order correction terms $\tilde{U}_{e3}$ remains exactly zero, to all orders in ϵ_i. The active-sterile mixing ($\tilde{U}_{\ell 4,5}$) is always proportional to ϵ_i, or in other words to a ratio of scales [cf. Eqs. (2.22) and (4.52)]. In the different scenarios discussed in the following subsections, the ϵ_i terms will have different magnitudes, depending on the right-handed neutrino spectrum. In those cases with significant values of ϵ_i (i.e., eV-scale sterile neutrinos) one must take into account both NLO seesaw corrections and higher-order corrections, whereas in cases with negligible ϵ_i (heavy sterile neutrinos) one need only worry about the higher-order correction terms controlled by y'_2, y'_3, w'_1, y'_μ and y'_τ.

Even if y'_2, y'_3 and w'_1 are small and mixing corrections from the neutrino sector are negligible, there are still effects from the charged lepton sector. Indeed, in order to keep the solar mixing angle within its allowed range [347], one has the constraint (assuming for definiteness $y'_2 = y'_3 = w'_1 = 0$ and $\epsilon_{1,2} \simeq 0$)

$$-0.4 \leq \left(\frac{y'_\mu}{y_\mu} + \frac{y'_\tau}{y_\tau}\right) \leq 0.95\,, \tag{4.72}$$

on the charged lepton Yukawa couplings; the extreme choice $y'_\mu/y_\mu = -y'_\tau/y_\tau$ gives the reactor mixing angle

$$\sin^2\theta_{13} \simeq 2r_1^2 \left(\frac{y'_\tau}{y_\tau}\right)^2 \simeq 0.02, \tag{4.73}$$

in both mass orderings, assuming that $y'_\tau \approx y_\tau$. In that case $\sin^2\theta_{23} \simeq 0.6$, and $\sin^2\theta_{12}$ retains its TBM value, see Eq. (4.3).

Explicit seesaw model scenarios

In order to illustrate the versatility of the model discussed, three scenarios with different mass spectra in the right-handed neutrino sector will be presented. Each case differs by the choice of FN charges F_2 and F_3, what one could call the "theoretical input"; the consequent neutrino phenomenology is described in detail. Table 4.4 summarises the key differences in each case.

In all cases it has been checked that Yukawa couplings of order 1 or 0.1 can fit the model to the active neutrino mass-squared differences [347], and, where appropriate, to sterile mass parameters [153]. The effects of the higher-order corrections discussed in Section 4.2.3 are described for each scenario. Due to the large number of parameters there will always be enough freedom to fit the masses to the data, so that one only needs to take care that mixing corrections are under control, particularly in the IO, as discussed above.

Scenario I: two eV-scale right-handed neutrinos

In this case the FN charges $F_1 = 9$, $F_{2,3} = 10$ are assigned, so that the right-handed neutrino masses are at the eV scale. It is now notable that $\epsilon_{1,2} = \mathcal{O}(0.1)$ can be expected, indicating that NLO seesaw terms should be considered. The effects are more pronounced in the IO case, since two of the active neutrinos are nearly degenerate and are more sensitive to corrections. The five neutrino mass eigenvalues are given by the full expressions in Eqs. (C.18) and (C.20).

In this scenario, there are no heavy right-handed neutrinos that could be used for leptogenesis (cf. Section 3.6.3). Neutrinoless double beta decay is also vanishing since the contributions from active and sterile neutrinos exactly cancel each other [see Eq. (3.40)], unless there are other new physics contributions. This is different to the phenomenological analysis in Section 3.4.2, since in that case sterile singlet states are simply added to an existing model, like in the effective model described above.

Table 4.4: Summary of the different scenarios discussed in the A_4 seesaw model. In each case the WDM sterile neutrino has a mass $M_1 = \mathcal{O}(\text{keV})$, and the corresponding active neutrino is approximately massless.

	F_1, F_2, F_3	Mass spectrum	$\lvert\tilde{U}_{\ell 4}\rvert$	$\lvert\tilde{U}_{\ell 5}\rvert$	$\lvert\langle m_{ee}\rangle\rvert$ NO	$\lvert\langle m_{ee}\rangle\rvert$ IO
I	9, 10, 10	$M_{2,3} = \mathcal{O}(\text{eV})$,	$\mathcal{O}(0.1)$	$\mathcal{O}(0.1)$	0	0
IIA	9, 10, 0	$M_2 = \mathcal{O}(\text{eV})$ $M_3 = \mathcal{O}(10^{11}\,\text{GeV})$	$\mathcal{O}(0.1)$	$\mathcal{O}(10^{-11})$	0	$\dfrac{2\sqrt{\Delta m^2_{\text{A}}}}{3}$
IIB	9, 0, 10	$M_2 = \mathcal{O}(10^{11}\,\text{GeV})$ $M_3 = \mathcal{O}(\text{eV})$	$\mathcal{O}(10^{-11})$	$\mathcal{O}(0.1)$	$\dfrac{\sqrt{\Delta m^2_{\text{S}}}}{3}$	$\dfrac{\sqrt{\Delta m^2_{\text{A}}}}{3}$
III	9, 5, 5	$M_{2,3} = \mathcal{O}(10\,\text{GeV})$	$\mathcal{O}(10^{-6})$	$\mathcal{O}(10^{-6})$	$\dfrac{\sqrt{\Delta m^2_{\text{S}}}}{3}$	$\sqrt{\Delta m^2_{\text{A}}}$

The eV-scale right-handed neutrinos offer an explanation for the short-baseline oscillation anomalies often attributed to them. In the NO case, one of the two sterile neutrinos could mix with ν_e via $\tilde{U}_{e4} \simeq \epsilon_1$. The reactor flux loss is therefore explained since part of the total flux of $\overline{\nu}_e$ oscillates into sterile neutrinos. However, one finds that the active-sterile mixing turns out to be too small to account for the reactor anomaly. That can be deduced from Eqs. (4.53) and (4.58): at leading order, $\epsilon_1^2 \propto m_2/m_4$. In the NO, $m_2 \simeq 0.009$ eV is fixed by the neutrino mass-squared differences, so that ϵ_1 cannot be large enough for an eV-scale m_4. The situation is different in the IO case, since $m_1 \simeq m_2 \simeq \sqrt{\Delta m^2_{\text{A}}} \simeq 0.05$ eV. Furthermore, both $\tilde{U}_{e4}$ and $\tilde{U}_{e5}$ are non-vanishing (see Fig. 4.3).

The effect of higher-order operators on the active-sterile mixing is very small. Switching on w_1' gives $|\tilde{U}_{e5}|^2 \simeq \mathcal{O}(r_1^2)\,\epsilon_2^2$ in the NO [cf. Eq. (4.67)], which will still not give sufficient mixing to explain the data. In the IO case, $|\tilde{U}_{e5}|^2 \simeq 4[1 + \mathcal{O}(r_1)]\epsilon_2^2$, so the small correction term makes little difference. Indeed, the allowed ranges illustrated in Fig. 4.3 already include the effects of higher-order operators. One observes that the desired active-sterile mixing can indeed be achieved in the IO case.

In what regards active neutrino mixing, deviations from TBM come from both NLO seesaw terms ($\propto \epsilon_i$) and higher-order operators ($\propto y_2', y_3', w_1', y_\mu', y_\tau'$). If one considers only higher-order corrections in the neutrino sector for simplicity, i.e., the $y_{2,3}'$ and w_1' terms in Eqs. (C.5) and (C.8) respectively, then Eqs. (4.66) and (4.68) show that only $\tilde{U}_{\mu 3} \propto \epsilon_2$ receives visible corrections in the NO, since ϵ_1 and the product $\sigma_+^N \mathcal{R}$ are both small. However, the higher-order terms related to the product $\sigma_+^I \mathcal{G}$ lead to sizable corrections to $|\tilde{U}_{e2}|^2$ in the IO case; $|\tilde{U}_{e2}|$ could be enhanced or reduced depending on the signs and magnitudes of $y_{2,3}'$ and w_1'. In addition, non-zero θ_{13} can be obtained from charged lepton corrections, as discussed above.

Scenario II: split seesaw with both eV-scale and heavy right-handed neutrinos

Equations (4.47) and (4.55) show that it is possible to get either normal or inverted ordering by choosing the alignment of the flavon VEV $\langle\varphi''\rangle$ correctly. If one assigns different FN charges to the two seesaw right-handed neutrinos there will be four distinct possibilities, depending on

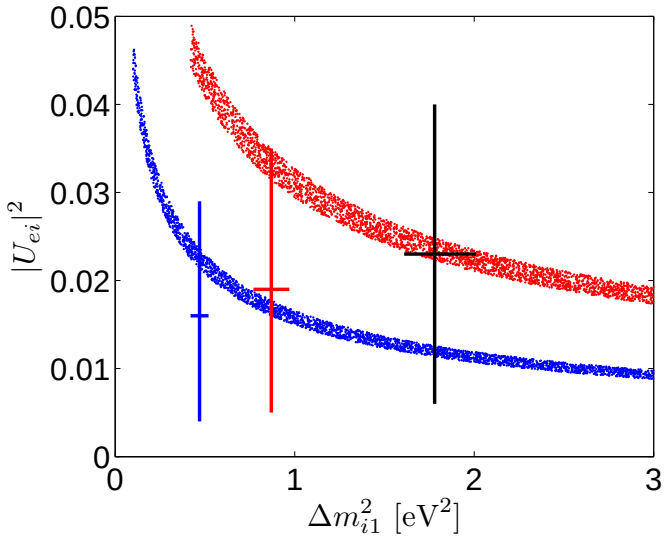

Figure 4.3: The allowed ranges of $|U_{e4}|^2 - \Delta m^2_{41}$ (blue) and $|U_{e5}|^2 - \Delta m^2_{51}$ (red) in the inverted ordering, requiring that the oscillation parameters lie in their currently allowed 2σ ranges. The blue and red vertical and horizontal error bars indicate the allowed 2σ range for the $3+2$ mass and mixing parameters from Refs. [153, 347], their intersection is the best-fit point. The black errors bars are for the $3+1$ case from Ref. [153], to be discussed in scenario II in Section 4.2.3. Note that charged lepton corrections are not included here.

the mass ordering (NO or IO) of active neutrinos and which sterile neutrino (ν_2^c or ν_3^c) is chosen as the heavy one. One can then use a two-stage seesaw, by integrating out the heavy sterile neutrino first and then applying the seesaw formula again (see the discussion in Section 2.2.1). With the assignments $F_1 = 9$, $F_2 = 10\,(0)$ and $F_3 = 0\,(10)$ the sterile neutrino ν_3^c (ν_2^c) has a mass in the 10^{11} GeV range, and is integrated out first, whereas ν_2^c (ν_3^c) is at the eV scale. The third (second) column of M_D is then used in the seesaw formula, leading to a 3×3 effective neutrino mass matrix of rank 1 that gives one of the active neutrinos masses. The full 4×4 mass matrix in the basis $(\nu_e, \nu_\mu, \nu_\tau, \nu^c_{2(3)})$ is

$$M_\nu^{4\times 4} = \begin{pmatrix} -[M_D]_{\ell i} M_i^{-1} [M_D^T]_{\ell i} & [M_D]_{\ell i} \\ [M_D^T]_{\ell i} & M_i \end{pmatrix}, \quad \ell = e,\mu,\tau, \quad i = 1 \text{ or } 2\,, \tag{4.74}$$

with M_D defined in Eqs. (4.49) or (4.56) and M_R from Eq. (4.50), leading to mixing between the active sector and the remaining eV-scale sterile neutrino ν_2^c (ν_3^c). Applying the same method and formulae outlined above results in a 4×4 mixing matrix, which can simply be obtained from the formulae in Eqs. (4.51) and (4.57) by removing the relevant row and column.

- **Case IIA: ν_3^c heavy, ($F_3 = 0$), ν_2^c light ($F_2 = 10$)**
  In this case one removes the fifth row and fifth column of U in Eqs. (4.51) and (4.57), giving the same 4×4 mixing matrix in both mass orderings, and the matrix elements $|U_{e5}|^2$ and $|U_{\mu 5}|^2$ are zero. The light neutrino mass eigenvalues m_i ($i = 1,2,3,4$) are given by the expressions in Eqs. (C.18) and (C.20) with ϵ_2 set to zero; the heavy neutrino has the mass $M_3 = w_3 u''$. It is the small value of F_3 that leads to $\epsilon_2 \simeq 0$ [Eq. (4.52)], so that m_3 (or m_1) does not receive any higher-order corrections, as this mass originates

from the high-scale of M_3, whose FN charge "cancelled" in the leading order seesaw formula. Although in this example $F_3 = 0$, so that $M_3 \simeq 10^{11}$ GeV, even with $F_3 = 5$ and $M_3 \simeq 10$ GeV, one has $\epsilon_2 \simeq 10^{-6}$ (see scenario III), so that NLO corrections would still be under control.

The FN charge $F_2 = 10$ of the eV-scale neutrino gives corrections to m_2 and m_4, via $\epsilon_1 \simeq 0.1$. With order one Yukawas and values for the VEVs as before, M_3 lies around 10^{11} GeV. The effective mass in $0\nu\beta\beta$ is given by the $(1,1)$ element of the 4×4 mass matrix, which, at leading order, is

$$|\langle m_{ee}\rangle|^{(\mathrm{NO})} = 0\,, \quad |\langle m_{ee}\rangle|^{(\mathrm{IO})} = \left|\frac{2m_1^{(0)}}{3}\right| = \frac{2\sqrt{\Delta m^2_{\mathrm{A}}}}{3} \simeq 0.032 \text{ eV}\,. \tag{4.75}$$

Here one can see that the contribution of the light neutrino of mass $m_2^{(0)}$ has cancelled with that of the light sterile neutrino ν_2^c, in both mass orderings. Note again that this is different from the usually discussed effects of sterile neutrinos in $0\nu\beta\beta$, and corresponds to the pairwise cancellation described in Section 3.4.4. The effective mass is zero in the NO since $U_{e3} = 0$ at leading order. A non-zero value of U_{e3} would give a very small contribution to the effective mass in the NO, and a completely negligible one in the IO.

- **Case IIB: ν_2^c heavy ($F_2 = 0$), ν_3^c light ($F_3 = 10$)**
  Here the mixing matrix is found by removing the fourth row and column of Eqs. (4.51) and (4.57), so that the matrix elements in Eqs. (4.67) and (4.69) can be relabelled $|\tilde{U}_{e5}|^2 \to |\tilde{U}_{e4}|^2$ and $|\tilde{U}_{\mu 5}|^2 \to |\tilde{U}_{\mu 4}|^2$. The light neutrino mass eigenvalues m_i $(i = 1,2,3,4)$ are now found by setting ϵ_1 to zero in Eqs. (C.18) and (C.20), with the relabelling $m_5 \to m_4$; the heavy neutrino has the mass $M_2 = w_2 u'$. The roles of the sterile neutrinos are swapped, and M_2 is situated at the 10^{11} GeV scale. The effective mass at leading order is

$$\begin{aligned} |\langle m_{ee}\rangle|^{(\mathrm{NO})} &= \left|\frac{m_2^{(0)}}{3}\right| = \frac{\sqrt{\Delta m^2_{\mathrm{S}}}}{3} \simeq 0.0029 \text{ eV}\,, \\ |\langle m_{ee}\rangle|^{(\mathrm{IO})} &= \left|\frac{m_2^{(0)}}{3}\right| \simeq \frac{\sqrt{\Delta m^2_{\mathrm{A}}}}{3} \simeq 0.016 \text{ eV}\,; \end{aligned} \tag{4.76}$$

  in this case the contribution of $m_3^{(0)}$ has cancelled. Again, corrections to the mixing angles give very small corrections to the effective mass.

In both cases IIA and IIB one could potentially explain the 3+1 neutrino mixing scenario [151, 153], with $|\tilde{U}_{e4}|^2 \simeq [1 + \mathcal{O}(r_1)]\,\epsilon_1^2$ in case IIA and $|\tilde{U}_{e4}|^2 \simeq 4[1 + \mathcal{O}(r_1)]\epsilon_2^2$ in the IO in case B. Once again only the IO fits the data: the allowed ranges in the mass-mixing plane for the IO in case IIA (IIB) are shown by the blue (red) points in Fig. 4.3. One can see that the best-fit point (the black cross) from Ref. [153] is compatible with case IIB. Finally, the effects of higher-order operators on both active-sterile mixing and active mixing are the same as in scenario I, except that one should switch off the effect of ϵ_2 (ϵ_1) in case IIA (IIB).

Scenario III: two heavy right-handed neutrinos

Here $F_1 = 9$, $F_{2,3} = 5$, so that one can estimate that the $\epsilon_i \simeq 10^{-6}$ $(i = 1,2)$ are suppressed, and the NLO seesaw terms in Eqs. (4.51) and (4.57) can be safely neglected. The 3×3 effective

neutrino mass matrix is given by Eq. (2.15), with M_D defined in Eqs. (4.49) or (4.56) and M_R from Eq. (4.50); the active neutrino masses are simply given by the leading order masses $m_i^{(0)}$. The heavy neutrinos have masses $M_2 = w_2 u' \lambda^{10}$ and $M_3 = w_3 u'' \lambda^{10}$. Without the effect of the ϵ_i terms, the only modifications to the TBM pattern come from the higher-order operators in Section 4.2.3.

The two heavy right-handed neutrinos that participate in the seesaw formula have masses around 5 GeV, assuming order one Yukawas and the usual values of the VEVs. Note that one could set $w_2 = w_3$ to obtain degenerate right-handed neutrinos $M_2 = M_3$. The choice of degenerate sterile neutrinos in the few-GeV regime would correspond to the νMSM paradigm, discussed in Section 3.6.3, where baryogenesis comes from oscillations. On the other hand, if $F_{2,3} = 0$ then $M_{2,3} \simeq 10^{11}$ GeV, so that the usual thermal leptogenesis scenario could be at play. The required CP violation may originate from complex Yukawa couplings.

Neutrinoless double beta decay is allowed in this scenario, and the right-handed neutrinos play no role in this process since their contribution $\sum_{i=2,3} S_i^2/M_i$ is strongly suppressed by the inverse of their mass. Explicitly, at leading order the effective mass from the $(1,1)$ entry of Eq. (2.15) is

$$|\langle m_{ee} \rangle|^{(\mathrm{NO})} = \left| \frac{m_2^{(0)}}{3} \right| = \frac{\sqrt{\Delta m^2_{\mathrm{S}}}}{3} \simeq 0.0029 \text{ eV} , \tag{4.77}$$

$$|\langle m_{ee} \rangle|^{(\mathrm{IO})} = \left| \frac{2m_1^{(0)}}{3} + \frac{m_2^{(0)}}{3} \right| \simeq \sqrt{\Delta m^2_{\mathrm{A}}} \simeq 0.049 \text{ eV} , \tag{4.78}$$

where the mass eigenvalues are real. If $m_1^{(0)}$ and $m_2^{(0)}$ are complex, the IO case becomes $|\langle m_{ee} \rangle|^{(\mathrm{IO})} \lesssim \sqrt{\Delta m^2_{\mathrm{A}}}$. Corrections from higher-order terms are again small.

Summary

The explicit model constructed in this section shows that the seesaw mechanism also works even if the scale of the sterile neutrinos is not the "natural" one of 10^{10} to 10^{15} GeV, as long as the Dirac mass matrix can also be suppressed such that M_D^2/M_R is small. Indeed, the observations pointing to sterile neutrinos at the eV and keV scales may require a modification of the usual seesaw framework. Although one can explain both eV-scale and keV-scale sterile neutrinos in a single model, it is not possible to have viable WDM, eV-scale neutrinos and heavy neutrinos for leptogenesis in a model containing just three right-handed neutrinos. In the study presented here the production mechanism of the WDM particle is not examined in detail; the purpose is rather to show that seesaw models with flavour symmetries have the required ingredients to provide a keV particle with the correct mass and small enough mixing with the active sector.

In the context of A_4 flavour symmetry models it is relatively straightforward to use the FN mechanism to suppress the masses of the right-handed neutrinos, and the required $U(1)_{\mathrm{FN}}$ symmetry is often already present in order to generate the charged lepton mass hierarchy. There are different possible spectra in the sterile sector: once the keV WDM neutrino is decoupled one can have the remaining two neutrinos at the eV scale or at a high scale (e.g, at either 10 GeV or close to the flavour symmetry breaking scale of $\simeq 10^{11}$ GeV). In each case there are distinct phenomenological consequences, both for neutrino mass and neutrinoless double beta decay. In particular, NLO corrections to the seesaw formula need to be taken into account when the

sterile neutrinos are at the eV scale, and in general active neutrino mixing angles will receive corrections of the same order. Higher-order operators are required in order to perturb the leading-order TBM pattern, but active-sterile mixing is rather robust, since it is proportional to the ratio of two scales.

4.3 Bimodal neutrinos in an S_3 model

4.3.1 Pseudo-Dirac vs. bimodal neutrinos

Pseudo-Dirac neutrinos were introduced in Section 2.2.1: a tiny Majorana mass is added for either one or both of the two two-component neutrino states that make up the Dirac neutrino. The stringent constraints on the pseudo-Dirac mass splitting from solar neutrino experiments have already been discussed: $\delta m_i^2 \lesssim 10^{-11}$ eV^2. The so-called bimodal or schizophrenic scenario is an intermediate possibility, first introduced in Ref. [27]. The key point is that one defines the Dirac or Majorana nature of neutrinos in terms of mass eigenstates instead of flavour eigenstates, thus allowing some mass eigenstates to be Dirac and others to be Majorana. The flavour eigenstates become "bimodal", in the sense that they contain large admixtures of both types of mass. One then needs to add as many sterile neutrino states to the standard model as there are Dirac mass eigenstates.

The bimodal flavour case ($M_D \simeq M_R$) is different from the pseudo-Dirac case ($M_D \gg M_R$) and the seesaw case ($M_D \ll M_R$) in the sense that the lepton number conserving and violating terms have comparable magnitude. Neutrino oscillations remain unaffected, unlike the case of pseudo-Dirac flavour neutrinos. In addition, bimodal neutrinos propagate in matter in the same way as those in the pure Majorana or pure Dirac case. However, the predictions for $0\nu\beta\beta$ will be markedly different from both the pure Majorana and pseudo-Dirac possibilities, as described in Section 3.4.3. From a model-building point of view, one needs to introduce symmetries that treat some mass eigenstates differently from others. In most realistic cases (without additional symmetries), the tree level Dirac mass eigenstate will receive a tiny ($\leq 10^{-14}$ eV) amount of Majorana mass from one-loop corrections, effectively making it pseudo-Dirac. This leads to the effects discussed in Section 3.5.2, since one could have one, two or three mass-eigenstates pseudo-Dirac, leading to different flavour ratios in neutrino telescopes.

An S_3 model with one Dirac mass eigenstate was first written down in Ref. [27], and has been extended in Ref. [348]; the main ingredients are summarised here.

4.3.2 Effective S_3 model with one Dirac mass eigenstate

The permutation group S_3 has six elements, corresponding to the symmetry of an equilateral triangle.[9] There are three irreducible representations: two singlets $\underline{1}$ and $\underline{1}'$ and a doublet $\underline{2}$, with the product rules

$$\underline{1}' \otimes \underline{1}' = \underline{1}, \quad \underline{2} \otimes \underline{1}' = \underline{2}, \quad \underline{2} \otimes \underline{2} = \underline{2} + \underline{1} + \underline{1}' . \tag{4.79}$$

For two doublets (a_1, a_1) and (b_1, b_2) the tensor product is

$$\begin{pmatrix} a_1 \\ a_2 \end{pmatrix}_{\underline{2}} \otimes \begin{pmatrix} b_1 \\ b_2 \end{pmatrix}_{\underline{2}} = (a_1 b_1 + a_2 b_2)_{\underline{1}} + (a_1 b_2 - a_2 b_1)_{\underline{1}'} + \begin{pmatrix} a_1 b_2 + a_2 b_1 \\ a_1 b_1 - a_2 b_2 \end{pmatrix}_{\underline{2}} , \tag{4.80}$$

[9] See Ref. [22] for a detailed description of the group theory of S_3.

Table 4.5: Particle assignments of the effective S_3 model, where the subscripts L and R for left- and right-handed fields have been dropped.

Field	L_2	(L_1, L_3)	e^c	μ^c	τ^c	N_2	(N_1, N_3)	$h_{u,d}$	σ_e	σ_μ	σ_τ
$SU(2)_L$	2	2	1	1	1	1	1	2	1	1	1
S_3	$\underline{1}$	$\underline{2}$	$\underline{1}'$	$\underline{1}'$	$\underline{1}'$	$\underline{1}$	$\underline{2}$	$\underline{1}$	$\underline{1}'$	$\underline{1}'$	$\underline{1}'$
Z_{2e}	+	+	−	+	+	+	+	+	−	+	+
$Z_{2\mu}$	+	+	+	−	+	+	+	+	+	−	+
$Z_{2\tau}$	+	+	+	+	−	+	+	+	+	+	−

which will be useful in constructing the S_3-invariant Lagrangian in what follows. The triplet representation is reducible, i.e., $\underline{3} = \underline{1} + \underline{2}$, which reflects the fact that S_3 is a subgroup of S_4, since the latter contains $\underline{3}$ as an irreducible representation. By separating the fermion generations into singlets and doublets one naturally obtains a hierarchy amongst them, see for instance Ref. [349]. Several authors have also applied S_3 to neutrino mixing [350, 351]. The discussion here follows the models in Refs. [27, 31].

With the particle assignments in Table 4.5, the S_3 symmetry permutes the three families of $SU(2)_L$ lepton doublets $(L_e, L_\mu, L_\tau) \sim \underline{3}$ amongst themselves, where the subscript L has been dropped. Decomposing the triplet representation into a singlet and doublet allows one to write the mass eigenstates as linear combinations of lepton doublet fields, *viz.*

$$\begin{aligned} L_2 &= \frac{1}{\sqrt{3}}(L_e + L_\mu + L_\tau) \sim \underline{1}\,, \\ (L_1, L_3) &= \left(\frac{1}{\sqrt{6}}(2L_e - L_\mu - L_\tau), \frac{1}{\sqrt{2}}(L_\mu - L_\tau)\right) \sim \underline{2}\,. \end{aligned} \tag{4.81}$$

The S_3 singlet field L_2 couples to the right-handed neutrino field $N_2 \sim \underline{1}$, which must be isolated from the other two right-handed neutrinos by additional quantum numbers that also forbid it from receiving a Majorana mass term. Details will be not be discussed here, since they relate to possible UV completions of the model. For instance, in one version with an anomaly-free $U(1)_{B-L}$ symmetry, the $B - L$ quantum number is chosen such that N_2 has $B - L = +5$ and $N_{1,3}$ each have $B - L = -4$ [348]. The $B - L$ breaking Higgs can be chosen to have quantum numbers such that only $N_{1,3}$ have large Majorana masses (see Ref. [27] for details). After integrating out the seesaw right-handed neutrinos N_1 and N_3, the effective lepton Dirac Yukawa coupling and dimension-five terms [cf. Eq. (2.8)] can be written as

$$\mathcal{L}_\nu = y_2 L_2 h_u N_2 + \frac{y_2^1}{M_{N_1}}(L_1 h_u)^2 + \frac{y_3^2}{M_{N_3}}(L_3 h_u)^2 + \text{h.c.}, \tag{4.82}$$

with y_i $(i = 1, 2, 3)$ dimensionless coupling constants and h_u the up-type Higgs doublet. After electroweak symmetry breaking, the neutrino sector has one Dirac neutrino corresponding to the mass eigenstate ν_2, two Majorana eigenstates ν_1 and ν_3, as well as TBM.

The Lagrangian in Eq. (4.82), together with the S_3 assignments in Eq. (4.81) and the group multiplication rules in Eqs. (4.79) and (4.80) allow one to construct the symmetric 4×4 neutrino

mass matrix in the flavour basis $(\nu_e, \nu_\mu, \nu_\tau, N_2)$, i.e.,

$$M_\nu = \frac{m_2}{\sqrt{3}} \left(\begin{array}{ccc|c} 0 & 0 & 0 & 1 \\ \cdot & 0 & 0 & 1 \\ \cdot & \cdot & 0 & 1 \\ \hline \cdot & \cdot & \cdot & 0 \end{array}\right) + \frac{m_1}{6} \left(\begin{array}{ccc|c} 4 & -2 & -2 & 0 \\ \cdot & 1 & 1 & 0 \\ \cdot & \cdot & 1 & 0 \\ \hline \cdot & \cdot & \cdot & 0 \end{array}\right) + \frac{m_3}{2} \left(\begin{array}{ccc|c} 0 & 0 & 0 & 0 \\ \cdot & 1 & -1 & 0 \\ \cdot & \cdot & 1 & 0 \\ \hline \cdot & \cdot & \cdot & 0 \end{array}\right)$$
$$= \left(\begin{array}{ccc|c} \frac{2m_1}{3} & -\frac{m_1}{3} & -\frac{m_1}{3} & \frac{m_2}{\sqrt{3}} \\ \cdot & \frac{m_1}{6}+\frac{m_3}{2} & \frac{m_1}{6}-\frac{m_3}{2} & \frac{m_2}{\sqrt{3}} \\ \cdot & \cdot & \frac{m_1}{6}+\frac{m_3}{2} & \frac{m_2}{\sqrt{3}} \\ \hline \cdot & \cdot & \cdot & 0 \end{array}\right), \tag{4.83}$$

with $m_1 = y_1^2 v_u^2 / M_{N_1}$, $m_3 = y_3^2 v_u^2 / M_{N_3}$, and $m_2 = y_2 v_u$, where $v_u = \langle h_u \rangle$. In order for the Majorana and Dirac mass matrix elements to have comparable magnitudes, the Yukawa coupling y_2 must be of order 10^{-12}. One motivation for this comes from supersymmetric versions of such models, where the right-handed sneutrino drives inflation and a small Dirac coupling is required to give consistent predictions (see Ref. [27] for details).

The leading order mass matrix in Eq. (4.83) will receive small Majorana corrections from one-loop effects [25, 27, 352, 353], if lepton number is not conserved. Indeed, the charged lepton mass terms break the symmetry in the effective low energy Lagrangian of Eq. (4.82), resulting in mixing between different mass eigenstates in the finite wave function renormalisation corrections that arise at the one-loop level. This leads to new terms of the form $\delta_{12} \bar{\nu}_2 \gamma^\mu \partial_\mu \nu_1$, where $\delta_{12} \sim \frac{G_F m_\tau^2}{16\pi^2\sqrt{6}} \sim 10^{-7}$; diagonalisation of the kinetic terms gives the new states $\nu_1' \approx \nu_1 + \delta_{12}\nu_2$. The Majorana mass term for ν_1 in the new basis leads to a Majorana mass of magnitude $\delta_{12}^2 m_1$ for ν_2. From these rough estimates, the pseudo-Dirac contribution to the Dirac eigenstate is of order $10^{-14}\sqrt{\Delta m^2_{\rm A}} \sim 10^{-15}$ eV, corresponding to an oscillation length of $\mathcal{O}(10)$ kpc. This implies that extra-galactic neutrinos from sources beyond 10 kpc will have half of their ν_2 component oscillate into sterile neutrinos, as described in the previous chapter in Section 3.5.2.

As far as corrections to neutrino mixing are concerned, if the $(4,4)$ entry of m_ν is perturbed to $\epsilon\, m_2$, the diagonalisation matrix is

$$U = \left(\begin{array}{cc} U_{\rm TBM} & 0_3^T \\ 0_3 & 1 \end{array}\right) \left(\begin{array}{cc} 1 & 0_3 \\ 0_3^T & R(\pi/4 + \epsilon/4) \end{array}\right), \tag{4.84}$$

where $0_3 = (0,0,0)$ and $R(\theta)$ is the 3×3 unitary rotation matrix

$$R(\theta) = \begin{pmatrix} \cos\theta & 0 & -\sin\theta \\ 0 & 1 & 0 \\ \sin\theta & 0 & \cos\theta \end{pmatrix}. \tag{4.85}$$

The diagonal mass matrix is $\tilde{m}_\nu = \mathrm{diag}(m_1, m_2(1+\epsilon/2), m_3, -m_2(1-\epsilon/2))$, to first order in ϵ.

The full PMNS matrix will include rotations from the charged lepton sector [cf. Eq. (2.20)], which can be described by writing down the most general Yukawa superpotential, *viz.*

$$\begin{aligned} \mathcal{W}_{\rm Y}^\ell &= \frac{1}{\Lambda} h_e h_d (L_e \sigma_e e^c + L_\mu \sigma_\mu \mu^c + L_\tau \sigma_\tau \tau^c) \\ &+ \frac{1}{\Lambda} h_\mu h_d (L_\mu \sigma_e e^c + L_\tau \sigma_\mu \mu^c + L_e \sigma_\tau \tau^c) \\ &+ \frac{1}{\Lambda} h_\tau h_d (L_\tau \sigma_e e^c + L_e \sigma_\mu \mu^c + L_\mu \sigma_\tau \tau^c) + \text{h.c.}, \end{aligned} \tag{4.86}$$

where $(\sigma_e, \sigma_\mu, \sigma_\tau)$ are gauge singlet superfields and h_α ($\alpha = e, \mu, \tau$) are Yukawa couplings. Three extra Z_2 symmetries that "glue" each charged lepton singlet (e^c, μ^c, τ^c) to the corresponding σ_α gauge singlet have been assumed [351], as shown in Table 4.5. This means that although the neutrino mass matrix is diagonalised by the TBM matrix, there are small corrections from the charged lepton sector via the matrix V_L^ℓ, see Eq. (2.7). The final PMNS matrix has a perturbed TBM form, and the complete diagonalisation matrix takes the same form as Eq. (4.84), with $U_{\rm TBM}$ replaced by $V_L^{\ell\dagger} U_{\rm TBM}$.

In this model only the ν_2 mass eigenstate has a Dirac mass, but the idea can easily be generalised in the sense that one or both of the other two neutrino mass eigenstates (ν_1 and/or ν_3) could be Dirac. The case in which two of the eigenstates are Dirac has been discussed in Ref. [31], where it was shown that a supersymmetric model with inverse seesaw can be constructed to obtain this scenario.

In summary, it is possible to construct models in which some neutrino mass eigenstates are Dirac while others are Majorana: the bimodal scenario. The S_3 symmetric model described above provides one example of embedding this idea into a flavour symmetry model. The deviation from TBM implied by current data can be accommodated by charged lepton corrections. Unfortunately the small Dirac masses are obtained at the price of tuning the Yukawa couplings; it would clearly be more desirable to be able to predict those small values from theory. The unusual signatures of bimodal neutrinos have already been described in the previous chapter. Indeed, measurements of the flux ratios of extra-galactic high energy neutrinos as well as the effective mass for $0\nu\beta\beta$ should be able to rule out this model for neutrino masses. On the other hand, if the bimodal hypothesis is supported by experiment it will not only provide a major departure from our current thinking about the nature of neutrino masses, but also its theoretical origin from physics beyond the SM.

4.4 Summary and conclusion

The models considered in this chapter are examples of neutrino mass models with light sterile neutrinos at different mass scales. They have been constructed in order to explain not only active neutrino masses and mixing but also the various anomalies and phenomenological hints for light sterile neutrinos summarised in Chapter 3. Although adding light states to existing effective models is a relatively simple exercise, one would like to build UV-complete models. The seesaw model in Section 4.2.3 is a step in this direction, but admittedly contains a large number of parameters and extra scalar fields, generic to flavour symmetry models. In addition, since the leading-order prediction for active neutrino mixing angles is disfavoured one might consider a new symmetry as a starting point. The same can be said for the S_3 bimodal model in Section 4.3. In that sense the models built here can be used as a rough guide for future sterile neutrino models with flavour symmetries.

Chapter 5

Lepton number and lepton flavour violation in the left-right symmetric model

5.1 Introduction

The "fully sterile" neutrinos in the models of the previous chapter only interact via their mixing with the active sector, which in the seesaw model case can be expressed as a ratio of two scales, $S \simeq M_D/M_R$. Those sterile states are gauge singlets, so that one is free to introduce as many as required (n_s). However, from a theoretical point of view it would be desirable to embed new particles into a larger framework, which is the idea behind GUTs. Once sterile neutrinos become "weakly sterile" they can also feel interactions from the new physics sector, which from a phenomenological perspective means new types of signatures. Embedding into a gauge theory results in interactions with new gauge bosons, which produce signatures at colliders, in experiments searching for lepton flavour violation and in neutrinoless double beta decay.

The left-right symmetric model is an example of a theory in which right-handed neutrinos are no longer gauge singlets, and light neutrino masses arise naturally from both type I and type II seesaw terms [cf. Eq. (2.51)], with neutrino mass connected to the restoration of parity at high energies. The magnitude of the two seesaw contributions is indistinguishable in neutrino oscillation experiments, so that one needs another approach to discover the neutrino mass generation mechanism. In particular, the particles responsible for neutrino mass can also mediate several different diagrams leading to $0\nu\beta\beta$ and LFV processes, and could be produced at colliders. It is however rather difficult to pin down the mechanism by which the $0\nu\beta\beta$ process occurs.

The phenomenology of the LRSM is only observable in current experiments if parity restoration occurs at the TeV scale, which will be assumed in what follows. Explicitly this means that $v_R \simeq$ TeV [cf. Eq. (2.48)]. Other limits on the scales in the model come from the quark sector, for instance from flavour changing processes in which right-handed W bosons are exchanged in loops, or from the neutron electric dipole moment. Ref. [354] provides a summary of the relevant constraints, which depend on whether one assumes charge or parity symmetry, see Section 2.3.2. One of the most important observables is the K meson mass difference, which leads to $m_{W_R} > 2.5$ TeV and $m_{H_1^0} > 7.7$ TeV. In the analysis that follows the mass of the W_R boson will be fixed to 3.5 TeV, which is still allowed by both LHC data as well as the indirect bounds from neutral meson mixing.

The connection between double beta decay, colliders and lepton flavour violation has recently been studied by several authors [94, 283, 355–359]. It is possible to simplify the analysis by assuming the dominance of either type I or type II seesaw terms; the latter case is particularly straightforward, and has been studied in the literature before [355, 357]. Here the number of parameters is greatly reduced since the right- and left-handed Majorana mass terms are proportional to each other. A detailed investigation of this case will be described below, with

LFV constraints included in the calculation of the $0\nu\beta\beta$ halflife.

The case of type I seesaw dominance is more complicated: there are some contributions to $0\nu\beta\beta$ that involve the left- and right-handed sectors individually as well as others that involve both sectors, through "left-right mixing". A simplified version was studied in Ref. [357], and a useful formula relating the various mass matrices of the theory was presented in Ref. [94], for the case of symmetric Dirac coupling. Particularly noteworthy is the fact that $0\nu\beta\beta$ processes involving left-right mixing could be enhanced for specific Dirac mass matrices, since that mixing is simply a ratio of the Dirac and Majorana mass scales. This enhancement [263] is also required for collider signatures of the TeV-scale seesaw mechanism, as discussed in Section 3.7.1 (see the review in Ref. [360]), and there have been several studies of related phenomenology [361–364]. In the LRSM case both the so-called λ- and η-diagrams could be enhanced, although the latter is further suppressed by the mixing between left- and right-handed gauge bosons. This idea has also been emphasised in extended seesaw versions of the LRSM [358, 359]. A thorough analysis of the type I seesaw scenario will be carried out here, with special attention paid to the correct nuclear matrix elements for the different diagrams as well as the often severe constraints from lepton flavour violating phenomena.

Due to the large number of competing mechanisms for $0\nu\beta\beta$ an independent test would provide valuable information about the nature of lepton number violation. The inverse neutrinoless double beta decay process described in Section 3.7.2 is one such test that could be performed at a linear collider. In the LRSM one could even produce the new gauge boson W_R in collisions with charged leptons. A recent analysis was performed in Ref. [295], excluding right-handed currents; here the process $e^-e^- \to W_L^- W_R^-$ is studied. This process is indeed the most interesting, which will be shown from kinematical arguments and an examination of the amplitudes for $0\nu\beta\beta$.

A detailed discussion of $0\nu\beta\beta$ and LFV processes in the LRSM will be provided in Sections 5.2 and 5.3, and there is a brief summary of LHC signatures in Section 5.4. A quantitative analysis of the various $0\nu\beta\beta$ amplitudes in the limit of type I or type II seesaw dominance is presented in Section 5.5, with details of decay widths and loop functions for LFV processes delegated to Appendix D. A complementary analysis of the linear collider process of inverse neutrinoless double beta decay can be found in Section 5.6. The theoretical details of the model have been introduced in Section 2.3, which provides the background necessary for the analysis of this chapter.

5.2 Neutrinoless double beta decay

5.2.1 Particle physics amplitudes

There are several possible diagrams for $0\nu\beta\beta$ in the LRSM, due to the presence of right-handed currents, heavy right-handed neutrinos and Higgs triplets (for one of the first analyses on this

topic, see Ref. [365]). The charged current Lagrangian in Eq. (2.61) can be written as

$$\begin{aligned}\mathcal{L}_{CC}^{\text{lep}} &= \frac{g}{\sqrt{2}}\sum_{i=1}^{6}\Big[\overline{e}\,\gamma^{\mu}(K_L)_{ei}P_L n_i(W_{1\mu}^{-}+\xi e^{i\alpha}W_{2\mu}^{-}) \\ &\quad + \overline{e}\,\gamma^{\mu}(K_R)_{ei}P_R n_i(-\xi e^{-i\alpha}W_{1\mu}^{-}+W_{2\mu}^{-})\Big] + \text{h.c.} \\ &= \frac{g}{\sqrt{2}}\sum_{i=1}^{3}\Big[\overline{e_L}\gamma^{\mu}(U_{ei}\nu_{Li}+S_{ei}N_{Ri}^{c})(W_{1\mu}^{-}+\xi e^{i\alpha}W_{2\mu}^{-}) \\ &\quad + \overline{e_R}\gamma^{\mu}(T_{ei}^{*}\nu_{Li}^{c}+V_{ei}^{*}N_{Ri})(-\xi e^{-i\alpha}W_{1\mu}^{-}+W_{2\mu}^{-})\Big] + \text{h.c.},\end{aligned} \tag{5.1}$$

where in the second line the charged leptons are assumed to be diagonal (this basis will be used from now on, so that $\tilde{U}=U$ and all processes can be expressed in terms of the matrices U, S, T and V). $0\nu\beta\beta$ amplitudes arise from second order terms in perturbation theory: it is clear that one can combine either two left-handed currents, two right-handed currents or one left- and one right-handed current. The relevant mixing matrix element also depends on whether light or heavy neutrinos are exchanged in the process; the matrices U, V, S and T are [cf. Eq. (2.13)]

$$\begin{aligned}&U \equiv \left[\mathbb{1}-\frac{1}{2}M_D M_R^{-1}(M_D M_R^{-1})^{\dagger}\right]V_{\nu}, \quad V \equiv \left[\mathbb{1}-\frac{1}{2}(M_D M_R^{-1})^{\dagger}M_D M_R^{-1}\right]V_R, \\ &S \equiv M_D M_R^{-1}V_R, \quad T \equiv -(M_D M_R^{-1})^{\dagger}V_{\nu}\,,\end{aligned} \tag{5.2}$$

to second order in M_D/M_R, which shows that light neutrino mixing is no longer unitary. The additional possibility of W_L-W_R mixing allows for diagrams with, for instance, two left-handed hadronic currents but one left- and one right-handed leptonic current [see Fig. 5.3(b)], with the corresponding suppression factor of $\tan\xi$ [Eq. (2.60)].

Neutrinoless double beta decay processes in the LRSM can be categorised in terms of their topology and the helicity of the final state electrons; the most relevant diagrams that will be discussed in detail in what follows are shown in Figs. 3.5, 3.11, 5.1, 5.2 and 5.3 (see Ref. [165] for a complete list). Limits on the particle physics parameters are calculated using the recent KamLAND-Zen limit [166] and are summarised in Table 5.1. Note that the chiral structure of the matrix element means that the neutrino propagator becomes [366]

$$P_{L,R}\frac{\not{q}+m_i}{q^2-m_i^2}P_{L,R} = \frac{m_i}{q^2-m_i^2} \quad \text{or} \quad P_{L,R}\frac{\not{q}+m_i}{q^2-m_i^2}P_{R,L} = \frac{\not{q}}{q^2-m_i^2}\,, \tag{5.3}$$

leading to mass or momentum dependence when the leptonic vertices have the same or opposite chirality, respectively, and providing a useful way to categorise the different possible mechanisms. In order to give a rough estimate of the relative magnitudes of $0\nu\beta\beta$ amplitudes, the masses of all particles belonging to the right-handed sector (M_i, W_R and δ_R) will be denoted as $R \simeq$ TeV, and those from the left-handed sector as $L \simeq 10^2$ GeV (corresponding to the weak scale, or the mass of the W_L). The matrices T and S describing left-right mixing can be written as L/R, and the gauge boson mixing angle ξ is of order $(L/R)^2$. Note that with this definition the order of magnitude of the type I seesaw contribution is $m_\nu \simeq L^2/R$, which is far too large in the naive case (without cancellations). As mentioned above, the TeV scale for R is a necessary choice if one wants to have signatures in current experiments.

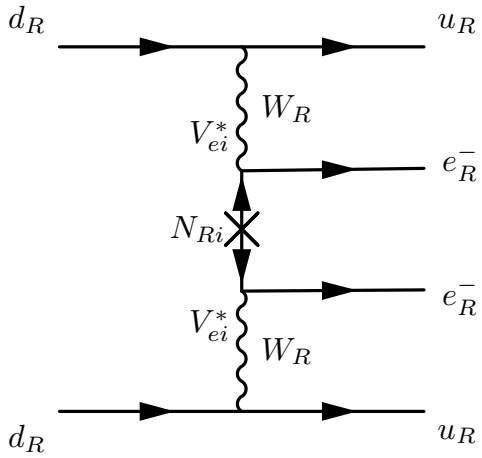

Figure 5.1: Feynman diagram of $0\nu\beta\beta$ in the LRSM, mediated by heavy neutrinos with right-handed currents ($\mathcal{A}^R_{N_R}$), analogous to Fig. 3.11. Diagrams with light neutrino exchange and right-handed currents are negligible.

Mass-dependent mechanisms

In this case the emitted electrons have the same chirality and there are either light or heavy neutrinos exchanged, with mass denoted by m_i and M_i. With both electrons left-handed the amplitude is proportional to

$$\mathcal{A}_{LL} \simeq G_F^2 \left(1 + 2\tan\xi + \tan^2\xi\right) \sum_i \left(\frac{U_{ei}^2 m_i}{q^2} - \frac{S_{ei}^2}{M_i}\right), \tag{5.4}$$

whereas if both are right-handed it becomes

$$\mathcal{A}_{RR} \simeq G_F^2 \left(\frac{m_{W_L}^4}{m_{W_R}^4} + 2\frac{m_{W_L}^2}{m_{W_R}^2}\tan\xi + \tan^2\xi\right) \sum_i \left(\frac{T_{ei}^{*\,2} m_i}{q^2} - \frac{V_{ei}^{*2}}{M_i}\right). \tag{5.5}$$

These expressions take into account diagrams with gauge boson mixing at one or both vertices, but the most relevant diagrams are:

- Fig. 3.5, the "standard" diagram, which has already been discussed in Section 3.4.1. The amplitude and particle physics parameter given in Eqs. (3.23) and (3.46) are repeated here for convenience:

  $$\mathcal{A}_\nu \simeq G_F^2 \frac{\langle m_{ee}\rangle_{3\nu}}{q^2}, \tag{5.6}$$

  with $\langle m_{ee}\rangle_{3\nu}$ defined in Eq. (3.25), and

  $$|\eta_\nu| = \frac{|\langle m_{ee}\rangle_{3\nu}|}{m_e} =\lesssim 7.1 \times 10^{-7}. \tag{5.7}$$

  Figure 3.6 displays the currently allowed regions of the effective mass.

- Fig. 3.11, discussed in the usual type I seesaw context in Section 3.4.4, in which heavy neutrinos are exchanged with purely left-handed currents. The amplitude is proportional to

  $$\mathcal{A}^L_{N_R} \simeq G_F^2 \sum_i \frac{S_{ei}^2}{M_i} \propto \frac{L^2}{R^3}, \tag{5.8}$$

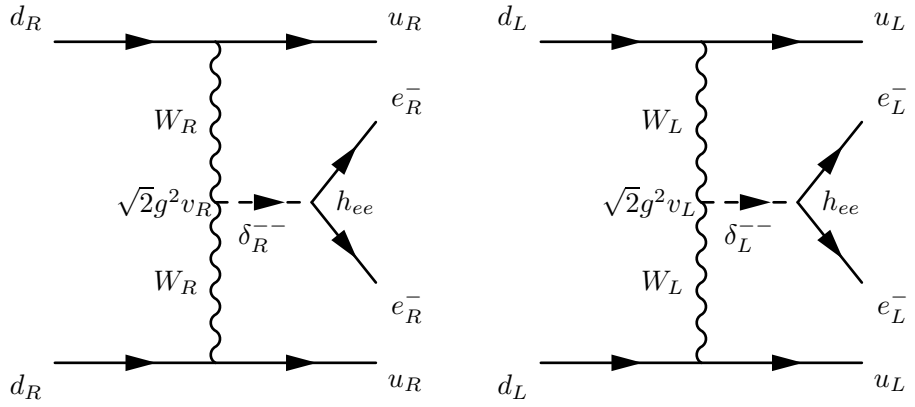

(a) $\mathcal{A}_{\delta_R}$ (b) $\mathcal{A}_{\delta_L}$

Figure 5.2: Feynman diagrams of $0\nu\beta\beta$ in the left-right symmetric model, mediated by doubly charged triplets: (a) triplet of $SU(2)_R$ and (b) triplet of $SU(2)_L$.

with $S \simeq L/R$ describing the mixing of the heavy neutrinos with left-handed currents. The limit is given in Eq. (3.47), i.e.,

$$\left|\eta^L_{N_R}\right| = m_p \left|\sum_i \frac{S^2_{ei}}{M_i}\right| \lesssim 7.0 \times 10^{-9}\,. \tag{5.9}$$

Note that the sum in Eq. (5.8) can be written as

$$\sum_i \frac{S^2_{ei}}{M_i} = \left[M_D M_R^{-1} M_R^{-1*} M_R^{-1} M_D^T\right]_{ee}\,, \tag{5.10}$$

which vanishes for negligible Dirac Yukawa couplings. It is also possible to have light neutrino exchange with right-handed currents [the term proportional to T in Eq. (5.5)], but that diagram is highly suppressed.

- Fig. 5.1, which is the analogous diagram with purely right-handed currents, mediated by right-handed neutrinos. The amplitude is proportional to

$$\mathcal{A}^R_{N_R} \simeq G_F^2 \left(\frac{m_{W_L}}{m_{W_R}}\right)^4 \sum_i \frac{V^{*2}_{ei}}{M_i} \propto \frac{L^4}{R^5}\,, \tag{5.11}$$

where m_{W_R} (m_{W_L}) is the mass of the right-handed W_R (left-handed W_L), M_i the mass of the heavy neutrinos and V the right-handed analogue of the PMNS matrix U. The dimensionless particle physics parameter is

$$\left|\eta^R_{N_R}\right| = m_p \left(\frac{m_{W_L}}{m_{W_R}}\right)^4 \left|\sum_i \frac{V^{*2}_{ei}}{M_i}\right| \lesssim 7.0 \times 10^{-9}\,. \tag{5.12}$$

Triplet exchange mechanisms

- Fig. 5.2(a) is a diagram with different topology, mediated by the triplet of $SU(2)_R$. The amplitude is given by

$$\mathcal{A}_{\delta_R} \simeq G_F^2 \left(\frac{m_{W_L}}{m_{W_R}}\right)^4 \sum_i \frac{V^2_{ei} M_i}{m^2_{\delta_R^{--}}} \propto \frac{L^4}{R^5}\,, \tag{5.13}$$

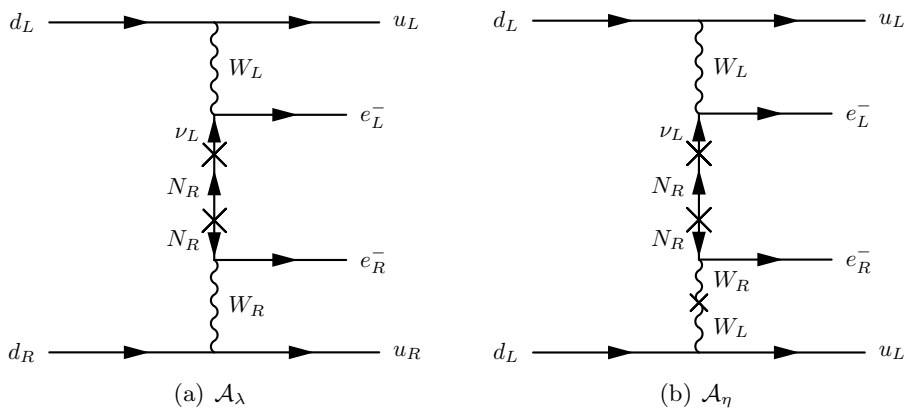

(a) $\mathcal{A}_\lambda$ (b) $\mathcal{A}_\eta$

Figure 5.3: Feynman diagrams of neutrinoless double beta decay in the left-right symmetric model with final state electrons of different helicity: (a) the λ-mechanism and (b) the η-mechanism due to gauge boson mixing.

and the dimensionless particle physics parameter is

$$|\eta_{\delta_R}| = \frac{\left|\sum_i V_{ei}^2 M_i\right|}{m_{\delta_R^{--}}^2 m_{W_R}^4} \frac{m_p}{G_F^2} \lesssim 7.0 \times 10^{-9} \,. \tag{5.14}$$

The dependence on the heavy neutrino mass comes from the fact that $\sqrt{2} v_R h_{ee}$ is nothing but the ee element of the right-handed Majorana neutrino mass matrix M_R diagonalised by V [cf. Eq. (2.51)], with v_R the VEV of the triplet δ_R and h_{ee} the coupling of the triplet with right-handed electrons;

- Fig. 5.2(b) is a diagram mediated by the triplet of $SU(2)_L$, also present in the usual type II seesaw model (without left-right symmetry). The amplitude is given by

$$\mathcal{A}_{\delta_L} \simeq G_F^2 \frac{h_{ee} v_L}{m_{\delta_L^{--}}^2} \,, \tag{5.15}$$

which is suppressed with respect to the standard light neutrino exchange by at least a factor $q^2/m_{\delta_L^{--}}^2$.

Momentum dependent mechanisms

In this case the emitted electrons have opposite helicity, and the amplitude is proportional to

$$\mathcal{A}_{LR} \simeq G_F^2 \left(\frac{m_{W_L}^2}{m_{W_R}^2} + \tan\xi + \frac{m_{W_L}^2}{m_{W_R}^2} \tan\xi + \tan^2\xi \right) \sum_i \left(U_{ei} T_{ei}^* \frac{1}{q} - S_{ei} V_{ei}^* \frac{q}{M_i^2} \right) ; \tag{5.16}$$

the most important diagrams are those involving light neutrinos and two powers of the left-right mixing in the prefactor, i.e.,

- The so-called λ-diagram in Fig. 5.3(a), with an amplitude

$$\mathcal{A}_\lambda \simeq G_F^2 \left(\frac{m_{W_L}}{m_{W_R}} \right)^2 \sum_i U_{ei} T_{ei}^* \frac{1}{q} \propto \frac{L^3}{R^3 q} \,, \tag{5.17}$$

and particle physics parameter

$$|\eta_\lambda| = \left(\frac{m_{W_L}}{m_{W_R}}\right)^2 \left|\sum_i U_{ei} T^*_{ei}\right| \lesssim 4.8 \times 10^{-7} \,. \tag{5.18}$$

Note that this is a long-range diagram with light neutrinos exchanged, with the matrix $T^*_{ei} = \mathcal{O}(M_D/M_R)$ quantifying the mixing of light neutrinos with right-handed currents.

- The η-diagram in Fig. 5.3(b), which also has mixed helicity and light neutrino exchange (long-range diagram). This is only possible due to $W_L - W_R$ mixing, described by the parameter $\tan\xi$ [see Eq. (2.57)]. The amplitude is

$$\mathcal{A}_\eta \simeq G_F^2 \tan\xi \sum_i U_{ei} T^*_{ei} \frac{1}{q} \propto \frac{L^3}{R^3 q} \,, \tag{5.19}$$

with particle physics parameter

$$|\eta_\eta| = \tan\xi \left|\sum_i U_{ei} T^*_{ei}\right| \lesssim 2.6 \times 10^{-9} \,. \tag{5.20}$$

Ref. [167] gives a detailed explanation of how a complicated cancellation of different nuclear physics amplitudes leads to a limit on the η-diagram that is much stronger than the one on the λ-diagram. The heavy neutrino contributions to both the λ- and η diagrams are further suppressed, being proportional to $\sum_i S_{ei} V^*_{ei} q/M_i^2$ [see Eq. (5.16)]. Using the mixing matrices in Eq. (5.2), the relevant sums become

$$\begin{aligned}
\sum_i U_{ei} T^*_{ei} &= \left[\left(\mathbb{1} - \frac{1}{2} M_D M_R^{-1} (M_D M_R^{-1})^\dagger\right) V_\nu \left(-(M_R^{-1})^T M_D^T V_\nu^*\right)^T\right]_{ee} \\
&\simeq -\left[M_D M_R^{-1}\right]_{ee} \,, \\
\sum_i S_{ei} V^*_{ei} &= \left[M_D M_R^{-1} V_R \left(\left(\mathbb{1} - \frac{1}{2}(M_D M_R^{-1})^T (M_D M_R^{-1})^*\right) V_R^*\right)^T\right]_{ee} \\
&\simeq \left[M_D M_R^{-1}\right]_{ee} \,,
\end{aligned} \tag{5.21}$$

neglecting third order terms, demonstrating that the left-right mixing is a ratio of two scales, M_D and M_R.

With all of the relevant diagrams written down one can make a rough estimate of their relative magnitudes in terms of $L \simeq 10^2$ GeV and $R \simeq$ TeV. Since the mixed λ- and η-diagrams in Fig. 5.3 are of order $(L/R)^3/q$ and the purely right-handed short-range diagrams in Figs. 5.1 (heavy neutrino exchange and right-handed currents) and 5.2(a) ($SU(2)_R$ triplet exchange and right-handed currents) are of order L^4/R^5, the mixed diagrams are expected to dominate by a factor $R^2/(Lq) \sim 10^5$. In the same way, the amplitudes of the mixed diagrams are also larger than the one for heavy neutrino exchange with left-handed currents in Fig. 3.11, proportional to L^2/R^3. The main point is that mixed diagrams should be examined more thoroughly, which will also be done in the context of inverse neutrinoless double beta decay in Section 5.6. It should be obvious that the light neutrino mass from type I seesaw, $m_\nu \simeq M_D^2/M_R \simeq L^2/R$ cannot be small enough without matrix cancellations; the crucial point is that the left-right mixing $M_D/M_R \simeq L/R$ can still be large in those cases.

The reliability of these rough approximations can be tested by calculating the ratios of amplitudes, using known bounds on the left-right mixing. The limits on the difference of the diagonal elements of the product $\epsilon_\alpha \equiv [SS^\dagger]_{\alpha\alpha} \simeq [T^\dagger T]_{\alpha\alpha}$ from lepton universality [367] are

$$\epsilon_e - \epsilon_\mu \lesssim 0.0022\,, \quad \epsilon_\mu - \epsilon_\tau \lesssim 0.0017\,, \quad \epsilon_e - \epsilon_\tau \lesssim 0.0039\,, \tag{5.22}$$

which give a rather weak bound on the left-right mixing. In the absence of cancellations (i.e., neglecting matrix structures) one finds a much stronger bound from the seesaw formula, namely

$$|S_{\alpha i}| \simeq |T^T_{\alpha i}| \simeq \sqrt{\frac{m_\nu}{M_i}} \lesssim 10^{-7} \left(\frac{\text{TeV}}{M_i}\right)^{1/2}, \quad (\alpha = e, \mu, \tau)\,, \tag{5.23}$$

which will be applied in the estimates that follow, along with the light neutrino mass scale $m_\nu \simeq 0.05$ eV and momentum exchange $|q| \simeq 100$ MeV.

For heavy neutrino exchange with right-handed currents [Fig. 5.1],

$$\frac{\mathcal{A}^R_{N_R}}{\mathcal{A}_\nu} \simeq \left(\frac{m_{W_L}}{m_{W_R}}\right)^4 \sum_i \frac{V^{*2}_{ei}}{M_i} \frac{q^2}{m_\nu} \simeq 8.36 \left(\frac{\text{TeV}}{m_{W_R}}\right)^4 \left(\frac{\text{TeV}}{M_i}\right), \tag{5.24}$$

whereas for heavy neutrino exchange with left-handed currents [Eq. (5.8)] the ratio is

$$\frac{\mathcal{A}^L_{N_R}}{\mathcal{A}_\nu} \simeq \sum_i \frac{S^2_{ei}}{M_i} \frac{q^2}{m_\nu} \lesssim \frac{q^2}{M_i^2} \simeq 10^{-8} \left(\frac{\text{TeV}}{M_R}\right)^2. \tag{5.25}$$

One sees immediately that this process requires cancellations to be enhanced.[1] However, for the λ- and η-diagrams [Fig. 5.3],

$$\frac{\mathcal{A}_\eta}{\mathcal{A}_\nu} \lesssim \frac{\mathcal{A}_\lambda}{\mathcal{A}_\nu} \simeq \left(\frac{m_{W_L}}{m_{W_R}}\right)^2 \sum_i U_{ei} T^*_{ei} \frac{q}{m_\nu} \lesssim \left(\frac{m_{W_L}}{m_{W_R}}\right)^2 \frac{q}{\sqrt{m_\nu M_i}} \simeq 2.89 \left(\frac{\text{TeV}}{m_{W_R}}\right)^2 \left(\frac{\text{TeV}}{M_R}\right)^{1/2}, \tag{5.26}$$

where the first inequality comes from the upper limit $|\xi| \lesssim \left(\frac{m_{W_L}}{m_{W_R}}\right)^2$. Without the bound in Eq. (5.23) that connects the left-right mixing T to light neutrino mass, $\mathcal{A}_\lambda$ and $\mathcal{A}_\eta$ could be even larger. However, even with such a stringent limit, Eq. (5.26) shows that the mixed helicity diagrams can compete with the standard light neutrino diagram. Depending on the relative magnitude of the bi-doublet VEVs κ_1 and κ_2, the amplitude $\mathcal{A}_\eta$ may be further suppressed [see Eq. (2.60)], but this could be compensated for by the fact that $\mathcal{M}^{0\nu}_\eta \simeq 10^2 \mathcal{M}^{0\nu}_\lambda$ (cf. Table 5.2). With the numerical values $m_{W_R} = 3.5$ TeV and $M_R = 500$ GeV, the naive estimates for $\mathcal{A}^R_{N_R}$, $\mathcal{A}_\lambda$ and $\mathcal{A}_\eta$ turn out to be quite close in magnitude, whereas the small value for $\mathcal{A}^L_{N_R}$ could still be enhanced by cancellations. Inverting the seesaw formula gives $M_D \simeq \sqrt{m_\nu M_R} \simeq 10^{-4}$ GeV, which means that the Yukawa matrices f and $\tilde{f}$ need to have non-trivial flavour structure in order to obtain the correct light neutrino mass [see Eq. (2.51)]. With $\mathcal{O}(1)$ couplings, $M_D \propto \kappa_i$, so that M_D would be near the electroweak scale of 10^2 GeV. Assuming that $\kappa_2 \ll \kappa_1$ (see also Ref. [89]) means that $M_D \simeq \kappa_1 f/\sqrt{2}$ and $M_\ell \simeq \kappa_2 \tilde{f}/\sqrt{2}$, so that one has the freedom to choose f without affecting the charged lepton sector.

[1] This case was also studied in Ref. [361, 363, 364, 368].

Table 5.1: Summary of relevant mechanisms for $0\nu\beta\beta$ in the left-right symmetric model, with limits on new physics parameters (written in bold face) in each case (see also Ref. [164]).

Mechanism	Amplitude	Current limit
light neutrino exchange ($\mathcal{A}_\nu$)	$\frac{G_F^2}{q^2}\left\|\boldsymbol{U_{ei}^2 m_i}\right\|$	0.36 eV
heavy neutrino exchange ($\mathcal{A}^L_{N_R}$)	$G_F^2\left\|\frac{\boldsymbol{S_{ei}^2}}{\boldsymbol{M_i}}\right\|$	7.4×10^{-9} GeV^{-1}
heavy neutrino exchange ($\mathcal{A}^R_{N_R}$)	$G_F^2 m_{W_L}^4\left\|\frac{\boldsymbol{V_{ei}^{*2}}}{\boldsymbol{M_i m_{W_R}^4}}\right\|$	1.7×10^{-16} GeV^{-5}
Higgs triplet exchange ($\mathcal{A}_{\delta_R}$)	$G_F^2 m_{W_L}^4\left\|\frac{\boldsymbol{V_{ei}^2 M_i}}{\boldsymbol{m^2_{\delta_R^{--}} m_{W_R}^4}}\right\|$	1.7×10^{-16} GeV^{-5}
λ-mechanism ($\mathcal{A}_\lambda$)	$G_F^2\frac{m_{W_L}^2}{q}\left\|\frac{\boldsymbol{U_{ei}T_{ei}^*}}{\boldsymbol{m_{W_R}^2}}\right\|$	7.5×10^{-11} GeV^{-2}
η-mechanism ($\mathcal{A}_\eta$)	$G_F^2\frac{1}{q}\left\|\boldsymbol{\tan\xi}\sum_i \boldsymbol{U_{ei}T_{ei}^*}\right\|$	2.6×10^{-9}

5.2.2 Nuclear matrix elements and lifetime

In order to translate the dimensionless particle physics parameters η_k into actual lifetimes of $0\nu\beta\beta$ processes for different isotopes, one needs the relevant nuclear matrix elements and phase space factors, discussed in Section 3.4.5. Most previous studies have focussed on the standard light neutrino exchange mechanism, with fewer groups calculating the matrix elements relevant to $0\nu\beta\beta$ in the LRSM. The QRPA calculation of the matrix elements for the mixed diagrams in Ref. [369] will be used in this analysis (see also Refs. [370, 371]).[2,3] In their notation, the lifetime of $0\nu\beta\beta$ can be written as

$$\begin{aligned}\left[T^{0\nu}_{1/2}\right]^{-1} = G^{0\nu}_{01}|\mathcal{M}^{0\nu}_{\rm GT}|^2\Big\{&|X_L|^2+|X_R|^2+\tilde{C}_2|\eta_\lambda||X_L|\cos\psi_1+\tilde{C}_3|\eta_\eta||X_L|\cos\psi_2\\&+\tilde{C}_4|\eta_\lambda|^2+\tilde{C}_5|\eta_\eta|^2+\tilde{C}_6|\eta_\lambda||\eta_\eta|\cos(\psi_1-\psi_2)+{\rm Re}\left[\tilde{C}_2X_R\eta_\lambda+\tilde{C}_3X_R\eta_\eta\right]\Big\}\,,\end{aligned}\tag{5.27}$$

where the coefficients $\tilde{C}_i$ are combinations of matrix elements and integrated kinematical factors, $G^{0\nu}_{01}$ is the usual phase space factor and ψ_i are complex phases. The parameters X_L (X_R) include all processes in which the final state electrons are both left-handed (right-handed), i.e.,

$$X_L \equiv \mathcal{M}'^{0\nu}_{\nu}\eta_\nu + \mathcal{M}'^{0\nu}_{N}\eta^L_{N_R} + \mathcal{M}'^{0\nu}_{N}\eta_{\delta_L}\,,\text{and}\quad X_R \equiv \mathcal{M}'^{0\nu}_{N}\eta^R_{N_R} + \mathcal{M}'^{0\nu}_{N}\eta_{\delta_R}\,,\tag{5.28}$$

with η_{δ_L} the lepton number violating parameter associated with Eq. (5.15). In Eq. (5.27) the interference term X_LX_R has been omitted: it is suppressed due to the different electron helicities ($e^-_Le^-_L$ vs $e^-_Re^-_R$). Interference terms with final states in which at least one of the electrons has

[2] p-n pairing effects [369] in general reduce the matrix elements compared to the ones reported in Ref. [370].
[3] There is also a shell model calculation [372] for ^{76}Ge, ^{82}Se and ^{136}Xe.

Table 5.2: Phase-space factors $G_{01}^{0\nu}$ [182, 369] and nuclear matrix elements for light ($\mathcal{M}_\nu^{0\nu}$) [181] and heavy ($\mathcal{M}_N^{0\nu}$) [183, 184] neutrino exchange, and for the λ- and η-diagrams [369, 371], for different isotopes and with $g_A = 1.25$ and $r_0 = 1.1$ fm [cf. Eq. (5.30)].

Isotope	$G_{01}^{0\nu}$ [10^{-14} yrs^{-1}] (old [369])	$G_{01}^{0\nu}$ [10^{-14} yrs^{-1}] (new [182])	$\mathcal{M}_\nu^{0\nu}$	$\mathcal{M}_N^{0\nu}$	$\mathcal{M}_\lambda^{0\nu}$	$\mathcal{M}_\eta^{0\nu}$
^{76}Ge	0.793	0.686	2.58–6.64	233–412	1.75–3.76	235–637
^{82}Se	3.53	2.95	2.42–5.92	226–408	2.54–3.69	209–234
^{130}Te	5.54	4.13	2.43–5.04	234–384	2.85–3.67	414–540
^{136}Xe	5.91	4.24	1.57–3.85	160–172	1.96–2.49	370–419

the same helicity have been included. The matrix elements $\mathcal{M}'^{0\nu}_\nu$ and $\mathcal{M}'^{0\nu}_N$ include Fermi and Gamow-Teller contributions.

An improved calculation of the phase space factor $G_{01}^{0\nu}$ for the light neutrino exchange mechanism has recently been performed in Ref. [182], taking into account the finite nuclear size of the Dirac wave function as well as electron screening effects and angular correlations. The factor is slightly lower, with the difference becoming more marked for heavier nuclei. The coefficients $\tilde{C}_i$ ($i = 2, 3, 4, 5, 6$) depend on different phase space factors [369, 373], which are assumed to be reduced by the same percentage as $G_{01}^{0\nu}$. More recent calculations [183, 184, 374] of light and heavy neutrino matrix elements include the Gamow-Teller factor $\mathcal{M}_{\rm GT}^{0\nu}$ in the relevant matrix elements $\mathcal{M}_\nu^{0\nu}$ and $\mathcal{M}_N^{0\nu}$. For consistency of notation one can define

$$\begin{aligned} \mathcal{M}_\nu^{0\nu} &\equiv \mathcal{M}_{\rm GT}^{0\nu}\mathcal{M}'^{0\nu}_\nu\,, \quad \mathcal{M}_N^{0\nu} \equiv \mathcal{M}_{\rm GT}^{0\nu}\mathcal{M}'^{0\nu}_N\,, \\ \mathcal{M}_\lambda^{0\nu} &\equiv \sqrt{|\mathcal{M}_{\rm GT}^{0\nu}|^2\tilde{C}_4}\,, \quad \mathcal{M}_\eta^{0\nu} \equiv \sqrt{|\mathcal{M}_{\rm GT}^{0\nu}|^2\tilde{C}_5}\,, \end{aligned} \tag{5.29}$$

so that the lifetime in Eq. (5.27) can be written as

$$\begin{aligned} \left[T_{1/2}^{0\nu}\right]^{-1} = G_{01}^{0\nu}\,\{&|\mathcal{M}_\nu^{0\nu}|^2|\eta_\nu|^2 + |\mathcal{M}_N^{0\nu}|^2|\eta_{N_R}^L|^2 + |\mathcal{M}_N^{0\nu}|^2|\eta_{N_R}^R + \eta_{\delta_R}|^2 \\ &+|\mathcal{M}_\lambda^{0\nu}|^2|\eta_\lambda|^2 + |\mathcal{M}_\eta^{0\nu}|^2|\eta_\eta|^2\} + \text{interference terms}. \end{aligned} \tag{5.30}$$

The corresponding matrix elements are reported in Table 5.2 and will be used in the analysis that follows. The new phase space numbers have been used to calculate limits.

In the limit of type II seesaw dominance, the expression in Eq. (5.30) will simplify considerably, whereas with type I seesaw dominance all six terms should be considered (neglecting the contribution stemming from the left-handed triplet δ_L, which is suppressed by light neutrino mass and $m_{\delta_L^{--}}$). The notation $[T_{1/2}^{0\nu}]_k$ ($k = \nu, N_R^{(R)}, N_R^{(L)}, \delta_R, \lambda, \eta$) is used to refer to the lifetime stemming from one particular diagram. The variation of the lifetime $[T_{1/2}^{0\nu}]_\nu$ with lightest neutrino mass was already displayed in Fig. 3.12; this plot will be repeated for other mechanisms.

5.3 Lepton flavour violation

Lepton flavour violating decays of charged leptons are important probes of new physics models at the TeV scale. The relevant processes and their corresponding limits have been introduced

in Section 3.7.3, with a focus on LFV decays of the muon, i.e., $\mu \to e\gamma$, $\mu \to 3e$ and $\mu \to e$ conversion. In the LRSM, the amplitudes for those processes receive contributions from (*i*) right-handed gauge bosons and Higgs triplets, suppressed by $(m_{W_L}/m_{W_R})^2$; (*ii*) left-handed gauge bosons, suppressed by $\simeq |M_D M_R^{-1}|^2$ and (*iii*) processes with $W_L - W_R$ mixing, suppressed by $\xi M_D M_R^{-1}$. Terms proportional to ξ^2 are expected to be small and are neglected here. All of the possible channels are in some way related to the right-handed neutrino mass, either directly as a virtual particle in the loop or indirectly since the couplings of the triplets to leptons are proportional to M_R.

A detailed calculation of the LFV decay widths and branching ratios in the LRSM has been performed in Ref. [375], where the results have been obtained by expanding to leading order in the ratios M_D/M_R and κ_+/v_R, and thus ignore any effects of left-right mixing. The results are (see also Refs. [376, 377])

$$\mathrm{BR}^{\mathrm{triplet}}_{\mu\to 3e} = \frac{1}{8}\left|\tilde{h}_{\mu e}\tilde{h}^*_{ee}\right|^2 \left(\frac{m^4_{W_L}}{m^4_{\delta^{++}_L}} + \frac{m^4_{W_L}}{m^4_{\delta^{++}_R}}\right), \tag{5.31}$$

for the tree-level process $\mu \to 3e$ and

$$\mathrm{BR}_{\mu\to e\gamma} \simeq 1.5\times 10^{-7}\,|g_{\mathrm{lfv}}|^2 \left(\frac{1\ \mathrm{TeV}}{m_{W_R}}\right)^4, \tag{5.32}$$

$$\mathrm{R}^{\mathrm{Au}}_{\mu\to e} \simeq 8\times 10^{-8}\,|g_{\mathrm{lfv}}|^2 \left(\frac{1\ \mathrm{TeV}}{m_{\delta^{++}_{L,R}}}\right)^4 \alpha \left(\log\frac{m^2_{\delta^{++}_{L,R}}}{m^2_\mu}\right)^2, \tag{5.33}$$

for the loop-suppressed decays $\mu \to e\gamma$ and $\mu \to e$ conversion (in gold nuclei), where the expressions are simplified by assuming the "commensurate mass spectrum" $M_i \simeq m_{W_R} \simeq m_{\delta^{++}_L} \simeq m_{\delta^{++}_R} \simeq m_{\delta^+_R}$. The parameters $\tilde{h}$ and g_{lfv} are defined to leading order in the ratio M_D/M_R by

$$\begin{aligned} \tilde{h}_{\alpha\beta} &\equiv \sum_{i=1}^{3} V_{\alpha i}V_{\beta i}\frac{M_i}{m_{W_R}} = \frac{[M_R]_{\alpha\beta}}{m_{W_R}}, \\ g_{\mathrm{lfv}} &\equiv \sum_{i=1}^{3} V_{\mu i}V^*_{ei}\left(\frac{M_i}{m_{W_R}}\right)^2 = \frac{[M_R M_R^*]_{\mu e}}{m^2_{W_R}}, \end{aligned} \tag{5.34}$$

assuming manifest left-right symmetry (see Appendix D). If one assumes that logarithmic terms [cf. Eq. (D.14)] from doubly charged Higgs diagrams dominate and that no cancellations occur amongst the LFV parameters ($|g_{\mathrm{lfv}}| \simeq |\tilde{h}_{\mu e}\tilde{h}^*_{ee}|$), one expects $\mathrm{BR}_{\mu\to 3e}$ to be roughly two orders of magnitude larger than $\mathrm{R}^{\mathrm{Au}}_{\mu\to e}$ for $\mathcal{O}$(TeV) Higgs triplet masses [375]. In that simplified case the limits on $\mu \to 3e$ will confine the model parameter space the most, which will be used in the analysis of the case of type II seesaw dominance.

However, with right-handed neutrinos around the TeV scale the left-right mixing could be enhanced, so that the usual type I seesaw contribution to LFV processes should also be considered. Those have been calculated in Refs. [363, 378–385]. Since the LRSM is effectively a type I+II seesaw model one needs to take into account LFV processes mediated by both heavy neutrinos and Higgs triplets, effectively allowing for interference between different amplitudes. Ref. [385] has presented the full expressions for $\mu \to e\gamma$; in the present analysis type I seesaw terms are included for $\mu \to 3e$ and $\mu \to e$ conversion, in the former case including possible

interference between loop and tree level diagrams. Detailed expressions for the decay widths including form factors and loop functions can be found in Appendix D; the most constraining processes will be summarised here. In the parameter scans in the type I dominance case all relevant contributions are taken into account.

It turns out that the most important constraints on the mixing $S \simeq M_D/M_R$ come from $\mu \to e\gamma$ and $\mu \to e$ conversion. In both cases the constraint is roughly

$$S^*_{\mu i} S_{ei} \mathcal{F}(x_i) \simeq S^*_{\mu i} S_{ei} \lesssim 10^{-5}\,, \tag{5.35}$$

where the loop function $\mathcal{F}(x_i)$ is taken to be of order one. This approximation is not always valid for very large right-handed neutrino masses, in which case $\mathcal{F}(x_i) \simeq \ln(M_i^2/m^2_{W_L})$, but since the mixing scales with $1/M_i$ the rate will vanish in the decoupling limit [384]. The decay rate of $\mu \to 3e$ depends on the same parameters as $\mu \to e$ conversion, but the limits are weaker in that case: the bound $\mathrm{BR}_{\mu\to 3e} < 1.0 \times 10^{-12}$ can be roughly translated into $S^*_{\mu i} S_{ei} \lesssim 10^{-3}$. These constraints come from diagrams with left-handed currents and left-right mixing, i.e. the terms proportional to S^2 in Eqs. (D.9), (D.14), (D.15) and (D.17), so that there is no other dependence on the heavy particle masses besides from the loop functions. Another interesting constraint comes from $\mu \to e\gamma$ diagrams in which gauge bosons mix: the chirality flip occurs within the loop, leading to a direct dependence on the Dirac mass matrix instead of the muon mass [Eq. (D.9)], in a similar way to the mixed diagrams in $0\nu\beta\beta$ (see also Refs. [382, 385, 386]). This enhances the contribution of mixed diagrams to $\mu \to e\gamma$ by a factor $SM_R/m_\mu \simeq M_D/m_\mu$, so that the product of the mixing angle ξ and the μe element of the Dirac mass matrix is constrained to be

$$|M^*_D|_{\mu e} \left(\frac{\xi}{10^{-5}}\right) \lesssim 0.2 \text{ GeV}\,. \tag{5.36}$$

In addition, the experimental limit of $|d_e| < 10^{-27}\, e$ cm [310] on the electric dipole moment of the electron [see Eq. (D.10)] constrains the ee element to be roughly

$$\mathrm{Im}\left\{[M_D]_{ee} e^{i\alpha}\right\} \left(\frac{\xi}{10^{-5}}\right) \lesssim 0.02 \text{ GeV}\,, \tag{5.37}$$

which also depends on the phase α. These limits effectively constrain the η-diagram in Fig. 5.3(b).

One might also expect large left-right mixing to allow loop-suppressed (type I) contributions to $\mu \to 3e$ to compete with the tree level triplet (type II) contribution. The full expression is given in Eq. (D.12), and the condition for comparable magnitudes of type I and type II contributions is roughly

$$S^*_{\mu i} S_{ei} \simeq 0.1 \left(\frac{5 \text{ TeV}}{m_{\delta^{++}}}\right)^2 \left(\frac{|M_{\mu e} M^*_{ee}|}{m^2_{W_R}}\right), \tag{5.38}$$

assuming $m_{\delta^{++}_L} = m_{\delta^{++}_R} \equiv m_{\delta^{++}}$. Thus for TeV-scale W_R the most restrictive bound on S^2 in Eq. (5.35) means that one needs right-handed neutrinos around the electroweak scale for the type I loop contribution to be competitive in $\mu \to 3e$ decay.

5.4 Signatures at the LHC

Collider searches provide a complementary probe of heavy neutrino models, as discussed in Section 3.7.1. Specifically, in the LRSM the right-handed W boson and right-handed neutrinos can be produced in pp collisions at the LHC via

$$pp \to W_R + X \to N_\ell + \ell + X\,, \quad (\ell = e, \mu), \tag{5.39}$$

followed by the decay into like-sign dileptons and two jets, i.e.,

$$W_R \to \ell_1 N_\ell \to \ell_1 \ell_2 W_R^* \to \ell_1 \ell_2 q q' \to \ell_1 \ell_2 jj \,, \tag{5.40}$$

which for the $\ell = e$ case is equivalent to the $0\nu\beta\beta$ diagram in Fig. 5.1. Several studies in this direction have been performed [87, 278, 355, 387], although the λ-diagram was not included.[4] Recently the CMS collaboration looked for this signature in both 7 TeV [390] and 8 TeV [391] data, where the integrated luminosity was 5.0 fb^{-1} and 3.6 fb^{-1}, respectively. Their analysis was simplified by assuming negligible mixing ($\xi \simeq 0$) between gauge bosons and between heavy neutrino mass eigenstates ($V \simeq \mathbb{1}$), so that the final states are either both electrons or both muons. ATLAS studied the same process with 2.1 fb^{-1} of data from 7 TeV collisions [392], and in addition examined the case of maximal mixing between the first two heavy neutrino mass eigenstates.

As a simple illustration of the complementarity of the different data sets the limits from the latest CMS data as well as from the KamLAND-Zen $0\nu\beta\beta$ experiment [166] are plotted in the $M_{N_e} - m_{W_R}$ parameter space in Fig. 5.4, using two different values for the mixing V_{e1}. Here one assumes that only one heavy neutrino flavour $N_e \simeq N_1$ is accessible, so that the LNV parameter in Eq. (5.12) simply becomes $|\eta^R_{N_R}| = m_p (m_{W_L}/m_{W_R})^4 |V^*_{e1}|^2 / M_1$. It is evident that colliders can place strong bounds on the parameter space.

It is also possible to probe the couplings $h_{\alpha\beta}$ of Higgs triplets to leptons [see Eq. (2.47)] with collider searches. The latest results from ATLAS [276] give the exclusion limits $m_{\delta_L^{\pm\pm}} > 409$ GeV and $m_{\delta_R^{\pm\pm}} > 322$ GeV for $e^\pm e^\pm$ final states and assuming a branching ratio of 100% to each final state. In order to compare those results to the $0\nu\beta\beta$ bounds one needs to take into account the other decay modes of doubly-charged Higgs scalars into gauge bosons and singly-charged scalars. The bounds extracted depend on the mass spectrum of the different components of the Higgs triplets $\Delta_{L,R}$, see the analysis in Ref. [275].

5.5 $0\nu\beta\beta$ amplitudes in the seesaw limits

In the most general case the light neutrino mass matrix

$$m_\nu = M_L - M_D M_R^{-1} M_D^T \,, \tag{5.41}$$

receives contributions from [see Eq. (2.52)] both the left-handed triplet (type II seesaw) and the heavy right-handed neutrinos (type I seesaw), making quantitative studies of the $0\nu\beta\beta$ amplitudes difficult. The two extreme cases of type II and type I dominance will be analysed here in detail; a complete study (i.e., type I+II) is beyond the scope of this work. In the type II case one sets the Dirac Yukawa couplings to zero, in the type I case one assumes that the triplet VEV vanishes, i.e., $v_L = 0$. The simpler case of type II seesaw dominance is dealt with first.

5.5.1 Type II seesaw dominance

With the approximations mentioned above, the lifetime in the limit of type II dominance is

$$\left[T^{0\nu}_{1/2}\right]^{-1}_{\text{type II}} = G^{0\nu}_{01} \left\{ \left|\mathcal{M}^{0\nu}_\nu\right|^2 |\eta_\nu|^2 + \left|\mathcal{M}^{0\nu}_N\right|^2 |\eta^R_{N_R} + \eta_{\delta_R}|^2 \right\} ; \tag{5.42}$$

with all terms proportional to M_D neglected, i.e., those with left-right mixing. Thus only heavy neutrino (Fig. 5.1) and triplet exchange [Fig. 5.2(a)] contributions remain, in addition to the

[4] For other collider probes of $0\nu\beta\beta$, see Ref. [388, 389].

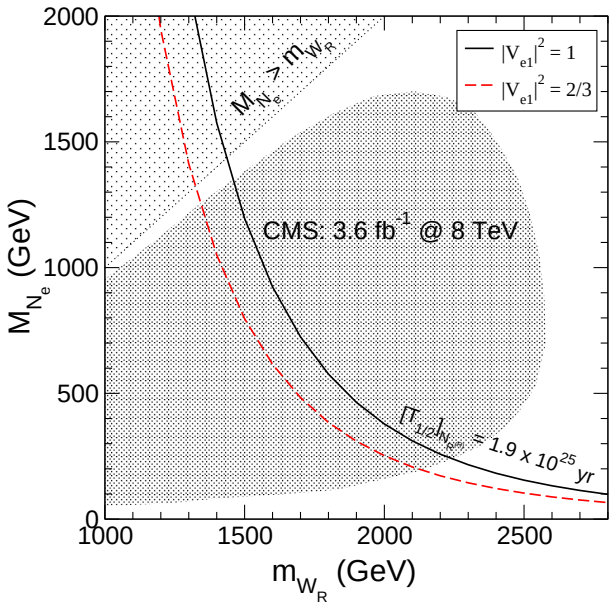

Figure 5.4: Comparison of the limits in $M_{N_e} - m_{W_R}$ parameter space from CMS and from the KamLAND-Zen limit on $0\nu\beta\beta$. The limit of 1.9×10^{25} yrs on the $0\nu\beta\beta$ halflife of ^{136}Xe means that all points to the left of the solid black line (dashed red line) are excluded, for $|V_{ei}|^2 = 1$ ($|V_{ei}|^2 = 2/3$), assuming that only heavy neutrinos contribute to $0\nu\beta\beta$, i.e. only $[T^{0\nu}_{1/2}]_{N_R^{(R)}}$. The shaded region is excluded by CMS at 95% C.L. [391].

standard diagram (Fig. 3.5) (the amplitude $\mathcal{A}^L_{N_R}$ also vanishes, being proportional to M_D). As discussed above, the interference term is suppressed, since the final state electrons in Fig. 3.5 are left-handed whereas those in Fig. 5.1 are right-handed.

In the case of type II dominance, the right-handed neutrino mass matrix can be expanded as [93]

$$M_R^{\text{type II}} \simeq \frac{v_R}{v_L e^{i\theta_L}} m_\nu + \kappa_+^2 h_D m_\nu^{-1} h_D^T - \kappa_+^4 \frac{v_L e^{i\theta_L}}{v_R} (h_D m_\nu^{-1} h_D) m_\nu^{-1} (h_D m_\nu^{-1} h_D)^T + \ldots , \quad (5.43)$$

and since $h_D \simeq 0$,

$$M_R^{\text{type II}} \simeq \frac{v_R}{v_L e^{i\theta_L}} m_\nu \, , \quad (5.44)$$

which simplifies the analysis considerably: the light and heavy neutrino spectra are proportional to each other, and $V = U$, up to an overall complex phase. In addition, both U and V become unitary in the limit that $M_D = 0$ [cf. Eq. (5.2)]. These assumptions were first used in Ref. [355] to quantify the heavy neutrino contribution to $0\nu\beta\beta$, with the triplet contribution neglected since the constraint from $\mu \to 3e$ leads to $M_R/m_{\delta_R} \ll 1$ over a large part of parameter space. Nevertheless, it is interesting to study this interplay more carefully. Replacing V with U in Eq. (5.12), the dimensionless lepton number violating parameter corresponding to heavy

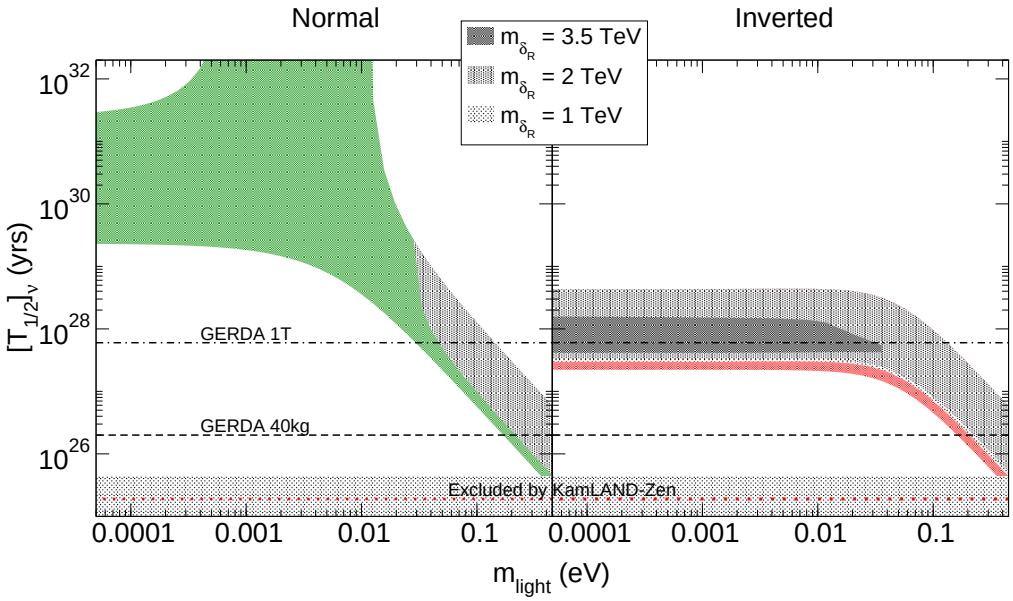

Figure 5.5: The standard light neutrino contribution to the $0\nu\beta\beta$ halflife of ^{76}Ge plotted against the lightest light neutrino mass, including the LFV constraint $\mathrm{BR}_{\mu\to 3e} \lesssim 10^{-12}$, for different values of the Higgs triplet mass, with $m_{W_R} = 3.5$ TeV and the heaviest right-handed neutrino $M_{\mathrm{heavy}} = 500$ GeV. Experimental limits are explained in the caption of Fig. 3.12.

neutrino exchange with right-handed currents ($\propto [M_R^{-1}]_{ee}$) can now be written as

$$[\eta^R_{N_R}]_{\mathrm{NO}} = m_p \left(\frac{m_{W_L}}{m_{W_R}}\right)^4 \left(\frac{m_3}{m_1}|U_{e1}|^2 + \frac{m_3}{m_2}|U_{e2}|^2 e^{-i\alpha} + |U_{e3}|^2 e^{-i\beta}\right) \frac{1}{M_3}\,, \tag{5.45}$$

$$[\eta^R_{N_R}]_{\mathrm{IO}} = m_p \left(\frac{m_{W_L}}{m_{W_R}}\right)^4 \left(\frac{m_2}{m_1}|U_{e1}|^2 + |U_{e2}|^2 e^{-i\alpha} + \frac{m_2}{m_3}|U_{e3}|^2 e^{-i\beta}\right) \frac{1}{M_2}\,, \tag{5.46}$$

for normal and inverted ordering, respectively, where α and β are Majorana phases. Similarly, the branching ratio for $\mu \to 3e$ in Eq. (5.31) depends on the product of the ee and μe elements of $\tilde{h} = M_R/m_{W_R}$, with

$$\begin{aligned}
[M_R]^{\mathrm{NO}}_{\sigma\rho} &= \left(\frac{m_1}{m_3}U_{\sigma 1}U_{\rho 1} + \frac{m_2}{m_3}U_{\sigma 2}U_{\rho 2}e^{i\alpha} + U_{\sigma 3}U_{\rho 3}e^{i\beta}\right) M_3 \\
[M_R]^{\mathrm{IO}}_{\sigma\rho} &= \left(\frac{m_1}{m_2}U_{\sigma 1}U_{\rho 1} + U_{\sigma 2}U_{\rho 2}e^{i\alpha} + \frac{m_3}{m_2}U_{\sigma 3}U_{\rho 3}e^{i\beta}\right) M_2\,.
\end{aligned} \tag{5.47}$$

In the following the triplet masses are assumed to be equal, $m_{\delta_L^{++}} = m_{\delta_R^{++}}$.

Following Ref. [355], by fixing $m_{W_R} = 3.5$ TeV and the heaviest right-handed neutrino mass $M_{\mathrm{heaviest}} = 500$ GeV, the three contributions can be plotted against the lightest light neutrino mass (see Figs. 5.5 and 5.6). It is clear that the right-handed contribution $[T_{1/2}]^{-1}_{N_R^{(R)}}$ [Fig. 5.6(a)] is proportional to the inverse of M_R, whereas the triplet contribution $[T_{1/2}]^{-1}_{\delta_R}$ [Fig. 5.6(b)] is proportional to M_R, and looks similar to the standard lifetime $[T_{1/2}]^{-1}_{\nu}$ (Fig. 5.5), since

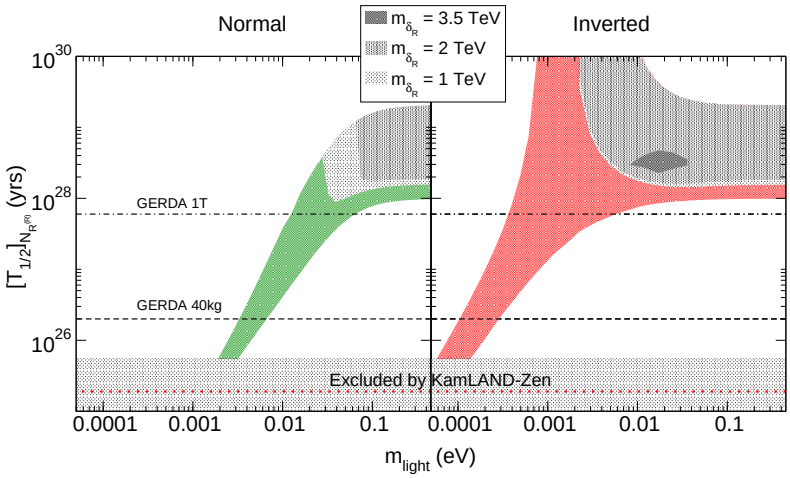

(a)

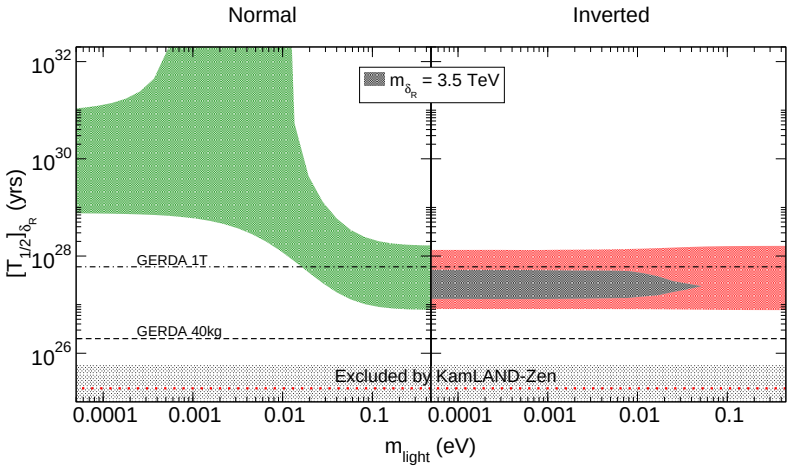

(b)

Figure 5.6: The contribution to the $0\nu\beta\beta$ halflife of ^{76}Ge from (a) heavy right-handed neutrinos and (b), right-handed Higgs triplets, plotted against the lightest light neutrino mass, with $m_{W_R} = 3.5$ TeV and $M_{\text{heavy}} = 500$ GeV. In plot (a) the grey shaded regions are excluded by LFV constraints, for different values of $m_{\delta_R^{++}}$, in plot (b) $m_{\delta_R^{++}} = m_{W_R} = 3.5$ TeV. Experimental limits are explained in the caption of Fig. 3.12.

$m_\nu \propto M_R$ in the type II limit. For $[T_{1/2}]^{-1}_{N_R^{(R)}}$, the inverted ordering can have infinite lifetime (zero effective mass), whereas the normal ordering cannot, so that the roles are reversed with respective to the standard case. In each plot the regions excluded by the limit on $\mu \to 3e$ are indicated, for different values of $m_{\delta_R^{++}}$: in the normal hierarchy the constraint only comes into play when the lightest mass is larger than about 0.01 eV, whereas in the inverted hierarchy the whole parameter space is affected.[5] In the case of the light neutrino and triplet contributions,

[5]These results agree with Fig. 2 of Ref. [355], which shows that $M_{\text{heavy}}/m_{\delta_R^{++}} \lesssim 0.1$ in the inverted ordering for all light neutrino masses, which corresponds to $m_{\delta_R^{++}} = 5$ TeV.

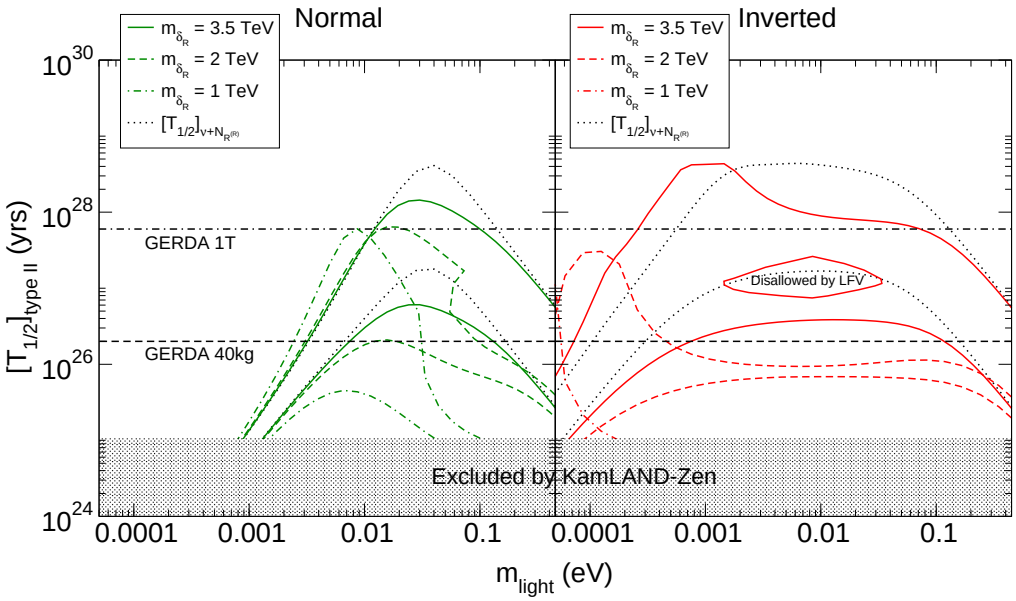

Figure 5.7: The total $0\nu\beta\beta$ halflife of ^{76}Ge including light neutrino, heavy neutrino and triplet contributions, plotted against the lightest light neutrino mass, with $m_{W_R} = 3.5$ TeV and $M_{\text{heavy}} = 500$ GeV. The solid, dashed and dashed-dotted lines show the allowed regions that satisfy $\text{BR}_{\mu\to 3e} \leq 10^{-12}$ for $m_{\delta_R^{++}}$ equal to 1, 2 and 3.5 TeV respectively; the black dotted lines enclose the regions allowed if one neglects the triplet contribution and LFV constraints. Experimental limits are explained in the caption of Fig. 3.12.

the only areas still allowed correspond to the largest possible value of $|\langle m_{ee}\rangle|$, i.e., when both Majorana phases are close to zero.

Figure 5.7 shows the total halflife, with all three contributions included. The chosen value of $m_{\delta_R^{++}}$ affects not only the LFV constraint but also the resulting halflife, due to the dependence of the triplet contribution on this quantity [Eq. (5.13)]. The black dotted lines show the halflife without the triplet contribution, and it is evident that the addition of the triplet part can shorten the halflife by several orders of magnitude, bringing it within reach of the GERDA experiment. There also exist regions where the lifetime can be longer, due to cancellations between the $\eta^R_{N_R}$ and η_{δ_R} contributions. The key point here is that the triplet contribution can still be allowed for certain values of the Majorana phases, even with the LFV constraint, thus enhancing the total amplitude for $0\nu\beta\beta$. This enhancement obviously depends on the triplet mass, so that if $m_{\delta_R^{++}} \gtrsim 5$ TeV the results of Ref. [355] are recovered.

5.5.2 Type I seesaw dominance

In the limit of type I seesaw dominance all the terms in Eq. (5.30) must be considered (neglecting the small contribution from η_{δ_L}, as discussed above). There are six contributing diagrams: (i) "standard" light neutrino exchange (η_ν); (ii) heavy neutrino exchange with left-handed currents ($\eta^L_{N_R}$); (iii) heavy neutrino exchange with right-handed currents ($\eta^R_{N_R}$); (iv) light neutrino exchange via the λ-diagram (η_λ); (v) light neutrino exchange via the η-diagram (η_η) and

(*vi*) right-handed triplet exchange (η_{δ_R}). Interference terms are also possible [see Eq. (5.27)], and distinguishing the different contribution becomes difficult. The contributions (*iv*) and (*v*) are usually neglected in the literature, but they can actually be significant, as shown in the rough estimates above.

Parameterising the relative magnitudes

In order to quantify the six contributions one needs more information about the right-handed sector, specifically the right-handed mixing matrix V_R and the mass spectrum M_i ($i = 1, 2, 3$) of right-handed neutrinos. The right-handed mass matrix M_R appears in the amplitudes $\mathcal{A}^L_{N_R}$, $\mathcal{A}^R_{N_R}$, $\mathcal{A}_{\delta_R}$, $\mathcal{A}_\lambda$ and $\mathcal{A}_\eta$, and in the case of type I seesaw dominance can be expanded as

$$M_R^{\text{type I}} = \kappa_+^2 h_D^T m_\nu^{-1} h_D + \kappa_+^4 \frac{v_L e^{i\theta_L}}{v_R} (h_D m_\nu^{-1} h_D)^T m_\nu^{-1} (h_D m_\nu^{-1} h_D) + \dots . \tag{5.48}$$

The leading term is a matrix product containing the unknown Dirac mass matrix, so that the simple relations in Eq. (5.44) no longer hold and a different approach is required. The authors of Ref. [357] simplify the analysis by assuming that (*i*) the Dirac mass matrix is diagonalised by V_R and (*ii*) the three Dirac Yukawas are equal. This scenario is very restrictive; another approach would be to insert an ansatz for the matrix of Dirac Yukawa couplings h_D. Often one uses the condition $M_u \simeq M_D = \kappa_+ h_D$, which holds at the GUT scale in $SO(10)$ models [393].

More generally, the Dirac mass matrix can be parameterised using the so called top-down or bi-unitary parameterisation,

$$M_D = U_L^\dagger \tilde{M}_D U_R, \tag{5.49}$$

where U_L and U_R are arbitrary unitary matrices and $\tilde{M}_D = \kappa_+ \,\mathrm{diag}(h_1, h_2, h_3)$. In the LRSM type I case, M_D has 18 parameters and M_R has 12 parameters, so that the left-right mixing $M_D M_R^{-1}$ depends on 30 parameters, making it difficult to learn anything from a parameter scan. An additional discrete parity (charged conjugation) symmetry [see Section 2.3.2] means that M_D becomes hermitian (symmetric) thus reducing the number of parameters by 6. However, it is still numerically difficult to find Dirac mass matrix structures that give large enough left-right mixing. One way is to start from a specific matrix structure in M_D that gives zero neutrino masses, and introduce small perturbations (see Refs. [263, 266]). It is also possible to scan the entire allowed parameter space using the orthogonal parameterisation, defined in Eq. (2.25). However, due to the large number of unknown parameters (6 in O, 3 in $\tilde{M}_R$ and 9 in V_R) it is difficult to learn anything. In addition, this approach does not allow one to define a symmetric or Hermitian Dirac mass matrix in a unique way.

An alternative method is to go to the basis where M_D is "diagonal" from the left. Starting with a general Majorana mass matrix M_R and the most general Dirac mass matrix in Eq. (5.49), one rotates the left-handed neutrino fields by U_L, leading to the light neutrino mass matrix

$$m'_\nu = -\tilde{M}_D U_R M_R^{-1} U_R^T \tilde{M}_D \equiv -\tilde{M}_D {M'_R}^{-1} \tilde{M}_D \,, \tag{5.50}$$

with ${M'_R}^{-1} = U_R M_R^{-1} U_R^T$. In this basis the mass matrix m'_ν can be diagonalised by the unitary matrix X_L, i.e. $m'_\nu = X_L \tilde{m}_\nu X_L^T$, so that the neutrino mass matrix in the flavour basis is

$$m_\nu = V_\nu \tilde{m}_\nu V_\nu^T = -V_\nu X_L^\dagger \left(\tilde{M}_D {M'_R}^{-1} \tilde{M}_D \right) X_L^* V_\nu^T \equiv -U_L^\dagger \left(\tilde{M}_D {M'_R}^{-1} \tilde{M}_D \right) U_L^* \,, \tag{5.51}$$

where V_ν is the light neutrino mixing matrix [Eq. (2.16)] defined by $V_\nu \equiv U_L^\dagger X_L$. Numerically, this means one need only fit the mass eigenvalues after diagonalising Eq. (5.50), decoupling the

PMNS mixing parameters, which turns out to be much more efficient than trying to fit both mass eigenvalues and mixing eigenvectors.[6] Put another way, one always has the freedom to choose U_L in order that the experimental values of V_ν are reproduced, for any choice of U_R. The authors of Ref. [368] used this approach to find matrix structures that could enhance the amplitude for $0\nu\beta\beta$ mediated by heavy sterile neutrinos ($\mathcal{A}^L_{N_R}$), albeit without right-handed currents. In the LRSM case those same structures will also enhance the amplitudes for the λ- and η-diagrams and influence the LFV branching ratios. However, one cannot recover the non-trivial mixing V_R in the right-handed sector simply by diagonalising ${M'_R}^{-1}$. Defining ${M'_R}^{-1} = X_R^* \tilde{M}_R^{-1} X_R^\dagger$ means that

$$V_R = U_R^T X_R \,, \tag{5.52}$$

so that the only way to find V_R is to invoke the symmetry (Hermiticity) of M_D, which gives $U_R = U_L^*$ ($U_R = U_L$). The right-handed mixing is then

$$V_R = U_L^\dagger X_R = V_\nu X_L^\dagger X_R \quad \text{or} \quad V_R = U_L^T X_R = V_\nu^* X_L^T X_R \,, \tag{5.53}$$

whereas the left-right mixing (in the flavour basis) is

$$M_D M_R^{-1} = U_L^\dagger \tilde{M}_D {M'_R}^{-1} U_L \quad \text{or} \quad M_D M_R^{-1} = U_L^\dagger \tilde{M}_D {M'_R}^{-1} U_L^* \,, \tag{5.54}$$

for symmetric or Hermitian M_D, respectively. The expression [cf. Eq.(5.10)] characterising the diagram with heavy neutrinos and left-handed currents is

$$M_D M_R^{-1} M_R^{-1^*} M_R^{-1} M_D^T = U_L^\dagger \tilde{M}_D {M'_R}^{-1} {M'_R}^{-1^*} {M'_R}^{-1} \tilde{M}_D U_L^* \,. \tag{5.55}$$

The corrected forms of U and V used for calculating $0\nu\beta\beta$ amplitudes and LFV branching ratios can be found from Eq. (5.2), but the terms second order in $B \simeq M_D M_R^{-1}$ make little numerical difference.

It has also been shown [94] that if the Dirac mass matrix is symmetric, there are only $2^3 = 8$ discrete solutions to the seesaw equation, given by $M_D = i\sqrt{M_\nu M_R^{-1}} M_R$. It is possible to obtained large left-right mixing solutions that are consistent with this formalism. In that case half of the eight solutions give large mixing, whereas the other half give small mixing.

Numerical example

In the most general case, obtaining zero light neutrino masses means solving the condition $M_D M_R^{-1} M_D^T = 0$, and it turns out that in the basis in Eq. (5.50) this equates to [368]

$$\tilde{M}_D \propto \text{diag}(0,0,1) \quad \text{and} \quad M'_R \propto \begin{pmatrix} 0 & 0 & 1 \\ 0 & 1 & 1 \\ 1 & 1 & 1 \end{pmatrix} . \tag{5.56}$$

Inserting small parameters instead of zeros leads to non-zero light neutrino masses, with the spectrum depending on any hierarchies introduced in $\tilde{M}_D$ and M_R. One particular example (from Ref. [368]) is

$$\tilde{M}_D = \kappa^+ \text{diag}(a\,\epsilon^2, b\,\epsilon, c), \quad {M'_R}^{-1} \simeq M^{-1} \begin{pmatrix} d & e & f \\ \cdot & g & h\,\epsilon \\ \cdot & \cdot & j\,\epsilon^2 \end{pmatrix} , \tag{5.57}$$

[6] This approach is discussed in Ref. [394].

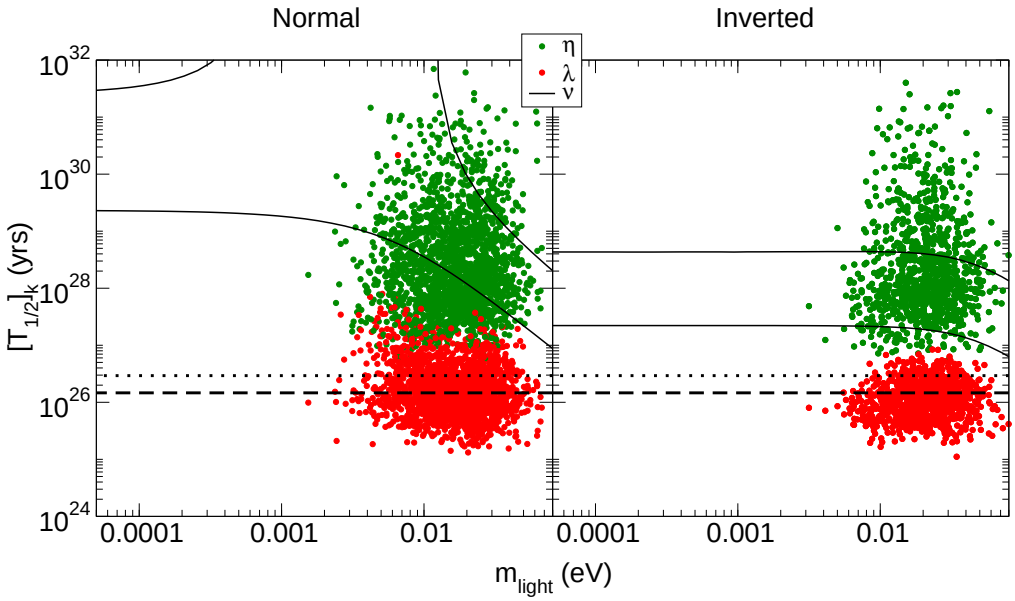

Figure 5.8: The contributions to the $0\nu\beta\beta$ halflife of ^{76}Ge from the λ- and η-diagrams plotted against the lightest light neutrino mass, for symmetric M_D. The standard contribution is indicated by the region outlined in black, and the dashed and dotted horizontal line correspond to the limits from Eqs. (5.18) and Eq. (5.20).

which leads to nonzero lightest neutrino mass. With all coefficients a, b, c etc. of order one one needs $|\epsilon| = \mathcal{O}(10^{-6})$ in order to get the correct mass for active neutrinos. Inverting ${M'_R}^{-1}$ would give a matrix with small $(1,1)$, $(1,2)$ and $(2,1)$ entries, but since ${M'_R}^{-1} = \left(U_R M_R^{-1} U_R^T\right)$, the matrix M_R can have large entries everywhere, which can enhance the LFV amplitudes. This is simply a manifestation of the fact that one cannot go to a basis where the right-handed neutrinos are diagonal without affecting the right-handed current, which is different to the conventional case. For the parameter scans the values $m_{W_R} = 3.5$ TeV and $m_{\delta_R^{++}} = 5$ TeV are chosen, and the gauge boson mixing angle is varied in the range $10^{-8} \leq \xi \leq 10^{-6}$, otherwise it would be difficult to evade the constraints from $\mu \to e\gamma$. The magnitudes of the complex parameters a, b, c etc. are varied in the range $[0.1, 1.0]$, and $|\epsilon|$ in the range $[10^{-12}, 10^{-5}]$. The phases are taken to be between 0 and 2π, and $\kappa^+ = 174$ GeV and $M = 1$ TeV are fixed. From Eqs. (2.51) and (2.59) the relation $M_R = \frac{2}{g} m_{W_R} h \simeq 3 m_{W_R} h$ holds, which is used to check perturbativity of the coupling h.

In the region of parameter space where cancellations are at play, one expects the different halflife contributions to have similar orders of magnitude, so that the amplitudes $\mathcal{A}^L_{N_R}$, $\mathcal{A}_\lambda$ and $\mathcal{A}_\eta$, which all depend on the left-right mixing, are enhanced. The halflives for the amplitudes $\mathcal{A}_\lambda$ and $\mathcal{A}_\eta$ are plotted in Fig. 5.8 and the halflives corresponding to heavy neutrino exchange, i.e., the amplitudes $\mathcal{A}^L_{N_R}$, $\mathcal{A}^R_{N_R}$ and $\mathcal{A}_{\delta_R}$ in Fig. 5.9, in both cases for a symmetric Dirac mass matrix. In each case the usual light neutrino contribution is shown for comparison, and one can see that there are regions of parameter space in which the λ and η contributions dominate over the light neutrino contribution. Remarkably the η contribution can still be sizeable, even with such small values of ξ: this is largely due to the larger value of the matrix element $\mathcal{M}^{0\nu}_\eta$ (cf. Table 5.2). The lightest mass could be smaller if the parameters a, b, c were allowed to be

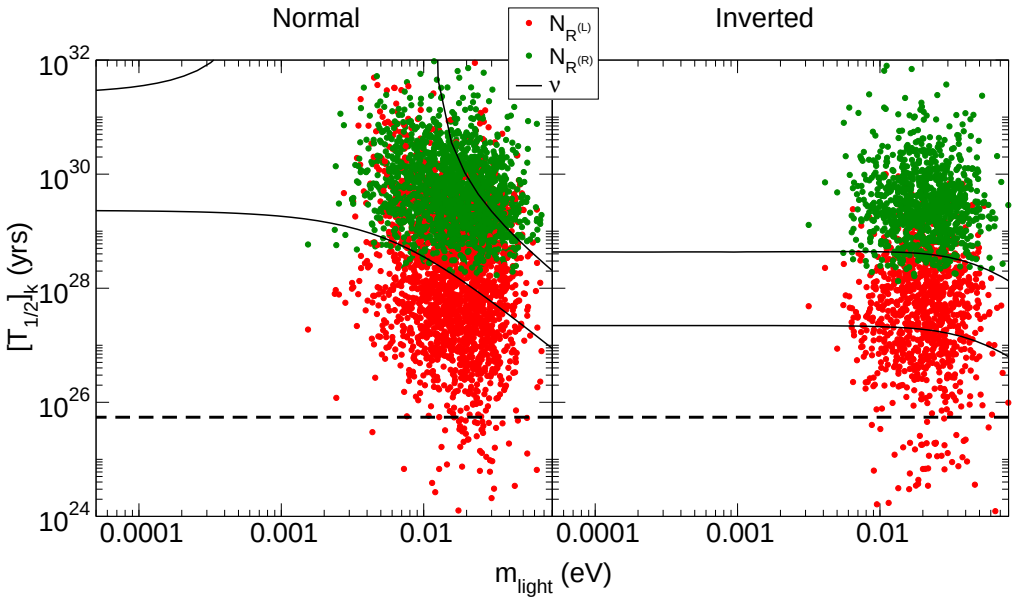

Figure 5.9: The contributions to the $0\nu\beta\beta$ halflife of ^{76}Ge from heavy right-handed neutrinos, with left- and right-handed currents ($\mathcal{A}^{L,R}_{N_R}$), for symmetric M_D. The standard contribution is indicated by the region outlined in black, and the dashed horizontal line corresponds to the limit from Eq. (3.47).

smaller than 0.1, although in the NO case the LFV constraints favour larger values of m_{light}. It also turns out that b and c need to be small in order to keep the left-right mixing small enough, since the rotation matrices in Eq. (5.54) can lead to large entries in the $(1,1)$, $(1,2)$ and $(2,1)$ positions of $M_D M_R^{-1}$, which enhance LFV processes.

In order to ascertain whether one diagram might dominate over another it is interesting to look at the ratios of different halflives. Some of those ratios are shown in Fig. 5.10, calculated for the example texture. As expected, the halflives $[T^{0\nu}_{1/2}]_{N^L_R}$ and $[T^{0\nu}_{1/2}]_\lambda$ can both be larger than the light neutrino contribution. Note that the possibility of interference terms has not been taken into account, as that would considerably complicate the analysis. Indeed, distinguishing the magnitude of different mechanisms in the presence of interference terms would require a multi-isotope investigation [184]. One way of checking the results of this section would be at a linear collider, which will now be discussed.

5.6 Inverse neutrinoless double beta decay

5.6.1 Relation to $0\nu\beta\beta$

The linear collider signatures of the the LRSM have been briefly mentioned in Section 3.7.2. Besides the existence of a new neutral gauge boson (Z') that could mediate four fermion interactions, there are also processes depending on the doubly charged Higgs scalars $\delta^{\pm\pm}_{L,R}$ [298, 300]. The detection of either of those particles would provide alternative tests of the left-right model, although the Z' has no immediate connection to $0\nu\beta\beta$. On the contrary, the process $e^-e^- \to W^-W^-$ (see Fig. 3.17) allows one to directly test the mechanism of $0\nu\beta\beta$.

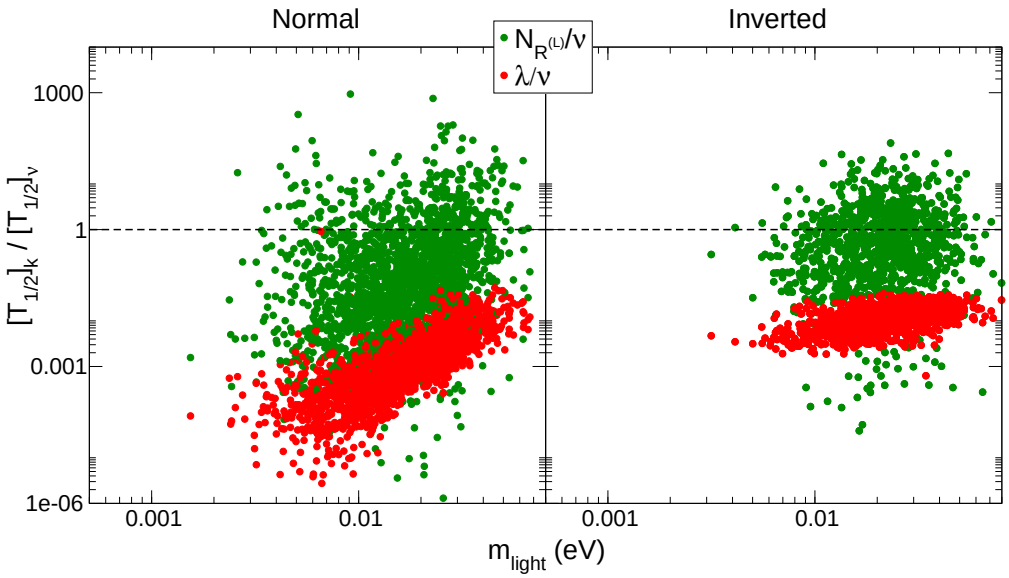

Figure 5.10: Ratios of halflife contributions, $[T^{0\nu}_{1/2}]_\lambda/[T^{0\nu}_{1/2}]_\nu$ and $[T^{0\nu}_{1/2}]_{N^L_R}/[T^{0\nu}_{1/2}]_\nu$.

In the present analysis the process in which left- and right-handed W bosons are produced [285, 287, 288],

$$e^- e^- \to W_L^- W_R^- \,, \tag{5.58}$$

will be discussed. Figure 5.11 shows the relevant Feynman diagrams, which correspond to the λ-mechanism for $0\nu\beta\beta$ shown in Fig. 5.3(a). This process can be tested not only at a linear collider, but also due to its unique angular distribution in $0\nu\beta\beta$, which could be measured by the SuperNEMO experiment [180]. It has not yet been studied at hadron colliders.

The fact that this particular process is dominant can be deduced by a process of elimination from the $0\nu\beta\beta$ diagrams in Figs. 3.5, 3.11, 5.1 and 5.3. Using crossing symmetry one can translate them into linear collider cross sections of the form $e^-e^- \to W^-W^-$. In each case the two gauge bosons can either have the same polarisation ($W_L^-W_L^-$ or $W_R^-W_R^-$), in which case the process can be mediated by either Majorana neutrinos or Higgs triplets, or opposite polarisations ($W_L^-W_R^-$), only possible with the exchange of Majorana neutrinos plus non-zero left-right mixing. Since the experimental limits on W_R are about 2.5 TeV (see Fig. 5.4), diagrams with two W_R are obviously disfavoured. In addition, for diagrams with two W_L, both the light and the heavy neutrino exchange contributions can be shown to be suppressed and unobservable, see Ref. [295] for a recent reanalysis. The cross section corresponding to left-handed triplet exchange [Fig. 5.2(b)] is proportional to $\sqrt{2}v_L h_{ee} = [M_L]_{ee}$ (see Eq. (2.51) and Ref. [298]), so that it is suppressed by light neutrino mass. The only diagrams remaining are those with only one W_R, i.e. the mixed diagrams from Fig. 5.3. Since the limit on the λ-diagram is less stringent by almost two orders of magnitude with respect to the one for η [compare Eqs. (5.18) and (5.20)], one is led to the conclusion that the λ-diagram is the most promising channel to study. Fig. 5.11 shows the relevant Feynman diagram; its cross section will be evaluated in what follows. The analysis presented here is complementary to those in Refs. [87, 278, 355, 387].

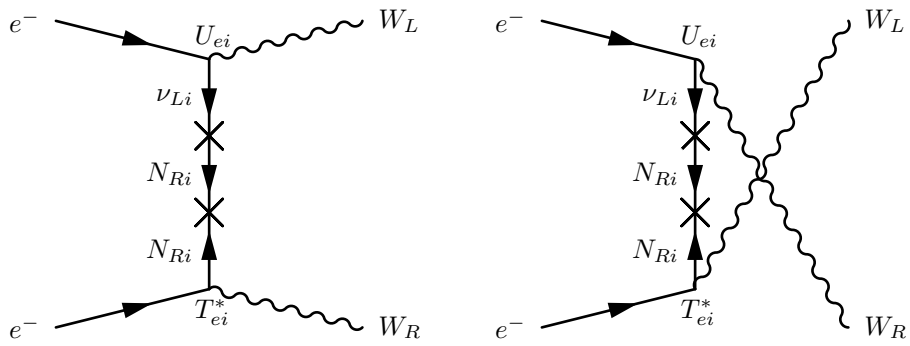

(a) t-channel production (b) u-channel production

Figure 5.11: Inverse neutrinoless double beta decay diagrams with W_L and W_R in the final state.

5.6.2 Cross section of $e^-e^- \to W_L^- W_R^-$

The two possible channels for the process $e^-(p_1)\, e^-(p_2) \to W_L^-(k_1, \mu)\, W_R^-(k_2, \nu)$ are shown in Fig. 5.11. Here $p_{1,2}$ and $k_{1,2}$ are the momenta of the particles and μ, ν the Lorentz indices of the W polarisation vectors. The matrix element is

$$-i\mathcal{M} = -i\,(\mathcal{M}_t + \mathcal{M}_u)\,, \tag{5.59}$$

where the subscript denotes the t- or u-channel process. The differential cross section,

$$\frac{d\sigma}{d\Omega} = \frac{1}{64\pi^2}\frac{1}{s}\frac{1}{4}|\overline{\mathcal{M}}|^2 \sqrt{\frac{\lambda(s, m_{W_L}^2, m_{W_R}^2)}{\lambda(s,0,0)}}\,, \tag{5.60}$$

where $\lambda(a,b,c) = a^2 + b^2 + c^2 - 2\,(a\,b + a\,c + b\,c)$, can be evaluated using the relations

$$|\overline{\mathcal{M}}|^2 = |\overline{\mathcal{M}_t}|^2 + |\overline{\mathcal{M}_u}|^2 + 2\mathrm{Re}\left(\overline{\mathcal{M}_t^*\,\mathcal{M}_u}\right). \tag{5.61}$$

The result is (neglecting m_{W_L})

$$\begin{aligned}
|\overline{\mathcal{M}_t}|^2 &= \frac{8\,G_F^2\,|\sum_i U_{ei}\,T_{ei}^*|^2}{(t-m_i^2)^2}\left(\frac{m_{W_L}}{m_{W_R}}\right)^2 \left\{4m_{W_L}^4 m_{W_R}^2(t-m_{W_R}^2) - t^2\left[t(s+t) - m_{W_R}^2(2s+t)\right]\right. \\
&\quad \left. + m_{W_L}^2 t\left[4m_{W_R}^4 + t(2s+t) - m_{W_R}^2(4s+5t)\right]\right\}, \\
|\overline{\mathcal{M}_u}|^2 &= |\overline{\mathcal{M}_t}|^2\,(t \leftrightarrow u)\,, \\
\overline{\mathcal{M}_t^*\,\mathcal{M}_u} &\propto \mathrm{Tr}\{P_R\gamma_\nu \not{q}\gamma_\mu \not{p}_1 \gamma_\alpha \not{q}\gamma_\beta \not{p}_2 P_L\} = 0\,.
\end{aligned} \tag{5.62}$$

The interference term vanishes because the final state particles are distinguishable. Fig. 5.12 shows the differential cross section $d\sigma/d\cos\theta$ as a function of $\cos\theta$, for $m_{W_R} = 2.5$ TeV and 2.7 TeV, normalised with respect to each other (the cross section for $m_{W_R} = 2.7$ TeV is actually a factor of two smaller). $d\sigma/d\cos\theta$ is practically flat, and approaches a straight line as m_{W_R} increases.

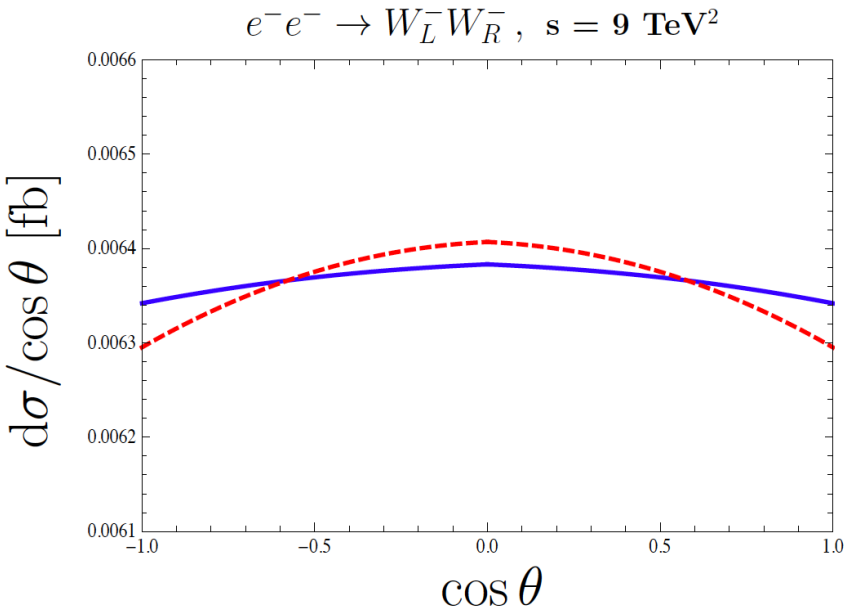

Figure 5.12: Differential cross section for $e^-e^- \to W_L^- W_R^-$ with $\sqrt{s} = 3$ TeV and for both $m_{W_R} = 2.5$ TeV (dashed red line) and 2.7 TeV (solid blue line), with the latter normalised to facilitate comparison.

It is interesting to study the high energy behaviour of the total cross section in the case of light neutrino exchange. In the limit that $\sqrt{s} \to \infty$, the cross section becomes

$$\sigma(e^-e^- \to W_L^- W_R^-) \simeq \frac{G_F^2\, m_{W_R}^2}{24\,\pi\, m_{W_L}^2}\, s\, |\eta_\lambda|^2 \leq 8.8 \times 10^{-5} \left(\frac{m_{W_R}}{\mathrm{TeV}}\right)^2 \left(\frac{\sqrt{s}}{\mathrm{TeV}}\right)^2 \left(\frac{|\eta_\lambda|}{9\times 10^{-7}}\right)^2 \mathrm{fb}\,, \tag{5.63}$$

where the upper bound on $|\eta_\lambda|$ is taken from Ref. [164] and the mass of the light neutrinos m_i have been neglected. The apparent violation of unitarity can be explained by taking the full theory into account, in which case the cross section will vanish when $\sqrt{s} \to \infty$ and unitarity is restored. Indeed, the high-energy limit of the cross section is obtained by neglecting the neutrino mass in the propagator [see Eq. (5.62)], i.e.,

$$\sigma \propto \left(\sum_i U_{ei} T_{ei}^*\right)^2 , \tag{5.64}$$

which does not seem to vanish. However, one needs to consider the full theory. In calculating the cross section one combines two terms from the Lagrangian in Eq. (5.1):

$$\sum_i \left[\overline{e}\,\gamma^\mu (K_L)_{ei} P_L n_i W_{L\mu}^-\right] \left[\overline{e}\,\gamma^\nu (K_R)_{ei} P_R n_i W_{R\nu}^-\right] . \tag{5.65}$$

The identity $\overline{e}\,\gamma^\nu P_R n_i = -\overline{n_i^c}\,\gamma^\nu P_L e^c$ allows one to contract $n_i \overline{n_i^c}$ to a propagator, so that in the high energy limit the amplitude is proportional to

$$\sum_i (K_L)_{ei} (K_R)_{ei} = [K_L K_R^T]_{ee}\,, \tag{5.66}$$

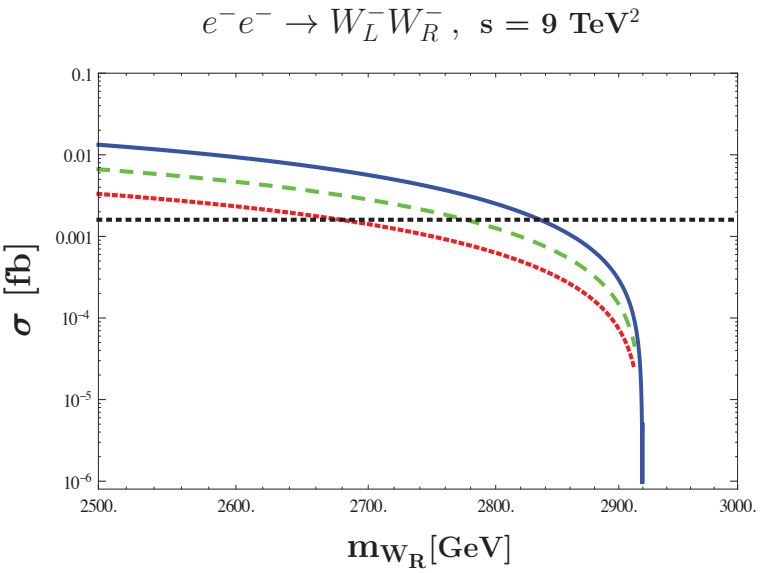

Figure 5.13: Cross section for $e^-e^- \to W_L^- W_R^-$ with $\sqrt{s} = 3$ TeV and three limits for the η_λ parameter: the solid (blue) line is for $|\eta_\lambda| = 9 \times 10^{-7}$, the dashed (green) line for $|\eta_\lambda| < 6.4 \times 10^{-7}$ and the dotted (red) line for $|\eta_\lambda| < 4.8 \times 10^{-7}$ [Eq. (5.18)]. The dotted (black) horizontal line corresponds to the cross section that would give five events at an integrated luminosity of 3000 fb^{-1}.

instead of $\sum_i U_{ei} T_{ei}^*$ as in the naive case. As shown in Section 2.3.2, $K_L K_R^T = 0$, which means that the cross section vanishes in the high energy limit and unitarity is ensured. The helicity amplitudes of the process are detailed in Appendix E, where their high-energy behaviour is also discussed.

There is also another diagram analogous to Fig. 5.11, with heavy neutrinos exchanged. The structure of the matrix elements is the same, one needs only to interchange $m_i \leftrightarrow M_i$, $U_{ei} \leftrightarrow V_{ei}^*$ and $T_{ei}^* \leftrightarrow S_{ei}$, where M_i is the mass of the heavy neutrinos and V_{ei}^* and S_{ei} are the mixing matrices defined in Eq. (2.13) [see also the expression in Eq. (5.16)]. In that case the rate for $0\nu\beta\beta$ will be suppressed with respect to the case of light neutrino exchange in the λ-diagram.

To calculate the total cross section the limits from $0\nu\beta\beta$ experiments as well as the allowed region for m_{W_R} must be taken into account. Fig. 5.13 shows the cross section for $e^-e^- \to W_L^- W_R^-$ as a function of m_{W_R} for $\sqrt{s} = 3$ TeV, assuming only light neutrinos are exchanged and with three different limits for $|\eta_\lambda|$: the solid (blue) line corresponds to $|\eta_\lambda| < 9 \times 10^{-7}$, the dashed (green) to $|\eta_\lambda| < 6.4 \times 10^{-7}$ and the (red) line to the limit in Eq. (5.18). Note that a factor of x improvement in $|\eta_\lambda|$ corresponds to a factor of x^2 improvement in lifetime. Also indicated is the cross section that would give five events at an integrated luminosity of 3000 fb^{-1} [395], corresponding to a few years of running. It is evident that for 2.5 TeV $\lesssim m_{W_R} \lesssim$ 2.7 TeV, enough events are possible in case $0\nu\beta\beta$ is observed soon, and caused by the λ-diagram. Note that since there is no SM background to the process, a small rate is tolerable. In the next subsection it will be shown that polarisation of the electron beams could be used to enhance the cross section by up to a factor of two. In addition, if different contributions to $0\nu\beta\beta$ interfere destructively, the bound on $|\eta_\lambda|$ would be relaxed and a larger cross section would be possible.

Table 5.3: Suppression or enhancement factors (with respect to the unpolarised case) of the cross section for inverse double beta decay with polarised beams.

Beam polarisation		$\mathcal{J}$
1	2	
0%	0%	1
90% RH	0%	1
50% LH	50% LH	0.75
50% LH	50% RH	1.25
80% LH	50% RH	1.40
90% LH	90% RH	1.81
90% LH	80% RH	1.72
100% LH	100% RH	2

5.6.3 Polarised beams

Future linear colliders have the possibility to polarise their beams. In order to quantify the effects on the process under discussion, one can define the polarisation for an electron beam $\mathcal{P}_{1,2}$ as follows:

$$\mathcal{P}_{1,2} \equiv \frac{\mathcal{N}_R^{1,2} - \mathcal{N}_L^{1,2}}{\mathcal{N}_R^{1,2} + \mathcal{N}_L^{1,2}}\,, \tag{5.67}$$

where $\mathcal{N}_R$ and $\mathcal{N}_L$ stand for the number of electrons having right- and left-handed helicity in the electron beam 1 or 2, respectively. If beam 1 is fully left-handed, $\mathcal{P}_1 = -1$, whereas for a fully right-handed beam, $\mathcal{P}_1 = +1$.

When the electron beam 1 has a polarisation of $\mathcal{P}_1$ and the electron beam 2 has a polarisation of $\mathcal{P}_2$, the total cross section $\sigma(\mathcal{P}_1, \mathcal{P}_2)$ of a process is calculated as

$$\begin{aligned}\sigma(\mathcal{P}_1, \mathcal{P}_2) = \frac{1}{4}\{&(1-\mathcal{P}_1)(1+\mathcal{P}_2)\sigma_{LR} + (1-\mathcal{P}_1)(1-\mathcal{P}_2)\sigma_{LL} \\ &+ (1+\mathcal{P}_1)(1+\mathcal{P}_2)\sigma_{RR} + (1+\mathcal{P}_1)(1-\mathcal{P}_2)\sigma_{RL}\}\,,\end{aligned} \tag{5.68}$$

where σ_{LR} stands for the cross section of the process when both electron beams are 100% polarised, one left-handed and the other right-handed; σ_{RL}, σ_{LL} and σ_{RR} are defined in a similar way. In our case for the λ-diagram $\sigma_{LL} = \sigma_{RR} = 0$, and σ_{LR} (σ_{RL}) is the cross section that would arise from the t-channel (u-channel) diagram only. Furthermore, $\sigma_{LR} = \sigma_{RL}$. Thus, equation (5.68) simply becomes

$$\sigma(\mathcal{P}_1, \mathcal{P}_2) = \sigma(\mathcal{P}_2, \mathcal{P}_1) = \frac{\sigma_{LR}}{2}\,(1 - \mathcal{P}_1\,\mathcal{P}_2)\,. \tag{5.69}$$

Table 5.3 gives numerical examples, where the ratio $\mathcal{J}$ between the cross section of polarised and unpolarised beams has been defined as

$$\mathcal{J} \equiv \frac{\sigma(\mathcal{P}_1, \mathcal{P}_2)}{\sigma(0,0)} = 1 - \mathcal{P}_1\,\mathcal{P}_2\,. \tag{5.70}$$

Obviously, $\sigma(0,0)$ is the total cross section calculated before. It is evident that the event numbers can in principle be doubled. Furthermore, polarisation could be used as an additional

method to distinguish different mechanisms for processes of the form $e^-e^- \to W^-W^-$. For instance, the process $e^-e^- \to 4$ jets [296] mediated by R-parity violating supersymmetry, involves slepton exchange, which couple mainly to left-handed electrons.

5.7 Summary and conclusions

Lepton number and lepton flavour violation provide complementary tools to study the parameter space of the LRSM, and are connected with the origin of neutrino mass in the model. The large number of contributions to $0\nu\beta\beta$, coupled with the possibility of interference terms, makes a comprehensive analysis rather difficult. In addition, both type I and type II seesaw terms are present in the neutrino mass matrix. The present study examines the resulting phenomenology of the type I and type II dominance for neutrino masses. Particular attention has been given to $0\nu\beta\beta$ diagrams usually neglected in the literature.

In the case of pure type II seesaw it has been shown that the triplet contribution to $0\nu\beta\beta$ should not be neglected for all light neutrino masses. For pure type I seesaw there exist regions of parameter space in which all diagrams can have similar orders of magnitude, which makes distinguishing the leading contribution difficult. In particular, the momentum-dependent λ-diagram is not negligible, even without enhancement from cancellations. The bounds from LFV are particularly severe in the type I case, and can be used to further restrict the parameter space. A comprehensive study should include the type I+II case, which is beyond the scope of this work.

Furthermore, the process $e^-e^- \to W_L^-W_R^-$ as a clean check of the so-called λ-diagram has been considered. Among the many possible diagrams for $0\nu\beta\beta$ that are possible in left-right symmetric theories, it was shown to be the most promising one at a linear collider. Indeed, it may be possible to observe the process at a linear collider that has a centre-of-mass energy of 3 TeV. It is however necessary that both the mass of the W_R and the life-time of $0\nu\beta\beta$ are close to their current experimental limits. Beam polarisation effects and the high energy behaviour of the total cross section were also considered; the individual helicity amplitudes are discussed in Appendix E.

Chapter 6

Conclusion

Sterile neutrinos are not only integral parts of most neutrino mass models but reveal themselves in a wide spectrum of physical phenomena at different energy scales. This thesis has summarised the different theoretical and phenomenological motivations for the existence of sterile neutrinos, specifically those at observable (low) mass scales, from sub-eV up to TeV scales. The usual premise of the seesaw mechanism with heavy GUT scale particles must necessarily be modified to allow for such light particles: several such models have been discussed and their consequences for phenomenology outlined. The background information in Chapter 2 serves to place sterile neutrinos within the general context of neutrino mass models, and describes various special cases of the type I seesaw mechanism when different assumptions as to the relative scales of the Dirac and Majorana mass terms are made. Mechanisms for obtaining light sterile neutrinos are outlined, the FN mechanism being the example employed in this work.

It is possible to study eV-scale sterile neutrinos in a purely model-independent manner. This was done in Sections 3.3, 3.4.2 and 3.6.1, where the signatures of those particles in beta decay, $0\nu\beta\beta$ and cosmology were outlined. In particular, $0\nu\beta\beta$ was focussed on, since the coherent sum of products of neutrino mixing matrix elements and neutrino masses (the effective mass $|\langle m_{ee}\rangle|$) can show markedly different behaviour in the presence of sterile neutrinos. The effects depend on the mass spectrum of sterile and active mass eigenstates: in the cases where the active neutrinos are lighter than the sterile ones (3+1 and 3+2) the effective mass can vanish even in the inverted ordering case, which it cannot in the usual three-neutrino scenario. Those cases are indeed favoured, since when active states are heavier than their sterile counterparts one generally runs into trouble with the bound on the sum of neutrino masses from cosmology. In fact, a factor of four improvement in the experimental limit on the effective mass could even rule such scenarios out. The different mass spectra are generally indistinguishable in oscillation experiments, with one exception being the appearance probabilities at short baselines in the case of two sterile neutrinos, discussed in Section 3.2.2. In principle one can distinguish between 3+2/2+3 and 1+3+1 cases, shown in Fig. 3.4.

The bimodal model contains sterile neutrinos at sub-eV scales, and is a subset of the pseudo-Dirac scenario, with the main difference being that flavour eigenstates contain large admixtures of both Dirac and Majorana type masses. Neutrino oscillations are unaffected, but there are striking signatures in the flavour flux ratios at neutrino telescopes as well as in $0\nu\beta\beta$, analysed in Sections 3.5.2 and 3.4.3, respectively. The plots in those sections show that a combination of measurements of the ratios of high energy astrophysical neutrinos and the effective mass in $0\nu\beta\beta$ should be able to confirm or rule out the bimodal model.

If some or all of the phenomena related to sterile neutrinos are observed one would like to explain their mass scales and mixing in theoretical models. The models described in Chapter 4 embed sterile states into flavour symmetry models and study the phenomenological consequences. An example of a model based on S_3 that can accommodate the bimodal scenario is given in Section 4.3. The leading order prediction of TBM must be modified by NLO cor-

rections, in this case from the charged lepton sector. The central focus of the model building chapter is on A_4 models augmented with the FN mechanism. Both an effective and a seesaw model were studied, in Sections 4.2.2 and 4.2.3, respectively. It was shown that light sterile neutrinos can naturally be accommodated in those models, with the active-sterile mixing correlated to the deviation from exact TBM. In both cases one requires higher-order operators to generate a non-zero θ_{13}; in the seesaw model that can be achieved by charged lepton corrections, studied in detail in Appendix C. Indeed, corrections to active neutrino mixing are generally larger than corrections to active-sterile mixing, which is a ratio of two scales. In seesaw models there are also higher-order terms from the seesaw expansion that should be taken into account. The departure from the initial mixing scheme is a general feature of such approaches.

The A_4 seesaw model in Section 4.2.3 contains one keV-scale neutrino, whereas the other two neutrinos could be at different mass scales, depending on the FN charges assigned to the respective right-handed fields. Various cases were studied, and it was shown that with one or two sterile neutrinos at the eV scale one can explain the SBL oscillation anomalies, albeit only in the inverted ordering case. There are distinct predictions for the effective mass in $0\nu\beta\beta$ in each of the scenarios under study: if all of the sterile neutrinos are lighter than about 100 MeV then the effective mass is zero, but as soon as one of the states is larger than 100 MeV one expects a non-zero value (in the absence of other interference terms). This exact cancellation is a well-known feature of seesaw models, and in the special case of the flavour symmetry model in Section 4.2.3 it was shown to occur pairwise, as described in detail in Section 3.4.4. Note that if one places the two sterile neutrinos at the GeV scale or higher it is possible to generate the baryon asymmetry of the universe via oscillations (as in the νMSM), although one relinquishes the explanation of eV neutrino anomalies. That would require additional sterile states above the three introduced, a possibility not discussed here. The main point is that if one departs from the common theoretical prejudice of right-handed neutrinos residing at around the GUT scale, various interesting model building options can arise. Further experimental data in the years to come will put those models to the test.

Once sterile neutrinos have been introduced, a natural question to ask is whether one can embed them into a larger theory. In that sense the models of Chapter 4 could be seen as "bottom-up" models, whereas the left-right symmetric model discussed in Chapter 5 is an example of a "top-down" model, where sterile neutrinos are embedded into doublets under $SU(2)_R$. The additional gauge symmetry means that the sterile states participate in (right-handed) gauge interactions at a higher scale, making them "weakly sterile". Those interactions manifest themselves in several phenomena in both the quark and lepton sectors, which allow one to constrain the parameters of the model. Processes involving leptons have been studied in detail, specifically the lepton number violating neutrinoless double beta decay and inverse neutrinoless double beta decay, both of which are connected to neutrino mass. A systematic description of all relevant $0\nu\beta\beta$ amplitudes was given, as well as a discussion of their expected relative magnitudes. The cases of type II and type I dominance for neutrino mass were studied in detail in Sections 5.5.1 and 5.5.2, respectively, with the relevant constraints from LFV taken into account in each case.

In the case of type II dominance the explicit effect of the branching ratio for $\mu \to 3e$ was taken into account across all of parameter space, and it was shown that there can be non-negligible interference between the contributions of right-handed neutrinos and Higgs triplets. In the type I dominance case it was emphasised that the λ- and η-diagrams could provide sizeable contributions to the lifetime of $0\nu\beta\beta$, and a specific matrix texture was studied in which light neutrino masses are small while left-right mixing is relatively enhanced. In that case the contribution of right-handed neutrinos with left-handed currents can also be sizeable.

The stringent constraints from the lepton flavour violating decays $\mu \to e\gamma$, $\mu \to 3e$ and $\mu \to e$ conversion in nuclei were taken into account, since those processes also depend on the left-right mixing. Explicit expressions for the relevant branching ratios, form factors and loop functions are detailed in Appendix D.

The related process of inverse neutrinoless double beta decay was studied in Section 5.6, in particular the process $e^-e^- \to W_L W_R$, the inverse of the λ-diagram. Out of all possible contributions associated with $0\nu\beta\beta$ in left-right models it was shown to be the largest, and its cross section was calculated. Observation of the process could be possible at future linear colliders, only if the mass of the right-handed W boson is small enough and $0\nu\beta\beta$ (caused by the λ-diagram) is observed soon. However, the cross section could in principle be enhanced by a factor of two by polarising the electron beams. Finally, the helicity amplitudes of the process have also been calculated, both in the general case and in the high-energy limit, and are given in Appendix E.

In summary, theoretical models and experimental signatures of sterile neutrinos at different mass scales are invariably intertwined, and it is an interesting exercise to study the connection between neutrino mass models, sterile neutrinos and beyond the SM phenomenology. In this thesis several models with sterile neutrinos have been outlined in detail, in particular models with flavour symmetries. The phenomenon of neutrinoless double beta decay as a tool to distinguish models with sterile neutrinos has been focussed on, in various contexts. In addition to a model-independent discussion of how the process is modified in the presence of sterile neutrinos, neutrinoless double beta decay has been studied in detail in the context of the left-right symmetric model. Several diagrams usually considered to be negligible have been shown to be important, and all relevant constraints from LFV have been taken into account. This thesis demonstrates that the large parameter space of neutrino mass models can only be disentangled using the discriminative power of different phenomena, in the present case those induced by sterile neutrinos, both with and without additional gauge interactions.

Appendices

Appendix A

Flavour conversion probabilities

Flavour flux ratios of bimodal neutrinos have been calculated in Section 3.5.2; explicit expressions for the deviation parameters and probabilities are reported here.

In the general case without pseudo-Dirac effects, the probability matrix P with elements $P_{\alpha\beta}$ can be approximated as

$$P \simeq \begin{pmatrix} 1-2c_{12}^2 s_{12}^2 & c_{12}^2 s_{12}^2 + \Delta & c_{12}^2 s_{12}^2 - \Delta \\ \cdot & \frac{1}{2}(1 - c_{12}^2 s_{12}^2) - \Delta & \frac{1}{2}(1 - c_{12}^2 s_{12}^2) \\ \cdot & \cdot & \frac{1}{2}(1 - c_{12}^2 s_{12}^2) + \Delta \end{pmatrix}, \tag{A.1}$$

where $s_{12}^2 \equiv \sin^2\theta_{12}$, $c_{12}^2 \equiv \cos^2\theta_{12}$ and the universal correction parameter is defined as [396, 397]

$$\Delta \equiv \frac{1}{4}(2\epsilon \sin^2 2\theta_{12} + \theta_{13}\cos\delta \sin 4\theta_{12}) = 2\epsilon s_{12}^2 c_{12}^2 + \frac{1}{4}\theta_{13}\cos\delta\sin 4\theta_{12}\,, \tag{A.2}$$

with ϵ parameterising the deviation from μ-τ symmetry [cf. Eq. (3.54)]. Terms of order $\mathcal{O}(\theta_{13}^2)$, $\mathcal{O}(\epsilon^2)$, and $\mathcal{O}(\theta_{13}\epsilon)$ have been neglected in this approximation. It can be shown that the flux ratio evolves as [396, 397]

$$(1:2:0) \longrightarrow (1+2\Delta) : (1-\Delta) : (1-\Delta)\,, \tag{A.3}$$

with the parameters ϵ and Δ in the ranges $-0.184 \leq \epsilon \leq 0.142$ and $-0.11 \leq \Delta \leq 0.09$ for the current 3σ ranges [23] of the oscillation parameters.[1]

This general framework can be applied to the pseudo-Dirac scenario: if one or more neutrinos are pseudo-Dirac, the probability matrix in Eq. (A.1) will be modified, leading to different final flux ratios in each case. The probabilities can be written (to first order in θ_{13} and ϵ) in terms of θ_{12}, θ_{13}, and the deviation parameters ϵ, Δ, and Γ, where

$$\Gamma \equiv \frac{1}{8}\theta_{13}\sin 2\theta_{12}\cos\delta = \frac{1}{4}\theta_{13}s_{12}c_{12}\cos\delta\,. \tag{A.4}$$

The parameter Γ is constrained to the range $-0.022 \leq \Gamma \leq 0.022$. The flavour conversion probabilities for each case are shown in Table A.1, which have been used to calculate the flavour ratios displayed in Section 3.5.2. The ratio $P_{\tau\tau}$ is omitted, as it is not needed to calculate flux ratios.

[1] "Next-to-next-to-leading order" terms of second order in ϵ and θ_{13} have been discussed in Refs. [398, 399].

Table A.1: Flavour conversion probabilities $P^{\nu_i}_{\alpha\beta}$ and $P^{\nu_{i,j}}_{\alpha\beta}$ for the cases where ν_i and $\nu_{i,j}$ are pseudo-Dirac, where rows denote initial flavour α and columns final flavour β.

	α \ β	e	μ	τ
$P^{\nu_1}_{\alpha\beta}$	e	$\frac{1}{2}c_{12}^4 + s_{12}^4$	$\frac{3}{4}(c_{12}^2 s_{12}^2 + \Delta) - \Gamma$	$\frac{3}{4}(c^2 12 s_{12}^2 - \Delta) + \Gamma$
	μ	$\times$	$\frac{1}{2} - \frac{1}{8}s_{12}^2\left(1 + 3c_{12}^2 + 4\epsilon\right) - \frac{3}{4}\Delta - \Gamma$	$\frac{1}{4} + \frac{1}{4}c_{12}^4 + \frac{1}{8}s_{12}^4$
$P^{\nu_{2,3}}_{\alpha\beta}$	e	$c_{12}^4 + \frac{1}{2}s_{12}^4$	$\frac{3}{4}(c_{12}^2 s_{12}^2 + \Delta) + \Gamma$	$\frac{3}{4}(c_{12}^2 s_{12}^2 - \Delta) - \Gamma$
	μ	$\times$	$\frac{1}{4} + \frac{1}{8}s_{12}^2(1 - 3c_{12}^2 + 4\epsilon) - \frac{3}{4}\Delta + \Gamma$	$\frac{1}{8} + \frac{1}{8}c_{12}^4 + \frac{1}{4}s_{12}^4$
$P^{\nu_2}_{\alpha\beta}$	e	$c_{12}^4 + \frac{1}{2}s_{12}^4$	$\frac{3}{4}(c_{12}^2 s_{12}^2 + \Delta) + \Gamma$	$\frac{3}{4}(c_{12}^2 s_{12}^2 - \Delta) - \Gamma$
	μ	$\times$	$\frac{1}{2} - \frac{1}{8}c_{12}^2(1 + 3s_{12}^2 + 4\epsilon) - \frac{3}{4}\Delta + \Gamma$	$\frac{1}{4} + \frac{1}{8}c_{12}^4 + \frac{1}{4}s_{12}^4$
$P^{\nu_{1,3}}_{\alpha\beta}$	e	$\frac{1}{2}c_{12}^4 + s_{12}^4$	$\frac{3}{4}(c_{12}^2 s_{12}^2 + \Delta) - \Gamma$	$\frac{3}{4}(c_{12}^2 s_{12}^2 - \Delta) + \Gamma$
	μ	$\times$	$\frac{1}{4} + \frac{1}{8}c_{12}^2(1 - 3s_{12}^2 + 4\epsilon) - \frac{3}{4}\Delta - \Gamma$	$\frac{1}{8} + \frac{1}{4}c_{12}^4 + \frac{1}{8}s_{12}^4$
$P^{\nu_3}_{\alpha\beta}$	e	$c_{12}^4 + s_{12}^4$	$c_{12}^2 s_{12}^2 + \Delta$	$c_{12}^2 s_{12}^2 - \Delta$
	μ	$\times$	$\frac{3}{8} + \frac{1}{2}\left(c_{12}^2 s_{12}^2 + \epsilon\right) - \Delta$	$\frac{3}{8} - \frac{1}{2}c_{12}^2 s_{12}^2$
$P^{\nu_{1,3}}_{\alpha\beta}$	e	$\frac{1}{2}(c_{12}^4 + s_{12}^4)$	$\frac{1}{2}(c_{12}^2 s_{12}^2 + \Delta)$	$\frac{1}{2}(c_{12}^2 s_{12}^2 - \Delta)$
	μ	$\times$	$\frac{3}{8} - \frac{1}{4}c_{12}^2 s_{12}^2 - \frac{1}{2}\epsilon - \frac{1}{2}\Delta$	$\frac{3}{8} - \frac{1}{4}c_{12}^2 s_{12}^2$

Appendix B

Group theory details

B.1 Group theory of A_4

A brief summary of group theory aspects, relevant for the models in Section 4.2, will be presented here. For a detailed discussion of the A_4 group see the reviews in Refs. [22, 313].

A_4 is the alternating group of order 4, the group of all even permutations of four objects, and is isomorphic to the group of rotational symmetries of the regular tetrahedron. It is a finite, non-Abelian subgroup of $SO(3)$ and $SU(3)$ with 12 elements. There are 4 irreducible representations, three one-dimensional representations and one three-dimensional representation: $\underline{1}$, $\underline{1}'$, $\underline{1}''$ and $\underline{3}$.

The symmetry group can be generated by two basic permutations $\tilde{S}$ and $\tilde{T}$, given by $\tilde{S} = (4321)$ and $\tilde{T} = (2314)$, where the generic permutation $(1,2,3,4) \to (n_1, n_2, n_3, n_4)$ is denoted by $(n_1 n_2 n_3 n_4)$. It follows that

$$\tilde{S}^2 = \tilde{T}^3 = (\tilde{S}\tilde{T})^3 = 1, \tag{B.1}$$

which defines a "presentation" of the group. The one-dimensional unitary representations are generated by

$$\begin{aligned} \underline{1}: &\quad \tilde{S} = 1 \quad \tilde{T} = 1\,, \\ \underline{1}': &\quad \tilde{S} = 1 \quad \tilde{T} = e^{i2\pi/3} \equiv \omega\,, \\ \underline{1}'': &\quad \tilde{S} = 1 \quad \tilde{T} = e^{i4\pi/3} \equiv \omega^2\,, \end{aligned} \tag{B.2}$$

and the three-dimensional unitary representation is built up from the generators

$$\tilde{T} = \begin{pmatrix} 1 & 0 & 0 \\ 0 & \omega & 0 \\ 0 & 0 & \omega^2 \end{pmatrix}, \quad \tilde{S} = \frac{1}{3}\begin{pmatrix} -1 & 2 & 2 \\ 2 & -1 & 2 \\ 2 & 2 & -1 \end{pmatrix}, \tag{B.3}$$

in the basis where $\tilde{T}$ is diagonal, employed in this thesis. $\omega \equiv e^{i2\pi/3}$ is the cube root of unity. The basis where $\tilde{S}$ is diagonal, related by a unitary transformation, has also been used in the literature, see the discussion in Refs. [28, 313].

The relevant multiplication rules are

$$\underline{1}' \otimes \underline{1}'' = \underline{1}\,, \quad \underline{1}' \otimes \underline{1}' = \underline{1}''\,, \quad \underline{1}'' \otimes \underline{1}'' = \underline{1}'\,, \tag{B.4}$$

for singlets and

$$\underline{3} \otimes \underline{3} = \underline{1} + \underline{1}' + 1'' + \underline{3}_{as} + \underline{3}_s\,, \tag{B.5}$$

for triplets, where $\underline{3}_{as}$ and $\underline{3}_{s}$ are asymmetric and symmetric combinations respectively. The product of two triplets in Eq. (B.5) can be decomposed as

$$\begin{aligned}\begin{pmatrix} a_1 \\ a_2 \\ a_3 \end{pmatrix}_{\underline{3}} \otimes \begin{pmatrix} b_1 \\ b_2 \\ b_3 \end{pmatrix}_{\underline{3}} &= (a_1b_1 + a_2b_3 + a_3b_2)_{\underline{1}} + (a_3b_3 + a_1b_2 + a_2b_1)_{\underline{1}'} + (a_2b_2 + a_1b_3 + a_3b_1)_{\underline{1}''} \\ &\quad + \frac{1}{3}\begin{pmatrix} a_2b_3 - a_3b_2 \\ a_1b_2 - a_2b_1 \\ a_1b_3 - a_3b_1 \end{pmatrix}_{\underline{3}_{as}} + \frac{1}{3}\begin{pmatrix} 2a_1b_1 - a_2b_3 - a_3b_2 \\ 2a_3b_3 - a_1b_2 - a_2b_1 \\ 2a_2b_2 - a_1b_3 - a_3b_1 \end{pmatrix}_{\underline{3}_{s}} . \end{aligned} \tag{B.6}$$

The symmetric combination $\underline{3}_{s}$ will be used extensively for model building, in particular for constructing Majorana mass matrices.

Note that the most general mass matrix leading to TBM [cf. Eq. (4.2)],

$$m_\nu^{\mathrm{TBM}} = \begin{pmatrix} A & B & B \\ \cdot & \frac{1}{2}(A+B+D) & \frac{1}{2}(A+B-D) \\ \cdot & \cdot & \frac{1}{2}(A+B+D) \end{pmatrix} , \tag{B.7}$$

is invariant with respect to $\tilde{S}$, i.e.,

$$\tilde{S}^T\, m_\nu^{\mathrm{TBM}} \tilde{S} = m_\nu^{\mathrm{TBM}} , \tag{B.8}$$

which means that A_4 is a suitable candidate to predict TBM in the neutrino sector. However, the symmetry must be broken in the correct way; see the discussion in Section 4.2.1 and the models that follow.

B.2 Residual μ-τ symmetries in extended A_4 models

In the model with one additional sterile neutrino described in Section (4.2.2), the 4×4 neutrino mass matrix has an eigenvector proportional to $(0,-1,1,0)^T$, see Eq. (4.22). This arises due to a generalised μ-τ symmetry, related to the properties of A_4. An arbitrary 4×4 Majorana mass matrix $M_\nu^{4\times4}$ will be invariant under μ-τ symmetry if the defining matrix $\tilde{P}_{\mu\tau}$ fulfils $\tilde{P}_{\mu\tau}^2 = \mathbb{1}$ and the invariance condition $\tilde{P}_{\mu\tau} M_\nu^{4\times4} \tilde{P}_{\mu\tau} = M_\nu^{4\times4}$, so that $\tilde{P}_{\mu\tau}$ and the resulting mass matrix are given by

$$\tilde{P}_{\mu\tau} = \begin{pmatrix} 1 & 0 & 0 & 0 \\ 0 & 0 & 1 & 0 \\ 0 & 1 & 0 & 0 \\ 0 & 0 & 0 & 1 \end{pmatrix} \quad \text{and} \quad M_\nu^{4\times4} = \begin{pmatrix} \tilde{a} & \tilde{b} & \tilde{b} & \tilde{d} \\ \cdot & \tilde{e} & \tilde{f} & \tilde{g} \\ \cdot & \cdot & \tilde{e} & \tilde{g} \\ \cdot & \cdot & \cdot & \tilde{m} \end{pmatrix} . \tag{B.9}$$

The eigenvalue $\tilde{e}-\tilde{f}$ of this mass matrix corresponds to an eigenvector proportional to $(0,-1,1,0)^T$. This Z_2 invariance, usually present in A_4 models [313], arises by spontaneous A_4 breaking, i.e., from the vacuum $\langle\varphi'\rangle = (v',v',v')$. There is also a second Z_2 under which $M_\nu^{4\times4}$ is invariant, defined by the generator

$$\tilde{P}_{\mathrm{sol}} = \frac{1}{3}\begin{pmatrix} -1 & 2 & 2 & 0 \\ 2 & -1 & 2 & 0 \\ 2 & 2 & -1 & 0 \\ 0 & 0 & 0 & 3 \end{pmatrix} . \tag{B.10}$$

Additional invariance under this Z_2 (note that $\tilde{P}_{\mu\tau}$ and $\tilde{P}_{\mathrm{sol}}$ commute) requires $\tilde{f} = \tilde{a} - \tilde{e} + \tilde{b}$ and $\tilde{d} = \tilde{g}$, so that the eigenvalue $2\tilde{e} - \tilde{b} - \tilde{a}$ has an eigenvector proportional to $(-2,1,1,0)^T$.

Furthermore, it holds that $U_{es} = U_{\mu s} = U_{\tau s}$. The main features of Eq. (4.17) are therefore explained by the two Z_2 symmetries. In addition, the simplicity of the A_4 model leads to $\tilde{e} = -2\tilde{b}$, but does not modify the mixing properties that arise from the two Z_2 symmetries.

Indeed, the upper left 3×3 part of $\tilde{P}_{\rm sol}$ corresponds to the generator $\tilde{S}$ shown in Eq. (B.3), which together with $\tilde{T}$ fulfils the condition in Eq. (B.1). The vacuum $\langle \varphi \rangle = (v, 0, 0)$ means that the charged lepton mass matrix $M_\ell M_\ell^\dagger$ remains invariant under $\tilde{T}$. In other words, the well-known features [313] of A_4 models are not altered by adding a sterile neutrino. Similar statements about the Z_2 invariance of properly extended $\tilde{P}_{\mu\tau}$ and $\tilde{P}_{\rm sol}$ symmetries can be made in the case with two sterile neutrinos [see the 5×5 mass matrix in Eq. (4.30)].

Appendix C

NLO corrections in the A_4 seesaw model

The presence of higher-order operators in the A_4 seesaw model in Section 4.2.3 leads to modifications to the mass matrices M_ℓ, M_D and M_R, so that there are corrections to the leading order lepton mixing matrix. Details of the calculation are presented here, where only corrections of relative order $r_1 \simeq 0.1$ [cf. Eq. (4.63)] have been taken into account. Explicit expressions for the corrected neutrino mass eigenvalues are also reported. This appendix was also published in Ref. [29].

C.1 Charged lepton sector

The corrections to M_ℓ from dimension-six operators come from coupling a second A_4 triplet or an A_4 singlet to each mass term. The addition of the flavon φ replicates the leading order pattern, since the triplet from the product $(\varphi\varphi)_3$ has a VEV in the same direction as φ [331]. Terms with the additional singlet ξ'' also leave the structure of the mass matrix unchanged, but the additional terms

$$\frac{y'_e}{\Lambda^2}\lambda^3\xi(\varphi' L h_d)e^c \,, \frac{y''_e}{\Lambda^2}\lambda^3\xi'(\varphi'' L h_d)'' e^c \quad \text{and} \quad \frac{y'''_e}{\Lambda^2}\lambda^3(\varphi'\varphi'' L h_d)e^c \tag{C.1}$$

are also present, for all three flavours. The first term gives the largest NLO contribution, *viz.*

$$\delta M_\ell^{(1)} = \frac{v_d u v'}{\Lambda^2}\begin{pmatrix} y'_e\lambda^3 & y'_\mu\lambda & y'_\tau \\ y'_e\lambda^3 & y'_\mu\lambda & y'_\tau \\ y'_e\lambda^3 & y'_\mu\lambda & y'_\tau \end{pmatrix}, \tag{C.2}$$

of relative order $r_1 \simeq 0.1$. The matrix diagonalising $(M_\ell + \delta M_\ell^{(1)})(M_\ell + \delta M_\ell^{(1)})^\dagger$ can be approximated by

$$V_L^\ell \simeq \begin{pmatrix} 1 & \frac{y'_\mu}{y_\mu}r_1 & \frac{y'_\tau}{y_\tau}r_1 \\ -\frac{y'_\mu}{y_\mu}r_1 & 1 & \frac{y'_\tau}{y_\tau}r_1 \\ -\frac{y'_\tau}{y_\tau}r_1 & -\frac{y'_\tau}{y_\tau}r_1 & 1 \end{pmatrix} + \mathcal{O}(r_1^2, \lambda^2)\,, \tag{C.3}$$

and the charged lepton masses become

$$m'_\ell = (y_\ell + y'_\ell r_1)\frac{v_d v}{\Lambda}\lambda^{F_\ell}, \qquad (\ell = e, \mu, \tau), \tag{C.4}$$

which amounts to a rescaling of Yukawa couplings.

C.2 Neutrino sector

Similarly to M_ℓ, corrections to M_D from adding the singlet ξ'' retain the leading order form, but there are also several terms with two triplet flavons. The latter are all suppressed by $r_2 \simeq 0.01$ and can be safely neglected. Of the nine different invariant dimension-six operators with one triplet and one singlet flavon, there are three of relative order $r_1 \simeq 0.1$, namely

$$\frac{y_1'}{\Lambda^2}\lambda^{F_1}\xi(\varphi' L h_u)\nu_1^c + \frac{y_2'}{\Lambda^2}\lambda^{F_2}\xi(\varphi'' L h_u)''\nu_2^c + \frac{y_3'}{\Lambda^2}\lambda^{F_3}\xi(\varphi L h_u)\nu_3^c\,, \tag{C.5}$$

leading to the corrections

$$\delta M_D^{(1N)} = \frac{v_u u}{\Lambda^2}\begin{pmatrix} y_1'v' & -y_2'v'' & y_3'v \\ y_1'v' & y_2'v'' & 0 \\ y_1'v' & 0 & 0 \end{pmatrix} F \quad \text{and} \quad \delta M_D^{(1I)} = \frac{v_u u}{\Lambda^2}\begin{pmatrix} y_1'v' & -y_2'v'' & y_3'v \\ y_1'v' & -y_2'v'' & 0 \\ y_1'v' & 2y_2'v'' & 0 \end{pmatrix} F\,, \tag{C.6}$$

in the normal and inverted ordering, respectively. Here the matrix of FN charges is

$$F = \mathrm{diag}(\lambda^{F_1}, \lambda^{F_2}, \lambda^{F_3})\,. \tag{C.7}$$

The corrections to M_R come from terms with two singlets and those with two triplets, e.g.,

$$\frac{w_1'}{\Lambda}\lambda^{F_1+F_3}\xi\xi\nu_1^c\nu_3^c + \ldots \quad \text{and} \quad \frac{w_1''}{\Lambda}\lambda^{F_1+F_3}(\varphi\varphi')\nu_1^c\nu_3^c + \ldots\,; \tag{C.8}$$

the singlet terms give the contribution

$$\delta M_R^{(1)} \propto \frac{1}{\Lambda}\begin{pmatrix} uu''\lambda^{2F_1} & 0 & uu\lambda^{F_1+F_3} \\ \cdot & u'u''\lambda^{2F_2} & u'u'\lambda^{F_2+F_3} \\ \cdot & \cdot & u''u''\lambda^{2F_3} \end{pmatrix}\,, \tag{C.9}$$

whereas the triplet terms are all suppressed by $r_2 \simeq 0.01$. Comparison of the leading order and NLO terms shows that the large ratio $r_1 \simeq 0.1$ only occurs in the $(1,3)$ element of $\delta M_R^{(1)}$, whereas the diagonal and $(2,3)$ elements receive small corrections of order $r_2 \simeq 0.01$. Ignoring the latter, the new mass matrix is

$$M_R' = M_R + \delta M_R^{(1)} = F\begin{pmatrix} w_1 u & 0 & w_1' u r_1 \\ \cdot & w_2 u' & 0 \\ \cdot & \cdot & w_3 u'' \end{pmatrix} F\,. \tag{C.10}$$

It is convenient to factor out the FN charges here, since they do not appear in the leading order seesaw formula. However, as emphasised before, they will play a role when considering NLO seesaw terms. Expanding in the small ratios $r_1 \simeq \frac{w_3 u''}{w_1 u} \simeq 0.1$, the matrix diagonalising M_R' can be approximated as

$$V_R \simeq F^{-1}\begin{pmatrix} 1 & 0 & -\frac{w_1'}{w_1}r_1 \\ 0 & 1 & 0 \\ \frac{w_1'}{w_1}r_1 & 0 & 1 \end{pmatrix} F + \mathcal{O}\left(\frac{w_3 u''}{w_1 u}r_1, r_1^2\right), \tag{C.11}$$

with the mass eigenvalues

$$\begin{aligned} M_1' &= w_1 u\lambda^{2F_1}\left(1 + \frac{{w_1'}^2}{w_1^2}r_1^2\right)\,, \\ M_2' &= w_2 u'\lambda^{2F_2}\,, \\ M_3' &= w_3 u''\lambda^{2F_3}\left(1 - \frac{{w_1'}^2}{w_1^2}r_1^2\right)\,. \end{aligned} \tag{C.12}$$

This shows that corrections to the masses $M_{1,3}$ are suppressed by r_1^2, and the WDM candidate ν_1^c remains in the keV range.

The diagonalisation matrix in Eq. (C.11) can be absorbed into M_D, so that the leading order neutrino mass matrix is

$$M'_\nu = -M'_D \mathrm{diag}(M_1'^{-1}, M_2'^{-1}, M_3'^{-1}) M_D'^{\,T}\,, \tag{C.13}$$

where $M'_D = \left(M_D + \delta M_D^{(1)}\right) V_R^*$ and the FN charges have cancelled. The Dirac mass matrices in Eqs. (4.49) and (4.56) plus the corrections terms in Eq. (C.6) lead to

$$M_D'^{\,(\mathrm{NO})} = \frac{v_u}{\Lambda} \begin{pmatrix} y_1 v + y_1' v' r_1 & y_2 v' - y_2' v'' r_1 & \left(y_3' v - y_1 v \frac{w_1'}{w_1}\right) r_1 \\ \left(y_1' v' - y_3 v'' \frac{w_1'}{w_1}\right) r_1 & y_2 v' + y_2' v'' r_1 & -y_3 v'' \\ \left(y_1' v' + y_3 v'' \frac{w_1'}{w_1}\right) r_1 & y_2 v' & y_3 v'' \end{pmatrix} F\,, \tag{C.14}$$

in the NO and

$$M_D'^{\,(\mathrm{IO})} = \frac{v_u}{\Lambda} \begin{pmatrix} y_1 v + \left(y_1' v' + 2 y_3 v'' \frac{w_1'}{w_1}\right) r_1 & y_2 v' - y_2' v'' r_1 & 2 y_3 v'' + \left(y_3' v - y_1 v \frac{w_1'}{w_1}\right) r_1 \\ \left(y_1' v' - y_3 v'' \frac{w_1'}{w_1}\right) r_1 & y_2 v' - y_2' v'' r_1 & -y_3 v'' \\ \left(y_1' v' - y_3 v'' \frac{w_1'}{w_1}\right) r_1 & y_2 v' + 2 y_2' v'' r_1 & -y_3 v'' \end{pmatrix} F\,, \tag{C.15}$$

in the IO, respectively, to first order in r_1. As shown explicitly in the main text, the dynamics of the right-handed sector are relatively unaffected: the new entries in the first column of the Dirac mass matrices in Eqs. (C.14) and (C.15) will induce mixing between the sterile neutrino ν_1^c and the μ and τ flavours, but of the same magnitude as the original θ_{e1}, so that θ_1^2 will not increase by that much [cf. Eqs. (4.64) and (4.65)]. Thus the entire first column of M'_D, suppressed by the mass $M'_1 = \mathcal{O}(\mathrm{keV})$, can be decoupled from the seesaw (assuming that $|w_1'| \lesssim |w_1|$). In addition, corrections to U_{e5} in Eqs. (4.51) and (4.57) will also be small (see Sects. 4.2.3 and 4.2.3 for a discussion of those effects).

The full 5×5 NLO neutrino mass matrix $M_\nu'^{\,5\times5}$ can now be constructed from the second and third columns of M'_D and $\mathrm{diag}(M'_2, M'_3)$, as in Eq. (4.48). Since NLO seesaw terms are important in the scenarios considered, the full 5×5 diagonalisation must once again be performed [cf. Eqs. (4.51) and (4.57)], including the new terms from higher-order operators in Eqs. (C.14) and (C.15). The matrix diagonalising $M_\nu'^{\,5\times5}$ is explicitly given by

$$U = \begin{pmatrix} U_{\mathrm{TBM}} & 0_{3\times2} \\ 0_{2\times3} & 1_{2\times2} \end{pmatrix} + \delta U \tag{C.16}$$

where, to first order in r_1 and second order in ϵ_i,

$$\delta U^{(\mathrm{NO})} \simeq \begin{pmatrix} \frac{\rho_2}{\sqrt{6}} & -\frac{\rho_2}{\sqrt{3}} & -\frac{1}{\sqrt{2}}\left(\chi-\rho_3+\sigma_+^N\frac{\mathcal{R}}{3}\right) & (1-\rho_2)\epsilon_1 & (\rho_3-\chi)\epsilon_2 \\ -\frac{\sigma_-^N}{\sqrt{6}} & -\frac{1}{2\sqrt{3}}\left(\sigma_-^N+\sigma_+^N\mathcal{R}\right) & -\frac{\sigma_+^N}{3\sqrt{2}}\mathcal{R} & (1+\rho_2)\epsilon_1 & -\epsilon_2 \\ \frac{\sigma_+^N}{\sqrt{6}} & \frac{\sigma_+^N}{2\sqrt{3}}(1+\mathcal{R}) & -\frac{\sigma_+^N}{3\sqrt{2}}\mathcal{R} & \epsilon_1 & \epsilon_2 \\ 0 & -\sqrt{3}\epsilon_1 & \frac{\sigma_+^N}{\sqrt{2}}(1+\mathcal{R})\epsilon_1 & 0 & 0 \\ 0 & -\frac{\sigma_+^N}{\sqrt{3}}\mathcal{R}\epsilon_2 & -\sqrt{2}\epsilon_2 & 0 & 0 \end{pmatrix}$$

$$+\begin{pmatrix} 0 & -\frac{\sqrt{3}}{2}(1-\rho_2)\epsilon_1^2 & \frac{1}{2\sqrt{2}}\left[2(\chi-\rho_3)\epsilon_2^2+\sigma_+^N\left(1+\mathcal{R}\right)\epsilon_1^2\right] & 0 & 0 \\ 0 & -\frac{1}{2\sqrt{3}}\left[3(1+\rho_2)\epsilon_1^2-\sigma_+^N\mathcal{R}\epsilon_2^2\right] & \frac{1}{2\sqrt{2}}\left[2\epsilon_2^2+\sigma_+^N\left(1+\mathcal{R}\right)\epsilon_1^2\right] & 0 & 0 \\ 0 & -\frac{1}{2\sqrt{3}}\left[3\epsilon_1^2+\sigma_+^N\mathcal{R}\epsilon_2^2\right] & -\frac{1}{2\sqrt{2}}\left[2\epsilon_2^2-\sigma_+^N\left(1+\mathcal{R}\right)\epsilon_1^2\right] & 0 & 0 \\ 0 & 0 & 0 & -\frac{3}{2}\epsilon_1^2 & \frac{1}{2}\sigma_+^N\epsilon_1\epsilon_2 \\ 0 & 0 & 0 & \frac{1}{2}\sigma_+^N\epsilon_1\epsilon_2 & -\epsilon_2^2 \end{pmatrix}, \tag{C.17}$$

in the normal ordering, where only first order terms in $\mathcal{R} \simeq \mathcal{O}(10^{-1})$ are kept [see Eq. (4.70)], and $\sigma_\pm^N = \chi \pm \rho_2 - \rho_3$. The new mass eigenvalues are

$$\begin{aligned}
m_1'^{(\mathrm{NO})} &= 0\,, \\
m_2'^{(\mathrm{NO})} &\simeq m_2^{(0)}\left\{1-3\epsilon_1^2-\frac{\rho_2}{3}\sigma_-^I-\frac{1}{2}\left[9\rho_2^2-4\rho_2(\chi-\rho_3)-(\chi-\rho_3)^2\right]\epsilon_1^2\right. \\
&\qquad \left.-\frac{\sigma_+^N}{3}\mathcal{R}\left[\rho_2(1-3\epsilon_1^2)-\sigma_+^N\epsilon_2^2\right]\right\}, \\
m_3'^{(\mathrm{NO})} &\simeq m_3^{(0)}\left\{1-2\epsilon_2^2+(\chi-\rho_3)^2(1-3\epsilon_2^2)-\frac{(\sigma_+^N)^2}{2}(1+2\mathcal{R})\epsilon_1^2\right. \\
&\qquad \left.+\frac{1}{6}\left[\rho_2^2+4\rho_2(\chi-\rho_3)+3(\chi-\rho_3)^2\right]\mathcal{R}(1-2\epsilon_2^2)\right\} \\
m_4'^{(\mathrm{NO})} &\simeq w_2u'\lambda^{2F_2}-m_2^{(0)}\left\{1-3\epsilon_1^2+\frac{2\rho_2^2}{3}(1-6\epsilon_1^2)-\frac{3(\sigma_+^N)^2}{8}\frac{m_3^{(0)}}{m_2^{(0)}}\epsilon_1^2\right\}, \\
m_5'^{(\mathrm{NO})} &\simeq w_3u''\lambda^{2F_3}-m_3^{(0)}\left\{1-2\epsilon_2^2+\frac{1}{2}(\chi-\rho_3)^2-\frac{1}{4}\left[8(\chi-\rho_3)^2+(\sigma_+^N)^2\mathcal{R}\right]\epsilon_2^2\right\},
\end{aligned} \tag{C.18}$$

which corresponds to Eq. (4.53) in the limit $(\chi, \rho_2, \rho_3) \to 0$. Here one can explicitly see that NLO seesaw corrections are controlled by ϵ_i, whereas corrections from higher-order operators are controlled by χ, ρ_2 and ρ_3. In those scenarios where the ϵ_i are negligible, i.e., scenario III, one could still have corrections from the latter, and those turn out to be small in the normal ordering.

In the inverted ordering, the full mixing matrix is

$$\delta U^{(\mathrm{IO})} \simeq \begin{pmatrix} \frac{1}{3\sqrt{6}}\left(3\rho_2+\sigma_+^I\mathcal{G}\right) & -\frac{1}{3\sqrt{3}}\left(3\rho_2+\sigma_+^I\mathcal{G}\right) & -\frac{\rho_2}{\sqrt{2}} & (1-\rho_2)\epsilon_1 & (2-\chi+\rho_3)\epsilon_2 \\ \frac{1}{3\sqrt{6}}\left(3\rho_2+\sigma_+^I\mathcal{G}\right) & -\frac{1}{6\sqrt{3}}\left(6\rho_2-\sigma_+^I\mathcal{G}\right) & -\frac{\rho_2}{\sqrt{2}} & (1-\rho_2)\epsilon_1 & -\epsilon_2 \\ \frac{1}{3\sqrt{6}}\left(3\rho_2+\sigma_+^I\mathcal{G}\right) & \frac{1}{6\sqrt{3}}\left(12\rho_2+\sigma_+^I\mathcal{G}\right) & -\frac{\rho_2}{\sqrt{2}} & (1+2\rho_2)\epsilon_1 & -\epsilon_2 \\ -\frac{\sigma_+^I}{\sqrt{6}}\mathcal{G}\,\epsilon_1 & -\sqrt{3}\,\epsilon_1 & 0 & 0 & 0 \\ -\sqrt{\frac{2}{3}}\left(3-\chi+\rho_3\right)\epsilon_2 & \frac{\sigma_+^I}{\sqrt{3}}\left(1+\mathcal{G}\right)\epsilon_2 & 0 & 0 & 0 \end{pmatrix} \tag{C.19}$$

$$+\begin{pmatrix} -\frac{1}{2\sqrt{6}}\left[2\left(6-5\left(\chi-\rho_3\right)\right)\epsilon_2^2+\sigma_+^I\mathcal{G}\epsilon_1^2\right] & -\frac{1}{2\sqrt{3}}\left[3(1-\rho_2)\epsilon_1^2-2\sigma_+^I(1+\mathcal{G})\epsilon_2^2\right] & 0 & 0 & 0 \\ \frac{1}{2\sqrt{6}}\left[2(3-\chi+\rho_3)\epsilon_2^2-\sigma_+^I\mathcal{G}\epsilon_1^2\right] & -\frac{1}{2\sqrt{3}}\left[3(1-\rho_2)\epsilon_1^2+\sigma_+^I(1+\mathcal{G})\epsilon_2^2\right] & 0 & 0 & 0 \\ \frac{1}{2\sqrt{6}}\left[2(3-\chi+\rho_3)\epsilon_2^2-\sigma_+^I\mathcal{G}\epsilon_1^2\right] & -\frac{1}{2\sqrt{3}}\left[3(1+2\rho_2)\epsilon_1^2+\sigma_+^I(1+\mathcal{G})\epsilon_2^2\right] & 0 & 0 & 0 \\ 0 & 0 & 0 & -\frac{3}{2}\epsilon_1^2 & \frac{\sigma_+^I\epsilon_1\epsilon_2}{2} \\ 0 & 0 & 0 & \frac{\sigma_+^I\epsilon_1\epsilon_2}{2} & -\left(3-2\chi+2\rho_3\right)\epsilon_2^2 \end{pmatrix},$$

to first order in χ and second order in ϵ_i, where σ_+^I and $\mathcal{G}=\mathcal{O}(10^2)$ are defined in Eq. (4.70). In this case one cannot expand in $\mathcal{G}$, in contrast to the NO case, where a first order expansion in $\mathcal{R}$ was performed. The new mass eigenvalues are

$$\begin{aligned}
m_1'^{(\mathrm{IO})} &\simeq m_1^{(0)}\left\{1-6\epsilon_2^2-\frac{1}{9}\left(\chi-\rho_3\right)\left(6-\sigma_-^I\right)+\left[8(\chi-\rho_3)+3\rho_2^2+4\rho_2(\chi-\rho_3)-4(\chi-\rho_3)^2\right]\epsilon_2^2\right. \\
&\quad\left.+\frac{1}{18}\left[9\rho_2^2-(\chi-\rho_3)^2\right]\mathcal{G}+\left[3\rho_2^2+4\rho_2(\chi-\rho_3)+(\chi-\rho_3)^2\right]\mathcal{G}\epsilon_2^2+\frac{(\sigma_+^I)^2}{18}\mathcal{G}^2\left(1-3\epsilon_1^2\right)\right\}, \\
m_2'^{(\mathrm{IO})} &\simeq m_2^{(0)}\left\{1-3(1+6\rho_2^2)\epsilon_1^2+4\rho_2^2+\frac{1}{18}\left[27\rho_2^2+12\rho_2(\chi-\rho_3)+(\chi-\rho_3)^2\right]\mathcal{G}(1-3\epsilon_1^2)\right. \\
&\quad\left.-\frac{(\sigma_+^I)^2}{18}\left[6(1+2\mathcal{G})\epsilon_2^2-\mathcal{G}^2(1-6\epsilon_2^2)\right]\right\}, \\
m_3'^{(\mathrm{IO})} &= 0\,, \\
m_4'^{(\mathrm{IO})} &\simeq w_2u'\lambda^{2F_2}-m_2^{(0)}\left\{1+2\rho_2^2-3(1+4\rho_2^2)\epsilon_1^2-\frac{(\sigma_+^I)^2}{8}\frac{m_1^{(0)}}{m_2^{(0)}}\epsilon_1^2\right\}, \\
m_5'^{(\mathrm{IO})} &\simeq w_3u''\lambda^{2F_3}-m_1^{(0)}\left\{1-6\epsilon_2^2-\frac{1}{6}\left[4(\chi-\rho_3)-(\chi-\rho_3)^2\right]\right. \\
&\quad\left.+\left[8(\chi-\rho_3)-\frac{14}{3}(\chi-\rho_3)^2\right]\epsilon_2^2-\frac{(\sigma_+^I)^2}{4}\frac{3m_2^{(0)}}{2m_1^{(0)}}\epsilon_2^2\right\}.
\end{aligned} \tag{C.20}$$

In this case the corrections very much depend on the scenario concerned, since the value of the ϵ_i terms can give cancellations. However, the correction to $|U_{e2}|^2$ constrains the parameters χ, ρ_2 and ρ_3 to be small (see discussion in the main text), and since $\mathcal{G}$ always occurs together with one of the three parameters the effect of $\mathcal{G}=\mathcal{O}(10^2)$ will always be suppressed. In the end there are enough parameters to fit the mass eigenvalues to the data.

Appendix D

Form factors and loop functions for LFV processes

Details of the different contributions to lepton flavour violating processes in the LRSM, used in the parameter scans in Chapter 5, are presented here.

D.1 Relevant Lagrangian terms

LFV decays proceed via the charged current in Eq. (2.61), repeated here for convenience, as well as the couplings of the charged components of Higgs triplets to lepton doublets in Eq. (2.47); the relevant terms are (with $h_L = h_R = h$)

$$\begin{aligned}
\mathcal{L}_{CC}^{\text{lep}} &= \frac{g}{\sqrt{2}}\left[\overline{\ell'}\gamma^\mu P_L \nu' W_{L\mu}^- + \overline{\ell'}\gamma^\mu P_R \nu' W_{R\mu}^-\right] + \text{h.c.}, \\
\mathcal{L}_{\delta_L^\pm} &= \frac{\delta_L^+}{\sqrt{2}}\left[\overline{\nu_L'^{\,c}} h \ell_L' + \overline{\ell_L'^{\,c}} h \nu_L'\right] + \text{h.c.}\,, \\
\mathcal{L}_{\delta_{L,R}^{\pm\pm}} &= \delta_{L,R}^{++}\overline{\ell'^c} h P_{L,R} \ell' + \delta_{L,R}^{--}\overline{\ell'} h^\dagger P_{R,L} \ell'^c\,.
\end{aligned} \tag{D.1}$$

Rotating the fields to the physical basis gives

$$\begin{aligned}
\mathcal{L}_{CC}^{\text{lep}} &= \frac{g}{\sqrt{2}}\left[\overline{\ell_L}\gamma^\mu K_L n_L (W_{1\mu}^- + \xi e^{i\alpha} W_{2\mu}^-) + \overline{\ell_R}\gamma^\mu K_R n_L^c (-\xi e^{-i\alpha} W_{1\mu}^- + W_{2\mu}^-)\right] + \text{h.c.}, \\
\mathcal{L}_{H_1} &= \frac{g}{\sqrt{2}}\left[H_1^+ \overline{n_L^c}\left(K_L^T \tilde{h}_L\right)\ell_L + H_1^- \overline{\ell_L}\left(\tilde{h}_L^\dagger K_L^*\right) n_L^c\right], \\
\mathcal{L}_{\delta_{L,R}^{\pm\pm}} &= \frac{g}{2}\left[\delta_{L,R}^{++}\overline{\ell^c}\tilde{h}_{L,R} P_{L,R}\ell + \delta_{L,R}^{--}\overline{\ell}\tilde{h}_{L,R}^\dagger P_{R,L}\ell^c\right],
\end{aligned} \tag{D.2}$$

which follows from Eqs. (2.51), (2.54), (2.57) and (2.59), with

$$\tilde{h}_{L,R} \equiv (V_{L,R}^\ell)^T V_R^\nu \frac{\tilde{M}_\nu}{m_{W_R}} V_R^{\nu T} V_{L,R}^\ell = (V_{L,R}^\ell)^T \frac{M_R}{m_{W_R}} V_{L,R}^\ell\,, \tag{D.3}$$

and $\tilde{M}_\nu = \text{diag}(m_1, m_2, m_3, M_1, M_2, M_3)$. The LFV parameter is

$$g_{\text{lfv}}^{L,R} \equiv \left[\tilde{h}_{L,R}^\dagger \tilde{h}_{L,R}\right]_{e\mu} = \left[V_{L,R}^{\ell\dagger} V_R^{\nu *}\left(\frac{\tilde{M}_\nu}{m_{W_R}}\right)^2 V_R^{\nu T} V_{L,R}^\ell\right]_{e\mu} = \left[V_{L,R}^{\ell\dagger}\frac{M_R^* M_R}{m_{W_R}^2} V_{L,R}^\ell\right]_{e\mu}. \tag{D.4}$$

In the manifest left-right symmetry case (discrete parity symmetry), $V_L^\ell = V_R^\ell$, so that these expressions become [375]

$$\tilde{h} \equiv \tilde{h}_L = \tilde{h}_R = K_R^* \frac{\tilde{M}_\nu}{m_{W_R}} K_R^\dagger, \quad \text{and} \quad g_{\text{lfv}} \equiv g_{\text{lfv}}^L = g_{\text{lfv}}^R = \left[K_R\left(\frac{\tilde{M}_\nu}{m_{W_R}}\right)^2 K_R^\dagger\right]_{e\mu}. \tag{D.5}$$

In the present analysis the charged lepton mixing matrices are taken to be diagonal so that all processes depend on a combination of the mixing matrices S and V [see Eq. (5.34)], depending on the helicity of the different particles.

D.2 Decay widths and branching ratios

The effective Lagrangian for μ to e conversion can be written as

$$\begin{aligned}\mathcal{L}_{\mu\to e} = &-\frac{eg^2}{4(4\pi)^2 m_{W_L}^2} m_\mu \overline{e}\sigma_{\mu\nu}(G_L^\gamma P_L + G_R^\gamma P_R)\mu F^{\mu\nu} \\ &-\frac{\alpha_W^2}{2m_{W_L}^2}\sum_q \left\{\overline{e}\gamma_\mu\left[W_L^q P_L + W_R^q P_R\right]\mu\,\overline{q}\gamma^\mu q\right\} + \text{h.c.},\end{aligned} \tag{D.6}$$

with $\sigma_{\mu\nu} \equiv \frac{i}{2}[\gamma_\mu, \gamma_\nu]$ and the form factors $G_{L,R}^\gamma$ and $W_{L,R}^{u,d}$. The full matrix element for $\mu \to e\gamma$ is given by

$$\begin{aligned}i\mathcal{M}(\mu\to e\gamma) = &\frac{e\alpha_W}{8\pi m_{W_L}^2}\epsilon_\gamma^\mu \overline{e}\left[\left(q^2\gamma_\mu - q_\mu \not{q}\right)\left(F_L^\gamma P_L + F_R^\gamma P_R\right)\right. \\ &\left. - im_\mu\sigma_{\mu\nu}q^\nu\left(G_L^\gamma P_L + G_R^\gamma P_R\right)\right]\mu,\end{aligned} \tag{D.7}$$

with the anapole and dipole form factors $F_{L,R}^\gamma$ and $G_{L,R}^\gamma$ defined in Eqs. (D.14) and (D.9).

The on-shell decay $\mu \to e\gamma$ only receives contributions from the $G_{L,R}^\gamma$ terms, the branching ratio turns out to be

$$\text{BR}_{\mu\to e\gamma} = \frac{\alpha_W^3 s_W^2 m_\mu^5}{256\pi^2 m_{W_L}^4 \Gamma_\nu}\left(|G_L^\gamma|^2 + |G_R^\gamma|^2\right) = \frac{3\alpha_{\text{em}}}{2\pi}\left(|G_L^\gamma|^2 + |G_R^\gamma|^2\right), \tag{D.8}$$

where

$$\begin{aligned}G_L^\gamma = &\sum_{i=1}^3\left\{V_{\mu i}V_{ei}^*|\xi|^2 G_1^\gamma(x_i) - S_{\mu i}^* V_{ei}^* \xi e^{-i\alpha} G_2^\gamma(x_i)\frac{M_i}{m_\mu}\right. \\ &\left. + V_{\mu i}V_{ei}^*\left[\frac{m_{W_L}^2}{m_{W_R}^2}G_1^\gamma(y_i) + \frac{2y_i}{3}\frac{m_{W_L}^2}{m_{\delta_R^{++}}^2}\right]\right\}, \\ G_R^\gamma = &\sum_{i=1}^3\left\{S_{\mu i}^* S_{ei} G_1^\gamma(x_i) - V_{\mu i}S_{ei}\xi e^{i\alpha} G_2^\gamma(x_i)\frac{M_i}{m_\mu}\right. \\ &\left. + V_{\mu i}V_{ei}^* y_i\left[\frac{2}{3}\frac{m_{W_L}^2}{m_{\delta_L^{++}}^2} + \frac{1}{12}\frac{m_{W_L}^2}{m_{H_1^+}^2}\right]\right\},\end{aligned} \tag{D.9}$$

with $x_i \equiv (M_i/m_{W_L})^2$, $y_i \equiv (M_i/m_{W_R})^2$ and the loop functions $G_{1,2}^\gamma(x)$ defined in Eq. (D.26). In addition, the electric dipole moment of charged lepton ℓ_α ($\alpha = e, \mu, \tau$) is given by [94, 385, 400]

$$d_\alpha = \frac{e\,\alpha_W}{8\pi m_{W_L}^2}\text{Im}\left[\sum_{i=1}^3 S_{\alpha i}V_{\alpha i}\xi e^{i\alpha} G_2^\gamma(x_i) M_i\right], \tag{D.10}$$

which is similar to the mixed diagram contribution in $\mu \to e\gamma$.

The tree level contribution to $\mu \to 3e$ in Eq. (5.31) can be rewritten as

$$\mathrm{BR}^{\mathrm{triplet}}_{\mu\to 3e} = \frac{\alpha_W^4 m_\mu^5}{24576\pi^3 m_{W_L}^4 \Gamma_\mu} \frac{(4\pi)^2}{2\alpha_W^2} \left|\tilde{h}_{\mu e}\tilde{h}^*_{ee}\right|^2 \left(\frac{m_{W_L}^4}{m_{\delta_L^{++}}^4} + \frac{m_{W_L}^4}{m_{\delta_R^{++}}^4}\right), \tag{D.11}$$

to be compared with the loop-suppressed type I seesaw contribution given by [380, 401]

$$\begin{aligned}
\mathrm{BR}^{\text{type I}}_{\mu\to 3e} = \frac{\alpha_W^4 m_\mu^5}{24576\pi^3 m_{W_L}^4 \Gamma_\mu} \Bigg\{ & 2\left[\left|\frac{1}{2}B_{LL}^{\mu eee} + F_L^{Z_1} - 2s_W^2(F_L^{Z_1} - F_L^\gamma)\right|^2 + \left|\frac{1}{2}B_{RR}^{\mu eee} - 2s_W^2(F_R^{Z_1} - F_R^\gamma)\right|^2\right] \\
& + \left|2s_W^2(F_L^{Z_1} - F_L^\gamma) - B_{LR}^{\mu eee}\right|^2 + \left|2s_W^2(F_R^{Z_1} - F_R^\gamma) - (F_R^{Z_1} + B_{RL}^{\mu eee})\right|^2 \\
& + 8s_W^2\left[\mathrm{Re}\left((2F_L^{Z_1} + B_{LL}^{\mu eee} + B_{LR}^{\mu eee})G_R^{\gamma\,*}\right) + \mathrm{Re}\left((F_R^{Z_1} + B_{RR}^{\mu eee} + B_{RL}^{\mu eee})G_L^{\gamma\,*}\right)\right] \\
& - 48s_W^4\left[\mathrm{Re}\left((F_L^{Z_1} - F_L^\gamma)G_R^{\gamma\,*}\right) + \mathrm{Re}\left((F_R^{Z_1} - F_R^\gamma)G_L^{\gamma\,*}\right)\right] \\
& + 32s_W^4\left(|G_L^\gamma|^2 + |G_R^\gamma|^2\right)\left[\ln\frac{m_\mu^2}{m_e^2} - \frac{11}{4}\right]\Bigg\}.
\end{aligned} \tag{D.12}$$

The interference terms between triplet exchange and gauge boson mediated loop and box diagrams are

$$\begin{aligned}
\mathrm{BR}^{\text{triplet+type I}}_{\mu\to 3e} = & \frac{\alpha_W^4 m_\mu^5}{24576\pi^3 m_{W_L}^4 \Gamma_\mu} \frac{2(4\pi)}{\alpha_W} \times \\
& \Bigg\{ \frac{m_{W_L}^2}{m_{\delta_L^{++}}^2}\mathrm{Re}\left[2s_W^2 T^* F_L^\gamma + 4s_W^2 T^* G_R^\gamma + T^* B_{LL}^{\mu eee} + T^* F_L^{Z_1}(1 - 2s_W^2)\right] \\
& + \frac{m_{W_L}^2}{m_{\delta_R^{++}}^2}\mathrm{Re}\left[2s_W^2 T^* F_R^\gamma + 4s_W^2 T^* G_L^\gamma + T^* B_{RR}^{\mu eee} - 2s_W^2 T^* F_R^{Z_1}\right]\Bigg\},
\end{aligned} \tag{D.13}$$

where $T \equiv \tilde{h}_{\mu e}\tilde{h}^*_{ee}$ and $\tilde{h}_{\alpha\beta}$ is defined in Eq. (5.34). Note that the triplet term effectively has the same structure as the box contribution (after Fierz transformations, see Ref. [402]), so one expects it to interfere with the other amplitudes in the same way.

The form factors for off-shell photon exchange are

$$\begin{aligned}
F_L^\gamma &= \sum_{i=1}^{3}\left\{S^*_{\mu i}S_{ei}F_\gamma(x_i) - V_{\mu i}V^*_{ei}\,y_i\left[\frac{2}{3}\frac{m_{W_L}^2}{m_{\delta_L^{++}}^2}\ln\frac{m_\mu^2}{m_{\delta_L^{++}}^2} + \frac{1}{18}\frac{m_{W_L}^2}{m_{H_1^+}^2}\right]\right\}, \\
F_R^\gamma &= \sum_{i=1}^{3} V_{\mu i}V^*_{ei}\left[|\xi|^2 F_\gamma(x_i) + \frac{m_{W_L}^2}{m_{W_R}^2}F_\gamma(y_i) - y_i\frac{2}{3}\frac{m_{W_L}^2}{m_{\delta_R^{++}}^2}\ln\frac{m_\mu^2}{m_{\delta_R^{++}}^2}\right],
\end{aligned} \tag{D.14}$$

where the logarithmic term is a simplified version of the usual triplet loop function [403], since the doubly charged scalar mass is taken to be much larger than the charged lepton masses

($m_{\delta_{L,R}} \gg m_{e,\mu,\tau}$). The Z_1-boson exchange terms[1] can be expressed as

$$\begin{aligned} F_L^{Z_1} &= \sum_{i,j=1}^{3} S^*_{\mu i} S_{ej} \left\{ \delta_{ij} \left(F_Z(x_i) + 2G_Z(0,x_i) \right) \right. \\ &\quad \left. + (S^T S^*)_{ij} \left[G_Z(x_i,x_j) - G_Z(0,x_i) - G_Z(0,x_j) \right] + (S^\dagger S)_{ij} H_Z(x_i,x_j) \right\}, \\ F_R^{Z_1} &\simeq \sum_{i=1}^{3} V_{\mu i} V^*_{ei} \left[\frac{1-2s_W^2}{2c_W^2} \frac{m_{W_L}^2}{m_{W_R}^2} \left(F_Z(y_i) + 2G_Z(0,y_i) - \frac{y_i}{2} \right) \right. \\ &\quad \left. + \frac{m_{W_L}^2}{m_{W_R}^2} D_Z(y_i,x_i) + \frac{m_{W_L}^2}{m_{W_R}^2} D_Z(y_i,z_i) \right]. \end{aligned} \tag{D.15}$$

where $z_i = (M_i/m_{H_2})^2$; the box diagram form factors are[2]

$$\begin{aligned} B_{LL}^{\mu eee} &= -2 \sum_{i=1}^{3} \left\{ S^*_{\mu i} S_{ei} \left[F_{\text{Xbox}}(0,x_i) - F_{\text{Xbox}}(0,0) \right] \right\} \\ &\quad + \sum_{i,j=1}^{3} S^*_{\mu i} S_{ej} \left\{ -2 S^*_{ej} S_{ei} \left[F_{\text{Xbox}}(x_i,x_j) - F_{\text{Xbox}}(0,x_j) - F_{\text{Xbox}}(0,x_i) + F_{\text{Xbox}}(0,0) \right] \right. \\ &\quad \left. + S^*_{ei} S_{ej} G_{\text{box}}(x_i,x_j,1) \right\}, \end{aligned} \tag{D.16}$$

$$\begin{aligned} B_{RR}^{\mu eee} &= -2 \frac{m_{W_L}^2}{m_{W_R}^2} \sum_{i=1}^{3} \left\{ V_{\mu i} V^*_{ei} \left[F_{\text{Xbox}}(0,y_i) - F_{\text{Xbox}}(0,0) \right] \right\} \\ &\quad + \sum_{i,j=1}^{3} V_{\mu i} V^*_{ej} \left\{ -2 V_{ej} V^*_{ei} \left[F_{\text{Xbox}}(y_i,y_j) - F_{\text{Xbox}}(0,y_j) - F_{\text{Xbox}}(0,y_i) + F_{\text{Xbox}}(0,0) \right] \right. \\ &\quad \left. + V_{ei} V^*_{ej} G_{\text{box}}(y_i,y_j,1) \right\}, \end{aligned} \tag{D.17}$$

for purely left- and right-handed contributions and

$$B_{LR}^{\mu eee} = \frac{1}{2} \frac{m_{W_L}^2}{m_{W_R}^2} \sum_{i,j=1}^{3} S^*_{\mu i} S_{ej} V_{ei} V^*_{ej} G_{\text{box}} \left(x_i, x_j, \frac{m_{W_L}^2}{m_{W_R}^2} \right), \tag{D.18}$$

$$B_{RL}^{\mu eee} = \frac{1}{2} \frac{m_{W_L}^2}{m_{W_R}^2} \sum_{i,j=1}^{3} V_{\mu i} V^*_{ej} S^*_{ei} S_{ej} G_{\text{box}} \left(x_i, x_j, \frac{m_{W_L}^2}{m_{W_R}^2} \right), \tag{D.19}$$

for diagrams with mixed helicity. The loop-suppressed amplitudes with right-handed currents contain the $\mathcal{O}(1)$ mixing matrix V as well as the additional suppression factor of $(m_{W_L}/m_{W_R})^2$; without the enhancement from large left-right mixing (in S) those contributions will be much smaller than the tree level one in Eq. (5.31). The mixed left-right box contributions come from an effective four fermion operator, as is the case in kaon mixing [88, 89, 354], with a factor of 1/2 coming from the Fierz transformation of a scalar to vector contribution (see Ref. [401]).

[1] Terms from the exchange of the heavier Z_2 boson are neglected.
[2] Terms proportional to $|\xi|^2$ are neglected.

$\mu \to e$ conversion in nuclei is similar to $\mu \to 3e$ and receives contributions from the same loop and box diagrams.[3] The $\mu \to e$ conversion rate is given by [375, 383, 384, 401]

$$\mathrm{R}_{\mu\to e}^{A(N,Z)} = \frac{\alpha_{\mathrm{em}}^3 \alpha_W^4 m_\mu^5}{16\pi^2 m_{W_L}^4 \Gamma_{\mathrm{capt}}} \frac{Z_{\mathrm{eff}}^4}{Z} \left|F(-m_\mu^2)\right|^2 \left(|Q_L^W|^2 + |Q_R^W|^2\right), \tag{D.20}$$

where

$$Q_{L,R}^W = (2Z+N)\left[W_{L,R}^u - \frac{2}{3}s_W^2 G_{R,L}^\gamma\right] + (Z+2N)\left[W_{L,R}^d + \frac{1}{3}s_W^2 G_{R,L}^\gamma\right], \tag{D.21}$$

and

$$\begin{aligned} W_{L,R}^u &= \frac{2}{3}s_W^2 F_{L,R}^\gamma + \left(-\frac{1}{4} + \frac{2}{3}s_W^2\right) F_{L,R}^{Z_1} + \frac{1}{4}\left(B_{LL,RR}^{\mu euu} + B_{LR,RL}^{\mu euu}\right), \\ W_{L,R}^d &= -\frac{1}{3}s_W^2 F_{L,R}^\gamma + \left(\frac{1}{4} - \frac{1}{3}s_W^2\right) F_{L,R}^{Z_1} + \frac{1}{4}\left(B_{LL,RR}^{\mu edd} + B_{LR,RL}^{\mu edd}\right), \end{aligned} \tag{D.22}$$

are composite form factors. Note that the expression in Eq. (D.20) is derived by approximating all interactions to be point-like and taking the proton and neutron densities to be equal. In that case the wavefunction overlap integrals D and $V^{(p,n)}$ calculated in Ref. [404] can be replaced by the quantities Z_{eff} and the form factor $F(-m_\mu^2)$, where

$$\frac{V^{(p)}}{\sqrt{Z}} = \frac{Z_{eff}^2 F(-m_\mu^2)\alpha_{\mathrm{em}}^{\frac{3}{2}}}{4\pi}, \tag{D.23}$$

and $V^{(p)}/Z \simeq V^{(n)}/N$. The relevant box diagram form factors are

$$\begin{aligned} B_{LL}^{\mu euu} &= \sum_{i=1}^{3} S_{\mu i}^* S_{ei} \left[F_{\mathrm{box}}(0,x_i) - F_{\mathrm{box}}(0,0)\right], \\ B_{LL}^{\mu edd} &\simeq \sum_{i=1}^{3} S_{\mu i}^* S_{ei} \left\{F_{\mathrm{Xbox}}(0,x_i) - F_{\mathrm{Xbox}}(0,0)\right. \\ &\quad \left. + |[V_{\mathrm{CKM}}]_{td}|^2 \left[F_{\mathrm{Xbox}}(x_t,x_i) - F_{\mathrm{Xbox}}(0,x_i) - F_{\mathrm{Xbox}}(0,x_t) + F_{\mathrm{Xbox}}(0,0)\right]\right\}, \\ B_{RR}^{\mu eqq} &= \frac{m_{W_L}^2}{m_{W_R}^2} B_{LL}^{\mu eqq}(S \leftrightarrow V^*\,;\, x_i \leftrightarrow y_i\,;\, x_t \leftrightarrow y_t), \end{aligned} \tag{D.24}$$

where $x_t = m_t^2/m_{W_L}^2$ and $y_t = m_t^2/m_{W_R}^2$.

Finally, the presence of non-unitary mixing in the light neutrino sector (due to the matrix $S \simeq M_D M_R^{-1}$) also affects the standard muon decay width, Γ_μ (and thus the determination of G_F), as well as the capture rate for muons on the nucleus, Γ_{capt}. Explicitly, one has

$$\Gamma_\mu \simeq \Gamma_\mu^{(0)}\left(\mathbb{1} - [SS^\dagger]_{ee} - [SS^\dagger]_{\mu\mu}\right) \quad \text{and} \quad \Gamma_{\mathrm{capt}} \simeq \Gamma_{\mathrm{capt}}^{(0)}\left(\mathbb{1} - [SS^\dagger]_{\mu\mu}\right), \tag{D.25}$$

where $\Gamma_\mu^{(0)}$ and $\Gamma_{\mathrm{capt}}^{(0)}$ are the SM values and terms of order S^4 have been omitted. Those expressions occur in the denominators of the branching ratio formulae in Eq. (3.80), and since the numerators are in general proportional to $\mathcal{O}(S^4)$ the effect will be negligible; in the numerical analysis the standard value $\Gamma_\mu = G_F^2 m_\mu^5/(192\pi^3)$ is used.

[3] Although the process can also be mediated at tree-level by neutral Higgs bosons, those particles have to be very heavy due to constraints from K^0-$\overline{K}^0$ mixing.

D.3 Loop functions

The relevant loop functions are

$$
\begin{aligned}
F_\gamma(x) &= \frac{7x^3 - x^2 - 12x}{12(1-x)^3} - \frac{x^4 - 10x^3 + 12x^2}{6(1-x)^4} \ln x \,, \\
G_1^\gamma(x) &= -\frac{2x^3 + 5x^2 - x}{4(1-x)^3} - \frac{3x^3}{2(1-x)^4} \ln x \,, \\
G_2^\gamma(x) &= \frac{x^2 - 11x + 4}{2(1-x)^2} - \frac{3x^2}{(1-x)^3} \ln x \,, \\
F_Z(x) &= -\frac{5x}{2(1-x)} - \frac{5x^2}{2(1-x)^2} \ln x \,, \\
G_Z(x,y) &= -\frac{1}{2(x-y)} \left[\frac{x^2(1-y)}{1-x} \ln x - \frac{y^2(1-x)}{1-y} \ln y \right] , \\
H_Z(x,y) &= \frac{\sqrt{xy}}{4(x-y)} \left[\frac{x^2 - 4x}{1-x} \ln x - \frac{y^2 - 4y}{1-y} \ln y \right] , \\
D_Z(x,y) &= x \left(2 - \ln \frac{y}{x} \right) + \frac{(-8x + 9x^2 - x^3) + (-8x^2 + x^3) \ln x}{(1-x)^2} \\
&\quad + \frac{x(y - y^2 + y^2 \ln y)}{(1-y)^2} + \frac{2xy(4-x) \ln x}{(1-x)(1-y)} + \frac{2x(x-4y) \ln \frac{y}{x}}{(1-y)(x-y)} \,, \\
F_{\text{box}} &= \left(4 + \frac{xy}{4} \right) I_2(x,y,1) - 2xy I_1(x,y,1) \,, \\
F_{\text{Xbox}}(x,y) &= -\left(1 + \frac{xy}{4} \right) I_2(x,y,1) - 2xy I_1(x,y,1) \,, \\
G_{\text{box}}(x,y,\eta) &= -\sqrt{xy} \left[(4 + xy\eta) I_1(x,y,\eta) - (1+\eta) I_2(x,y,\eta) \right] ,
\end{aligned}
\tag{D.26}
$$

where

$$
\begin{aligned}
I_1(x,y,\eta) &= \left[\frac{x \ln x}{(1-x)(1-\eta x)(x-y)} + (x \leftrightarrow y) \right] - \frac{\eta \ln \eta}{(1-\eta)(1-\eta x)(1-\eta y)} \,, \\
I_2(x,y,\eta) &= \left[\frac{x^2 \ln x}{(1-x)(1-\eta x)(x-y)} + (x \leftrightarrow y) \right] - \frac{\ln \eta}{(1-\eta)(1-\eta x)(1-\eta y)} \,, \\
I_i(x,y,1) &\equiv \lim_{\eta \to 1} I_i(x,y,\eta) \,,
\end{aligned}
\tag{D.27}
$$

and the limiting values are

$$
\begin{aligned}
G_Z(0,x) &= -\frac{x \ln x}{2(1-x)} \,, \\
F_{\text{box}}(0,x) &= \frac{4}{1-x} + \frac{4x}{(1-x)^2} \ln x \,, \\
F_{\text{Xbox}}(0,x) &= -\frac{1}{1-x} - \frac{x \ln x}{(1-x)^2} \,.
\end{aligned}
\tag{D.28}
$$

Appendix E

Helicity amplitudes for $e^-e^- \to W_L^- W_R^-$

It is an illustrative exercise to study the helicity amplitudes of the inverse double beta decay process studied in Section 5.6. An explicit evaluation for the process $e^-e^- \to W_L^- W_R^-$ has been performed, with the helicity of the electrons and the polarisation of the W bosons fixed. This appendix was also published in Ref. [32].

Denoting electron (W boson) momenta with p_i (k_i), $(i = 1, 2)$, the process is

$$e^-(p_1, \lambda_1)\, e^-(p_2, \lambda_2) \to W_L^-(k_1, \tau_1)\, W_R^-(k_2, \tau_2)\,, \tag{E.1}$$

where $\lambda_{1,2} = \pm\frac{1}{2}$ and $\tau_{1,2} = 0, \pm 1$. Without loss of generality, one can choose p_1 and p_2 to be in the $\pm z$-directions, and assume that the final state particles propagate in the x–z plane. The momenta are then given by

$$p_{1,2}^\mu = (E, 0, 0, \pm E)\,, \quad k_{1,2}^\mu = (E_{1,2}, \pm|k|\vec{\mathbf{n}})\,, \tag{E.2}$$

where $\vec{\mathbf{n}} = (\sin\theta, 0, \cos\theta)$ and

$$E = \frac{\sqrt{s}}{2}\,, \quad E_{1,2} = \frac{s \pm m_{W_L}^2 \mp m_{W_R}^2}{2\sqrt{s}}\,, \quad |k| = \frac{\sqrt{\lambda(s, m_{W_L}^2, m_{W_R}^2)}}{2\sqrt{s}}\,. \tag{E.3}$$

The gauge boson polarisation vectors can be defined by

$$\epsilon_{\tau_{1,2}=0}(k_1, k_2) = \pm\frac{1}{m_{W_{L,R}}}(\pm|k|, E_{1,2}\sin\theta, 0, E_{1,2}\cos\theta)\,, \tag{E.4}$$

$$\epsilon_{\tau_{1,2}=\pm1}(k_1, k_2) = \frac{1}{\sqrt{2}}(0, \mp\tau_{1,2}\cos\theta, -i, \pm\tau_{1,2}\sin\theta)\,. \tag{E.5}$$

The helicity amplitudes are calculated from

$$\begin{aligned}\mathcal{M}_{\lambda_1\lambda_2\tau_1\tau_2} = {} & \frac{g^2}{2(t - m_i^2)}\bar{u}(p_1, \lambda_1)\gamma_\mu \not{k}_1 \gamma_\nu P_L v(p_2, \lambda_2)\epsilon^{\mu*}(k_1, \tau_1)\epsilon^{\nu*}(k_2, \tau_2) \\ & + \frac{g^2}{2(u - m_i^2)}\bar{u}(p_1, \lambda_1)\gamma_\mu \not{k}_2 \gamma_\nu P_R v(p_2, \lambda_2)\epsilon^{\mu*}(k_2, \tau_2)\epsilon^{\nu*}(k_1, \tau_1)\,,\end{aligned} \tag{E.6}$$

resulting in

$$
\begin{aligned}
\mathcal{M}_{\lambda\lambda 00} &= -\lambda g^2 \sin\theta \\
&\quad \times \frac{\left\{\sqrt{\lambda(s, m_{W_L}^2, m_{W_R}^2)}\left(s + m_{W_L}^2 + m_{W_R}^2\right) - 2\lambda\cos\theta\left[\left(m_{W_L}^2 - m_{W_R}^2\right)^2 - s^2\right]\right\}}{4 m_{W_L} m_{W_R}\left(q^2 - m_i^2\right)}, \\
\mathcal{M}_{\lambda\lambda 0\tau} &= \lambda g^2 \sqrt{s}\left[(1+2\lambda\tau)\cos^2\frac{\theta}{2} + (1-2\lambda\tau)\sin^2\frac{\theta}{2}\right] \\
&\quad \times \frac{\cos\theta\left(s + m_{W_L}^2 - m_{W_R}^2\right) - 4\lambda\tau m_{W_L}^2 + 2\lambda\sqrt{\lambda\left(s, m_{W_L}^2, m_{W_R}^2\right)}}{2\sqrt{2} m_{W_L}\left(q^2 - m_i^2\right)}, \\
\mathcal{M}_{\lambda\lambda\tau 0} &= -\lambda g^2 \sqrt{s}\left[(1-2\lambda\tau)\cos^2\frac{\theta}{2} + (1+2\lambda\tau)\sin^2\frac{\theta}{2}\right] \\
&\quad \times \frac{\cos\theta\left(s - m_{W_L}^2 + m_{W_R}^2\right) + 4\lambda\tau m_{W_L}^2 + 2\lambda\sqrt{\lambda\left(s, m_{W_L}^2, m_{W_R}^2\right)}}{2\sqrt{2} m_{W_L}\left(q^2 - m_i^2\right)}, \\
\mathcal{M}_{\lambda\lambda\tau\tau} &= g^2 \frac{\sin\theta\left[2\lambda\sqrt{\lambda\left(s, m_{W_L}^2, m_{W_R}^2\right)} - 2\lambda\tau\left(m_{W_L}^2 - m_{W_R}^2\right) + s\cos\theta\right]}{4\left(q^2 - m_i^2\right)}, \\
\mathcal{M}_{\lambda\lambda\tau-\tau} &= -\frac{g^2 s \sin\theta(\cos\theta - 2\lambda\tau)}{4\left(q^2 - m_i^2\right)}, \\
\mathcal{M}_{\lambda-\lambda 00} &= \mathcal{M}_{\lambda-\lambda 0\tau} = \mathcal{M}_{\lambda-\lambda\tau 0} = \mathcal{M}_{\lambda-\lambda\tau\tau} = \mathcal{M}_{\lambda-\lambda\tau-\tau} = 0,
\end{aligned}
\tag{E.7}
$$

where $\lambda = \pm\frac{1}{2}$ and $\tau = \pm 1$, and $q^2 = t(u)$ when $\lambda = -\frac{1}{2}\left(+\frac{1}{2}\right)$. The amplitude vanishes whenever $\lambda_1 = -\lambda_2$, or in other words, when the two electrons have the same spin (note that one electron is described by a v spinor in Eq. (E.6), which means that its actual helicity is the opposite of the spinor's helicity). The amplitude is only non-zero when the electrons have opposite spin ($\lambda_1 = \lambda_2$); squaring and summing over boson polarisations gives the polarised cross sections σ_{LR} and σ_{RL} in Eq. (5.68), which correspond to the t- and u-channels respectively.

It is interesting to study the high energy behaviour of these helicity amplitudes. Explicitly, in the limit $\sqrt{s} \to \infty$ and neglecting neutrino mass one gets

$$
\begin{aligned}
\mathcal{M}_{\lambda\lambda 00} &\xrightarrow{\sqrt{s}\to\infty} -\lambda\frac{g^2 \sin\theta\, s}{2 m_{W_L} m_{W_R}}, \\
\mathcal{M}_{\lambda\lambda 0\tau} &\xrightarrow{\sqrt{s}\to\infty} -\frac{g^2\sqrt{s}\left[(1+2\lambda\tau)\cos^2\frac{\theta}{2} + (1-2\lambda\tau)\sin^2\frac{\theta}{2}\right]}{2\sqrt{2} m_{W_L}}, \\
\mathcal{M}_{\lambda\lambda\tau 0} &\xrightarrow{\sqrt{s}\to\infty} \frac{g^2\sqrt{s}\left[(1-2\lambda\tau)\cos^2\frac{\theta}{2} + (1+2\lambda\tau)\sin^2\frac{\theta}{2}\right]}{2\sqrt{2} m_{W_L}}, \\
\mathcal{M}_{\lambda\lambda\tau\tau} &\xrightarrow{\sqrt{s}\to\infty} -\lambda g^2 \sin\theta, \\
\mathcal{M}_{\lambda\lambda\tau-\tau} &\xrightarrow{\sqrt{s}\to\infty} -\lambda\tau\frac{g^2 \sin\theta(1 - 2\lambda\tau\cos\theta)}{1 + 2\lambda\cos\theta}.
\end{aligned}
\tag{E.8}
$$

The amplitudes that contain at least one longitudinally polarised W boson ($\tau_{1,2} = 0$) are divergent, whereas those with only transverse polarisations ($\tau_{1,2} = \pm 1$) are finite. Summing over fermion spins and boson polarisations gives the result in Eq. (5.63), and proper consideration of the full theory will lead to a well-behaved total amplitude, as discussed in the main text.

List of Tables

3.1 Best fit and 3σ ranges of neutrino oscillation parameters 24
3.2 Best-fit and estimated 2σ values of the sterile neutrino parameters 29
3.3 Phase-space factors and NMEs for light and heavy neutrino exchange 42
3.4 Observed Φ_μ/Φ_e flux ratio assuming the initial flux ratios of $1:2:0$ and exact μ-τ symmetry 45

4.1 Simplified classification of A_4 models in the literature 62
4.2 Particle assignments of effective A_4 model with one sterile neutrino 64
4.3 Particle assignments of A_4 type I seesaw model 73
4.4 Summary of the different scenarios discussed in the A_4 seesaw model 80
4.5 Particle assignments of the effective S_3 model 85

5.1 Summary of relevant mechanisms and limits for $0\nu\beta\beta$ in the LRSM 97
5.2 Phase-space factors and NMEs for light and heavy neutrino exchange, and for the λ- and η-diagrams, for different isotopes 98
5.3 Suppression or enhancement factors of the cross section for inverse double beta decay cross section with polarised beams 114

A.1 Flavour conversion probabilities for different pseudo-Dirac combinations 124

List of Figures

1.1 Graphic summarising the connections between the main topics of the thesis . . 4

2.1 Feynman diagram for the type I seesaw model 8
2.2 Feynman diagram for the type II seesaw model 14

3.1 The two possible active neutrino mass orderings 23
3.2 Mass spectra of sterile neutrino schemes with one sterile neutrino 25
3.3 Mass spectra of sterile neutrino schemes with two sterile neutrinos 26
3.4 Oscillation probabilities vs. L/E in the 3+2/2+3 and 1+3+1 case 28
3.5 Feynman diagram for $0\nu\beta\beta$ with light neutrino exchange 31
3.6 The effective mass $|\langle m_{ee}\rangle|$ as a function of the lightest neutrino mass in both the normal and inverted ordering 32
3.7 The allowed ranges in the $|\langle m_{ee}\rangle| - m_{\text{light}}$ parameter space for the 3+1 and 1+3 cases 33
3.8 Same as Fig. 3.7, for the 3+2 and 2+3 cases 35
3.9 Allowed regions in the $|\langle m_{ee}\rangle| - \sum m_\nu$ plane for the three different cases of one pseudo-Dirac neutrino 37
3.10 Same as Fig. 3.9 for the three different cases of two pseudo-Dirac neutrinos . . 38
3.11 Heavy neutrino contribution to $0\nu\beta\beta$ in the type I seesaw model 40
3.12 The standard light neutrino contribution to the $0\nu\beta\beta$ halflife of ^{76}Ge plotted against the lightest light neutrino mass 43
3.13 The flux ratio Φ_μ/Φ_e against $\sin^2\theta_{12}$, assuming the initial neutrino flux ratios of $1:2:0$ 47
3.14 Same as Fig. 3.13 for the observable flux ratio Φ_e/Φ_τ 48
3.15 The observable flux ratio Φ_μ/Φ_e against n, assuming the initial neutrino flux ratios of $1:n:0$ 50
3.16 Same as Fig. 3.15 for the observable flux ratio Φ_e/Φ_τ 51
3.17 Inverse double beta decay mediated by light Majorana neutrinos 57

4.1 The allowed values in $a-d$ and $a-e$ parameter space for normal and inverted ordering 68
4.2 $\sin^2\theta_{14}$ against $\sin^2\theta_{12}$ and $\sin^2\theta_{23}$, for both the normal and inverted ordering . 69
4.3 The allowed ranges of $|U_{e4}|^2 - \Delta m^2_{41}$ and $|U_{e5}|^2 - \Delta m^2_{51}$ in the inverted ordering 81

5.1 Feynman diagram of $0\nu\beta\beta$ in the LRSM, mediated by heavy neutrinos with right-handed currents 92
5.2 Feynman diagrams of $0\nu\beta\beta$ in the LRSM, mediated by doubly charged triplets 93
5.3 Feynman diagrams of the λ- and η-mechanisms for $0\nu\beta\beta$ in the LRSM 94
5.4 Comparison of the limits in $M_{N_e} - m_{W_R}$ parameter space from CMS and from the KamLAND-Zen limit on $0\nu\beta\beta$ 102

5.5 The standard light neutrino contribution to the $0\nu\beta\beta$ halflife of ^{76}Ge plotted against the lightest light neutrino mass, including LFV constraints 103
5.6 The contribution to the $0\nu\beta\beta$ halflife of ^{76}Ge from heavy right-handed neutrinos and right-handed Higgs triplets 104
5.7 The total $0\nu\beta\beta$ halflife of ^{76}Ge including light neutrino, heavy neutrino and triplet contributions, plotted against the lightest light neutrino mass 105
5.8 The contributions to the $0\nu\beta\beta$ halflife of ^{76}Ge from the λ- and η-diagrams plotted against the lightest light neutrino mass 108
5.9 The contributions to the $0\nu\beta\beta$ halflife of ^{76}Ge from heavy right-handed neutrinos, with left- and right-handed currents 109
5.10 Ratios of halflife contributions 110
5.11 Inverse neutrinoless double beta decay diagrams with W_L and W_R in the final state 111
5.12 Differential cross section for $e^-e^- \to W_L^- W_R^-$ with $\sqrt{s} = 3$ TeV 112
5.13 Cross section for $e^-e^- \to W_L^- W_R^-$ with $\sqrt{s} = 3$ TeV 113

List of Acronyms

$0\nu\beta\beta$	neutrinoless double beta decay
ACT	Atacama Cosmology Telescope
AGN	active-galactic nuclei
ATLAS	A Toroidal LHC Apparatus
BAO	Baryonic Acoustic Oscillation
BAU	baryon asymmetry of the universe
BBN	Big Bang Nucleosynthesis
BM	bimodal
CDM	cold dark matter
CKM	Cabibbo-Kobayashi-Maskawa
CMB	cosmic microwave background
CMS	Compact Muon Solenoid
COMET	COherent Muon to Electron Transition
DAEδALUS	Decay At rest Experiment for δ studies At the Laboratory for Underground Science
DM	dark matter
EXO	Enriched Xenon Observatory
EWPO	electroweak precision observables
FN	Froggatt-Nielsen
GALLEX	Gallium Experiment
GERDA	GERmanium Detector Array
GIM	Glashow-Iliopoulos-Maiani
GRB	gamma-ray burst
GUT	Grand Unified Theory
HDM	hot dark matter

HM	Heidelberg-Moscow
HST	Hubble Space Telescope
ILL	Institut Laue-Langevin
INO	India-based Neutrino Observatory
IO	inverted ordering
K2K	KEK to Super-Kamiokande
KamLAND	Kamioka Liquid scintillator AntiNeutrino Detector
KamLAND-Zen	KamLAND Zero Neutrino double beta decay
KARMEN	KArlsruhe Rutherford Medium Energy Neutrino experiment
KATRIN	KArlsruhe TRItium Neutrino experiment
LBL	long-baseline
LBNE	Long-Baseline Neutrino Experiment
LEP	Large Electron-Positron Collider
LFV	lepton flavour violation
LHC	Large Hadron Collider
LNV	lepton number violation
LRSM	left-right symmetric model
LSND	Liquid Scintillator Neutrino Detector
LSS	large scale structure
Ly-α	Lyman-alpha
MEG	MuEGamma
MiniBooNE	Mini-Booster Neutrino Experiment
MINOS	Main Injector Neutrino Oscillation Search
MSSM	minimal supersymmetric standard model
MSW	Mikheyev-Smirnov-Wolfenstein
NLO	next-to-leading order
NME	nuclear matrix element
NO	normal ordering
νMSM	neutrino Minimal Standard Model

NSM	Nuclear Shell Model
NOνA	NuMI Off-Axis Neutrino Appearance
PINGU	Phased Icecube Next Generation Upgrade
PMNS	Pontecorvo-Maki-Nakagawa-Sakata
PRIME	PRIsm Mu E experiment
PRISM	Phase-Rotated Intense Slow Muon source
QED	Quantum Electrodynamics
QRPA	Quasi-Random Phase Approximation
RENO	Reactor Experiment for Neutrino Oscillation
SAGE	Soviet-American Gallium Experiment
SBL	short-baseline
SciBooNE	SciBar Booster Neutrino Experiment
SDSS	Sloan Digital Sky Survey
SM	Standard Model
SNO	Sudbury Neutrino Observatory
SPT	South Pole Telescope
SuperNEMO	Super-Neutrino Ettore Majorana Observatory
T2K	Tokai to Kamioka
T2KK	Tokai to Kamioka to Korea
TBM	tri-bimaximal mixing
UV	ultraviolet
VEV	vacuum expectation value
WDM	warm dark matter
WIMP	weakly interacting massive particle
WMAP	Wilkinson Microwave Anisotropy Probe

References

[1] **ATLAS Collaboration**, G. Aad *et al.*, "*Observation of a new particle in the search for the Standard Model Higgs boson with the ATLAS detector at the LHC*," Phys. Lett. **B716** (2012) 1–29, arXiv:1207.7214.

[2] **CMS Collaboration**, S. Chatrchyan *et al.*, "*Observation of a new boson at a mass of 125 GeV with the CMS experiment at the LHC*," Phys. Lett. **B716** (2012) 30–61, arXiv:1207.7235.

[3] P. Minkowski, "$\mu \to e\gamma$ *at a Rate of One Out of 1-Billion Muon Decays?*," Phys. Lett. **B67** (1977) 421.

[4] T. Yanagida, "*Horizontal Gauge Symmetry And Masses Of Neutrinos*," in *Proc. Workshop on the Baryon Number of the Universe and Unified Theories*, O. Sawada and A. Sugamoto, eds., p. 95. 1979.

[5] M. Gell-Mann, P. Ramond, and R. Slansky, "*Horizontal gauge symmetry and masses of neutrinos*," in *Supergravity*, P. van Nieuwenhuizen and D. Freedman, eds., p. 315. 1979.

[6] S. L. Glashow, "*The future of elementary particle physics*," in *Proceedings of the 1979 Cargese Summer Institute on Quarks and Leptons*, M. Levy, J.-L. Basdevant, D. Speiser, J. Weyers, R. Gastmans, and M. Jaco, eds., p. 687. 1980.

[7] R. N. Mohapatra and G. Senjanovic, "*Neutrino Mass and Spontaneous Parity Violation*," Phys. Rev. Lett. **44** (1980) 912.

[8] T. P. Cheng and L.-F. Li, "*Neutrino Masses, Mixings and Oscillations in* $SU(2) \times U(1)$ *Models of Electroweak Interactions*," Phys. Rev. **D22** (1980) 2860.

[9] G. Lazarides, Q. Shafi, and C. Wetterich, "*Proton Lifetime and Fermion Masses in an SO(10) Model*," Nucl. Phys. **B181** (1981) 287.

[10] M. Magg and C. Wetterich, "*Neutrino mass problem and gauge hierarchy*," Phys. Lett. **B94** (1980) 61.

[11] R. N. Mohapatra and G. Senjanovic, "*Neutrino Masses and Mixings in Gauge Models with Spontaneous Parity Violation*," Phys. Rev. **D23** (1981) 165.

[12] J. Schechter and J. W. F. Valle, "*Neutrino Masses in* $SU(2) \times U(1)$ *Theories*," Phys. Rev. **D22** (1980) 2227.

[13] C. Wetterich, "*Neutrino Masses and the Scale of B-L Violation*," Nucl. Phys. **B187** (1981) 343.

[14] G. G. Ross, *Grand Unified Theories*. Westview Press, 1985.

[15] G. Bertone, ed., *Particle dark matter: Observations, models and searches*. Cambridge, UK: Univ. Pr., 2010.

[16] S. Dodelson and L. M. Widrow, "*Sterile-neutrinos as dark matter*," Phys. Rev. Lett. **72** (1994) 17–20, arXiv:hep-ph/9303287.

[17] **LSND Collaboration**, A. Aguilar-Arevalo *et al.*, "*Evidence for neutrino oscillations from the observation of anti-neutrino(electron) appearance in a anti-neutrino(muon) beam*," Phys. Rev. **D64** (2001) 112007, arXiv:hep-ex/0104049.

[18] **MiniBooNE Collaboration**, A. Aguilar-Arevalo *et al.*, "*A Combined $\nu_\mu \to \nu_e$ and $\bar{\nu}_\mu \to \bar{\nu}_e$ Oscillation Analysis of the MiniBooNE Excesses*," arXiv:1207.4809.

[19] G. Mention, M. Fechner, T. Lasserre, T. Mueller, D. Lhuillier, *et al.*, "*The Reactor Antineutrino Anomaly*," Phys. Rev. **D83** (2011) 073006, arXiv:1101.2755.

[20] S. Hannestad, "*Neutrino physics from precision cosmology*," Prog. Part. Nucl. Phys. **65** (2010) 185–208, arXiv:1007.0658.

[21] K. Abazajian, M. Acero, S. Agarwalla, A. Aguilar-Arevalo, C. Albright, *et al.*, "*Light Sterile Neutrinos: A White Paper*," arXiv:1204.5379.

[22] H. Ishimori, T. Kobayashi, H. Ohki, Y. Shimizu, H. Okada, *et al.*, "*Non-Abelian Discrete Symmetries in Particle Physics*," Prog. Theor. Phys. Suppl. **183** (2010) 1–163, arXiv:1003.3552.

[23] D. Forero, M. Tortola, and J. Valle, "*Global status of neutrino oscillation parameters after Neutrino-2012*," Phys. Rev. **D86** (2012) 073012, arXiv:1205.4018.

[24] L. Wolfenstein, "*Different Varieties of Massive Dirac Neutrinos*," Nucl. Phys. **B186** (1981) 147.

[25] S. Petcov, "*On Pseudodirac Neutrinos, Neutrino Oscillations and Neutrinoless Double beta Decay*," Phys. Lett. **B110** (1982) 245–249.

[26] A. de Gouvea, W.-C. Huang, and J. Jenkins, "*Pseudo-Dirac Neutrinos in the New Standard Model*," Phys. Rev. **D80** (2009) 073007, arXiv:0906.1611.

[27] R. Allahverdi, B. Dutta, and R. N. Mohapatra, "*Schizophrenic Neutrinos and ν-less Double Beta Decay*," Phys. Lett. **B695** (2011) 181–184, arXiv:1008.1232.

[28] J. Barry and W. Rodejohann, "*Deviations from tribimaximal mixing due to the vacuum expectation value misalignment in A_4 models*," Phys. Rev. **D81** (2010) 093002, arXiv:1003.2385.

[29] J. Barry, W. Rodejohann, and H. Zhang, "*Sterile Neutrinos for Warm Dark Matter and the Reactor Anomaly in Flavor Symmetry Models*," JCAP **1201** (2012) 052, arXiv:1110.6382.

[30] I. M. Varzielas, C. Hambrock, G. Hiller, M. Jung, P. Leser, *et al.*, "*Proceedings of the 2nd Workshop on Flavor Symmetries and Consequences in Accelerators and Cosmology (FLASY12)*," arXiv:1210.6239.

[31] J. Barry, R. N. Mohapatra, and W. Rodejohann, "*Testing the Bimodal/Schizophrenic Neutrino Hypothesis in Neutrino-less Double Beta Decay and Neutrino Telescopes*," Phys. Rev. **D83** (2011) 113012, arXiv:1012.1761.

[32] J. Barry, L. Dorame, and W. Rodejohann, "*Linear Collider Test of a Neutrinoless Double Beta Decay Mechanism in left-right Symmetric Theories*," Eur. Phys. J. **C72** (2012) 2023, arXiv:1203.3365.

[33] **Particle Data Group**, J. Beringer *et al.*, "*Review of Particle Physics (RPP)*," Phys. Rev. **D86** (2012) 010001.

[34] O. Eberhardt, G. Herbert, H. Lacker, A. Lenz, A. Menzel, *et al.*, "*Impact of a Higgs boson at a mass of 126 GeV on the standard model with three and four fermion generations*," Phys. Rev. Lett. **109** (2012) 241802, arXiv:1209.1101.

[35] S. Weinberg, "*Baryon and Lepton Nonconserving Processes*," Phys. Rev. Lett. **43** (1979) 1566–1570.

[36] B. Pontecorvo, "*Inverse beta processes and nonconservation of lepton charge*," Sov. Phys. JETP **7** (1958) 172–173.

[37] Z. Maki, M. Nakagawa, and S. Sakata, "*Remarks on the unified model of elementary particles*," Prog. Theor. Phys. **28** (1962) 870.

[38] B. Pontecorvo, "*Neutrino Experiments and the Problem of Conservation of Leptonic Charge*," Sov. Phys. JETP **26** (1968) 984–988.

[39] A. Abada, C. Biggio, F. Bonnet, M. B. Gavela, and T. Hambye, "*Low energy effects of neutrino masses*," JHEP **12** (2007) 061, arXiv:0707.4058.

[40] G. (ed.) 't Hooft, C. (ed.) Itzykson, A. (ed.) Jaffe, H. (ed.) Lehmann, P. (ed.) Mitter, *et al.*, "*Recent Developments in Gauge Theories. Proceedings, Nato Advanced Study Institute, Cargese, France, August 26 - September 8, 1979*," NATO Adv.Study Inst.Ser.B Phys. **59** (1980) 1–438.

[41] **ALEPH Collaboration, DELPHI Collaboration, L3 Collaboration, OPAL Collaboration, SLD Collaboration, LEP Electroweak Working Group, SLD Electroweak Group, SLD Heavy Flavour Group**, S. Schael *et al.*, "*Precision electroweak measurements on the Z resonance*," Phys. Rept. **427** (2006) 257–454, arXiv:hep-ex/0509008.

[42] J. Schechter and J. W. F. Valle, "*Neutrino Decay and Spontaneous Violation of Lepton Number*," Phys. Rev. **D25** (1982) 774.

[43] W. Grimus and L. Lavoura, "*The Seesaw mechanism at arbitrary order: Disentangling the small scale from the large scale*," JHEP **0011** (2000) 042, arXiv:hep-ph/0008179.

[44] H. Hettmansperger, M. Lindner, and W. Rodejohann, "*Phenomenological Consequences of sub-leading Terms in See-Saw Formulas*," JHEP **1104** (2011) 123, arXiv:1102.3432.

[45] R. Mohapatra, *Unification and Supersymmetry. The Frontiers of Quark-Lepton Physics*. Springer, 1986.

[46] P. Langacker, "*A Mechanism for ordinary sterile neutrino mixing*," Phys. Rev. **D58** (1998) 093017, arXiv:hep-ph/9805281.

[47] N. Arkani-Hamed, S. Dimopoulos, G. Dvali, and J. March-Russell, "*Neutrino masses from large extra dimensions*," Phys. Rev. **D65** (2002) 024032, arXiv:hep-ph/9811448.

[48] M. Doi, M. Kenmoku, T. Kotani, H. Nishiura, and E. Takasugi, "*Pseudodirac neutrino*," Prog. Theor. Phys. **70** (1983) 1331.

[49] J. Valle, "*Neutrinoless double beta decay with quasi Dirac neutrinos*," Phys. Rev. **D27** (1983) 1672–1674.

[50] J. Casas and A. Ibarra, "*Oscillating neutrinos and $\mu \to e, \gamma$*," Nucl. Phys. **B618** (2001) 171–204, arXiv:hep-ph/0103065.

[51] A. de Gouvea, J. Jenkins, and N. Vasudevan, "*Neutrino Phenomenology of Very Low-Energy Seesaws*," Phys. Rev. **D75** (2007) 013003, arXiv:hep-ph/0608147.

[52] J. Fan and P. Langacker, "*Light Sterile Neutrinos and Short Baseline Neutrino Oscillation Anomalies*," JHEP **1204** (2012) 083, arXiv:1201.6662.

[53] A. Kusenko, F. Takahashi, and T. T. Yanagida, "*Dark Matter from Split Seesaw*," Phys. Lett. **B693** (2010) 144–148, arXiv:1006.1731.

[54] A. Adulpravitchai and R. Takahashi, "*A4 Flavor Models in Split Seesaw Mechanism*," JHEP **1109** (2011) 127, arXiv:1107.3829.

[55] S. Petcov and W. Rodejohann, "*Flavor symmetry L(e) - L(mu) - L(tau), atmospheric neutrino mixing and CP violation in the lepton sector*," Phys. Rev. **D71** (2005) 073002, arXiv:hep-ph/0409135.

[56] M. Shaposhnikov, "*A Possible symmetry of the nuMSM*," Nucl. Phys. **B763** (2007) 49–59, arXiv:hep-ph/0605047.

[57] M. Lindner, A. Merle, and V. Niro, "*Soft $L_e - L_\mu - L_\tau$ flavour symmetry breaking and sterile neutrino keV Dark Matter*," JCAP **1101** (2011) 034, arXiv:1011.4950.

[58] T. Araki and Y. Li, "*Q_6 flavor symmetry model for the extension of the minimal standard model by three right-handed sterile neutrinos*," Phys. Rev. **D85** (2012) 065016, arXiv:1112.5819.

[59] C. Froggatt and H. B. Nielsen, "*Hierarchy of Quark Masses, Cabibbo Angles and CP Violation*," Nucl. Phys. **B147** (1979) 277.

[60] A. Merle and V. Niro, "*Deriving Models for keV sterile Neutrino Dark Matter with the Froggatt-Nielsen mechanism*," JCAP **1107** (2011) 023, arXiv:1105.5136.

[61] H. Zhang, "*Light Sterile Neutrino in the Minimal Extended Seesaw*," Phys. Lett. **B714** (2012) 262–266, arXiv:1110.6838.

[62] E. Chun, A. S. Joshipura, and A. Smirnov, "*Models of light singlet fermion and neutrino phenomenology*," Phys. Lett. **B357** (1995) 608–615, arXiv:hep-ph/9505275.

[63] R. Mohapatra, "*Mechanism for understanding small neutrino mass in superstring theories*," Phys. Rev. Lett. **56** (1986) 561–563.

[64] R. Mohapatra and J. Valle, "*Neutrino Mass and Baryon Number Nonconservation in Superstring Models*," Phys. Rev. **D34** (1986) 1642.

[65] E. K. Akhmedov, M. Lindner, E. Schnapka, and J. Valle, "*Dynamical left-right symmetry breaking*," Phys. Rev. **D53** (1996) 2752–2780, arXiv:hep-ph/9509255.

[66] S. Barr, "*A Different seesaw formula for neutrino masses*," Phys. Rev. Lett. **92** (2004) 101601, arXiv:hep-ph/0309152.

[67] R. Foot, H. Lew, X. G. He, and G. C. Joshi, "*Seesaw neutrino masses induced by a triplet of leptons*," Z. Phys. **C44** (1989) 441.

[68] A. Zee, "*Charged Scalar Field and Quantum Number Violations*," Phys. Lett. **B161** (1985) 141.

[69] A. Zee, "*Quantum numbers of Majorana neutrino masses*," Nucl. Phys. **B264** (1986) 99.

[70] K. S. Babu, "*Model of 'Calculable' Majorana Neutrino Masses*," Phys. Lett. **B203** (1988) 132.

[71] K. S. Babu and C. Macesanu, "*Two-loop neutrino mass generation and its experimental consequences*," Phys. Rev. **D67** (2003) 073010, arXiv:hep-ph/0212058.

[72] D. Aristizabal Sierra and M. Hirsch, "*Experimental tests for the Babu-Zee two-loop model of Majorana neutrino masses*," JHEP **0612** (2006) 052, arXiv:hep-ph/0609307.

[73] F. Bonnet, M. Hirsch, T. Ota, and W. Winter, "*Systematic study of the d=5 Weinberg operator at one-loop order*," JHEP **1207** (2012) 153, arXiv:1204.5862.

[74] F. Bonnet, D. Hernandez, T. Ota, and W. Winter, "*Neutrino masses from higher than d=5 effective operators*," JHEP **0910** (2009) 076, arXiv:0907.3143.

[75] S. Kanemura and T. Ota, "*Neutrino Masses from Loop-induced $d \geq 7$ Operators*," Phys. Lett. **B694** (2010) 233–237, arXiv:1009.3845.

[76] E. Ma, "*Verifiable radiative seesaw mechanism of neutrino mass and dark matter*," Phys. Rev. **D73** (2006) 077301, arXiv:hep-ph/0601225.

[77] E. Ma, "*Utility of a Special Second Scalar Doublet*," Mod. Phys. Lett. **A23** (2008) 647–652, arXiv:0802.2917.

[78] E. Ma, A. Natale, and A. Rashed, "*Scotogenic A_4 Neutrino Model for Nonzero θ_{13} and Large δ_{CP}*," Int. J. Mod. Phys. **A27** (2012) 1250134, arXiv:1206.1570.

[79] A. Ibarra and C. Simonetto, "*Understanding neutrino properties from decoupling right-handed neutrinos and extra Higgs doublets*," JHEP **1111** (2011) 022, arXiv:1107.2386.

[80] D. Hehn and A. Ibarra, "*A radiative model with a naturally mild neutrino mass hierarchy*," Phys. Lett. **B718** (2013) 988–991, arXiv:1208.3162.

[81] M. Goldhaber, L. Grodzins, and A. Sunyar, "*Helicity of neutrinos*," Phys. Rev. **109** (1958) 1015–1017.

[82] R. Mohapatra and J. C. Pati, "*A Natural Left-Right Symmetry*," Phys. Rev. **D11** (1975) 2558.

[83] J. C. Pati and A. Salam, "*Lepton Number as the Fourth Color*," Phys. Rev. **D10** (1974) 275–289.

[84] G. Senjanovic and R. N. Mohapatra, "*Exact Left-Right Symmetry and Spontaneous Violation of Parity*," Phys. Rev. **D12** (1975) 1502.

[85] G. Senjanovic, "*Spontaneous Breakdown of Parity in a Class of Gauge Theories*," Nucl. Phys. **B153** (1979) 334.

[86] Riazuddin, R. Marshak, and R. N. Mohapatra, "*Majorana neutrinos and low-energy tests of electroweak models*," Phys. Rev. **D24** (1981) 1310–1317.

[87] W.-Y. Keung and G. Senjanović, "*Majorana neutrinos and the production of the right-handed charged gauge boson*," Phys. Rev. Lett. **50** (1983) 1427.

[88] R. N. Mohapatra, G. Senjanovic, and M. D. Tran, "*Strangeness changing processes and the limit on the right-handed gauge boson mass*," Phys. Rev. **D28** (1983) 546.

[89] Y. Zhang, H. An, X. Ji, and R. N. Mohapatra, "*General CP Violation in Minimal Left-Right Symmetric Model and Constraints on the Right-Handed Scale*," Nucl. Phys. **B802** (2008) 247–279, arXiv:0712.4218.

[90] D. Guadagnoli and R. N. Mohapatra, "*TeV Scale Left Right Symmetry and Flavor Changing Neutral Higgs Effects*," Phys. Lett. **B694** (2011) 386–392, arXiv:1008.1074.

[91] N. Deshpande, J. Gunion, B. Kayser, and F. I. Olness, "*Left-right symmetric electroweak models with triplet Higgs*," Phys. Rev. **D44** (1991) 837–858.

[92] R. R. Volkas, "*Introduction to sterile neutrinos*," Prog. Part. Nucl. Phys. **48** (2002) 161–174, arXiv:hep-ph/0111326.

[93] E. K. Akhmedov and M. Frigerio, "*Interplay of type I and type II seesaw contributions to neutrino mass*," JHEP **0701** (2007) 043, arXiv:hep-ph/0609046.

[94] M. Nemevsek, G. Senjanovic, and V. Tello, "*Left-Right Symmetry: from Majorana to Dirac*," arXiv:1211.2837.

[95] P. Duka, J. Gluza, and M. Zralek, "*Quantization and renormalization of the manifest left-right symmetric model of electroweak interactions*," Annals Phys. **280** (2000) 336–408, arXiv:hep-ph/9910279.

[96] P. Langacker and S. U. Sankar, "*Bounds on the Mass of W(R) and the W(L)-W(R) Mixing Angle xi in General SU(2)-L x SU(2)-R x U(1) Models*," Phys. Rev. **D40** (1989) 1569–1585.

[97] R. Barbieri and R. N. Mohapatra, "*Limits on right-handed interactions from SN1987A observations*," Phys. Rev. **D39** (1989) 1229.

[98] F. del Aguila, J. de Blas, and M. Perez-Victoria, "*Electroweak Limits on General New Vector Bosons*," JHEP **1009** (2010) 033, arXiv:1005.3998.

[99] J. Barry, W. Rodejohann, and H. Zhang, "*Light Sterile Neutrinos: Models and Phenomenology*," JHEP **1107** (2011) 091, arXiv:1105.3911.

[100] **Super-Kamiokande**, Y. Fukuda *et al.*, "*Evidence for oscillation of atmospheric neutrinos*," Phys. Rev. Lett. **81** (1998) 1562–1567, arXiv:hep-ex/9807003.

[101] **K2K**, M. H. Ahn *et al.*, "*Measurement of Neutrino Oscillation by the K2K Experiment*," Phys. Rev. D **74** (2006) 072003, arXiv:hep-ex/0606032.

[102] **T2K Collaboration**, K. Abe *et al.*, "*Indication of Electron Neutrino Appearance from an Accelerator-produced Off-axis Muon Neutrino Beam*," Phys. Rev. Lett. **107** (2011) 041801, arXiv:1106.2822.

[103] **T2K Collaboration**, K. Abe *et al.*, "*First Muon-Neutrino Disappearance Study with an Off-Axis Beam*," Phys. Rev. **D85** (2012) 031103, arXiv:1201.1386.

[104] **MINOS Collaboration**, P. Adamson *et al.*, "*Electron neutrino and antineutrino appearance in the full MINOS data sample*," Phys. Rev. Lett. (2013) , arXiv:1301.4581.

[105] **DAYA-BAY Collaboration**, F. An *et al.*, "*Observation of electron-antineutrino disappearance at Daya Bay*," Phys. Rev. Lett. **108** (2012) 171803, arXiv:1203.1669.

[106] **RENO collaboration**, J. Ahn *et al.*, "*Observation of Reactor Electron Antineutrino Disappearance in the RENO Experiment*," Phys. Rev. Lett. **108** (2012) 191802, arXiv:1204.0626.

[107] **DOUBLE-CHOOZ Collaboration**, Y. Abe *et al.*, "*Indication for the disappearance of reactor electron antineutrinos in the Double Chooz experiment*," Phys. Rev. Lett. **108** (2012) 131801, arXiv:1112.6353.

[108] **MINOS Collaboration**, P. Adamson *et al.*, "*Improved search for muon-neutrino to electron-neutrino oscillations in MINOS*," Phys. Rev. Lett. **107** (2011) 181802, arXiv:1108.0015.

[109] **SNO Collaboration**, B. Aharmim *et al.*, "*An Independent Measurement of the Total Active B-8 Solar Neutrino Flux Using an Array of He-3 Proportional Counters at the Sudbury Neutrino Observatory*," Phys. Rev. Lett. **101** (2008) 111301, arXiv:0806.0989.

[110] **Borexino**, C. Arpesella *et al.*, "*Direct Measurement of the Be-7 Solar Neutrino Flux with 192 Days of Borexino Data*," Phys. Rev. Lett. **101** (2008) 091302, arXiv:0805.3843.

[111] F. Calaprice, C. Galbiati, A. Wright, and A. Ianni, "*Results from the Borexino Solar Neutrino Experiment*," Ann. Rev. Nucl. Part. Sci. **62** (2012) 315–336.

[112] **KamLAND Collaboration**, S. Abe *et al.*, "*Precision Measurement of Neutrino Oscillation Parameters with KamLAND*," Phys. Rev. Lett. **100** (2008) 221803, arXiv:0801.4589.

[113] L. Wolfenstein, "*Neutrino oscillations in matter*," Phys. Rev. **D17** (1978) 2369.

[114] S. P. Mikheev and A. Y. Smirnov, "*Resonance enhancement of oscillations in matter and solar neutrino spectroscopy*," Sov. J. Nucl. Phys. **42** (1985) 913–917.

[115] A. de Gouvea, "*Neutrino physics*," in *TASI lectures on neutrino physics, Boulder, Colorado, 6 June - 2 July*. 2004. arXiv:hep-ph/0411274.

[116] A. Ghosh, T. Thakore, and S. Choubey, "*Determining the Neutrino Mass Hierarchy with INO, T2K, NOvA and Reactor Experiments*," arXiv:1212.1305.

[117] E. K. Akhmedov, S. Razzaque, and A. Y. Smirnov, "*Mass hierarchy, 2-3 mixing and CP-phase with Huge Atmospheric Neutrino Detectors*," JHEP **02** (2013) 082, arXiv:1205.7071.

[118] **NOvA Collaboration**, R. Patterson, "*The NOvA Experiment: Status and Outlook*," arXiv:1209.0716.

[119] **LBNE Collaboration**, T. Akiri *et al.*, "*The 2010 Interim Report of the Long-Baseline Neutrino Experiment Collaboration Physics Working Groups*," arXiv:1110.6249.

[120] J. Tang and W. Winter, "*Requirements for a New Detector at the South Pole Receiving an Accelerator Neutrino Beam*," JHEP **1202** (2012) 028, arXiv:1110.5908.

[121] A. S. Dighe and A. Y. Smirnov, "*Identifying the neutrino mass spectrum from the neutrino burst from a supernova*," Phys. Rev. **D62** (2000) 033007, arXiv:hep-ph/9907423.

[122] E. Borriello, S. Chakraborty, A. Mirizzi, P. D. Serpico, and I. Tamborra, "*(Down-to-)Earth matter effect in supernova neutrinos*," Phys. Rev. **D86** (2012) 083004, arXiv:1207.5049.

[123] P. Ghoshal and S. Petcov, "*Neutrino Mass Hierarchy Determination Using Reactor Antineutrinos*," JHEP **1103** (2011) 058, arXiv:1011.1646.

[124] P. Ghoshal and S. Petcov, "*Addendum: Neutrino Mass Hierarchy Determination Using Reactor Antineutrinos*," JHEP **1209** (2012) 115, arXiv:1208.6473.

[125] G. Fogli, E. Lisi, A. Marrone, D. Montanino, A. Palazzo, *et al.*, "*Global analysis of neutrino masses, mixings and phases: entering the era of leptonic CP violation searches*," Phys. Rev. **D86** (2012) 013012, arXiv:1205.5254.

[126] M. Gonzalez-Garcia, M. Maltoni, J. Salvado, and T. Schwetz, "*Global fit to three neutrino mixing: critical look at present precision*," JHEP **1212** (2012) 123, arXiv:1209.3023.

[127] H. Nunokawa, S. J. Parke, and J. W. Valle, "*CP Violation and Neutrino Oscillations*," Prog. Part. Nucl. Phys. **60** (2008) 338–402, arXiv:0710.0554.

[128] F. Dufour, T. Kajita, E. Kearns, and K. Okumura, "*Further study of neutrino oscillation with two detectors in Kamioka and Korea*," Phys. Rev. **D81** (2010) 093001, arXiv:1001.5165.

[129] V. Barger, M. Bishai, D. Bogert, C. Bromberg, A. Curioni, *et al.*, "*Report of the US long baseline neutrino experiment study*," arXiv:0705.4396.

[130] J. Conrad and M. Shaevitz, "*Multiple Cyclotron Method to Search for CP Violation in the Neutrino Sector*," Phys. Rev. Lett. **104** (2010) 141802, arXiv:0912.4079.

[131] S. K. Agarwalla, P. Huber, J. M. Link, and D. Mohapatra, "*A new approach to anti-neutrino running in long baseline neutrino oscillation experiments*," JHEP **1104** (2011) 099, arXiv:1005.4055.

[132] P. Huber, M. Lindner, and W. Winter, "*Superbeams versus neutrino factories*," Nucl. Phys. **B645** (2002) 3–48, arXiv:hep-ph/0204352.

[133] S. K. Agarwalla, P. Huber, J. Tang, and W. Winter, "*Optimization of the Neutrino Factory, revisited*," JHEP **1101** (2011) 120, arXiv:1012.1872.

[134] C. Giunti and M. Laveder, "*3+1 and 3+2 Sterile Neutrino Fits*," Phys. Rev. **D84** (2011) 073008, arXiv:1107.1452.

[135] S. Goswami and W. Rodejohann, "*MiniBooNE results and neutrino schemes with 2 sterile neutrinos: Possible mass orderings and observables related to neutrino masses*," JHEP **0710** (2007) 073, arXiv:0706.1462.

[136] G. Karagiorgi, Z. Djurcic, J. Conrad, M. Shaevitz, and M. Sorel, "*Viability of $\Delta m^2 \sim 1\ eV^2$ sterile neutrino mixing models in light of MiniBooNE electron neutrino and antineutrino data from the Booster and NuMI beamlines*," Phys. Rev. **D80** (2009) 073001, arXiv:0906.1997.

[137] **KARMEN Collaboration**, B. Armbruster *et al.*, "*Upper limits for neutrino oscillations $\bar{\nu}_\mu \to \bar{\nu}_e$ from muon decay at rest*," Phys. Rev. **D65** (2002) 112001, arXiv:hep-ex/0203021.

[138] **MiniBooNE Collaboration**, A. Aguilar-Arevalo *et al.*, "*A Search for electron neutrino appearance at the $\Delta m^2 \sim 1eV^2$ scale*," Phys. Rev. Lett. **98** (2007) 231801, arXiv:0704.1500.

[139] **MiniBooNE Collaboration**, A. Aguilar-Arevalo *et al.*, "*Unexplained Excess of Electron-Like Events From a 1-GeV Neutrino Beam*," Phys. Rev. Lett. **102** (2009) 101802, arXiv:0812.2243.

[140] M. Martini, M. Ericson, G. Chanfray, and J. Marteau, "*Neutrino and antineutrino quasielastic interactions with nuclei*," Phys. Rev. **C81** (2010) 045502, arXiv:1002.4538.

[141] J. Nieves, F. Sanchez, I. Ruiz Simo, and M. Vicente Vacas, "*Neutrino Energy Reconstruction and the Shape of the CCQE-like Total Cross Section*," Phys. Rev. **D85** (2012) 113008, arXiv:1204.5404.

[142] F. Kaether, W. Hampel, G. Heusser, J. Kiko, and T. Kirsten, "*Reanalysis of the GALLEX solar neutrino flux and source experiments*," Phys. Lett. **B685** (2010) 47–54, arXiv:1001.2731.

[143] C. Giunti and M. Laveder, "*Statistical Significance of the Gallium Anomaly*," Phys. Rev. **C83** (2011) 065504, arXiv:1006.3244.

[144] P. Huber, "*On the determination of anti-neutrino spectra from nuclear reactors*," Phys. Rev. **C84** (2011) 024617, arXiv:1106.0687.

[145] T. Lasserre, "*Testing the Reactor and Gallium Anomalies with Intense (Anti)Neutrino Emitters*," arXiv:1209.5090.

[146] **Nucifer Collaboration**, A. S. Cucoanes, "*Status of the Nucifer experiment*," J. Phys. Conf. Ser. **375** (2012) 042063.

[147] **MINOS Collaboration**, P. Adamson *et al.*, "*Active to sterile neutrino mixing limits from neutral-current interactions in MINOS*," Phys. Rev. Lett. **107** (2011) 011802, arXiv:1104.3922.

[148] **MiniBooNE Collaboration, SciBooNE Collaboration**, G. Cheng *et al.*, "*Dual baseline search for muon antineutrino disappearance at* $0.1\text{eV}^2 < \Delta m^2 < 100\text{eV}^2$," Phys. Rev. **D86** (2012) 052009, arXiv:1208.0322.

[149] S. Razzaque and A. Y. Smirnov, "*Searches for sterile neutrinos with IceCube DeepCore*," Phys. Rev. **D85** (2012) 093010, arXiv:1203.5406.

[150] C. Giunti, M. Laveder, Y. Li, Q. Liu, and H. Long, "*Update of Short-Baseline Electron Neutrino and Antineutrino Disappearance*," Phys. Rev. **D86** (2012) 113014, arXiv:1210.5715.

[151] C. Giunti and M. Laveder, "*Status of 3+1 Neutrino Mixing*," Phys. Rev. **D84** (2011) 093006, arXiv:1109.4033.

[152] M. Archidiacono, N. Fornengo, C. Giunti, S. Hannestad, and A. Melchiorri, "*Sterile Neutrinos: Cosmology vs Short-BaseLine Experiments*," arXiv:1302.6720.

[153] J. Kopp, M. Maltoni, and T. Schwetz, "*Are there sterile neutrinos at the eV scale?*," Phys. Rev. Lett. **107** (2011) 091801, arXiv:1103.4570.

[154] J. Kopp, P. A. N. Machado, M. Maltoni, and T. Schwetz, "*Sterile Neutrino Oscillations: The Global Picture*," arXiv:1303.3011.

[155] C. Kraus *et al.*, "*Final Results from phase II of the Mainz Neutrino Mass Search in Tritium β Decay*," Eur. Phys. J. **C40** (2005) 447–468, arXiv:hep-ex/0412056.

[156] V. M. Lobashev *et al.*, "*Direct search for mass of neutrino and anomaly in the tritium beta-spectrum*," Phys. Lett. **B460** (1999) 227–235.

[157] C. Giunti and M. Laveder, "*Short-Baseline Electron Neutrino Disappearance, Tritium Beta Decay and Neutrinoless Double-Beta Decay*," Phys. Rev. **D82** (2010) 053005, arXiv:1005.4599.

[158] **KATRIN Collaboration**, A. Osipowicz *et al.*, "*KATRIN: A Next generation tritium beta decay experiment with sub-eV sensitivity for the electron neutrino mass. Letter of intent*," arXiv:hep-ex/0109033.

[159] A. S. Riis and S. Hannestad, "*Detecting sterile neutrinos with KATRIN like experiments*," JCAP **1102** (2011) 011, arXiv:1008.1495.

[160] J. Formaggio and J. Barrett, "*Resolving the Reactor Neutrino Anomaly with the KATRIN Neutrino Experiment*," Phys. Lett. **B706** (2011) 68–71, arXiv:1105.1326.

[161] C. Giunti and C. Kim, *Fundamentals of Neutrino Physics and Astrophysics*. Oxford University Press, 2007.

[162] J. Bonn, K. Eitel, F. Gluck, D. Sevilla-Sanchez, and N. Titov, "*The KATRIN sensitivity to the neutrino mass and to right-handed currents in beta decay*," Phys. Lett. **B703** (2011) 310–312, arXiv:0704.3930.

[163] J. Schechter and J. Valle, "*Neutrinoless Double beta Decay in SU(2) x U(1) Theories*," Phys. Rev. **D25** (1982) 2951.

[164] W. Rodejohann, "*Neutrino-less Double Beta Decay and Particle Physics*," Int. J. Mod. Phys. **E20** (2011) 1833–1930, arXiv:1106.1334.

[165] J. Vergados, H. Ejiri, and F. Simkovic, "*Theory of Neutrinoless Double Beta Decay*," Rept. Prog. Phys. **75** (2012) 106301, arXiv:1205.0649.

[166] **KamLAND-Zen Collaboration**, A. Gando *et al.*, "*Limit on Neutrinoless $\beta\beta$ Decay of Xe-136 from the First Phase of KamLAND-Zen and Comparison with the Positive Claim in Ge-76*," Phys. Rev. Lett. **110** (2013) 062502, arXiv:1211.3863.

[167] J. Vergados, "*The Neutrinoless double beta decay from a modern perspective*," Phys. Rept. **361** (2002) 1–56, arXiv:hep-ph/0209347.

[168] S. Goswami and W. Rodejohann, "*Constraining mass spectra with sterile neutrinos from neutrinoless double beta decay, tritium beta decay and cosmology*," Phys. Rev. **D73** (2006) 113003, arXiv:hep-ph/0512234.

[169] M. Cirelli, G. Marandella, A. Strumia, and F. Vissani, "*Probing oscillations into sterile neutrinos with cosmology, astrophysics and experiments*," Nucl. Phys. **B708** (2005) 215–267, arXiv:hep-ph/0403158.

[170] M. Gonzalez-Garcia, M. Maltoni, and J. Salvado, "*Updated global fit to three neutrino mixing: status of the hints of $\theta_{13} > 0$*," JHEP **1004** (2010) 056, arXiv:1001.4524.

[171] M. Blennow, E. Fernandez-Martinez, J. Lopez-Pavon, and J. Menendez, "*Neutrinoless double beta decay in seesaw models*," JHEP **1007** (2010) 096, arXiv:1005.3240.

[172] M.-C. Chen and S. F. King, "*A4 See-Saw Models and Form Dominance*," JHEP **0906** (2009) 072, arXiv:0903.0125.

[173] S. Choubey, S. King, and M. Mitra, "*On the Vanishing of the CP Asymmetry in Leptogenesis due to Form Dominance*," Phys. Rev. **D82** (2010) 033002, arXiv:1004.3756.

[174] **EXO Collaboration**, M. Auger *et al.*, "*Search for Neutrinoless Double-Beta Decay in ^{136}Xe with EXO-200*," Phys. Rev. Lett. **109** (2012) 032505, arXiv:1205.5608.

[175] H. V. Klapdor-Kleingrothaus *et al.*, "*Latest Results from the Heidelberg-Moscow Double Beta Decay Experiment*," Eur. Phys. J. **A12** (2001) 147–154, arXiv:hep-ph/0103062.

[176] H. V. Klapdor-Kleingrothaus, I. V. Krivosheina, A. Dietz, and O. Chkvorets, "*Search for neutrinoless double beta decay with enriched 76Ge in Gran Sasso 1990-2003*," Phys. Lett. B **586** (2004) 198–212, arXiv:hep-ph/0404088.

[177] C. E. Aalseth *et al.*, "*Comment on 'Evidence for Neutrinoless Double Beta Decay'*," Mod. Phys. Lett. **A17** (2002) 1475–1478, arXiv:hep-ex/0202018.

[178] S. R. Elliott and J. Engel, "*Double beta decay*," J. Phys. **G30** (2004) R183, arXiv:hep-ph/0405078.

[179] **GERDA Collaboration**, K.-H. Ackermann *et al.*, "*The GERDA experiment for the search of $0\nu\beta\beta$ decay in ^{76}Ge*," arXiv:1212.4067.

[180] **SuperNEMO Collaboration**, R. Arnold *et al.*, "*Probing New Physics Models of Neutrinoless Double Beta Decay with SuperNEMO*," Eur. Phys. J. **C70** (2010) 927–943, arXiv:1005.1241.

[181] A. Dueck, W. Rodejohann, and K. Zuber, "*Neutrinoless Double Beta Decay, the Inverted Hierarchy and Precision Determination of theta(12)*," Phys. Rev. **D83** (2011) 113010, arXiv:1103.4152.

[182] J. Kotila and F. Iachello, "*Phase space factors for double-β decay*," Phys. Rev. **C85** (2012) 034316, arXiv:1209.5722.

[183] A. Faessler, A. Meroni, S. T. Petcov, F. Simkovic, and J. Vergados, "*Uncovering Multiple CP-Nonconserving Mechanisms of $\beta\beta$-Decay*," Phys. Rev. **D83** (2011) 113003, arXiv:1103.2434.

[184] A. Faessler, G. L. Fogli, E. Lisi, A. M. Rotunno, and F. Simkovic, "*Multi-isotope degeneracy of neutrinoless double beta decay mechanisms in the quasi-particle random phase approximation*," Phys. Rev. **D83** (2011) 113015, arXiv:1103.2504.

[185] W. Haxton, "*Neutrino Astrophysics*," arXiv:1209.3743.

[186] P. de Holanda and A. Y. Smirnov, "*Homestake result, sterile neutrinos and low-energy solar neutrino experiments*," Phys. Rev. **D69** (2004) 113002, arXiv:hep-ph/0307266.

[187] P. de Holanda and A. Y. Smirnov, "*Solar neutrino spectrum, sterile neutrinos and additional radiation in the Universe*," Phys. Rev. **D83** (2011) 113011, arXiv:1012.5627.

[188] A. Palazzo, "*Testing the very-short-baseline neutrino anomalies at the solar sector*," Phys. Rev. **D83** (2011) 113013, arXiv:1105.1705.

[189] J. Fetter, G. McLaughlin, A. Balantekin, and G. Fuller, "*Active sterile neutrino conversion: Consequences for the r process and supernova neutrino detection*," Astropart. Phys. **18** (2003) 433–448, arXiv:hep-ph/0205029.

[190] J. Beun, G. McLaughlin, R. Surman, and W. Hix, "*Fission cycling in supernova nucleosynthesis: Active-sterile neutrino oscillations*," Phys. Rev. **D73** (2006) 093007, arXiv:hep-ph/0602012.

[191] S. Choubey, N. Harries, and G. Ross, "*Turbulent supernova shock waves and the sterile neutrino signature in megaton water detectors*," Phys. Rev. **D76** (2007) 073013, arXiv:hep-ph/0703092.

[192] I. Tamborra, G. G. Raffelt, L. Hudepohl, and H.-T. Janka, "*Impact of eV-mass sterile neutrinos on neutrino-driven supernova outflows*," JCAP **1201** (2012) 013, arXiv:1110.2104.

[193] **IceCube Collaboration**, J. A. Aguilar, "*Neutrino searches with the IceCube telescope*," arXiv:1301.6504.

[194] S. Pakvasa, "*Neutrino Flavor Goniometry by High Energy Astrophysical Beams*," Mod. Phys. Lett. **A23** (2008) 1313–1324, arXiv:0803.1701.

[195] S. Pakvasa, "*Neutrino Flavor Detection at Neutrino Telescopes and Its Uses*," arXiv:1004.5413.

[196] D. Hollander, "*Astrophysical neutrino flavor ratios in the presence of sterile neutrinos*," arXiv:1301.5313.

[197] J. G. Learned and S. Pakvasa, "*Detecting tau-neutrino oscillations at PeV energies*," Astropart. Phys. **3** (1995) 267–274, arXiv:hep-ph/9405296.

[198] L. A. Anchordoqui, H. Goldberg, F. Halzen, and T. J. Weiler, "*Galactic point sources of TeV antineutrinos*," Phys. Lett. **B593** (2004) 42, arXiv:astro-ph/0311002.

[199] L. A. Anchordoqui, H. Goldberg, F. Halzen, and T. J. Weiler, "*Neutrinos as a diagnostic of high energy astrophysical processes*," Phys. Lett. **B621** (2005) 18–21, arXiv:hep-ph/0410003.

[200] J. P. Rachen and P. Meszaros, "*Photohadronic neutrinos from transients in astrophysical sources*," Phys. Rev. **D58** (1998) 123005, arXiv:astro-ph/9802280.

[201] M. Kachelriess, S. Ostapchenko, and R. Tomas, "*High energy neutrino yields from astrophysical sources. 2. Magnetized sources*," Phys. Rev. **D77** (2008) 023007, arXiv:0708.3047.

[202] S. Choubey and W. Rodejohann, "*Flavor Composition of UHE Neutrinos at Source and at Neutrino Telescopes*," Phys. Rev. **D80** (2009) 113006, arXiv:0909.1219.

[203] A. Esmaili, "*Pseudo-Dirac Neutrino Scenario: Cosmic Neutrinos at Neutrino Telescopes*," Phys. Rev. **D81** (2010) 013006, arXiv:0909.5410.

[204] J. F. Beacom, N. F. Bell, D. Hooper, J. G. Learned, S. Pakvasa, *et al.*, "*PseudoDirac neutrinos: A Challenge for neutrino telescopes*," Phys. Rev. Lett. **92** (2004) 011101, arXiv:hep-ph/0307151.

[205] P. Keranen, J. Maalampi, M. Myyrylainen, and J. Riittinen, "*Effects of sterile neutrinos on the ultrahigh-energy cosmic neutrino flux*," Phys. Lett. **B574** (2003) 162–168, arXiv:hep-ph/0307041.

[206] A. Bhattacharya, S. Choubey, R. Gandhi, and A. Watanabe, "*Ultra-high neutrino fluxes as a probe for non-standard physics*," JCAP **1009** (2010) 009, arXiv:1006.3082.

[207] J. Lesgourgues and S. Pastor, "*Massive neutrinos and cosmology*," Phys. Rept. **429** (2006) 307–379, arXiv:astro-ph/0603494.

[208] Y. Y. Wong, "*Neutrino mass in cosmology: status and prospects*," Ann. Rev. Nucl. Part. Sci. **61** (2011) 69–98, arXiv:1111.1436.

[209] A. Kusenko, "*Sterile neutrinos: The Dark side of the light fermions*," Phys. Rept. **481** (2009) 1–28, arXiv:0906.2968.

[210] S. Davidson, E. Nardi, and Y. Nir, "*Leptogenesis*," Phys. Rept. **466** (2008) 105–177, arXiv:0802.2962.

[211] G. Mangano, G. Miele, S. Pastor, T. Pinto, O. Pisanti, *et al.*, "*Relic neutrino decoupling including flavor oscillations*," Nucl. Phys. **B729** (2005) 221–234, arXiv:hep-ph/0506164.

[212] K. N. Abazajian, "*Telling three from four neutrinos with cosmology*," Astropart. Phys. **19** (2003) 303–312, arXiv:astro-ph/0205238.

[213] D. Kirilova, "*Neutrino spectrum distortion due to oscillations and its BBN effect*," Int. J. Mod. Phys. **D13** (2004) 831–842, arXiv:hep-ph/0209104.

[214] S. Gershtein and Y. Z. and, "*Rest Mass of Muonic Neutrino and Cosmology*," JETP Lett. **4** (1966) 120–122.

[215] R. Cowsik and J. McClelland, "*An Upper Limit on the Neutrino Rest Mass*," Phys. Rev. Lett. **29** (1972) 669–670.

[216] G. Hinshaw, D. Larson, E. Komatsu, D. Spergel, C. Bennett, *et al.*, "*Nine-Year Wilkinson Microwave Anisotropy Probe (WMAP) Observations: Cosmological Parameter Results*," arXiv:1212.5226.

[217] E. Di Valentino, S. Galli, M. Lattanzi, A. Melchiorri, P. Natoli, *et al.*, "*Tickling the CMB damping tail: scrutinizing the tension between the ACT and SPT experiments*," arXiv:1301.7343.

[218] R. H. Cyburt, B. D. Fields, K. A. Olive, and E. Skillman, "*New BBN limits on physics beyond the standard model from He-4*," Astropart. Phys. **23** (2005) 313–323, arXiv:astro-ph/0408033.

[219] Y. Izotov and T. Thuan, "*The primordial abundance of 4He: evidence for non-standard big bang nucleosynthesis*," Astrophys. J. **710** (2010) L67–L71, arXiv:1001.4440.

[220] E. Aver, K. A. Olive, and E. D. Skillman, "*A New Approach to Systematic Uncertainties and Self-Consistency in Helium Abundance Determinations*," JCAP **1005** (2010) 003, arXiv:1001.5218.

[221] G. Steigman, "*Neutrinos And Big Bang Nucleosynthesis*," Adv. High Energy Phys. **2012** (2012) 268321, arXiv:1208.0032.

[222] J. Hamann, S. Hannestad, G. G. Raffelt, I. Tamborra, and Y. Y. Wong, "*Cosmology seeking friendship with sterile neutrinos*," Phys. Rev. Lett. **105** (2010) 181301, arXiv:1006.5276.

[223] E. Giusarma, M. Corsi, M. Archidiacono, R. de Putter, A. Melchiorri, *et al.*, "*Constraints on massive sterile neutrino species from current and future cosmological data*," Phys. Rev. **D83** (2011) 115023, arXiv:1102.4774.

[224] N. Saviano, A. Mirizzi, O. Pisanti, P. D. Serpico, G. Mangano, *et al.*, "*Multi-momentum and multi-flavour active-sterile neutrino oscillations in the early universe: role of neutrino asymmetries and effects on nucleosynthesis*," arXiv:1302.1200.

[225] D. Hooper, F. S. Queiroz, and N. Y. Gnedin, "*Non-Thermal Dark Matter Mimicking An Additional Neutrino Species In The Early Universe*," Phys. Rev. **D85** (2012) 063513, arXiv:1111.6599.

[226] W. Hu, D. J. Eisenstein, and M. Tegmark, "*Weighing neutrinos with galaxy surveys*," Phys. Rev. Lett. **80** (1998) 5255–5258, arXiv:astro-ph/9712057.

[227] B. A. Reid, W. J. Percival, D. J. Eisenstein, L. Verde, D. N. Spergel, *et al.*, "*Cosmological Constraints from the Clustering of the Sloan Digital Sky Survey DR7 Luminous Red Galaxies*," Mon. Not. Roy. Astron. Soc. **404** (2010) 60–85, arXiv:0907.1659.

[228] F. De Bernardis, T. D. Kitching, A. Heavens, and A. Melchiorri, "*Determining the Neutrino Mass Hierarchy with Cosmology*," Phys. Rev. **D80** (2009) 123509, arXiv:0907.1917.

[229] Y. Oyama, A. Shimizu, and K. Kohri, "*Determination of neutrino mass hierarchy by 21 cm line and CMB B-mode polarization observations*," Phys. Lett. **B718** (2013) 1186–1193, arXiv:1205.5223.

[230] J. Hamann, S. Hannestad, and Y. Y. Wong, "*Measuring neutrino masses with a future galaxy survey*," JCAP **1211** (2012) 052, arXiv:1209.1043.

[231] F. De Bernardis, P. Serra, A. Cooray, and A. Melchiorri, "*An improved limit on the neutrino mass with CMB and redshift-dependent halo bias-mass relations from SDSS, DEEP2, and Lyman-Break Galaxies*," Phys. Rev. **D78** (2008) 083535, arXiv:0809.1095.

[232] J. Hamann, S. Hannestad, G. G. Raffelt, and Y. Y. Wong, "*Sterile neutrinos with eV masses in cosmology: How disfavoured exactly?*," JCAP **1109** (2011) 034, arXiv:1108.4136.

[233] S. Hannestad, I. Tamborra, and T. Tram, "*Thermalisation of light sterile neutrinos in the early universe*," JCAP **1207** (2012) 025, arXiv:1204.5861.

[234] S. Joudaki, K. N. Abazajian, and M. Kaplinghat, "*Are Light Sterile Neutrinos Preferred or Disfavored by Cosmology?*," Phys. Rev. **D87** (2013) 065003, arXiv:1208.4354.

[235] T. D. Jacques, L. M. Krauss, and C. Lunardini, "*Additional Light Sterile Neutrinos and Cosmology*," arXiv:1301.3119.

[236] C. M. Ho and R. J. Scherrer, "*Sterile Neutrinos and Light Dark Matter Save Each Other*," arXiv:1212.1689.

[237] G. Steigman, "*Equivalent Neutrinos, Light WIMPs, and the Chimera of Dark Radiation*," arXiv:1303.0049.

[238] H. Motohashi, A. A. Starobinsky, and J. Yokoyama, "*Cosmology based on f(R) Gravity admits 1 eV Sterile Neutrinos*," arXiv:1203.6828.

[239] M. Davis, G. Efstathiou, C. S. Frenk, and S. D. White, "*The Evolution of Large Scale Structure in a Universe Dominated by Cold Dark Matter*," Astrophys. J. **292** (1985) 371–394.

[240] P. Bode, J. P. Ostriker, and N. Turok, "*Halo formation in warm dark matter models*," Astrophys. J. **556** (2001) 93–107, arXiv:astro-ph/0010389.

[241] A. Dolgov and S. Hansen, "*Massive sterile neutrinos as warm dark matter*," Astropart. Phys. **16** (2002) 339–344, arXiv:hep-ph/0009083.

[242] K. Abazajian, G. M. Fuller, and M. Patel, "*Sterile neutrino hot, warm, and cold dark matter*," Phys. Rev. **D64** (2001) 023501, arXiv:astro-ph/0101524.

[243] A. Kusenko and G. Segre, "*Neutral current induced neutrino oscillations in a supernova*," Phys. Lett. **B396** (1997) 197–200, arXiv:hep-ph/9701311.

[244] G. M. Fuller, A. Kusenko, I. Mocioiu, and S. Pascoli, "*Pulsar kicks from a dark-matter sterile neutrino*," Phys. Rev. **D68** (2003) 103002, arXiv:astro-ph/0307267.

[245] S. Tremaine and J. Gunn, "*Dynamical Role of Light Neutral Leptons in Cosmology*," Phys. Rev. Lett. **42** (1979) 407–410.

[246] A. Boyarsky, A. Neronov, O. Ruchayskiy, M. Shaposhnikov, and I. Tkachev, "*Where to find a dark matter sterile neutrino?*," Phys. Rev. Lett. **97** (2006) 261302, arXiv:astro-ph/0603660.

[247] A. Boyarsky, J. Lesgourgues, O. Ruchayskiy, and M. Viel, "*Lyman-alpha constraints on warm and on warm-plus-cold dark matter models*," JCAP **0905** (2009) 012, arXiv:0812.0010.

[248] X.-D. Shi and G. M. Fuller, "*A New dark matter candidate: Nonthermal sterile neutrinos*," Phys. Rev. Lett. **82** (1999) 2832–2835, arXiv:astro-ph/9810076.

[249] A. Boyarsky, J. Lesgourgues, O. Ruchayskiy, and M. Viel, "*Realistic sterile neutrino dark matter with keV mass does not contradict cosmological bounds*," Phys. Rev. Lett. **102** (2009) 201304, arXiv:0812.3256.

[250] M. Shaposhnikov and I. Tkachev, "*The nuMSM, inflation, and dark matter*," Phys. Lett. **B639** (2006) 414–417, arXiv:hep-ph/0604236.

[251] A. Kusenko, "*Sterile neutrinos, dark matter, and the pulsar velocities in models with a Higgs singlet*," Phys. Rev. Lett. **97** (2006) 241301, arXiv:hep-ph/0609081.

[252] F. Bezrukov, H. Hettmansperger, and M. Lindner, "*keV sterile neutrino Dark Matter in gauge extensions of the Standard Model*," Phys. Rev. **D81** (2010) 085032, arXiv:0912.4415.

[253] M. Nemevsek, G. Senjanovic, and Y. Zhang, "*Warm Dark Matter in Low Scale Left-Right Theory*," JCAP **1207** (2012) 006, arXiv:1205.0844.

[254] T. Asaka, S. Blanchet, and M. Shaposhnikov, "*The nuMSM, dark matter and neutrino masses*," Phys. Lett. **B631** (2005) 151–156, arXiv:hep-ph/0503065.

[255] A. Boyarsky, O. Ruchayskiy, and M. Shaposhnikov, "*The role of sterile neutrinos in cosmology and astrophysics*," Ann. Rev. Nucl. Part. Sci. **59** (2009) 191–214, arXiv:0901.0011.

[256] S. Davidson and A. Ibarra, "*A Lower bound on the right-handed neutrino mass from leptogenesis*," Phys. Lett. **B535** (2002) 25–32, arXiv:hep-ph/0202239.

[257] E. K. Akhmedov, V. Rubakov, and A. Y. Smirnov, "*Baryogenesis via neutrino oscillations*," Phys. Rev. Lett. **81** (1998) 1359–1362, arXiv:hep-ph/9803255.

[258] A. Pilaftsis and T. E. J. Underwood, "*Resonant leptogenesis*," Nucl. Phys. **B692** (2004) 303–345, arXiv:hep-ph/0309342.

[259] L. Canetti, M. Drewes, and M. Shaposhnikov, "*Sterile Neutrinos as the Origin of Dark and Baryonic Matter*," Phys. Rev. Lett. **110** (2013) 061801, arXiv:1204.3902.

[260] L. Canetti, M. Drewes, T. Frossard, and M. Shaposhnikov, "*Dark Matter, Baryogenesis and Neutrino Oscillations from Right Handed Neutrinos*," arXiv:1208.4607.

[261] X.-G. He, T. Li, and W. Liao, "*Symmetry, dark matter and LHC phenomenology of the minimal nu SM*," Phys. Rev. **D81** (2010) 033006, arXiv:0911.1598.

[262] A. Pilaftsis, "*Radiatively induced neutrino masses and large Higgs neutrino couplings in the standard model with Majorana fields*," Z. Phys. **C55** (1992) 275–282, arXiv:hep-ph/9901206.

[263] J. Kersten and A. Y. Smirnov, "*Right-Handed Neutrinos at LHC and the Mechanism of Neutrino Mass Generation*," Phys. Rev. **D76** (2007) 073005.

[264] H. Zhang and S. Zhou, "*The Minimal Seesaw Model at the TeV Scale*," Phys. Lett. **B685** (2010) 297–301, arXiv:0912.2661.

[265] R. Adhikari and A. Raychaudhuri, "*Light neutrinos from massless texture and below TeV seesaw scale*," Phys. Rev. **D84** (2011) 033002, arXiv:1004.5111.

[266] A. de Gouvea, "*GeV seesaw, accidentally small neutrino masses, and Higgs decays to neutrinos*," arXiv:0706.1732.

[267] J.-H. Chen, X.-G. He, J. Tandean, and L.-H. Tsai, "*Effect on Higgs Boson Decays from Large Light-Heavy Neutrino Mixing in Seesaw Models*," Phys. Rev. **D81** (2010) 113004, arXiv:1001.5215.

[268] C. G. Cely, A. Ibarra, E. Molinaro, and S. Petcov, "*Higgs Decays in the Low Scale Type I See-Saw Model*," Phys. Lett. **B718** (2013) 957–964, arXiv:1208.3654.

[269] P. Bhupal Dev, R. Franceschini, and R. Mohapatra, "*Bounds on TeV Seesaw Models from LHC Higgs Data*," Phys. Rev. **D86** (2012) 093010, arXiv:1207.2756.

[270] A. G. Akeroyd and M. Aoki, "*Single and pair production of doubly charged Higgs bosons at hadron colliders*," Phys. Rev. **D72** (2005) 035011, arXiv:hep-ph/0506176.

[271] T. Han, B. Mukhopadhyaya, Z. Si, and K. Wang, "*Pair Production of Doubly-Charged Scalars: Neutrino Mass Constraints and Signals at the LHC*," Phys. Rev. **D76** (2007) 075013, arXiv:0706.0441.

[272] W. Chao, Z.-G. Si, Z. zhong Xing, and S. Zhou, "*Correlative signatures of heavy Majorana neutrinos and doubly-charged Higgs bosons at the Large Hadron Collider*," Phys. Lett. **B666** (2008) 451–454, arXiv:0804.1265.

[273] E. J. Chun, K. Y. Lee, and S. C. Park, "*Testing Higgs triplet model and neutrino mass patterns*," Phys. Lett. **B566** (2003) 142–151, arXiv:hep-ph/0304069.

[274] S. T. Petcov, H. Sugiyama, and Y. Takanishi, "*Neutrinoless Double Beta Decay and $H^{\pm\pm} \to l'^{\pm} l^{\pm}$ Decays in the Higgs Triplet Model*," Phys. Rev. **D80** (2009) 015005, arXiv:0904.0759.

[275] A. Melfo, M. Nemevsek, F. Nesti, G. Senjanovic, and Y. Zhang, "*Type II Seesaw at LHC: The Roadmap*," Phys. Rev. **D85** (2012) 055018, arXiv:1108.4416.

[276] **ATLAS Collaboration**, G. Aad *et al.*, "*Search for doubly-charged Higgs bosons in like-sign dilepton final states at $\sqrt{s} = 7$ TeV with the ATLAS detector*," Eur. Phys. J. **C72** (2012) 2244, arXiv:1210.5070.

[277] F. del Aguila and J. A. Aguilar-Saavedra, "*Distinguishing seesaw models at LHC with multi-lepton signals*," Nucl. Phys. **B813** (2009) 22–90, arXiv:808.2468.

[278] A. Ferrari, J. Collot, M.-L. Andrieux, B. Belhorma, P. de Saintignon, *et al.*, "*Sensitivity study for new gauge bosons and right-handed Majorana neutrinos in pp collisions at s = 14-TeV*," Phys. Rev. **D62** (2000) 013001.

[279] P. Langacker, "*The Physics of Heavy Z' Gauge Bosons*," Rev. Mod. Phys. **81** (2009) 1199–1228, arXiv:0801.1345.

[280] K. Huitu, J. Maalampi, A. Pietila, and M. Raidal, "*Doubly charged Higgs at LHC*," Nucl. Phys. **B487** (1997) 27–42, arXiv:hep-ph/9606311.

[281] C.-Y. Chen and P. B. Dev, "*Multi-Lepton Collider Signatures of Heavy Dirac and Majorana Neutrinos*," Phys. Rev. **D85** (2012) 093018, arXiv:1112.6419.

[282] J. Aguilar-Saavedra and F. Joaquim, "*Measuring heavy neutrino couplings at the LHC*," Phys. Rev. **D86** (2012) 073005, arXiv:1207.4193.

[283] S. Das, F. Deppisch, O. Kittel, and J. Valle, "*Heavy Neutrinos and Lepton Flavour Violation in Left-Right Symmetric Models at the LHC*," Phys. Rev. **D86** (2012) 055006, arXiv:1206.0256.

[284] T. G. Rizzo, "*Inverse neutrinoless double beta decay*," Phys. Lett. **B116** (1982) 23.

[285] D. London, G. Belanger, and J. Ng, "*New tests of lepton number violation at electron - electron colliders*," Phys. Lett. **B188** (1987) 155.

[286] T. G. Rizzo, "*Single W_R production in e^-e^- collisions at the NLC*," Phys. Rev. **D50** (1994) 5602–5606, arXiv:hep-ph/9404225.

[287] P. Helde, K. Huitu, J. Maalampi, and M. Raidal, "*Vector boson pair production in e^-e^- collisions with polarized beams*," Nucl. Phys. **B437** (1995) 305–318, arXiv:hep-ph/9409320.

[288] J. Gluza and M. Zralek, "*Inverse neutrinoless double beta decay in gauge theories with CP violation*," Phys. Rev. **D52** (1995) 6238–6248, arXiv:hep-ph/9502284.

[289] G. Belanger, F. Boudjema, D. London, and H. Nadeau, "*Inverse neutrinoless double beta decay revisited*," Phys. Rev. **D53** (1996) 6292–6301, arXiv:hep-ph/9508317.

[290] B. Ananthanarayan and P. Minkowski, "*CP violation in heavy neutrino mediated $e^-e^- \to W^-W^-$*," Phys. Lett. **B373** (1996) 130–134, arXiv:hep-ph/9512271.

[291] C. A. Heusch and P. Minkowski, "*Neutrinoless double beta decay and its 'inverse'*," arXiv:hep-ph/9611353.

[292] J. Gluza, "*Constraints on neutrino parameters and doubly charged Higgs particles in the $e^-e^- \to W^-W^-$ process*," Phys. Lett. **B403** (1997) 304–308, arXiv:hep-ph/9704202.

[293] P. Duka, J. Gluza, and M. Zralek, "*Influence of the left-handed part of the neutrino mass matrix on the lepton number violating $e^-e^- \to W^-W^-$ process*," Phys. Rev. **D58** (1998) 053009, arXiv:hep-ph/9804372.

[294] J. Maalampi and N. Romanenko, "*Production of $qq\bar{q}\bar{q}$ final states in e^-e^- collisions in the left-right symmetric model*," Phys. Rev. **D60** (1999) 055002, arXiv:hep-ph/9810528.

[295] W. Rodejohann, "*Inverse Neutrino-less Double Beta Decay Revisited: Neutrinos, Higgs Triplets and a Muon Collider*," Phys. Rev. **D81** (2010) 114001, arXiv:1005.2854.

[296] C. Kom and W. Rodejohann, "*Four-jet final state in same-sign lepton colliders and neutrinoless double beta decay mechanisms*," Phys. Rev. **D85** (2012) 015013, arXiv:1110.3220.

[297] J. F. Gunion, "*Probing Lepton-Number Violating Couplings of Doubly Charged Higgs Bosons at an e^-e^- Collider*," Int. J. Mod. Phys. **A11** (1996) 1551–1562, arXiv:hep-ph/9510350.

[298] W. Rodejohann and H. Zhang, "*Higgs triplets at like-sign linear colliders and neutrino mixing*," Phys. Rev. **D83** (2011) 073005, arXiv:1011.3606.

[299] F. J. Almeida, Y. D. A. Coutinho, J. A. Martins Simoes, J. Ponciano, A. Ramalho, *et al.*, "*Minimal left-right symmetric models and new Z' properties at future electron-positron colliders*," Eur. Phys. J. **C38** (2004) 115–122, arXiv:hep-ph/0405020.

[300] G. Barenboim, K. Huitu, J. Maalampi, and M. Raidal, "*Constraints on doubly charged Higgs interactions at linear collider*," Phys. Lett. **B394** (1997) 132–138, arXiv:hep-ph/9611362.

[301] **MEG Collaboration**, J. Adam *et al.*, "*New constraint on the existence of the $\mu^+ \to e^+\gamma$ decay*," arXiv:1303.0754.

[302] **MEG collaboration**, J. Adam *et al.*, "*New limit on the lepton-flavour violating decay $\mu^+ \to e^+\gamma$*," Phys. Rev. Lett. **107** (2011) 171801, arXiv:1107.5547.

[303] **SINDRUM II Collaboration**, W. H. Bertl *et al.*, "*A Search for muon to electron conversion in muonic gold*," Eur. Phys. J. **C47** (2006) 337–346.

[304] **SINDRUM Collaboration**, U. Bellgardt *et al.*, "*Search for the Decay $\mu^+ \to e^+e^+e^-$*," Nucl. Phys. **B299** (1988) 1.

[305] A. Baldini, F. Cei, C. Cerri, S. Dussoni, L. Galli, *et al.*, "*MEG Upgrade Proposal*," arXiv:1301.7225.

[306] A. Blondel, A. Bravar, M. Pohl, S. Bachmann, N. Berger, *et al.*, "*Research Proposal for an Experiment to Search for the Decay $\mu \to eee$*," arXiv:1301.6113.

[307] **COMET Collaboration**, A. Kurup, "*The COherent Muon to Electron Transition (COMET) experiment*," Nucl. Phys. Proc. Suppl. **218** (2011) 38–43.

[308] Y. Kuno, "*PRISM/PRIME*," Nucl. Phys. Proc. Suppl. **149** (2005) 376–378.

[309] M. Koike, Y. Kuno, J. Sato, and M. Yamanaka, "*A new idea to search for charged lepton flavor violation using a muonic atom*," Phys. Rev. Lett. **105** (2010) 121601, arXiv:1003.1578.

[310] J. Hudson, D. Kara, I. Smallman, B. Sauer, M. Tarbutt, *et al.*, "*Improved measurement of the shape of the electron*," Nature **473** (2011) 493–496.

[311] S. Antusch, C. Biggio, E. Fernandez-Martinez, M. Gavela, and J. Lopez-Pavon, "*Unitarity of the Leptonic Mixing Matrix*," JHEP **0610** (2006) 084, arXiv:hep-ph/0607020.

[312] E. Akhmedov, A. Kartavtsev, M. Lindner, L. Michaels, and J. Smirnov, "*Improving Electro-Weak Fits with TeV-scale Sterile Neutrinos*," arXiv:1302.1872.

[313] G. Altarelli and F. Feruglio, "*Discrete Flavor Symmetries and Models of Neutrino Mixing*," Rev. Mod. Phys. **82** (2010) 2701–2729, arXiv:1002.0211.

[314] P. F. Harrison, D. H. Perkins, and W. G. Scott, "*Tri-bimaximal mixing and the neutrino oscillation data*," Phys. Lett. **B530** (2002) 167, arXiv:hep-ph/0202074.

[315] C. H. Albright, A. Dueck, and W. Rodejohann, "*Possible Alternatives to Tri-bimaximal Mixing*," Eur. Phys. J. **C70** (2010) 1099–1110, arXiv:1004.2798.

[316] K. M. Parattu and A. Wingerter, "*Tribimaximal Mixing From Small Groups*," Phys. Rev. **D84** (2011) 013011, arXiv:1012.2842.

[317] R. de Adelhart Toorop, F. Feruglio, and C. Hagedorn, "*Finite Modular Groups and Lepton Mixing*," Nucl. Phys. **B858** (2012) 437–467, arXiv:1112.1340.

[318] M. Holthausen, K. S. Lim, and M. Lindner, "*Lepton Mixing Patterns from a Scan of Finite Discrete Groups*," to appear in Phys. Lett. B. (2013) , arXiv:1212.2411. In press.

[319] S. F. King and C. Luhn, "*Trimaximal neutrino mixing from vacuum alignment in A4 and S4 models*," JHEP **09** (2011) 042, arXiv:1107.5332.

[320] F. Plentinger and W. Rodejohann, "*Deviations from tribimaximal neutrino mixing*," Phys. Lett. **B625** (2005) 264–276, arXiv:hep-ph/0507143.

[321] S. Boudjemaa and S. F. King, "*Deviations from Tri-bimaximal Mixing: Charged Lepton Corrections and Renormalization Group Running*," Phys. Rev. **D79** (2009) 033001, arXiv:0808.2782.

[322] S. Goswami, S. T. Petcov, S. Ray, and W. Rodejohann, "*Large U_{e3} and Tri-bimaximal Mixing*," Phys. Rev. **D80** (2009) 053013, arXiv:0907.2869.

[323] L. J. Hall, H. Murayama, and N. Weiner, "*Neutrino mass anarchy*," Phys. Rev. Lett. **84** (2000) 2572–2575, arXiv:hep-ph/9911341.

[324] A. de Gouvea and H. Murayama, "*Statistical test of anarchy*," Phys. Lett. **B573** (2003) 94–100, arXiv:hep-ph/0301050.

[325] A. de Gouvea and H. Murayama, "*Neutrino Mixing Anarchy: Alive and Kicking*," arXiv:1204.1249.

[326] J. Heeck and W. Rodejohann, "*Sterile neutrino anarchy*," Phys.Rev. **D87** (2013) 037301, arXiv:1211.5295.

[327] G. Altarelli, F. Feruglio, I. Masina, and L. Merlo, "*Repressing Anarchy in Neutrino Mass Textures*," JHEP **1211** (2012) 139, arXiv:1207.0587.

[328] G. Altarelli and F. Feruglio, "*Tri-bimaximal neutrino mixing from discrete symmetry in extra dimensions*," Nucl. Phys. **B720** (2005) 64–88, arXiv:hep-ph/0504165.

[329] E. Ma, "*A(4) origin of the neutrino mass matrix*," Phys. Rev. D **70** (2004) 031901, arXiv:hep-ph/0404199.

[330] E. Ma and G. Rajasekaran, "*Softly broken A(4) symmetry for nearly degenerate neutrino masses*," Phys. Rev. **D64** (2001) 113012, arXiv:hep-ph/0106291.

[331] G. Altarelli and F. Feruglio, "*Tri-Bimaximal Neutrino Mixing, A4 and the Modular Symmetry*," Nucl. Phys. **B741** (2006) 215–235, arXiv:hep-ph/0512103.

[332] E. Ma, "*Tetrahedral family symmetry and the neutrino mixing matrix*," Mod. Phys. Lett. **A20** (2005) 2601–2606, arXiv:hep-ph/0508099.

[333] L. Lavoura and H. Kuhbock, "*Predictions of an A_4 model with a five-parameter neutrino mass matrix*," Mod. Phys. Lett. **A22** (2007) 181, arXiv:hep-ph/0610050.

[334] P. H. Frampton and S. Matsuzaki, "*Renormalizable A_4 Model for Lepton Sector*," arXiv:0806.4592.

[335] S. F. King and M. Malinsky, "*A4 family symmetry and quark-lepton unification*," Phys. Lett. **B645** (2007) 351–357, arXiv:hep-ph/0610250.

[336] G.-J. Ding and D. Meloni, "*A Model for Tri-bimaximal Mixing from a Completely Broken A_4*," Nucl. Phys. **B855** (2012) 21–45, arXiv:1108.2733.

[337] K. Babu and S. Gabriel, "*Semidirect Product Groups, Vacuum Alignment and Tribimaximal Neutrino Mixing*," Phys. Rev. **D82** (2010) 073014, arXiv:1006.0203.

[338] M. Holthausen and M. A. Schmidt, "*Natural Vacuum Alignment from Group Theory: The Minimal Case*," JHEP **1201** (2012) 126, arXiv:1111.1730.

[339] J. Barry and W. Rodejohann, "*Neutrino Mass Sum-rules in Flavor Symmetry Models*," Nucl. Phys. **B842** (2011) 33–50, arXiv:1007.5217.

[340] M. Honda and M. Tanimoto, "*Deviation from tri-bimaximal neutrino mixing in A4 flavor symmetry*," Prog. Theor. Phys. **119** (2008) 583–598, arXiv:0801.0181.

[341] T. Schwetz, M. Tortola, and J. W. F. Valle, "*Global neutrino data and recent reactor fluxes: status of three-flavour oscillation parameters*," New J. Phys. **13** (2011) 063004, arXiv:1103.0734.

[342] S. Antusch and S. F. King, "*Sequential dominance*," New J. Phys. **6** (2004) 110, arXiv:hep-ph/0405272.

[343] S. F. King, "*Invariant see-saw models and sequential dominance*," Nucl. Phys. **B786** (2007) 52–83, arXiv:hep-ph/0610239.

[344] S. F. King and C. Luhn, "*On the origin of neutrino flavour symmetry*," JHEP **10** (2009) 093, arXiv:0908.1897.

[345] P. Frampton, S. Glashow, and T. Yanagida, "*Cosmological sign of neutrino CP violation*," Phys. Lett. **B548** (2002) 119–121, arXiv:hep-ph/0208157.

[346] W.-L. Guo, Z.-Z. Xing, and S. Zhou, "*Neutrino Masses, Lepton Flavor Mixing and Leptogenesis in the Minimal Seesaw Model*," Int. J. Mod. Phys. **E16** (2007) 1–50, arXiv:hep-ph/0612033.

[347] T. Schwetz, M. Tortola, and J. Valle, "*Where we are on θ_{13}: addendum to 'Global neutrino data and recent reactor fluxes: status of three-flavour oscillation parameters'*," New J. Phys. **13** (2011) 109401, arXiv:1108.1376.

[348] A. Machado and V. Pleitez, "*Schizophrenic active neutrinos and exotic sterile neutrinos*," Phys. Lett. **B698** (2011) 128–130, arXiv:1008.4572.

[349] L. J. Hall and H. Murayama, "*A Geometry of the generations*," Phys. Rev. Lett. **75** (1995) 3985–3988, arXiv:hep-ph/9508296.

[350] E. Ma, "*Permutation symmetry for neutrino and charged lepton mass matrices*," Phys. Rev. **D61** (2000) 033012, arXiv:hep-ph/9909249.

[351] R. Mohapatra, S. Nasri, and H.-B. Yu, "*S(3) symmetry and tri-bimaximal mixing*," Phys. Lett. **B639** (2006) 318–321, arXiv:hep-ph/0605020.

[352] C. N. Leung and S. Petcov, "*A comment on the coexistence of Dirac and Majorana massive neutrinos*," Phys. Lett. **B125** (1983) 461.

[353] S. Petcov and S. Toshev, "*Conservation of lepton charges, massive Majorana and massless neutrinos*," Phys. Lett. **B143** (1984) 175.

[354] A. Maiezza, M. Nemevsek, F. Nesti, and G. Senjanovic, "*Left-Right Symmetry at LHC*," Phys. Rev. **D82** (2010) 055022, arXiv:1005.5160.

[355] V. Tello, M. Nemevsek, F. Nesti, G. Senjanovic, and F. Vissani, "*Left-Right Symmetry: from LHC to Neutrinoless Double Beta Decay*," Phys. Rev. Lett. **106** (2011) 151801, arXiv:1011.3522.

[356] F. F. Deppisch, M. Hirsch, and H. Pas, "*Neutrinoless Double Beta Decay and Physics Beyond the Standard Model*," J. Phys. **G39** (2012) 124007, arXiv:1208.0727.

[357] J. Chakrabortty, H. Z. Devi, S. Goswami, and S. Patra, "*Neutrinoless double-β decay in TeV scale Left-Right symmetric models*," JHEP **1208** (2012) 008, arXiv:1204.2527.

[358] M. Parida and S. Patra, "*Left-right models with light neutrino mass prediction and dominant neutrinoless double beta decay rate*," Phys. Lett. **B718** (2013) 1407–1412, arXiv:1211.5000.

[359] R. L. Awasthi, M. Parida, and S. Patra, "*Neutrino masses, dominant neutrinoless double beta decay, and observable lepton flavor violation in left-right models and SO(10) grand unification with low mass W_R, Z_R bosons*," arXiv:1302.0672.

[360] M.-C. Chen and J. Huang, "*TeV Scale Models of Neutrino Masses and Their Phenomenology*," Mod. Phys. Lett. **A26** (2011) 1147–1167, arXiv:1105.3188.

[361] A. Ibarra, E. Molinaro, and S. Petcov, "*TeV Scale See-Saw Mechanisms of Neutrino Mass Generation, the Majorana Nature of the Heavy Singlet Neutrinos and $(\beta\beta)_{0\nu}$-Decay*," JHEP **1009** (2010) 108, arXiv:1007.2378.

[362] A. Ibarra, E. Molinaro, and S. Petcov, "*Low Energy Signatures of the TeV Scale See-Saw Mechanism*," Phys. Rev. **D84** (2011) 013005, arXiv:1103.6217.

[363] D. Dinh, A. Ibarra, E. Molinaro, and S. Petcov, "*The $\mu \to e$ Conversion in Nuclei, $\mu \to e\gamma$, $\mu \to 3e$ Decays and TeV Scale See-Saw Scenarios of Neutrino Mass Generation*," JHEP **1208** (2012) 125, arXiv:1205.4671.

[364] J. Lopez-Pavon, S. Pascoli, and C. fai Wong, "*Can heavy neutrinos dominate neutrinoless double beta decay?*," arXiv:1209.5342.

[365] M. Hirsch, H. V. Klapdor-Kleingrothaus, and O. Panella, "*Double beta decay in left-right symmetric models*," Phys. Lett. **B374** (1996) 7–12, arXiv:hep-ph/9602306.

[366] H. Pas, M. Hirsch, H. Klapdor-Kleingrothaus, and S. Kovalenko, "*Towards a superformula for neutrinoless double beta decay*," Phys. Lett. **B453** (1999) 194–198.

[367] W. Loinaz, N. Okamura, S. Rayyan, T. Takeuchi, and L. Wijewardhana, "*The NuTeV anomaly, lepton universality, and nonuniversal neutrino gauge couplings*," Phys. Rev. **D70** (2004) 113004, arXiv:hep-ph/0403306.

[368] M. Mitra, G. Senjanovic, and F. Vissani, "*Neutrinoless Double Beta Decay and Heavy Sterile Neutrinos*," Nucl. Phys. **B856** (2012) 26–73, arXiv:1108.0004.

[369] G. Pantis, F. Simkovic, J. Vergados, and A. Faessler, "*Neutrinoless double beta decay within QRPA with proton - neutron pairing*," Phys. Rev. **C53** (1996) 695–707, arXiv:nucl-th/9612036.

[370] K. Muto, E. Bender, and H. Klapdor, "*Nuclear structure effects on the neutrinoless double beta decay*," Z. Phys. **A334** (1989) 187–194.

[371] J. Suhonen and O. Civitarese, "*Weak-interaction and nuclear-structure aspects of nuclear double beta decay*," Phys. Rept. **300** (1998) 123–214.

[372] E. Caurier, F. Nowacki, A. Poves, and J. Retamosa, "*Shell Model Studies of the Double Beta Decays of Ge-76, Se-82, and Xe-136*," Phys. Rev. Lett. **77** (1996) 1954–1957.

[373] M. Doi, T. Kotani, and E. Takasugi, "*Double beta Decay and Majorana Neutrino*," Prog. Theor. Phys. Suppl. **83** (1985) 1.

[374] F. Simkovic, G. Pantis, J. Vergados, and A. Faessler, "*Additional nucleon current contributions to neutrinoless double beta decay*," Phys. Rev. **C60** (1999) 055502, arXiv:hep-ph/9905509.

[375] V. Cirigliano, A. Kurylov, M. Ramsey-Musolf, and P. Vogel, "*Lepton flavor violation without supersymmetry*," Phys. Rev. **D70** (2004) 075007, arXiv:hep-ph/0404233.

[376] G. Leontaris, K. Tamvakis, and J. Vergados, "*Lepton and family number violation from exotic scalars*," Phys. Lett. **B162** (1985) 153.

[377] M. L. Swartz, "*Limits on doubly charged Higgs bosons and lepton flavor violation*," Phys. Rev. **D40** (1989) 1521.

[378] S. M. Bilenky, S. Petcov, and B. Pontecorvo, "*Lepton Mixing, $\mu \to e\gamma$ Decay and Neutrino Oscillations*," Phys. Lett. **B67** (1977) 309.

[379] T. Cheng and L.-F. Li, "*$\mu \to e\gamma$ in theories with Dirac and Majorana neutrino mass terms*," Phys. Rev. Lett. **45** (1980) 1908.

[380] A. Ilakovac and A. Pilaftsis, "*Flavor violating charged lepton decays in seesaw-type models*," Nucl. Phys. **B437** (1995) 491, arXiv:hep-ph/9403398.

[381] A. Ioannisian and A. Pilaftsis, "*Cumulative nondecoupling effects of Kaluza-Klein neutrinos in electroweak processes*," Phys. Rev. **D62** (2000) 066001, arXiv:hep-ph/9907522.

[382] L. Lavoura, "*General formulae for $f(1) \to f(2)\gamma$*," Eur. Phys. J. **C29** (2003) 191–195, arXiv:hep-ph/0302221.

[383] A. Pilaftsis and T. E. J. Underwood, "*Electroweak-scale resonant leptogenesis*," Phys. Rev. **D72** (2005) 113001, arXiv:hep-ph/0506107.

[384] R. Alonso, M. Dhen, M. Gavela, and T. Hambye, "*Muon conversion to electron in nuclei in type-I seesaw models*," arXiv:1209.2679.

[385] V. Tello, *Connections between the high and low energy violation of lepton and flavor numbers in the minimal left-right symmetric model*. PhD thesis, SISSA, Sept., 2012. http://www.sissa.it/tpp//phdsection/AlumniThesis/.

[386] B. He, T. Cheng, and L.-F. Li, "*A Less suppressed $\mu \to e\gamma$ loop amplitude and extra dimension theories*," Phys. Lett. **B553** (2003) 277–283, arXiv:hep-ph/0209175.

[387] M. Nemevsek, F. Nesti, G. Senjanovic, and V. Tello, "*Neutrinoless Double Beta Decay: Low Left-Right Symmetry Scale?*," arXiv:1112.3061.

[388] B. Allanach, C. Kom, and H. Pas, "*Large Hadron Collider probe of supersymmetric neutrinoless double beta decay mechanism*," Phys. Rev. Lett. **103** (2009) 091801, arXiv:0902.4697.

[389] B. Allanach, C. Kom, and H. Pas, "*LHC and B physics probes of neutrinoless double beta decay in supersymmetry without R-parity*," JHEP **0910** (2009) 026, arXiv:0903.0347.

[390] **CMS Collaboration**, S. Chatrchyan *et al.*, "*Search for heavy neutrinos and W[R] bosons with right-handed couplings in a left-right symmetric model in pp collisions at sqrt(s) = 7 TeV*," Phys.Rev.Lett. **109** (2012) 261802, arXiv:1210.2402.

[391] **CMS Collaboration**, "*Search for a heavy neutrino and right-handed W of the left-right symmetric model in pp collisions at 8 TeV*," CMS-PAS-EXO-12-017 (2012) . http://inspirehep.net/record/1199140/files/EXO-12-017-pas.pdf.

[392] **ATLAS Collaboration**, G. Aad *et al.*, "*Search for heavy neutrinos and right-handed W bosons in events with two leptons and jets in pp collisions at $\sqrt{s} = 7$ TeV with the ATLAS detector*," Eur. Phys. J. **C72** (2012) 2056, arXiv:1203.5420.

[393] P. Hosteins, S. Lavignac, and C. A. Savoy, "*Quark-Lepton Unification and Eight-Fold Ambiguity in the Left-Right Symmetric Seesaw Mechanism*," Nucl. Phys. **B755** (2006) 137–163, arXiv:hep-ph/0606078.

[394] J. Casas, A. Ibarra, and F. Jimenez-Alburquerque, "*Hints on the high-energy seesaw mechanism from the low-energy neutrino spectrum*," JHEP **0704** (2007) 064, arXiv:hep-ph/0612289.

[395] E. Adli *et al.*, "*A multi-TeV Linear Collider based on CLIC Technology: CLIC Conceptual Design Report*,". http://project-clic-cdr.web.cern.ch/project-CLIC-CDR/.

[396] Z. zhong Xing, "*Neutrino Telescopes as a Probe of Broken mu- tau Symmetry*," Phys. Rev. **D74** (2006) 013009, arXiv:hep-ph/0605219.

[397] W. Rodejohann, "*Neutrino Mixing and Neutrino Telescopes*," JCAP **0701** (2007) 029, arXiv:hep-ph/0612047.

[398] S. Pakvasa, W. Rodejohann, and T. J. Weiler, "*Flavor Ratios of Astrophysical Neutrinos: Implications for Precision Measurements*," JHEP **0802** (2008) 005, arXiv:0711.4517.

[399] D. Meloni and T. Ohlsson, "*Neutrino flux ratios at neutrino telescopes: The Role of uncertainties of neutrino mixing parameters and applications to neutrino decay*," Phys. Rev. **D75** (2007) 125017, arXiv:hep-ph/0612279.

[400] J. Nieves, D. Chang, and P. Pal, "*Electric dipole moment of the electron in left-right symmetric theories*," Phys. Rev. **D33** (1986) 3324–3328.

[401] A. Ilakovac, A. Pilaftsis, and L. Popov, "*Charged Lepton Flavour Violation in Supersymmetric Low-Scale Seesaw Models*," arXiv:1212.5939.

[402] F. Cuypers and S. Davidson, "*Bileptons: Present limits and future prospects*," Eur. Phys. J. **C2** (1998) 503–528, arXiv:hep-ph/9609487.

[403] M. Raidal and A. Santamaria, "*Muon electron conversion in nuclei versus $\mu \to e\gamma$: An Effective field theory point of view*," Phys. Lett. **B421** (1998) 250–258, arXiv:hep-ph/9710389.

[404] R. Kitano, M. Koike, and Y. Okada, "*Detailed calculation of lepton flavor violating muon electron conversion rate for various nuclei*," Phys. Rev. **D66** (2002) 096002, arXiv:hep-ph/0203110.